

# Advanced migration assays for studying chemotaxis of slow moving cells

Doctoral thesis

submitted in partial fulfilment of the requirements  
for the degree of

Doctor rerum naturalium (Dr. rer. nat.)

to the

Mathematisch-Naturwissenschaftlichen Fakultät der  
Rheinischen Friedrich-Wilhelms-Universität Bonn

by

Lea Tomášová  
from Pardubice, Czech Republic

Bonn, June 2021



---

Angefertigt mit Genehmigung der Mathematisch-Naturwissenschaftlichen Fakultät der Rheinischen Friedrich-Wilhelms-Universität Bonn.

1<sup>st</sup> referee: Prof. Dr. Rudolf Merkel  
2<sup>nd</sup> referee: Prof. Dr. Ulrich Kubitscheck

Year of publication: 2021  
Day of oral examination: 29.09.2021



# Abstract

Chemotaxis of slow moving cells plays a crucial role in numerous physiological and pathophysiological processes; including tumour metastasis, development, and wound healing. Therefore, a comprehensive understanding of chemotactic behaviour, and the characterisation of extracellular signals and cues that prompt directed cell migration is highly desirable. The state-of-the-art chemotaxis assays are in general designed either with respect to the migration characteristics of fast moving cells (such as cells of the immune system), or focus on an in-depth investigation of chemotactic behaviour, requiring a time-demanding and labour-intensive analysis of individual cell trajectories. Such approach poses a limitation for experiments challenged by an increased number of samples; e.g., screenings for chemoattractants, or molecules and genetic mutations with the potential to inhibit or promote the chemotactic effect.

Therefore, the first aim of this thesis was to develop a novel chemotaxis assay suitable for slow moving cells (e.g., keratinocytes, cancer cells), which would enable fast and effortless evaluation of the chemotactic response. For that purpose, advanced stimuli-responsive materials and micro-patterning methods were applied, and a chemotaxis chamber with hydrogel migration arena was established. The assay employs a gradient generator that maintains a well-defined long-term stable chemical gradient, essential for the investigation of chemotaxis in slow moving cells. The design of the assay enables evaluation of the chemotactic effect from the end-point state of the experiment. This method substantially facilitates the analysis, providing for an increased experimental throughput.

Characterisation and quantification of the chemotactic behaviour of whole cell populations provide the fundamental information on the chemotaxis-inducing stimuli and the relevant response, which is often cell-type specific. However, to get a complete picture of cell behaviour during chemotaxis, further detailed investigations of single cells in conditions close to their physiological environment is required. Therefore, in another part of the thesis, the focus was set on establishment of experimental procedures for studying the migratory behaviour of single chemotaxing cells in long-term stable gradients with advanced imaging techniques, such as traction force microscopy, and light-sheet fluorescence microscopy.

Finally, the novel tool was employed to investigate the chemotaxis of primary keratino-

cytes, slow moving cells that play a central role in re-epithelialisation of wounds. For the first time, the normal human epithelial keratinocytes (nHEK) were exposed to chemical gradients of several growth factors over long time-periods. The chemotactic response to a range of varying chemical conditions was evaluated quantitatively with the end-point assay. From the tested substances, the epithelial growth factor (EGF) and transforming growth factor  $\alpha$  (TGF $\alpha$ ) were most potent in inducing the directed migration of nHEK cells. The identification and quantification of the parameters that prompt keratinocyte chemotaxis made it possible to establish a model for further investigations of gradient sensing and directed migration of epithelial cells, aiming for new therapeutic strategies to promote wound repair.

# Contents

<b>1</b>	<b>Introduction</b>	<b>1</b>
1.1	Goals and objectives of the thesis . . . . .	6
1.1.1	End-point read-out of the chemotactic effect . . . . .	6
1.1.2	Chemotaxis of keratinocytes . . . . .	7
1.1.3	Combined assays for the observation of cell migration in long-term stable chemical gradients with advanced microscopy techniques . . . . .	8
<b>2</b>	<b>Foundations</b>	<b>13</b>
2.1	Cell in motion . . . . .	14
2.1.1	Actin cytoskeleton drives cell migration . . . . .	14
2.1.2	Cell migration over 2D surfaces . . . . .	17
2.1.3	Cell migration in 3D environment . . . . .	19
2.2	Chemotaxis: navigating cells through a chemically heterogeneous environment .	21
2.2.1	Molecular basis of the directional response . . . . .	21
2.2.2	Gradient sensing in slow moving cells . . . . .	22
2.2.3	Problems with the compass: an alternative view on chemotaxis . . . . .	24
2.3	The evolution of chemotaxis assays . . . . .	26
2.3.1	Gradient generation in chemotaxis assays . . . . .	26
2.3.2	Standard chemotaxis assays . . . . .	27
2.3.3	Microfluidics-based assays . . . . .	31
2.3.4	$\mu$ -Slide Chemotaxis . . . . .	33
2.3.5	Evaluation of the chemotactic effect with the $\mu$ -Slide Chemotaxis assay .	34
2.4	Micro-patterning and micro-structuring - methods of surface functionalisation for cell-based experiments . . . . .	37
2.4.1	Micro-patterning of flat 2D micro-environments . . . . .	38
2.4.2	Micro-engineered 3D environments . . . . .	41
<b>3</b>	<b>Materials and Methods</b>	<b>43</b>
3.1	Micro-structuring and micro-patterning . . . . .	43
3.1.1	Fabrication of PEG-DMA micro-wells . . . . .	43
3.1.2	Fabrication of fibronectin-patterned surfaces with a silicon stencil . . . . .	44
3.1.3	In-channel micro-patterning . . . . .	46

3.1.4	Photopolymerisation of PEG-norbornene hydrogel . . . . .	48
3.2	Cell-based experiments . . . . .	49
3.2.1	Cell culture . . . . .	49
3.2.2	Viability assay . . . . .	51
3.2.3	$\mu$ -Slide Chemotaxis assay . . . . .	52
3.2.4	Migration arena chemotaxis assay . . . . .	52
3.2.5	End-point evaluation of chemotaxis in the migration arena assay . . . . .	53
3.2.6	Time-lapse microscopy . . . . .	54
3.2.7	Traction Force Microscopy of chemotaxing cells . . . . .	55
3.2.8	Light-sheet Fluorescence Microscopy . . . . .	56
3.3	Statistical analysis . . . . .	57
<b>4</b>	<b>Establishment of a direct end-point chemotaxis assay: Results and Discussion</b>	<b>59</b>
4.1	Establishment of a 2D end-point chemotaxis assay: micro-wells and micro-patterns	61
4.1.1	PEG-DMA micro-wells for 2D chemotaxis assay . . . . .	61
4.1.2	Surface functionalisation in the chemotaxis chamber by 2D micro-patterning methods . . . . .	62
4.2	2D/3D migration arena enclosed by a cell repellent 3D hydrogel . . . . .	65
4.2.1	Fabrication of barriers from a 3D PEG-based hydrogel . . . . .	66
4.2.2	Visualisation of gradient formation in the migration arena . . . . .	67
4.2.3	Validation of the migration arena chemotaxis assay on the example of HT1080 chemotaxis in a FBS gradient . . . . .	68
4.3	Discussion . . . . .	77
4.3.1	Limitations regarding chemical functionalisations in the gradient area of the $\mu$ -Slide Chemotaxis . . . . .	77
4.3.2	Migration arena chemotaxis assay . . . . .	78
<b>5</b>	<b>Chemotaxis of primary keratinocytes: Results and Discussion</b>	<b>83</b>
5.1	Effect of growth factors on nHEK migration—time development of the chemo- tactic response . . . . .	84
5.2	TGF $\alpha$ , EGF, and BPE induce chemotaxis of nHEKs . . . . .	89
5.2.1	Cell proliferation does not bias the measured chemotaxis effect . . . . .	90
5.2.2	Interplay of signals: chemotactic response to gradients of mixed GFs . . . . .	92
5.2.3	Specificity of the EGF- and TGF $\alpha$ -induced chemotactic response - in- hibitor test . . . . .	93
5.3	Discussion . . . . .	95
<b>6</b>	<b>Combined assays for studying single cell behaviour in response to chemical gradients with             advanced microscopy techniques: Results and Discussion</b>	<b>99</b>
6.1	Chemotaxis chamber for Traction Force Microscopy . . . . .	99



6.1.1	Fabrication of the TFM/chemotaxis chamber . . . . .	100
6.1.2	Traction forces of keratinocytes during chemotaxis and chemokinesis . .	101
6.2	Chemotaxis set-up for Light-sheet Fluorescence Microscopy . . . . .	104
6.2.1	FEP chamber for generation of a chemical gradient . . . . .	104
6.3	Discussion . . . . .	107
6.3.1	TFM/chemotaxis assay . . . . .	107
6.3.2	Light-sheet microscopy . . . . .	109
7	Conclusions and outlook	<b>111</b>
	Bibliography	<b>115</b>
	List of figures	<b>136</b>
	Acknowledgements	<b>138</b>
	Appendix A. List of abbreviations	<b>141</b>
	Appendix B. List of materials	<b>144</b>



# 1 Introduction

Cell migration, the locomotion of cells through their environment, is a fundamental feature of both prokaryotic and eukaryotic life. In higher multicellular systems, the ability to actively migrate through the surrounding tissues is reserved to specialised cell types, and is orchestrated and coordinated with a great balance in space and time by a multitude of extracellular signals [1–4]. The fashion of cell locomotion varies in regard to the specific function and whereabouts of the cells [5–7]. On their way through the body, cells move along two-dimensional structures, through confined spaces, or invade dense three-dimensional matrices [8–11]; some cell types proceed fast to reach an assigned destination, as do the immune cells recruited to a site of infection [12]; others move slower, such as fibroblasts steering through the connective tissue, rebuilding the surrounding matrix [13]. Cell migration is a complex, integrated process regulated by guidance cues of both physical, and chemical substance, presented to the cells by the constantly changing environments that surround them [9, 14].

With the development of live-cell imaging techniques, the ability to study cell migration in detail emerged. To the present day, advanced imaging methods enable direct observation of cells encapsulated in a 3D matrix [15], visualisation of sub-cellular structures thanks to non-invasive labelling methods [16], or direct visualisation of cell migration *in vivo* [17]. Hand in hand with the outburst of live-cell imaging, a multitude of investigative tools that enable studying cell migration *in vitro* under specific parameters has been established [18]. In the recent decade, much effort has been dedicated to the development of advanced bio-compatible materials in the pursue of building synthetic matrices and micro-environments mimicking the physiological environment of the cell as close as possible [19–23].

Most of the cells migrating *in vivo* are exposed to a dynamic chemical environment. The cells are able to sense the changes in the concentrations of substances relevant for their function, and react to them by changing the direction of locomotion [2, 3]. This phenomenon is known as chemotaxis, where *taxis* signifies a movement responding to an external stimuli, and *chemo-*specifies the nature of the signal [24]. Its central role in numerous physiological and pathophysiological processes makes chemotaxis of the highest research interest. In cancer, as metastatic cells disseminate from the primary tumour, they orient towards chemical signals that navigate them through the tissues towards blood vessels and further up to the site of a secondary tumour [25]. In the process of wound healing, chemotaxis is involved on multiple cellular levels: first, the chemical signals released on the injury site attract inflammatory cells, being followed by fibroblasts, which secrete extracellular matrix (ECM) composites to repair the tissue, and

---

endothelial cells that vascularise the newly formed matrix [26–28]. All the cells that approach the wound secrete further molecules to recruit more cells. Finally, the cells of the upper skin layers, the keratinocytes, are attracted to the wound to close the injury and restore the skin integrity [29, 30]. Besides, chemotaxis also underpins crucial processes during embryogenesis, and immune responses [31, 32].

Although the long history of chemotaxis research is laced with important discoveries that shed light on the basic mechanisms of cell movement, much remains to be revealed yet in order to fully comprehend the process; especially its specific characteristics in various cell types [33]. Historically, the seminal research activities focused on chemotaxis of bacteria and fast moving eukaryotic cells, such as the amoeba *Dictyostellium discoideum* (one of the earliest model organisms of cell migration), or the cells of the immune system [34, 35]. Chemotactic response of these cells is almost immediate and the directed migration can be observed in real-time within a relatively short time period [36]. Subsequently, also specific tools for the investigation of chemotaxis were designed to suit the migration characteristics of the highly motile cells. Yet, the accumulating evidence proves that there are differences between the mechanisms employed by chemotaxing fast moving cells, and other cell types that move at considerably lower speed [33]. Cells that are designated as slow moving, such as fibroblasts, keratinocytes, endothelial cells, and many types of cancer cells, cover approximately one cell-body length per hour (i.e., 50-100  $\mu\text{m}/\text{h}$ ); hence migrating at speed rates 10-30x slower than the fast moving cells (leukocytes or amoebas) [12, 14, 37]. Thus, for a reliable analysis of the chemotactic behaviour of slow moving cells, it is necessary to employ investigative tools that generate defined gradients that remain stable over several hours [38]. Up to date, only a handful of ready-to-use systems for observing cell migration under long-term gradient conditions are available; all of them belonging to the category of microfluidic devices and chambers [39–41].

Typically, evaluation of the chemotactic behaviour in such assays is based on reconstructing the complete migration trajectories of cells [39]. Such analysis provides detailed information on cell migration [42]; however, it is a time-consuming and tedious procedure; especially, since manual tracking is usually the method of choice for reconstructing the cells paths. In spite of the intensive endeavour and fast advances in the field of automated cell tracking in recent years, it has not yet reached the reliability of a human observer in recognizing one moving cell in two subsequent frames of a time-lapse sequence [43]. Furthermore, the lengthy and challenging analytical process complicates the application of such chemotaxis assays in high-throughput studies, typical for biomedical and clinical research. Hence, there is a lack of investigative tools that at the same time provide a long-time stable chemical gradient, and enable fast and simple quantification of the chemotactic effect. As a consequence, not many specific chemoattractants of particular slow moving cell types were identified yet, relative to the fast moving cells [38]. Yet, the substantial role the slow moving cells play in numerous physiological and pathological processes dictates the necessity of understanding how their behaviour is regulated in tissues. For example, chemotactic regulation of slow migrating cells can be observed on several levels

---

during tumour metastasis [44,45]. Along with chemical signals that guide the metastatic cells on their way towards the site of the secondary tumour, the production of chemotactic factors by cancer cells also controls the migration of endothelial cells and vascularisation of tumour tissues [28,46]. Likewise, several types of slow moving cells are involved in the chemically triggered recolonisation of injured tissues during wound healing; namely, fibroblasts, endothelial cells, and keratinocytes [26,27,30].

This thesis deals mostly with the chemotactic behaviour of human primary keratinocytes. As noted above, these cells play a major role in wound closure [29]. In the epithelialisation phase of the process, keratinocytes migrate across the newly formed tissue of the wound bed to close the gap of the injured area, and are thus responsible for restoring the integrity of the skin barrier. A successful re-epithelialisation is an essential component of the wound healing process; impaired epithelialisation leads to chronic wounds [47]. Therefore, comprehension of the mechanisms that regulate keratinocyte migration could help to reveal new therapeutic methods to promote wound healing [48].

### Keratinocyte migration in wound closure

Keratinocytes (KCs) are relatively slow moving cells of the upper skin layers (epidermis), rich in intermediate filaments of keratin that form a dense cross-linked meshwork in the cytoplasm [49]. KCs of a normal (uninjured) skin are closely interconnected with the neighbouring cells, forming a confluent layer attached to the basal membrane. Characteristic is the baso-apical polarity of epithelial cells. However, following a cutaneous wound, KCs undergo a dramatic morphological change and become flat, persistently migrating cells, with a broad lamellipodium at the cell front, and thin retraction fibres at the rear [50]. Junctions that mediated KCs connection with the basal membrane (hemodesmosomes) and with other cells (desmosomes) are disassembled and internalised; both the intermediate filament and microfilament networks are reorganised and contractile stress fibres are formed across the cell body [49]. As the KCs acquire the migratory phenotype, they invade the wounded epidermis, they proliferate, and ultimately they close the wound gap. Multiple signals contribute to the KC activation and their navigation into the wound [51,52]. An acute wound substantially changes the environment and signal input of the cells, provoking many molecular events on cellular and extracellular level in both epidermis and dermis [29]. A provisional matrix, the fibrin cloth, is formed over the wound, containing blood platelets and adhesion proteins, foremost fibrin and fibronectin [53]. Immune cells and fibroblasts are lured into the wound by tissue factors, chemokines and growth factors (GFs) that are released after the injury,<sup>1</sup> and once there, they secrete additional factors. Basal KCs start to migrate into the wound several hours after the injury, following the immune cells and fibroblast [27].

---

<sup>1</sup>For example, the platelet-derived growth factor (PDGF), secreted by the platelets and macrophages present in the wound, is known to attract fibroblast into the injured dermis [26,54].

The exposure to the GFs and other soluble or substrate bound agents secreted by those cells is one of the most important triggers of KC activation. The migrating KCs themselves leave behind tracks of ECM proteins that are used as paths by other cells [49, 55]. Besides, the loss of tight contacts with the neighbour cells (i.e., loss of contact inhibition) also actuates the KC transition from sedentary to migratory phenotypes, and the free edges at the wound margin act as mechanical stimuli leading to KC colonisation of the bare area of the wounded epidermis [56, 57]. Relative to fibroblast-like cells, migrating KCs still form quite strong cell-cell contacts—engaging with other cells, and collective migration is the hallmark of KC migration [58]. While fibroblasts migrate rather independently *in vitro*, without any significant reaction to an occasional collision with other cells; colliding KCs tend to “stick together” and stall for a few minutes before proceeding in the forward migration, often in a new direction.

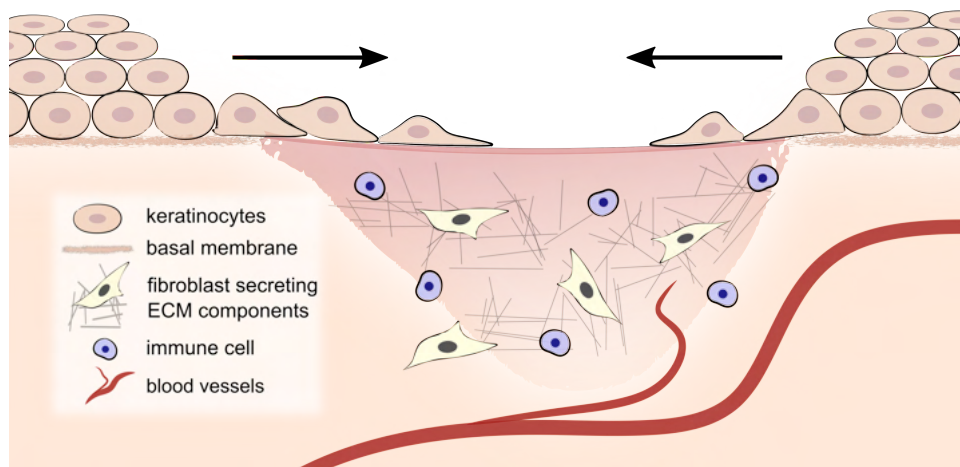


Figure 1.1: Scheme of the wound closure process. In the initial, inflammatory and proliferative phases of wound healing, immune cells and fibroblasts are recruited to the site of injury. Fibroblasts produce components of extracellular matrix (ECM), such as collagen and fibronectin, and fill the wound bed with a new matrix. Both cell types secrete further signal molecules that attract other cells into the wound bed, and promote angiogenesis (i.e., the formation of new blood vessels). During the re-epithelialisation phase, proliferation and motility of the keratinocytes of the basal layer at the wound margins is activated, the cells gain a migratory phenotype and move over the wound. The arrows indicate the direction of their migration from the wound margins towards the middle of the wound bed, where the two migrating sheets meet and close the gap.

### Role of growth factors in keratinocyte migration

The numerous growth and tissue factors produced in the injured area affect basal keratinocytes at the wound margin, acting as mito- and/or motogens (factors inducing cell division, or cell motility, respectively). The role of the diverse GFs in the activation of the wound KCs, their navigation into the wound, and finally their proliferation, was thoroughly studied in the last

---

decades. In 1988, Martinet *et al.* [59] described that KC migration is stimulated by the wound fluid, as well as with fibroblast and smooth muscle cells conditioned media. Later, numerous specific GFs and chemokines with chemokinetic effect on KCs were identified, as reviewed in [30, 49, 51, 60, 61]. It is presumable that the basal keratinocytes are guided into the wound bed not only in result of the natural cell tendency to colonise cell-free areas and by haptotaxis, but also chemotactically.

A multitude of chemical factors that activate keratinocytes at the wound margins and stimulate their migration over the wound have been identified so far [30, 51]. However, the evidence on the capacity of these factors to induce a truly directional migratory response (in contrast to general stimulation of cell motility and speed) remains inconclusive. Furthermore, along with chemical gradients, cell behaviour is regulated by diverse mechanical stimuli [9, 10]; which is also the case for keratinocytes in the re-epithelialisation process [56, 57]. Understanding how the diverse chemical and mechanical stimuli are integrated, and discerning the specific role of particular signals in directed migration of keratinocytes could lead to the identification of novel therapeutic targets or approaches for promoting a successful wound closure.

Therefore, the focus of this thesis was set on analysing the chemotactic behaviour of human keratinocytes exposed to long-term gradients of diverse growth factors. For that purpose, an end-point chemotaxis assay suitable for the investigation of slow-moving cells under multiple parallel conditions was established. Identification of specific keratinocyte chemoattractants, and quantification of the chemotactic effect allowed to specify the parameters that reliably and reproducibly induce directed migration; thus providing an epithelial chemotaxis model for further investigations on directed migration of these cells. The increased experimental throughput of the end-point assay permitted to quantitatively analyse the chemotactic capacity of multiple growth factors towards the cells. Besides, experimental set-ups for investigation of cell migration in long-term stable chemical gradients with advanced imaging techniques were established. That was namely the traction force microscopy, and the light-sheet fluorescent microscopy, making it possible to study the motility of single cells under multiple defined parameters in further detail. The rationale of the three sub-goals of this work is summarised in the next chapter.

---

## 1.1 Goals and objectives of the thesis

The goal of this thesis is the development of advanced chemotaxis assays suitable for studying the migratory response of slow moving cells, and characterisation of the chemotactic response of primary human keratinocytes in defined gradients of growth factors. The aims of the work can be divided in three parts:

1. Establishment of an end-point chemotaxis assay for a fast and simple evaluation of the chemotactic effect
2. Characterisation of the chemotactic effect of growth factors on normal human epithelial keratinocytes (nHEKs)
3. Designing experimental tools that combine chemical gradients and advanced imaging techniques for an in-depth analysis of the chemotactic behaviour

### 1.1.1 End-point read-out of the chemotactic effect

In order to fasten and simplify the analysis of the chemotactic behaviour of slow moving cells, a diffusion-based gradient generator for direct-observation of cell migration will be modified in a way that will enable evaluation of the chemotactic effect solely from the end-point of the experiment. This can be achieved by confining the cell migration in the chemotaxis chamber to defined areas. This will allow to monitor the changes in cell distribution over time simply by optical observation at any time-point of the experiment. The underlying idea is that the application of a chemical gradient triggers a chemotactic response in cells that are initially distributed evenly over the defined area, leading to directed migration towards the increasing chemoattractant concentration. Due to the confinement, the chemotaxing cells will accumulate in one part of the restriction area, proximal to the chemoattractant source (Fig 1.2). Thus, it should be then possible to identify the chemotactic effect from the change of cell distribution between the initial, and end-point state. In other words, the chemotactic effect will be represented by the displacement of the total cell mass in the defined area.

The area of cell migration will be outlined by a spatially defined functionalisation of the surface of the chemotaxis chamber with materials that enhance, or prevent cell adhesion, respectively. For that purpose, advanced, bio-compatible materials will be employed and micro-patterned or micro-structured in the chemotaxis chamber by UV-photolithography. The basic principles of surface-functionalisation techniques will be explained in Chapter 2.4.

The objectives of this part of the work include analysing the possibilities of modifying the chemotaxis chamber with diverse micro-patterning and micro-structuring methods, optimisation of a fabrication procedure yielding the cell migration restrictive areas in the chemotaxis chamber, and the establishment of an end-point based analytical method for quantifying the chemotactic effect. In order to validate the assay and verify the results obtained by the end-point analysis, the chemotaxis of HT1080 fibrosarcoma cell line in gradients of fetal bovine



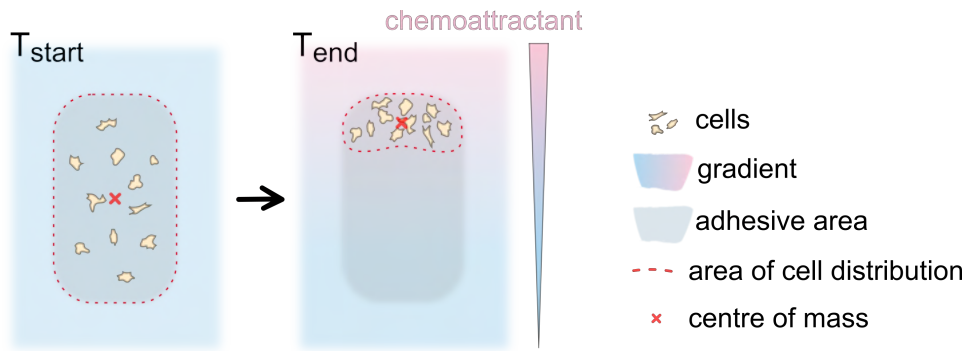


Figure 1.2: Scheme of the basic idea of the end-point evaluation of chemotaxis. Cell migration in the chemotaxis chamber is restricted to a defined adhesive area (grey). Initially, cells are distributed evenly in the whole adhesive area ( $T_{\text{start}}$ ). When a gradient of a chemoattractant is applied, cells migrate towards the chemoattractant source, which results in an accumulation of the cell mass in one part of the adhesive pattern ( $T_{\text{end}}$ ). The chemotactic effect can be evaluated by comparing the cell distribution at the start and end of the experiment based on the displacement of the centre of the cell mass.

serum (FBS) will be analysed, which is a well established model of chemotaxis of slow moving cells [39, 62]. HT1080 are fibroblast-like mesenchymal cells that are widely used in 2D and 3D migration experiments *in vitro* for their ability of spontaneous locomotion on extracellular matrix components, and for their high invasive potential in 3D matrices [63–66]. Chemotaxis of HT1080 cells can be induced by a gradient of 0-10% FBS [39]. In contrast, the cells move randomly in all directions when exposed to a uniform concentration of FBS. Uniformly applied FBS (10%) stimulates the random migration of HT1080; i.e., induces chemokinesis. Therefore, in order to verify that the end-point chemotaxis assay allows to discern the chemotactic effect from random migration and chemokinesis, HT1080 exposed to uniform, both serum-free (0% FBS), and 10% FBS conditions, will be included in the experiments as a control.

The results of this part of the work are presented in Chapter 4.

### 1.1.2 Chemotaxis of keratinocytes

In the next part of this work, the previously established end-point chemotaxis assay will be employed to identify a chemoattractant of normal human epithelial keratinocytes (nHEK), and to quantitatively characterise their chemotactic response.

By the present day, a number of chemokines and growth factors have been reported to stimulate KCs migration, or even induce chemotaxis [30, 49, 51]. However, the assay of choice practically in all studies of chemically induced KC migration was the Boyden chamber assay, or its modifications [59, 67–74]. As will be discussed in detail in Chapter 2.3.2, this type of assay is not optimal for studying chemotaxis of slow moving cells, and it cannot discern chemotaxis from a general increase in random locomotion. Therefore, such experiments could reveal the chemokinetic capacity of the tested agent, but are inconclusive in regard to the

---

genuine chemotactic effect and directionality of the cell response. Among the agents that were reported to induce KC chemotaxis in these experiments were chemokines, such as interferon- $\gamma$  (IFN- $\gamma$ ), interleukin-1 $\alpha$  (IL-1 $\alpha$ ), or interleukin-8 (IL-8) [67, 69, 70, 75]; GFs of the epithelial growth factor (EGF) family [68, 71, 76], transforming growth factor  $\beta$ -1 (TGF $\beta$ ), and platelet-derived growth factor (PDGF) [68]; or the  $\beta$ -amyloid precursor protein sAPP [74].

In this study, the chemotactic capacity of five different agents in varying gradient parameters will be analysed, including the epithelial growth factor (EGF), transforming growth factor  $\alpha$  (TGF $\alpha$ ), transforming growth factor  $\beta$ -1 (TGF $\beta$ ), insulin, and the bovine pituitary extract (BPE). These growth factors were chosen for being previously reported as the most potent modifiers of keratinocyte migration [69, 71, 75–79]. The migratory response of KCs *in vitro* has been by now only examined in experiments that exposed the cells either to an uniform concentration, or steep and unstable gradients of the chemical in question. The aim of this thesis is to investigate the long-term chemotactic response of KCs exposed to stable linear gradients of varying steepness.

The findings on the chemotaxis of nHEK cells are described in Chapter 5.

### 1.1.3 Combined assays for the observation of cell migration in long-term stable chemical gradients with advanced microscopy techniques

The end-point chemotaxis tool should enable a robust analysis of the chemotactic behaviour on the cell population level, and provide for a rapid screening for chemotactically active extracellular substances, as well as for signalling molecules that are involved in the intracellular machinery responsible for gradient sensing and relevant migratory response. However, a comprehensive understanding of the chemotactic behaviour requires a subsequent detailed characterisation of the migration on a single cell level; taking into account the multiple parameters of the micro-environments that cells face *in vivo*. Therefore, the next aim of the thesis is to develop tools and experimental set-ups that would combine long-term stable gradients with advanced microscopy techniques, in order to enable an in-depth insight in single cell migratory behaviour under chemotactic conditions. Taken together, the end-point chemotaxis assay will make it possible to identify and tune such parameters that reproducibly induce chemotaxis in a given cell type. The entailed challenge is to apply these parameters with specialised tools to visualise specific components of the directed migration, such as the traction forces applied by cells on the substrate, or the cell-substrate and cell-cell interplay within 3D environments.

---

## Traction Force Microscopy

An indispensable component of cell motility are traction forces that are applied by the migrating cells on the substrate to ensure the net displacement of cell body [80]. The cell traction forces are applied to the substrate via focal adhesions, which mediate the inside-out interactions of the cytoskeleton and the surrounding matrix.

The forces generated on the cell-surface interface depend on the specific cell type and the mode of its migration (e.g., the speed, or strength of the adhesion to the substrate), as well as on the mechanical and chemical conditions of the surrounding micro-environment [81–84]. In respect to these factors, the forces can differ in the magnitude, orientation, duration, or spatial distribution. For example, it was observed that in anchorage-dependent cells, such as fibroblasts or epithelial cells, the sites of the active force generation are the adhesions on the cell leading edge [85–87]; whereas in high-speed moving cells (e.g., *Dictyostelium*, neutrophils, or fish keratocytes), which are less dependent on adhesion, and their propulsion is driven by the actomyosin contraction of the cortical cytoskeleton, the propulsive forces are localised at the cell rear respective to the direction of the migration [80, 88, 89].

Typically, the traction forces have been analysed in cells moving through a chemically uniform environment. Except from that, Jannat *et al.* investigated the traction forces of neutrophils chemotaxing on stiff and soft substrates in chemoattractant gradients of varying steepness. They found a correlation between the force magnitude and the directional motion, but only in case of cell migration in steep gradients on stiff substrates [88]. These data indicate that the chemically induced direction of migration could affect cell forces, and that this effect depends on the mechanical properties of the environment.

Traction Force Microscopy (TFM) is an imaging method that enables visualisation and estimation of the forces applied on the interface of the cells and the substrate. In TFM, the cells adhere to a soft, elastomeric substrate that can be deformed in respect to the traction forces [90]. The deformations are visualised and quantified by implementing fluorescent nanobeads within the elastomer. As the cell migrates over the substrate, the applied traction forces lead to a displacement of the nanobeads (Fig 1.3); and knowing the mechanical properties of the elastomer, it is possible to recover the traction forces from the bead displacement [91]. Measuring of the forces on the cell-substrate interface helps to characterise and comprehend the migratory process.

The goal of this work is to combine a chemotaxis chamber with an elastomeric substrate decorated with covalently bound fluorescent beads, in order to characterise the traction forces generated by chemotaxing cells exposed to a long-term stable gradient of a chemoattractant. The experimental set-up, and a study of forces exerted by chemotaxing and randomly migrating keratinocytes, is presented in Chapter 6.1.

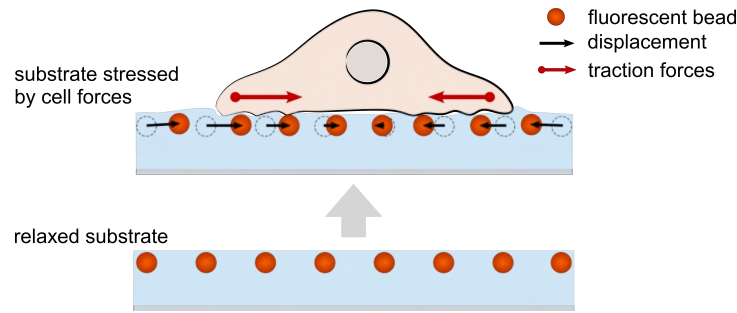


Figure 1.3: Scheme of the Traction Force Microscopy. In TFM, cells migrate over a well characterised elastic substrate (blue) with embedded fluorescent beads (in red). The traction forces generated by the migrating cells on the soft elastomer translate in a deformation of the substrate that can be quantified from the displacement of the beads by particle image velocimetry. Subsequently, based on the known mechanical properties of the elastomeric substrate and the measurement of the bead displacement, the traction forces can be estimated. In the scheme, the beads displacement is represented by the black arrows; dotted lines outline the initial position of beads in the substrate when in relaxed state.

### Light-sheet microscopy

The light-sheet fluorescence microscopy (LSFM) is a non-destructive imaging technique with a good optical sectioning capacity that enables multidimensional, high-speed visualisation of structures deep within large specimens, such as tissue samples and whole organs, embryos, and whole organisms [92–95]. LSFM uses a laser light-sheet to illuminate only a thin section of the specimen at a time. Hence, relative to other fluorescent microscopy methods, the excitation-induced phototoxic stress imposed on the cells is considerably diminished [96]. This enables observation of spatio-temporal changes on subcellular level in living multicellular specimens over long time periods. Therefore, LSFM could make an interesting tool for an in-depth investigation of the migration of slow moving cells within complex 3D micro-environments.

Since the focus of this thesis lies on the development of methods for studying chemotaxis, the challenge is to search for a suitable strategy to generate a long-term stable chemical gradient across a LSFM sample. In the light-sheet microscope, the specimen is illuminated by the light-sheet from sides; i.e., perpendicular from the direction of the detection objective (Fig 1.4). Such arrangement poses a specific challenge on the sample mounting. Typically, the sample is placed vertically in the LSFM chamber, which is filled with a water-based immersion medium (e.g., such set-up is employed in the commercially available LSFM system Lightsheet Z.1 from Zeiss). The specimen is usually embedded in a cylinder of a soft transparent 3D gel (e.g., agarose) that is extruded from a glass capillary hanging from above the chamber [92].

However, in order to sustain a chemical gradient, it will be necessary to isolate the specimen from the immersion medium in the sample chamber. It is important that the material chosen to enclose the sample matches the refractive index of water (1.335), so that the light path is not disturbed as it traverses the sample container, and the imaging quality is maintained.

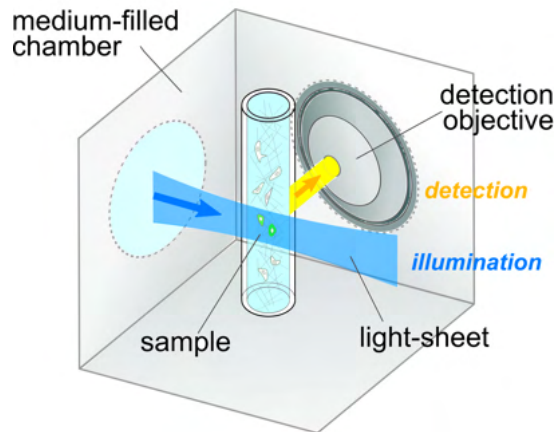


Figure 1.4: Scheme of the sample placement in a light-sheet fluorescence microscope. The sample in LSFM is situated vertically in a medium-filled chamber. A thin plane of the specimen is illuminated from sides with a laser light-sheet (direction indicated with the blue arrow), and the excited fluorescent signal is detected by a microscope objective placed orthogonally from the light-sheet (yellow arrow).

This requirement is met in the fluoropolymer fluorinated ethylene propylene (FEP),<sup>2</sup> a biocompatible plastics with the refractive index of 1.334. Tubes of FEP were used previously in LSFM to hold samples of zebra-fish embryos [95], or plant seedlings [98,99].

Therefore, in order to be able to observe the migratory behaviour of slow moving cells exposed to a long-term gradient within a 3D collagen matrix, the last goal of this work is to analyse the possibility of using a FEP tube as a container that would enable mounting such sample in the light-sheet microscope, and to establish an experimental procedure to apply a chemical gradient on the cells within the FEP tube.

The results of this work are presented in Chapter 6.2.

---

<sup>2</sup>FEP is a copolymer of tetrafluoroethylene and hexafluoropropylene, also known under the brandname Teflon<sup>®</sup> FEP [97].



## 2 Foundations

...and I must say, for my part, that no more pleasant sight has ever yet come before my eye than these many thousands of living creatures, seen all alive in a little drop of water, moving among one another, each several creature having its own proper motion.

---

— Anthony van Leeuwenhoek [100]

The ability of cell bodies to move through their environment fascinates scientists since the time of Anthony van Leeuwenhoek, who already in 1674 described his microscopic observations of the minuscule objects (which he called "animalcules") moving in a drop of water [100, 101]. Chemically directed migration—*chemotaxis*—as an object of scientific scrutiny can be traced back to late 19<sup>th</sup> century to the investigations of bacterial behaviour by W. Pfeffer and T. W. Engelmann,<sup>1</sup> or the discoveries of the nobelist I. I. Mechnikov, who described chemotaxis as the first step of the phagocytosis of a pathogen [104]. Chemotaxis is a directional migratory response of an organism to a chemical stimuli applied in a concentration gradient. The response can be *positive*; i.e., directed migration along the gradient direction, towards the source of a chemical stimuli, the *chemoattractant*. Contrariwise, a bacteria escaping a phagocyte represents *negative* chemotaxis, triggered by sensing a *chemorepellent*. If a chemical agent induces non-directional migration—random walk—we talk about chemokinesis [24]. Chemotaxis is an ubiquitous biological phenomenon, present in various types of motile cells that employ diverse migration strategies: from the flagella-driven swimming of bacteria and spermatozoa [102, 105], to the coordinated crawling of the amoeba *Dictyostelium discoideum* [106], amoeboid-like locomotion of a leukocyte on the pursuit of a pathogen [107], or slow, adhesion-dependent roaming of fibroblasts or metastatic cells through the connective tissue [25].

This thesis focuses on the migration and chemotaxis of slow moving eukaryotic cells; fibroblast and epithelial cells in particular. The migration mechanisms of fast moving cells such as bacteria or amoebas have already been intensively studied, basically since the light microscopy made it accessible for observations. The outburst of modern cell and molecular biology in the

---

<sup>1</sup>The physiologists W. Pfeffer and T. W. Engelmann studied the bacterial response to various stimuli, such as light, oxygen, salt, and other nutrients. Pfeffer used for the first time the term chemotaxis to describe the tendency of bacteria to move towards (or away from) diverse substances [102]. Engelmann observed the positive chemotaxis of bacteria towards oxygen and their attraction to algae chloroplasts, and deduced that it is the locus of oxygen production. Engelmann also utilised the aerotactic bacterial behaviour in experiments that revealed the action spectrum of photosynthesis [103].

---

second half of the 20<sup>th</sup> century led to development of novel imaging techniques and cell culture methods that facilitated the investigation of a broader spectrum of cell types, including cells that move at considerably slower rates. With the time, accumulating scientific data have provided numerous proofs of the importance of chemotaxis of slow moving cells in critical physiological and pathological processes, including wound healing and tumour metastasis [25, 30]. The recognition of the clinical relevance of chemotaxis in turn led to development of novel methods and tools for studying cell migratory behaviour [39–41]. The evolution of chemotaxis assays is summarised in Chapter 2.3. However, before addressing the chemotactic behaviour and the means of its investigation, it is first necessary to introduce the basic machinery of cell locomotion (Chapter 2.1). Chapter 2.2 then reviews the current understandings of how the external chemical stimuli influence the course of a migrating cell, and what are the mechanisms that mediate the chemotactic response. Finally, the basic principles of micro-patterning and micro-structuring techniques are described in Chapter 2.4, as these methods were employed in the process of development of the novel chemotaxis assay in this thesis.

## 2.1 Cell in motion

Indispensable for the motility of eukaryotic cells is the cytoskeleton, the micro-scaled parallel to the human musculoskeletal system. The cytoskeleton is a protein-based meshwork of filaments and tubules that provides a structural basis of cell body, organises its intracellular contents, and mediates cell motility [108]. It is formed by three types of filaments: thin and dynamic microfilaments (actin filaments); thick and firm microtubules, and flexible, cell type-specific intermediate filaments.<sup>2</sup>

### 2.1.1 Actin cytoskeleton drives cell migration

The cytoskeletal filaments are interconnected by numerous accessory proteins with one another and with other cellular compartments [108]. The microfilaments, attached to the cytoplasmic membrane, are responsible for moving the cell surface; whereas microtubules organise the intracellular movements, such as transport of molecules between organelles, cytokinesis, or endocytosis. Intermediate filaments are formed from a variety of proteins, depending on the cell type, and their function is mostly structural. From the three interconnected systems, it is the actin cytoskeleton that plays the central role in the processes that underlie cell migration [110].

Actin filaments (AF) localised in the cytoplasm are arranged by cross-linking proteins into bundles and meshes that form different AF subcompartments [108, 110]. A dense meshwork of cortical actin underlays the plasma membrane. Contractile actin bundles, called arcs, and stress fibres are strung across the cell body (Fig 2.2). Stress fibres are connected to the membrane via

---

<sup>2</sup>Although the three highly conserved cytoskeletal filaments are unique to eukaryotic cells, homologue filamentous proteins were found in prokaryota; e.g., the tubulin-related protein FtsZ, or the actin ortholog MreB [109].



clusters of proteins—focal adhesions (FAs). FAs mediate the contact of the cytoskeleton and the extracellular matrix (ECM) through the membrane-bound ECM receptors, integrins. FAs have not only a structural function, but serve also as important signalling nodes, transducing chemical as well as mechanical stimuli between the cytoskeleton and the ECM [111–113].

### Actin assembly by treadmilling

Microfilaments are formed by polarised assembly of globular actin monomers (termed G-actin) on the account of adenosine triphosphate (ATP) hydrolysis. Actin subunits have a binding cleft for the nucleotide. Following the assembly of the filamentous actin polymer (F-actin), the actin-bound ATP is hydrolysed, and the  $\gamma$ -phosphate slowly dissociates. Therefore, the subunits in the F-actin polymer bind adenosine diphosphate (ADP), except for a few subunits at the growing end (Fig 2.1). The actin-bound nucleotide significantly affects the assembly rate of the monomers: although the polymerisation of both ATP-actin and ADP-actin occurs spontaneously *in vitro*, the critical polymerisation concentration of ATP-actin is notably lower than the one of ADP-actin [114]. In result, the F-actin assembly is faster on one end of the fibre (the +, or “barbed” end), where new monomers of ATP-actin are added, and the subsequent ATP hydrolysis leads to disassembly of the ADP-subunits on the other, “pointed” (–) end. The filaments are in the state of dynamic instability: continuously growing at the barbed end and depolymerizing on the pointed end, which at the end results in a net forward displacement of the filament. This process—“treadmilling”—plays an important role in generating the

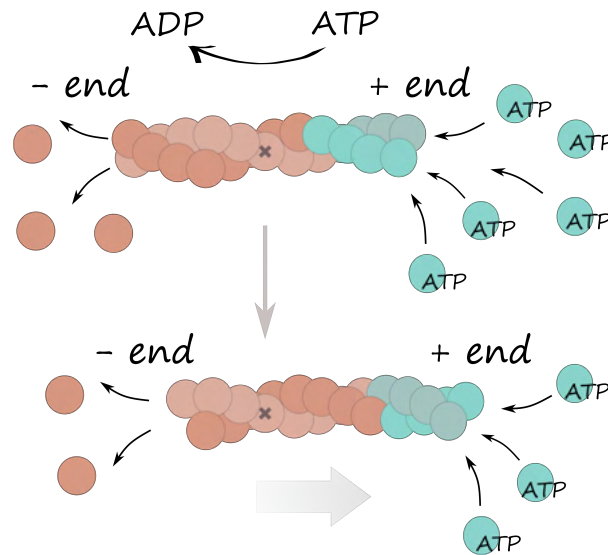


Figure 2.1: Actin treadmilling. Microfilaments consist of two helical strands of actin subunits. ATP-actin (in green) assembles at the + end of the F-actin filament. The polymerisation is followed by ATP hydrolysis; therefore, except for an “ATP cap” at the + end, F-actin is formed of ADP-binding subunits (orange). F-actin depolymerise at the - end. The treadmilling results in overall forward motion of the filament that drives the protrusion of cell membrane at the leading edge.

---

protrusive forces crucial for forward motion of the cell [115].

The dynamic state of actin filaments enables fast and spatially localised control over its polymerisation, in reaction to incoming stimuli. The assembly and remodelling of actin cytoskeleton is extensively regulated by numerous accessory proteins, that control and alternate the kinetic and localisation of actin polymerisation in the cell [116]. For example, profilin stimulates addition of actin monomers to the filament and promotes nucleotide exchange of ADP for ATP in G-actin; thymosin sequesters the soluble monomers, thus preventing the polymerisation; cofilin severs the filaments and promotes F-actin dissociation; capping proteins stabilise the filament ends. Nucleation proteins initiate AF polymerisation: protein complex Arp2/3 is responsible for nucleation of the new “branches” of F-actin from pre-existing filaments, and formins nucleate new, unbranched polymers [117]. The activity and localisation of the regulation proteins, and therefore the remodelling of the cytoskeleton in the whole cell, is coordinated and orchestrated by small G proteins of the Rho family [2].

### Rho GTPases as regulators of the actin cytoskeleton

The Rho family of small guanosine triphosphate (GTP)-binding proteins (GTPases) plays a central role in the coordination of processes that lead to cell migration. Rho GTPases are small proteins that work as a molecular signalling switch: when binding GTP, the protein is in an active conformation and interacts with its downstream effector proteins, while hydrolysis of GTP leads to deactivation, and the signalling pathway is “switched off”. The activity of the GTPases is controlled by three groups of proteins: (1) GTPase activating proteins (GAPs) catalyse GTP hydrolysis, and thus inactivate the GTPase signalling. (2) Guanosine nucleotide exchange factors (GEFs) activate GTPases by inducing the release of GDP (guanosine diphosphate) from the inactive protein and binding of a new GTP. Most of the Rho GTPases are prenylated and anchored in the cytoplasmic membrane, where they locally activate their downstream targets and interact with the regulatory proteins. (3) Guanine nucleotide dissociation inhibitors (GDIs) block the isoprenyl anchor, thus preventing GTPase localisation at the membrane and signal transduction. In every cell, there are numerous GEFs, GAPs and GDIs that are recruited in response to diverse extracellular stimuli. Upon activation of a signalling pathway downstream of the respective surface receptor, the GTPase regulating proteins are brought to the proximity of the membrane, where they interact with the GTPase [118, 119].

Rac1, RhoA, and Cdc42 belong to the most highly conserved and best studied GTPases of the Rho family, each of them playing a specific role in cell migration [120–122]. In general, Rac1 is associated with lamellipodia formation, Cdc42 with filopodia protrusion, and RhoA with actomyosin contraction. Among the downstream effectors are various proteins responsible for regulating the actomyosin cytoskeleton and other migration related processes, such as formation of adhesion complexes [2, 118, 123]. For example, Rac1 and Cdc42 stimulate WASP/WAVE proteins that activate the Arp2/3 nucleation factor; and RhoA activates the ROCK kinase, which controls the phosphorylation of myosin light-chain (MLC), important for the activity of

the motor protein myosin II and the contractility of stress fibres.

### 2.1.2 Cell migration over 2D surfaces

Continuous remodelling of the actin cytoskeleton, adhesion to the substrate, and force generation are the key processes that drive cell locomotion. The mechanism of cell migration can be described as a repeating cycle of four steps (Fig 2.2): 1) polarisation of the cell body and its protrusion on the cell front; 2) adhesion of the cell front to the substrate; 3) contraction of the cell body and its movement forward; and finally 4) release and retraction of the rear end [1, 5].

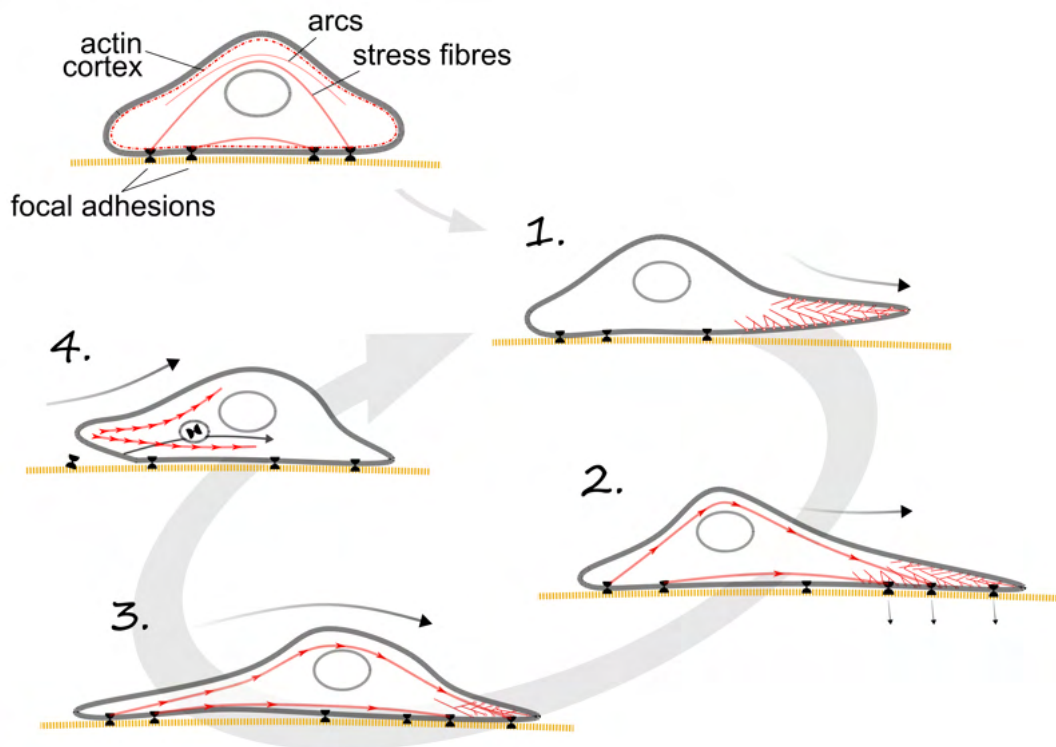


Figure 2.2: Cell migration along 2D substrate. In upper left corner, scheme of actin subcompartments in a sessile, non-polarised cell. Migration cycle: 1. Polarisation: polymerisation of new barbed ends at the leading edge generates protrusive forces that pushes the membrane forward, forming a lamellipodium. 2. The protrusion of the cell front is stabilised by adhesion to the substrate. Traction is built up across the cell body. 3. Cell body and nucleus move forward by contraction of stress fibres. 4. Retraction of cell rear. Integrin-based adhesions are recycled by endocytosis, or left behind, bound to the substrate. Actin cytoskeleton is figured in red. Arrows indicate the direction of traction and/or movement.

- 
1. During polarisation, the cell body forms a morphologically distinguishable cell front (“the leading edge”) and a rear end, following changes in distribution of F-actin, membrane-bound receptors, Rho GTPases and other signalling molecules [107]. The process can be triggered by sensing a directional extracellular stimulus, such as a soluble, or substrate-bound chemical gradient. However, cell polarisation can be as well completely intrinsic, or prompted by a short local fluctuation of an otherwise uniformly present chemical agent (chemokinesis) [124].

The polarity is sustained by Rac1 and RhoA GTPases. Active Rac1 localise at the cell front, whereas RhoA activity is limited to the cell rear. RhoA and Rac1 maintain this distribution by suppressing each other’s activity [125,126]. Rac1 at the cell front stimulates membrane ruffling and formation of protrusions: planar lamellipodia, or elongated, cylindrical filopodia. The protrusions are rich in actin filaments that are in filopodia organised in thick parallel bundles. In lamellipodia, new actin filaments are nucleated in 45° angle on the pre-existing ones, thus building up a planar web of barbed ends. Crucial molecule responsible for the nucleation of novel actin fibres in the lamellipodia is the Arp2/3 complex, activated by Rac1 and Cdc42 signalling [120,121]. Actin polymerisation in the polarised cell is localised at the leading edge, with the barbed ends of the filaments facing the membrane [127]. The nucleation and outgrowth of new filaments generate the propulsive forces needed for the forward motion of the cell [80,116].

2. The protruding membrane adheres to the surface. Binding of the integrin receptors to the substrate ligands stimulates formation of early focal contacts and activation of Rho dependent signalling pathways [122,128]. The adhesions convert the protrusion into forward cell movement. As the cell body slides over them, the adhesions subsequently travel backwards (in relation to the cell centre), towards the cell rear, and grow into mature focal adhesions.
3. As the cell front protrudes and adheres to the substrate, a gradient of binding and traction forces is formed across the cell [129]. In result, the cell body and the nucleus are pulled forward. The increasing traction forces are mediated along the cell through the actin stress fibres. The FAs stay in contact with the substrate the whole time. An important role in establishing an effective traction plays the actin-related motor protein, myosin II. Bundles of myosin interact with the actin filaments and—in the same manner as during a muscle contraction—cause contraction and shortening of stress fibres [130]. The actomyosin contraction is controlled by the Rho-ROCK signalling pathway [131,132].
4. Finally, the cell contraction leads to disassembly of the mature FAs, de-adhesion of the cell rear from the substrate, and retraction of the cell tail. The integrins are either ripped out of the membrane, remaining on the substrate; or dissociate from their ligands, are internalised by endocytosis, and trafficked through the cytoplasm back to the cell front to be recycled.

---

The model described here is based on *in vitro* migration of fibroblasts; i.e., strongly adherent cells, across a 2D substrate. *In vivo*, cells migrate in a complex 3D environment, and the migratory strategy of each cell type varies according to its function and localisation in the body. It is evident that the locomotion in 2D is dependent on cell adhesion—or more specifically, on the balance between the adhesion and subsequent detachment from the substrate. The strength of the adhesion determines the rate of migration—too strong attachment can slow down the cell, or anchor it on the spot [133]. Contrariwise, some chemokines activate cell motility by means of weakening the adhesions [134, 135]. In general, fibroblast-like cells move at the rate of tens  $\mu\text{m}$  per hour; while cells with weaker adhesions, such as amoebas or leukocytes, migrate 10x–60x faster, advancing at several  $\mu\text{m}/\text{min}$  [80]. The next chapter will show that in the 3D matrix, some cells adopt a migration strategy that is independent on focal adhesions. Still, the basic principles demonstrated in the model are valid in both 2D and 3D in a wide spectrum of cell types.

### 2.1.3 Cell migration in 3D environment

*In vivo*, migrating cells encounter a 3D environment that differs in many aspects from the 2D conditions *in vitro* [129]. The extracellular matrix is formed by the basal membrane and a gel-like interstitial matrix composed of cell-secreted fibrous proteins; e.g., collagen and fibronectin, glykoproteins and proteoglycans [136]. The exact composition and structure of the ECM depends on the type and function of the connective tissue, and its cell constitution. Numerous signalling and adhesive molecules are present, soluble or bound to the ECM—provided to the cell in much higher density and variety than in 2D. ECM surrounds the cell with a complex landscape of biochemical and biophysical signals that affect not only its migratory behaviour, but also its growth, differentiation and survival [9, 137]. The meshwork of collagen fibres represents a substrate orders of magnitude softer than the plastic surface of a culture dish, which has impact on the cellular forces and cell morphology [82, 138]. Unlike in 2D, the cells in 3D have to deal with the matrix rigidity in order to overcome mechanical barriers as they move through the tissue,<sup>3</sup> and they choose different strategies how to do so.

#### Mesenchymal and amoeboid mode of migration

The migration strategies employed by cells in 3D alter in the dependency on integrin-mediated adhesions and proteolytic ECM degradation [6]. The slow moving, mesenchymal-like cells overcome the spatial barriers of the 3D environment by rebuilding the surrounding matrix and tunnelling its way through; whereas the fast moving, amoeboid-like cells dynamically adapt their morphology and squeeze through the pores in the ECM.

---

<sup>3</sup>Cells migrating on a 2D substrate have to face the viscous drag of the liquid medium; however the forces needed to overcome the viscous resistance are negligible [101, 139].

---

1. Integrin-dependent, mesenchymal migration:

Fibroblasts, endothelial cells, and many types of cancer cells utilise membrane-bound and secreted matrix metalloproteinases (MMPs) to cleave the ECM proteins. Mesenchymal-like migration is dependent on integrin-mediated interaction with the ECM. The cells move along the ECM fibres in a manner corresponding to the mechanism of 2D migration described sooner, with the addition of a step reflecting the matrix degradation at the leading edge that follows cell protrusion and adhesion [13, 140]. Mesenchymal cells are large, with a prolonged and spindle-shaped morphology that is given by the traction forces of the adhesions at the cell front and rear. The interaction with the ECM and activation of integrin signalling is necessary for generating the traction forces, and stimulates the expression of MMPs. By digesting and remodelling the ECM, the cells create passages through which they move forward [6]. Integrin-dependent migration is relatively slow, with the rate of approximately one cell length (ca. 50  $\mu\text{m}$ ) per hour. The direction of cell migration can be biased by the orientation of the collagen fibres due to the contact guidance—i.e., cell tendency to migrate along mechanical structures [141, 142].<sup>4</sup> The distribution of the adhesion sites in the ECM determines the course of the migration (cells can only walk along existing fibres); therefore, the locomotion is less persistent and more diffusive than the migration of amoeboid cells [144].

2. Integrin-independent, amoeboid migration:

Leukocytes and other amoeboid-like cells move through the tissues in a focal adhesion-independent manner. Instead of degradation of the surrounding matrix, they push the ECM and squeeze through the pores between the collagen fibres. In this way, they can move fast (at the speed of tens of  $\mu\text{m}/\text{min}$ ) directly towards their destination. However, the movement is limited by the density of the ECM—the meshwork pores have to be large enough to allow the nucleus to pass through [15]. In comparison to mesenchymal cells, amoeboid cells are small and rounded. Their locomotion is based on cyclic extension of pseudopods and retraction, driven by cytoplasmic streaming and constriction of the actomyosin cortex, controlled by the Rho-ROCK signalling pathway [123, 140, 144]. Interestingly, invasive metastatic cells can gain the ability to switch from mesenchymal to amoeboid mode of migration if the MMP-mediated ECM degradation is impaired [63].

As the cells move through tissues, they are exposed to a variety of promigratory signals of biochemical or physical character. Such cues are often applied in a gradual manner, affecting the direction of cell migration. The next chapter will address the question of how the cells “sense” the gradient and what mechanisms underlie the directional response.

---

<sup>4</sup>Contact guidance affect cell migration in 2D as well; e.g., cells tend to migrate along the edge of a coverslip, or other topographical irregularities of the surface [143].

---

## 2.2 Chemotaxis: navigating cells through a chemically heterogeneous environment

A variety of external signals can stimulate cell motility and impose a preferred direction on the course of migration. Cells are able to respond to physical cues, including light (*phototaxis*), or electric and magnetic fields (*galvanotaxis*, *magnetotaxis*); mechanical properties of the environment, such as surface stiffness (*durotaxis*), or chemicals—either bound to the substrate (*haptotaxis*), or soluble (*chemotaxis*). A directional migratory response to an asymmetrically applied stimuli—*taxis*—is distinguished from a non-directional increase in motility, usually termed *kinesis*. As a cell moves through the tissues, it is steered by signal molecules, such as chemokines and growth factors that attract the cell to the site of its physiological function. It is likely that the cells migrating *in vivo* are simultaneously exposed to multiple types of cues that they have to evaluate in order to effectively reach their assigned destination (e.g., mesenchymal cells closely interacting with the ECM are subject not only to chemotaxis, but also haptotaxis and durotaxis) [33].

The process of chemotaxis comprises of three procedures: motility, polarity, and gradient sensing [145]. Cell motility is based on the continuous extension of protrusions driven by actin polymerisation, as described in Chapter 2.1. Gradient sensing biases the migration in one favoured direction which is sustained by the polarisation of the cell body. It was mentioned above that the cell polarisation can appear in reaction to, or independently from a directional external signal; and that it is maintained by a differential activity of signalling proteins and actomyosin cytoskeleton at the front and the rear of the cell. The molecular machinery at both ends of the chemotaxis process—i.e., receptor-mediated detection of the external signal, and local actin polymerisation leading to protrusion formation—is well understood, but the exact mechanism of the initial interpretation of the external gradient into the directional response is still a subject of discussions [146–148].

### 2.2.1 Molecular basis of the directional response

Gradient sensing in eukaryotic cells is spatial—the cell reacts to the relative difference in the chemoattractant concentration across its body.<sup>5</sup> The decreasing receptor occupancy from the prospective cell front to the rear is translated in an asymmetric distribution of intracellular signalling proteins [150]. In amoebas and leukocytes, the internal gradient of signalling molecules can be amplified relative to the external gradient, which enables the cells to react to shallow chemoattractant gradients [151, 152]. The signalling-centred approach dominating the field in

---

<sup>5</sup>In contrast, bacterial cells, considerably smaller than eukaryotic cells and relatively fast swimming, can only detect the changes in chemoattractant concentration over time, as they move up or down the gradient. Bacteria move by alternating series of persistent *runs* (a period of direct motion along an almost straight track) and erratic *tumbles* (a period of fast turns and changes of the course). Chemoattractants bias the otherwise random migration by prolonging the runs in the gradient direction [102, 104, 149].

---

the last decades expects the existence of an inner *chemotaxis compass*—a signal molecule that “recognises” the “correct” direction, and intrinsically steers the cell up (or down) the gradient by locally affecting actin polymerisation and prompting the outgrowth of new protrusions in the desired direction [153, 154].

The molecular basis of chemotaxis was most thoroughly studied in *Dictyostelium* and leukocytes; i.e., in fast moving cells. Although the cues that direct the motility of different cell types are unlike, and are recognised by distinct type of surface receptors, the chemotactic events trigger the same, conserved core signalling pathways [33, 148, 152]. The selective activity of the antagonistic GTPases RhoA and Rac1 at the opposing poles of the cell was already described (Chapter 2.1.1). The same polar distribution of effectors (or their activity) was observed in other pathways as well; notably, the signalling pathway of phosphatidylinositol-3,4,5-phosphate (PIP<sub>3</sub>) is considered to be the main mediator of gradient sensing [106, 155].

### Phosphoinositide pathway as the chemotaxis compass

As a guidance mechanism conserved in *Dictyostelium*, neutrophils, and fibroblasts, the PIP<sub>3</sub> signalling cascade was assigned the role of an universal chemotactic compass [150, 155]. The activation of chemoattractant receptors in all three model systems leads to the relocation of phosphoinositide 3-kinase (PI3K) towards the cell area facing the highest chemoattractant concentration. Here—at the prospective cell front—the PI3K produces the second messenger lipid, the PIP<sub>3</sub>. PIP<sub>3</sub> then recruits to the membrane a wide range of signalling proteins that contain PIP<sub>3</sub>-binding domains, such as the pleckstrin-homology (PH) domain; including regulators of Rho GTPases [151]. Thus, the local accumulation of PIP<sub>3</sub> results in a local induction of actin polymerisation and formation of a new protrusion at the newly established leading edge. The extension of protrusions in other directions is prevented by the accumulation of antagonistic signals at the cell rear and sides. In *Dictyostelium*, the PIP<sub>3</sub>-regulating phosphatase PTEN translocates to the cell rear, actively restricting the PIP<sub>3</sub> to the cell front [156]. In neutrophils, a positive feedback loop involving Rac1 GTPase induce a massive PI3K activation on the cell front [150], and the Rac1 activity is spatially controlled by RhoA activity at the cell rear and sides [126] (Fig 2.3).

### 2.2.2 Gradient sensing in slow moving cells

In contrast to the amoeboid chemotaxis, the chemically induced directed migration of slow moving cells is still poorly understood [33, 38]. Although the polar distribution of PI3K and PIP<sub>3</sub> has been observed in chemotaxing fibroblasts as well [157, 158], the dynamics and the upstream signal transduction differ in many aspects from the signalling events described in amoebas and leukocytes. These differences reflect the specific functions and migration characteristics of the respective cell types, discussed in the previous chapter (2.1.3). In fast moving cells, the asymmetric lipid distribution is established within several seconds, whereas in fi-



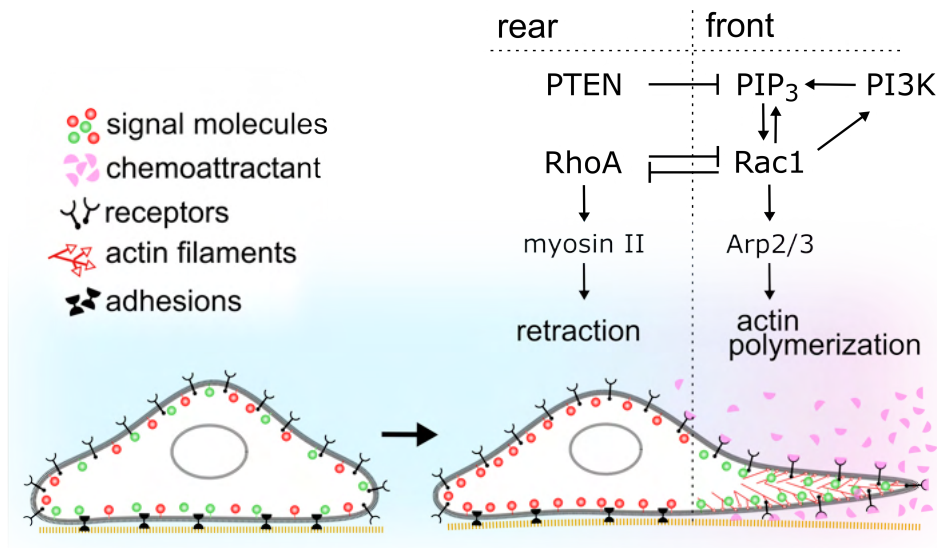


Figure 2.3: Scheme of the asymmetric activity and localisation of signal molecules in a cell sensing a gradient. Gradient sensing leads to relocation of signalling molecules in the cell—PI3K, PIP<sub>3</sub>, and active Rac1 (in green) accumulate at the cell front and induce actin polymerisation and the extension of a new protrusion. Rac1 also promotes the PI3K activity and a further production of PIP<sub>3</sub>. Activity of antagonistic PTEN and RhoA (in red) is localised at the cell rear where RhoA stimulates the activity of myosin II and the actomyosin contractility.

broblasts it takes 5-10 minutes before a steady state is reached [155]. Also, the range of the external chemoattractant gradient is not amplified internally in slow moving cells. Compared to amoebas and leukocytes, the polarisation of fibroblasts is weaker, and the cells often form multiple competing protrusions [159]. In result, the migration tracks of mesenchymal cells are more diffusive than the persistent trajectories of amoeboid cells, which tend to proceed almost directly towards the chemoattractant [33,37]. Besides, another phenomenon typical for amoeboid chemotaxis is lacking in fibroblast: the ability to adapt to a constant external signal. The adaptation enables fast moving cell to perceive the relative steepness of the gradient along the cell body (i.e., the percentage difference in the chemoattractant concentration at the cell front and rear), and thus react to a wide range of absolute chemoattractant concentration [160]. In contrast, slow moving cells are not sensitive to very shallow gradients, and their chemotactic response is more dependent on the midpoint chemoattractant concentration (i.e., the average concentration between the front and rear of the cell) [158].

The divergence in the dynamics of the same central signalling module (PIP<sub>3</sub>) in fast and slow moving cells is a result of a distinct processing of the signal upstream of PI3K [33,155]. The chemoattractants of *Dictyostelium* (cAMP) and leukocytes (chemokines released from the inflammation sites, and bacterial N-formyl peptides) activate the G-protein coupled receptors (GPCR); whereas the molecules with a chemoattractant activity towards mesenchymal cells are typically growth factors (e.g., the platelet-derived growth factor (PDGF) attracts fibro-

---

last into wounded tissues) that are recognised by the receptors of the receptor tyrosine kinase (RTK) class. GPCR signal transduction is fast, mediated by the dissociation of the intracellular receptor subunits  $G_\alpha$  and  $G_{\beta/\gamma}$ , which directly interact with the downstream targets. Typical for GPCR signalling is desensitisation and rapid attenuation of the response when continuously exposed to the signal (i.e., adaptation). RTK-mediated signal transmission is based on phosphorylation of many intracellular substrates, translocation of proteins to the membrane, and formation of signalling protein clusters. Usually, it takes several steps to activate the downstream effector [161]. Besides, the downregulation of RTKs, being dependent on endocytosis and ubiquitin-proteasome pathways, is relatively slow [162].

### 2.2.3 Problems with the compass: an alternative view on chemotaxis

The thorough research of directed migration in amoeboid cells uncovered numerous players involved in the chemotaxis-related signalling [148]. The identification of multiple redundant signalling pathways and complex negative and positive feedback loops that participate in the process complicated the initially simple and elegant concept of the universal internal chemotaxis compass. Besides, some experiments of the last decade directly challenged the  $PIP_3$  compass model, showing that neither PI3K, nor Rho GTPases, and not even the Arp2/3 complex are essential for cells to effectively sense and react to the gradient, even though the motility is defective in absence of these molecules [163–165]. Other data also show that the temporal course of the intracellular signalling events contradicts the expected model. It was measured in mesenchymal cells that the asymmetric localisation of PI3K and Rac1 activity is established after, not before the formation of the leading edge; thus rather stabilizing than initiating the protrusion [126, 166, 167]. The signalling module responsible for the initial interpretation of the receptor-mediated gradient sensing remains elusive.

#### Pseudopod-centred chemotaxis model

Since the experimental data do not completely support the signalling-centred model of chemotaxis driven by an internal compass, alternative concepts of chemotactic behaviour were proposed [35, 168]. For example, the pseudopod-centred<sup>6</sup> model offers an alternative, more probabilistic conceptual approach to chemotaxis, suggesting that the directional response is a result of a gradient-introduced bias of the otherwise random outgrowth of cell protrusions (pseudopods). The chemotactic-compass model expects an internally prompted repolarisation of the cell, followed by the formation of a new protrusion in the direction of the chemoattractant signal. The chemotactic-bias model again proposes that the protrusions are formed spontaneously all around the cell surface, and the external gradient leads to stabilisation and favoured outgrowth of the pseudopods pointing towards the chemoattractant [147, 168, 169]. Thus, the

---

<sup>6</sup>Pseudopod is a general term for a membrane protrusion; i.e., lamellipodia and filopodia. However, it is usually used in relation to amoeboid cells.

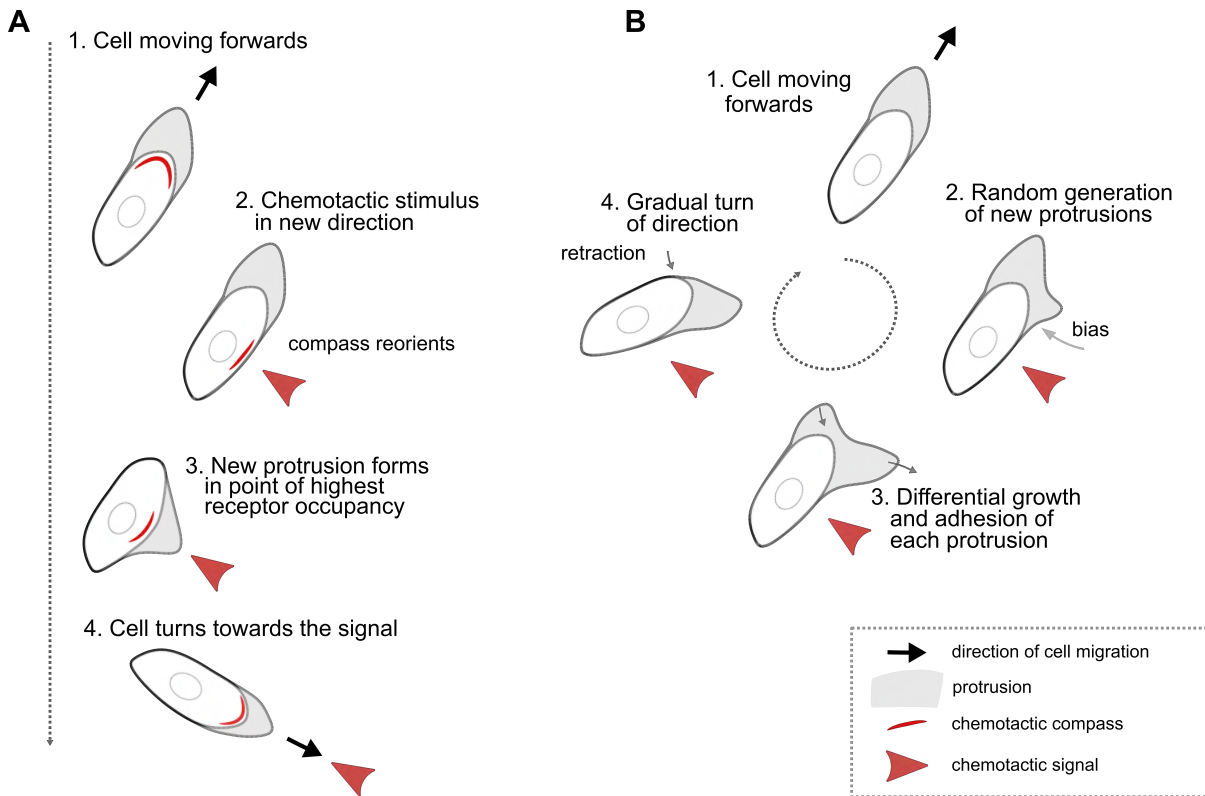


Figure 2.4: **A.** Chemotaxis compass model. Sensing of a chemotactic stimuli leads to repolarisation of the migrating cell, and to an internally induced formation of a new protrusion in the gradient direction. **B.** Pseudopod-centred model of chemotaxis. Chemoattractant gradient bias the migration course by differential stabilisation of the randomly formed protrusions. Growth of protrusions heading toward the increasing chemoattractant concentration results in gradual turn of the cell. Figure adapted from [147] by permission from Springer Nature.

reaction of the cell to a sudden change in the gradient direction is not immediate; instead, the cell would change its course gradually in small turns, until finally persisting the migration in the “correct” direction (Fig 2.4). Such behaviour was indeed observed in amoeboid cells in reaction to shallow gradients [170], while an immediate cell reorientation in accord to the compass model is more typical in very steep gradients [171].

Directed migration is a complex process involving multiple well-coordinated cellular procedures. Several decades of intensive research helped to shed light on the central mechanisms of cell motility, and elucidated the role of many signalling molecules involved in the chemotaxis machinery. However, side by side with the increasing understanding of the chemotactic behaviour, new questions and problems arise that remain to be investigated and answered. For that purpose, advanced experimental methods are applied, and novel tools and assays for studying chemotaxis are continuously being developed.

---

## 2.3 The evolution of chemotaxis assays

The increasing understanding of chemotaxis and the recognition of its importance in vital biological processes fuel the evolution of *in vitro* chemotaxis assays. Specific experimental requirements that arise along with the research, such as better optical accessibility, increased stability of the gradient, improved controllability of the assay parameters, or a closer approximation to the physiological conditions constantly generate the need for development of novel investigation tools and assays.

### 2.3.1 Gradient generation in chemotaxis assays

Formation of a chemical gradient is in most of the chemotaxis assays based on diffusion between two reservoirs filled with chemoattractant solutions—the “source” reservoir containing the maximal chemoattractant concentration, and the “sink” reservoir filled with a solution of a lower concentration, or with a chemoattractant-free solvent (Fig 2.5).

In an idealised case of infinitely large reservoirs (i.e., never-depleted source, and a perfectly absorbing sink), a lasting stable gradient would be established after a transient period of gradient formation [172]. The time necessary for the gradient formation is determined by the diffusion coefficient of the molecule, and the length of the gradient area. In general, the diffusion coefficient correlates with the size, shape and molecular weight of the molecule [173]; therefore, it will take longer for a gradient of larger molecules to reach the stable state. However, in practice the volumes of the source and the sink are finite; thus, the concentrations in the reservoirs equilibrate with time. As the difference in concentrations between the reservoirs decreases, the gradient starts to decay. The duration of the period of the gradient stability and constant shape is determined by the volume of the reservoirs, as well as by the proportions of the gradient area [172].

The source and sink are arranged in various ways in the different assays, and the specific geometry and proportions of the chemotaxis chambers define the stability and shape of the gradient. In one of the simplest experimental set-ups, the source is represented by a pipette containing chemoattractant solution, submerged in the medium of a cell culture vessel (sink) [174]. On the other spectrum of chemotaxis assays are elaborate microfluidic devices developed in the last decade, with miniaturised chamber dimensions, and gradients formed by diffusion between two continuous flow streams that substitute for the source and sink reservoirs.

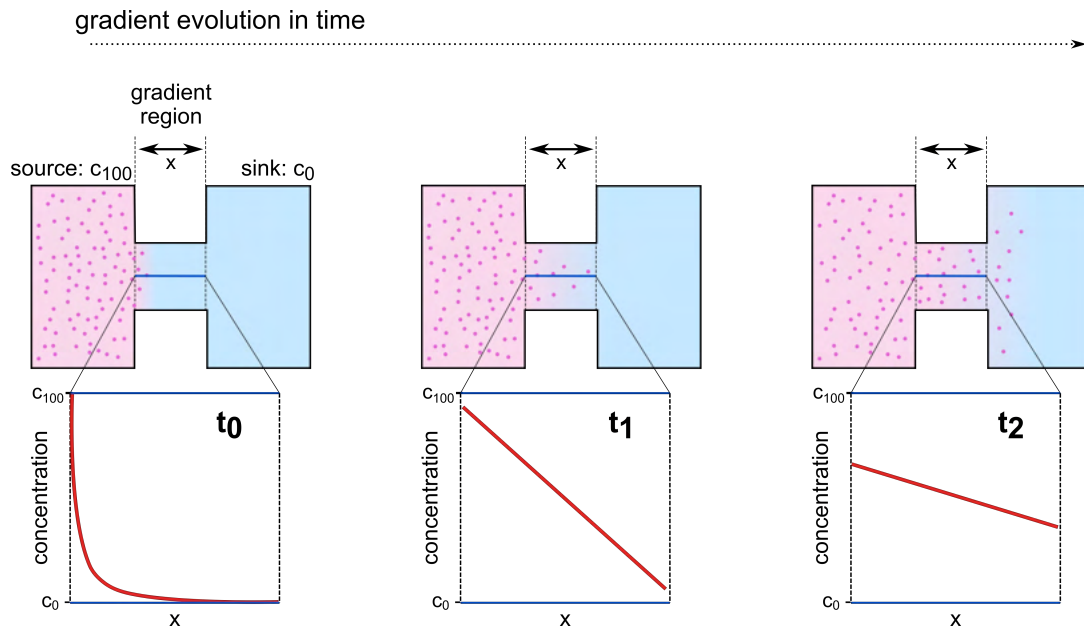


Figure 2.5: Evolution of a diffusion-based gradient. A stable linear gradient is formed in the region between a reservoir filled with a chemoattractant solution (source, pink), and a reservoir filled with a chemoattractant-free solvent (sink, blue). Gradient evolution: an initial period when the gradient is formed between the reservoirs ( $t_0$ ) is followed by a period of a relative stability ( $t_1$ ), until the source becomes depleted and the concentration of the solute in the sink raises, and the gradient decays ( $t_2$ ). The red curves represent the concentration profile of the chemoattractant in the gradient region.

### 2.3.2 Standard chemotaxis assays

Some of the most widely used migration assays originate in the 1960's - 1970's; e.g., the Boyden chamber [175], the micropipette assay [174], or the under-agarose assay [176]. The initial chemotaxis assays generated gradients in static conditions, i.e., without flow stream; and in most cases provided only poorly controllable and unreproducible, short-lived gradients. Therefore, such assays are mostly used for investigation of migratory response of fast moving cells, such as protozoa, *Dictyostelium*, or leukocytes.

#### Micropipette assay

A micropipette releasing a guidance cue into a free medium in a culture vessel represents a simple point-source gradient generator (Fig 2.6). The micropipette chemotaxis assay enables rapid application of chemicals and direct observation of the single-cell response. In the early experimental designs, the gradient formation relied on simple diffusion of the chemoattractant from the pipette tip [174]. Later, more elaborate modifications evolved in more precise, thin micropipettes mounted on micro-manipulators, equipped with pneumatically driven release of chemoattractant; so that the stimulus could be delivered in a small volume at a defined distance from the observed cell [151,177,178]. However, the diffusion of the chemoattractant into the free

---

medium is during the course of the experiment being disturbed by the convective currents in the medium vessel and it is difficult to accurately determine the parameters of the gradient [177]. Therefore, the gradients are only short-lived, poorly controllable, and not reproducible. Another disadvantage of the assay is its low-throughput, since only the cells in the vicinity of the tip of the pipette are exposed to the gradient. The assay is best suited for an in-depth investigation of the single-cell migratory behaviour of fast moving cells, typically bacteria or amoebas, which react promptly to sudden changes in stimulus direction [151, 174].

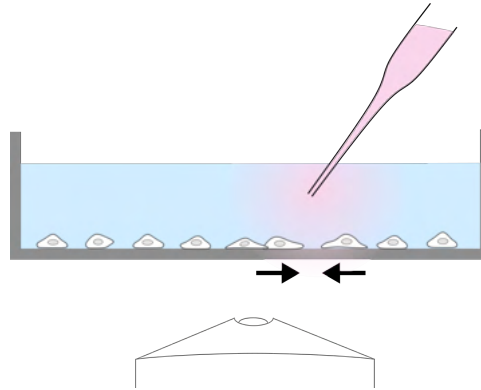


Figure 2.6: Scheme of micropipette chemotaxis assay. Chemoattractant dissolves from a micropipette tip submerged in the medium in a culture dish. Black arrows indicate the direction of the migration of the chemotaxing cells.

### Hydrogel-based assays

Another group of chemotactic assays is based on the diffusion of a chemoattractant through biocompatible hydrogels, mostly agarose, but also collagen, or fibrin [172, 176, 179–182]. Originally, the cells in the under-agarose assay were seeded in one of two wells cut out of an agarose layer in a culture dish. The other well was filled with chemoattractant solution, and as the substance started diffusing through the gel, cells became exposed to the evolving gradient and started to migrate over the surface of the culture dish, under the agarose [176]. The migration and the chemotactic response could be directly observed. In later modifications of the assay, the cells could be mixed directly into the gel matrix (using collagen or other matrices that enable cell migration), and the chemoattractant is applied in a more defined manner; e.g., by printing of small volume drops of varying chemoattractant concentration on the top of the gel [172, 180, 183]. The preparation and evaluation of the assay is usually very simple; the cell displacement from the seeding well toward the chemoattractant can be evaluated even by naked eye.

In contrast to the micropipette assay, the hydrogel assays are mostly suited for observation of collective cell behaviour, since the 3D system complicates detailed cell visualisation and cell tracking. The main advantage of the assay is the possibility to expose the cells to combinatorial gradients of multiple factors at once (i.e., by introduction of multiple source wells), which is

---

closely relevant to the *in vivo* conditions. However, the diffusion in the gel and the nature of the gradients is defined by the gel micro-architecture, thus the reproducibility of the assay is poor. Besides, the gradients is unstable and not controllable. Another disadvantage is the low-throughput of the experiment.

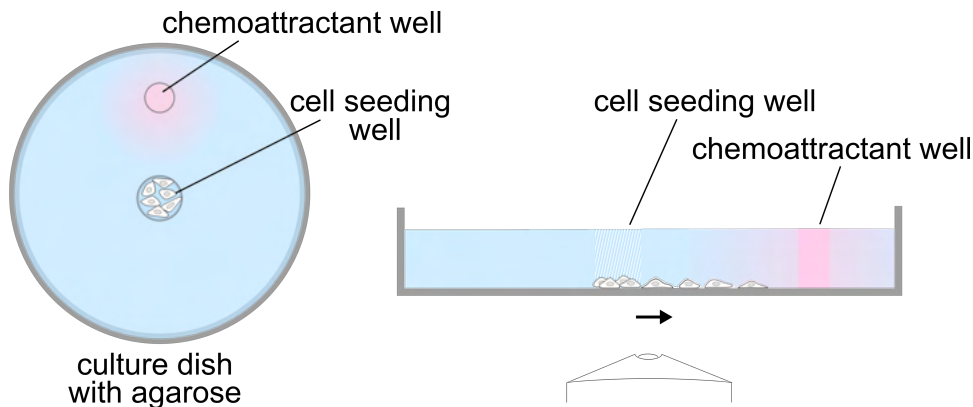


Figure 2.7: Scheme of the under-agarose chemotaxis assay. Two wells are cut in a layer of agarose in a culture dish. The cells are seeded in one well, and the other is filled with the chemoattractant solution. As the chemoattractant diffuses into the gel, cells sense the gradient and migrate along the 2D dish surface towards the stimulus (direction of the chemotactic response is indicated by the arrow). The cell migration can be directly observed with an inverted microscope.

### Boyden chamber assay

In contrast to the previously described methods, experiments in the Boyden chamber assay can be easily parallellised; and the assay became widely adopted by the research community for its ease of use and fast and simple evaluation. Together with the related transwell assay, the Boyden chamber remains until present days one of the most used migration assays and is often used for investigation of chemotaxis. The Boyden chamber was designed as a population-based migration assay in 1962 [175]. Its design is based on a two well system—the lower well is filled with a chemoattractant solution and the upper well, whose bottom is formed by a permeable membrane, contains the cell suspension (Fig 2.8). The diameter of the pores of the membrane is in scale of several  $\mu\text{m}$  (typically 3-12  $\mu\text{m}$ , depending on the cell type under study), i.e., smaller than the cell bodies; thus, in order to cross from one well to another, the cells have to actively squeeze through the pores. As the chemoattractant diffuses through the membrane, a short-term gradient is formed, and the cells migrate through the pores into the lower well. At the end-point of the experiment, the cells that migrated through the membrane are fixed, stained and counted [175]. However, the gradient formed between the wells is steep and undefined, and varies over time and space. Besides, the cell behaviour cannot be optically controlled during the course of the experiment; therefore, the mechanisms of cell migration cannot be further characterised. Comparative studies showed that relative to direct-viewing migration assays,

---

the sensitivity and precision of the Boyden chamber assay is limited [42]. Furthermore, it is not possible to discern, whether the increased migration through the membrane resulted from an overall stimulation of the cell motility; i.e., chemokinesis, or from the actual directed migration towards the chemical agent. Several modifications were presented to optimise the system for chemotaxis studies; e.g., the “checkerboard assay”, that relies on comparison of the cell response to a gradient and to an uniform concentration of the chemokinetic agent [36]. However, such approach is also not completely reliable [184]. The Boyden chamber/transwell assay is a helpful tool to evaluate the migratory response of cells in multiple parallel chemical conditions; however, the observed effect cannot be correlated with the gradient characteristics [182]. Moreover, the steep and short-lived gradients make the assay unsuitable for studying chemotaxis of slow moving cells [33, 38, 39].

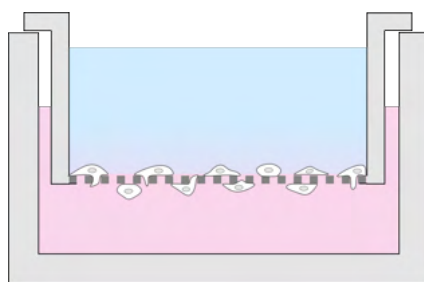


Figure 2.8: Scheme of Boyden chamber/transwell assay. The cells in the Boyden chamber/transwell are placed on a porous membrane between two wells. To cross the membrane, cells have to actively migrate through the pores. The lower well is filled with the chemoattractant solution and a short-term gradient is formed at the membrane. In response to sensing the chemoattractant, cells migrate to the lower reservoir.

### Bridge assays

The necessity of an in-depth characterisation of the chemotactic response on cellular and sub-cellular level led to the development of chemotaxis assays that enable direct observation and real-time tracking of cell migration and at the same time provide a well-defined, controllable chemical gradient. First of such assays was the Zigmond chemotaxis chamber [40]. The assay consists of a glass slide, in which two parallel channels are etched, representing the source and sink reservoirs. The channels are filled with chemoattractant solutions of different concentrations, and overlaid with a coverslip, on which the studied cells are seeded. The glass slide and the coverslip are assembled so that a 3-10  $\mu\text{m}$  high and 1 mm wide gap is formed between the coverslip and the ridge that separates the reservoirs (Fig 2.9). The cells migrating in this “bridge” area are exposed to a linear and relatively stable gradient that is formed between the reservoirs, as described in Chapter 2.3.1. The cell behaviour can be visualised in real time and the chemotactic response is evaluated based on the analysis of cell trajectories [40]. The gradient generated over the bridge is predictable and well-defined. However, the assay was



---

developed for leukocytes, and the short life span of the gradient (approximately 1 h) limits the use to fast moving cells.

The stability of the gradient in the Zigmond chamber suffers from high evaporation in the system [182]. This problem is addressed by the Dunn assay [185] that also exploits the bridge design to generate the gradient, but the reservoirs are arranged as two concentric circular wells (Fig 2.9B). Therefore, the cell-bearing coverslip that overlays the chamber completely seals the reservoirs, thus reducing the evaporation and improving the stability of the gradient. Yet, the stable state of the gradient is maintained only over several hours. Also, the radically symmetric design complicates the evaluation of the experiment, since the cells need to be tracked using the polar instead of cartesian coordinates [182].

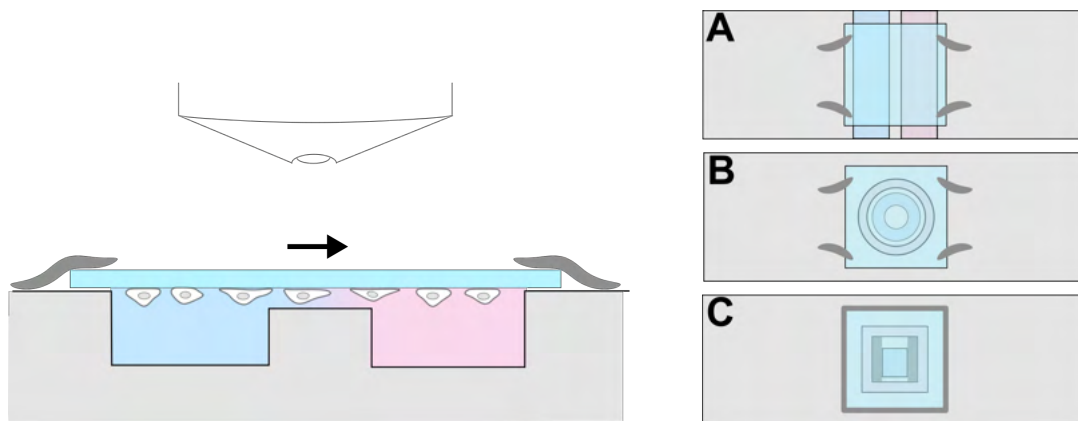


Figure 2.9: Scheme of bridge assays. In the Zigmond chamber (A), and its derivatives, the Dunn chamber (B), and the Insall chamber (C), cells seeded on a glass coverslip are exposed to a linear gradient that is formed across a “bridge” that connects two wells filled with differential concentrations of the chemoattractant. The arrow indicates the direction of chemotaxing cells.

Yet another modification of the Zigmond and Dunn chambers is the Insall chamber, introducing further improvements, mainly by maintaining the gradient stable for longer time periods (up to 24 hours) [186]. Besides, two parallel gradients of different steepness are generated in one chamber, and the imaging quality is improved by optimising the design so that a normal thin coverslips can be used to overlay the chamber. In the Zigmond and Dunn assay, thicker glass coverslips have to be employed in order to prevent its bending in the bridge area. Nevertheless, a common disadvantage of these assays is the low throughput, resulting from the rather labour-intensive experimental procedure and the challenging handling with the chambers. Another chemotaxis assay based on the “bridge” design is the commercially available, disposable  $\mu$ -Slide Chemotaxis (ibidi, Gräfelfing, Germany), which will be described in detail in the Chapter 2.3.4.

### 2.3.3 Microfluidics-based assays

A novel and fast evolving chapter in the field of chemotaxis research represent the microfluidic gradient generators. The development of advanced biocompatible materials, micro-

fabrication techniques, and microfluidic technologies in the last decades enabled an expansion of microfluidic-based migration assays with elaborate designs that can closely mimic complex *in vivo* environments and provide problem-specific experimental platforms [187]. Microfluidics operates with low-volume chambers on the scale of micro- and nanoliters. Miniaturisation of the experiments has many advantages; for example, smaller amount of cells and chemical agents are needed, which leads to cost optimisation and facilitates examination of cells that are difficult to isolate, or cells of patient samples [188]. The invention of micro-fabrication techniques such as soft-lithography enabled uncomplicated fabrication of chambers and precisely defined micro-environments of various geometries by molding a biocompatible silicone-based elastomer, the polydimethylsiloxane (PDMS), against a master wafer [189,190].

In relation to chemotaxis research, microfluidic devices can generate well-defined, combinatorial gradients that can be precisely controlled in time and space. Methods of gradient generation and microfluidic chemotaxis assays were summarised in several review articles in the recent years [182,187,188,190–194]. Typically, the gradient in microfluidic platforms is formed by diffusion between two flow streams of chemoattractant solutions of differential concentrations. The streams and cells can flow side-by-side in one channel, or be directed in channels separated by a hydrogel [195,196], or by an array of perpendicularly arranged microchannels, through which the cells migrate towards the chemoattractant (ladder-shaped devices; Fig 2.10) [197–202]. Characteristic for fluids at the micrometer scale is laminar flow (given the low Reynolds number). Therefore, the streams in the flow-based gradient generators flow side-by-side without turbulent mixing; the gradient forming between them relies on diffusion of the attractant molecules [191]. The diffusive mixing is (as compared to the macro scale) fast [172] and the resulting gradient is well defined [187]. The absence of stochastic mixing and the well-predictable diffusion kinetic in microfluidics allows a precise control and fine tuning of the gradient profile in the chemotaxis devices [187,190].

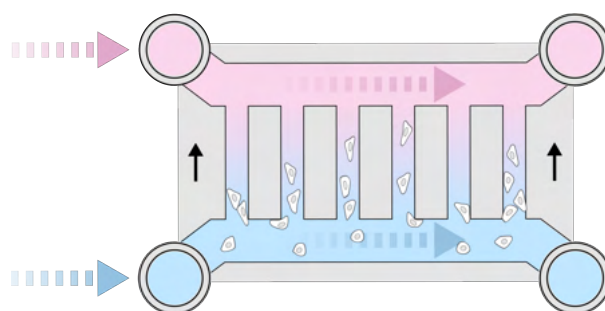


Figure 2.10: Scheme of a possible design of a microfluidic chemotaxis assay. The gradient is formed across microchannels that connect two flow streams with different concentration of chemoattractant. Cells migrate through the microchannels in the gradient area.

However, the presence of flow imposes a considerable shear stress on the cells that also affects their migration paths [203]. Studying cell chemotaxis under constant laminar flow is physiologically relevant only in the case of leukocyte transmigration from blood vessels [188].

---

Besides, specialised equipment such as a pump system and tubing is required to maintain the flow, and the application of microfluidic devices can be challenging for non-specialist users [187]. A less numerous group of microfluidic chemotaxis assays is based on designs independent of flow, generating the gradient in a stationary medium, in a similar principle to the standard assays described in Chapter 2.3.2 [39, 204–207]. Except for several microfluidic devices that were specifically designed for high-throughput studies [205, 207–209], most of the microfluidic platforms are oriented on an in-depth analysis of single-cell response. Furthermore, the set-up of the assays and manipulation with the microfluidic devices is in most cases rather difficult, yielding only low experimental throughput.

Another reason that prevents the general adoption of microfluidics in chemotaxis research is a lack of versatile, ready-to-use tools. As mentioned above, most of the microfluidic devices are designed in respect to a study-specific problem, and suited for the peculiar cell type under study. The variable conditions under which the cell migration is examined in the different microfluidic assays make it difficult to compare the results between individual studies. The several commercially available microfluidic-based chemotaxis assays are typically tailored for a specific biomedical application addressing fast moving cells [207, 210]. Exceptions from the rule are the flow-based CellDirector by Gradientech (Uppsala, Sweden) [41], and the  $\mu$ -Slide Chemotaxis (ibidi, Gräfelfing, Germany) [39], suitable for studying various cell types under static conditions.

### 2.3.4 $\mu$ -Slide Chemotaxis

The  $\mu$ -Slide Chemotaxis from the company ibidi is a disposable chemotaxis tool that conveniently combines the advantages of static and microfluidic assays. The design is based on the Zigmond chamber; i.e., bridge assays, and it operates with low volumes of chemoattractant and cell solutions. The bridge area is represented by a narrow, 70  $\mu\text{m}$  high channel that separates two symmetrical reservoirs of 65  $\mu\text{l}$  apiece (Fig 2.11A). The volume of the bridge channel at the cross-section with the reservoirs is 140 nl. Each reservoir and the middle channel have individual filling ports that are closed with specially designed plugs, so that every department can be filled independently. The cells are seeded in the middle channel, either to attach directly on the 2D surface, or embedded in a 3D matrix (e.g., collagen gel). After the cells adhere, or the matrix gelifies, respectively, the reservoirs are filled with chemoattractant solutions of different concentration and the chamber is sealed with the plugs in order to prevent convection that would disturb the gradient. A well-defined linear gradient forms across the channel within several hours and remains stable for over 48 hours [39, 211]. The longevity of the gradient makes the assay optimal also for studying chemotaxis of slow moving cells.

The cell migration in the gradient area can be visualised directly by an inverted microscope. The chemotaxis effect is assessed based on reconstruction of individual cell migration tracks (Fig 2.11B). Such analysis provides a detailed in-depth information on single-cell chemotactic behaviour. The  $\mu$ -Slide Chemotaxis assay has the form of a typical glass microscopic slide, and

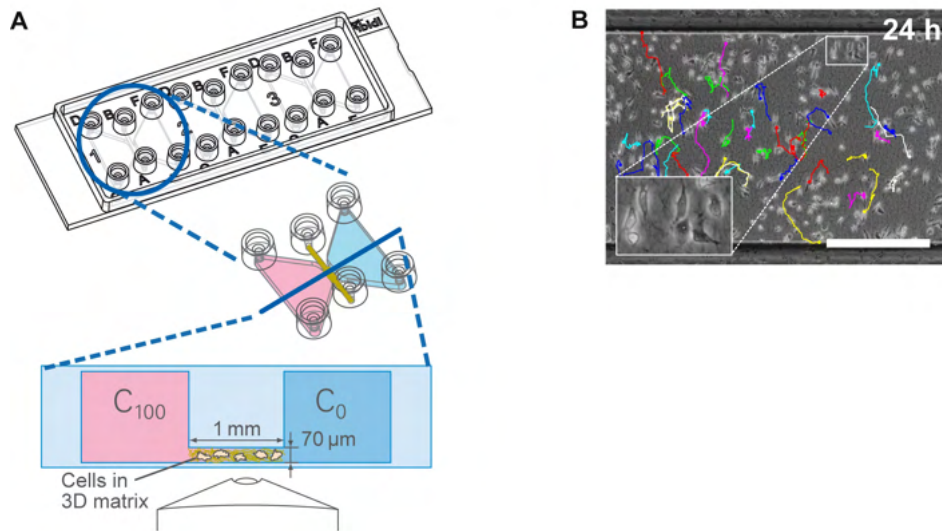


Figure 2.11:  $\mu$ -Slide Chemotaxis. **A.** The  $\mu$ -Slide Chemotaxis is a tool in the size of a microscopic slide and carries three independent chemotaxis chambers. The gradient is formed across the low volume, cell-containing middle channel at its cross-section with the reservoirs, which are filled with a medium (blue), and a chemoattractant solution (pink), respectively. The cells in the gradient area can be directly observed with an inverted microscope. **B.** Representative image of the observation area shows MDA-MB-231 cells embedded in a collagen gel with an overlay of the manually tracked cell trajectories at time point 24 h. Scale bar = 500  $\mu\text{m}$ . Figure adapted from [211] under the terms of the Creative Commons Attribution 4.0 License.

each  $\mu$ -Slide carries three autonomous chemotaxis chambers (Fig 2.11A). With a microscope equipped with a motorised stage, cell migration in up to four  $\mu$ -Slides can be recorded in parallel. Thus, the experimental throughput is substantially increased in comparison to the standard bridge chambers, or similar microfluidic-based assays. However, high-throughput experiments cannot be handled by the assay, especially the analysis of the cell trajectories, which is a time-consuming and labour-intensive procedure. Automated computer cell tracking could shorten the time required for the analysis, but the accuracy of the available tracking algorithms at the current state is suboptimal [43], especially at the rather high cell densities ( $> 10^4$  cells/cm<sup>2</sup>) typical for the  $\mu$ -Slide assay. Therefore, the lengthy and tedious manual tracking is usually the method of choice for retrieving the cell paths.

### 2.3.5 Evaluation of the chemotactic effect with the $\mu$ -Slide Chemotaxis assay

Time-lapse imaging followed by the analysis of complete cell trajectories is essential for a reliable identification of a preferred direction of cell migration. Since the cells are distributed homogeneously in the bridge area and they can migrate freely in and out to the reservoirs, it is not possible to detect a chemotactic effect solely from the distribution of the cells at the end-time of the experiment. The migration of slow moving cells is typically recorded for a time

period over 12 hours, with 5–10 min time-lapse interval [38, 39, 211]. For statistically relevant results, 30–40 cells in the gradient arena are manually tracked; i.e., the cell coordinates are determined in every frame of the time-lapse sequence. Several parameters that can be computed from the trajectories were identified for a reproducible quantification of migration and chemotaxis; e.g., forward migration indices (FMI), centre of mass (COM), cell velocity, and directness, as described in [39].

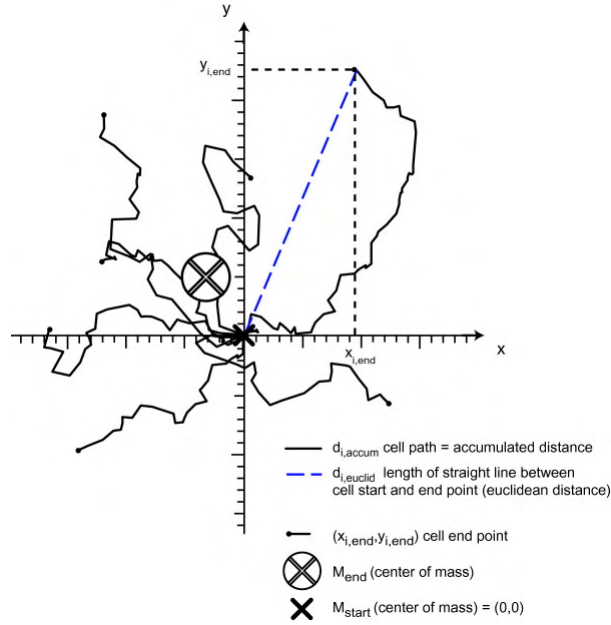


Figure 2.12: Parameters for analysing chemotaxis in the  $\mu$ -Slide Chemotaxis. The different parameters are defined in the trajectory plot. All cell trajectories are transformed by setting their starting point to  $(x_{i,start}, y_{i,start}) = (0,0)$  at time  $t = 0$ . Figure reproduced from [39] under the terms of the Creative Commons Attribution 4.0 License.

## Forward Migration Indices

The directionality of cell migration is evaluated by the forward migration indices parallel, and perpendicular to the gradient,  $FMI^{\parallel}$ , and  $FMI^{\perp}$ , respectively. The FMI represents the efficiency of a cell to migrate forward in the given direction. With the coordinate system chosen so that the y-axis is parallel to the gradient, and the cell trajectories extrapolated to  $(x, y) = 0$  at time 0 h, the FMI of  $n$  analyzed cells is:

$$\sum y_{i,start} = 0; \sum x_{i,start} = 0$$

$$FMI^{\parallel} = \frac{1}{n} \sum_{i=1}^n \frac{y_{i,end}}{d_{i,accum}}$$

$$FMI^\perp = \frac{1}{n} \sum_{i=1}^n \frac{x_{i,end}}{d_{i,accum}},$$

where  $x_{i,end}$ ,  $y_{i,end}$  are the coordinates of the cell end point position; and  $d_{i,accum}$ , the accumulated distance, is the length of the cell path; i.e., the sum of all incremental movements of the cell between all frames.

$FMI^\parallel$  significantly higher than  $FMI^\perp$  indicates chemotaxis—the cells are moving in a preferred direction, which is imposed by the gradient of the guidance cue.

### Displacement of centre of mass (COM)

The centre of mass represents the spatial average of positions of all  $n$  cells. The displacement of the centre of mass (COM) is the difference between the initial centre of mass at the beginning of the experiment ( $M_{start}$ ), and at its end point ( $M_{end}$ ):

$$\vec{M}_{start} = \frac{1}{n} \sum_{i=1}^n (x_{i,start}, y_{i,start}) = (0, 0); \vec{M}_{end} = \frac{1}{n} \sum_{i=1}^n (x_{i,end}, y_{i,end})$$

$$COM = |M_{end} - M_{start}|$$

### Cell velocity and directness

The velocity and the directness are parameters that reflect changes in overall cell migration; i.e., chemokinesis. The directness expresses how straight the cell path is, irrespective to the gradient direction; and is calculated as the ratio of the Euclidian and accumulated distance travelled by the cell. The Euclidian distance ( $d_{i,euclid}$ ) is the direct length of a straight line connecting the initial and end-point cell position:

$$d_{euclid} = \sqrt{(x_{i,end} - x_{i,start})^2 + (y_{i,end} - y_{i,start})^2}$$

$$D = \frac{1}{n} \sum_{i=1}^n \frac{d_{i,euclid}}{d_{i,accum}}$$

Increased cell velocity and directness indicates chemokinesis; i.e., an increase in random, persistent cell migration.

The  $\mu$ -Slide Chemotaxis has been successfully applied during the last years for the characterisation of chemotactic behaviour of multiple cell types, both fast moving; e.g., neutrophils [212,213], or macrophages [16,214]; and slow moving cells, such as fibroblasts [215,216]; neurons [217]; endothelial cells [38]; and cancer cells, including fibrosarcoma cells HT1080 [39], or human breast cancer cells MDA-MB-231 [211,218].

---

During the long era of the chemotaxis research, numerous tools for the investigation of the directed cell migration were invented. The choice of a chemotaxis assay depends on the specific research problem that is being addressed. Indirect assays such as the Boyden chamber are optimal for a high-throughput estimation of the migratory response to multiple cues in parallel experiments. For an accurate analysis of the chemotactic behaviour, assays enabling direct cell observation have to be employed. Furthermore, the stability of the gradient generated by the device should suit the migratory characteristics of the studied cell type. Among other criteria that could be required for an optimal chemotaxis assay is the possibility to study chemotaxis in physiological-like conditions (e.g., in 3D gels), or under multiple gradients. The advantages and the limitations of the most prevalent chemotaxis tools were described in this chapter. With respect to the research of chemotaxis of slow moving cells, only several tools can sustain the long-term stable gradient that is necessary for a reliable evaluation of the chemotactic response of these cells. Furthermore, such assays suffer from a low experimental throughput, which limits the use in studies with a high number of samples (e.g., screening for chemoattractants, testing of perturbations on the molecular level, examinations of clinical samples, or similar). The investigation and understanding of the chemotactic behaviour of slow moving cells is hindered by the lack of a suitable chemotaxis platform that would provide a stable and controlled gradient and, at the same time, enable a reliable, high-throughput evaluation of the chemotactic response. The recent advances in microfabrication techniques and the development of novel stimuli-responsive biomaterials could make it possible to address the limitations of chemotaxis tools in innovative ways in the future.

## 2.4 Micro-patterning and micro-structuring - methods of surface functionalisation for cell-based experiments

In many applications of the cell research it is desirable to control the geometry and area of cell adhesion and spreading. *In vivo*, after all, a constant confinement is imposed on cells by the topography of the environment, which greatly affects the cell behaviour [14]. In contrast, cells in standard *in vitro* culture vessels are free to spread and move indefinitely in all directions. Therefore, to mimic more physiologically relevant conditions, several techniques that enable spatially selective functionalisation of cell culture surfaces have been developed. The ability of cells to adhere to a substrate depends strongly on the hydrophobicity and the surface charge. With micro-patterning methods, the protein-adsorbing capacity of surfaces can be altered by introducing defined patterns of areas that promote, or prevent cell adhesion, respectively.

It has been shown that not only cell adhesion, but subsequently also other processes including the morphology, proliferation, migration, and respective signalling mechanisms in cells are affected by the composition, concentration and conformation of the proteins that are adsorbed to the surface from cell medium [219]. Therefore, micro-patterning methods, providing

---

a control over the chemical properties of the surface, are widely applied to study various aspects of cell behaviour [219, 220]. As discussed above, adhesion to the substrate is essential for effective locomotion of mesenchymal cells. Thus, by micro-patterning, cell migration can be restricted to predefined parts of the substrate. This way, the degrees of freedom of the cell motion are reduced, which makes it possible to break down the complex process and isolate particular features of the migratory behaviour, in respect to the chosen geometry of the micro-pattern. For example, triangular or tear-shape patterns enable investigation of polarisation and cytoskeletal architecture in immobilised cells [221, 222]; while thin micro-patterned adhesive stripes were produced to analyse the formation of protrusions in cancer cells responding to chemotactic stimuli [223]; or to study cell movement in a 1D-like environment that closely reproduces the conditions of migration along collagen fibres in a 3D ECM [224, 225]. Besides, micro-patterning—or micro-structuring of 3D hydrogels—can be used to generate arrays of standardised micro-environments that can be readily accessed for the analysis of cell behaviour, hence simplifying the evaluation of multiple experiments in parallel [226–230].

In the next chapters, the most prevalent methods used for functionalisation of 2D surfaces and engineered 3D substrates will be presented.

### 2.4.1 Micro-patterning of flat 2D micro-environments

In order to restrict cell adhesion to specific parts of the surface, the surface material is patterned with molecules that enhance cell adhesion; mostly ECM proteins such as fibronectin, collagen or laminin; or synthetic polypeptides derived from cell binding motifs (e.g., the Arginin-Glycin-Aspartate (RGD)-peptide<sup>7</sup>, or poly-L-lysine) [231, 232]. To ensure a specific adhesion of cells only to the patterned areas, the surrounding surface is usually passivated with polymers that suppress non-specific adsorption of proteins or other adhesion-supporting molecules from the cell culture media. Typically, copolymers of polyethylene glycol (PEG) are used as the cell-repellent moiety. The conformation of PEG chains deposited as a layer on the surface sterically blocks the adsorption of proteins and the cell adhesion [233, 234]. The PEG chains are often linked to a residue that mediates the linkage with the surface material [235]. To the most frequently used passivation agents belong the PEG block copolymers poly(propylene-oxide)-PEG (PEG-PPO-PEG, also known as Pluronics), and poly-L-lysine (PLL)-PEG [236]. The choice of the passivation molecule depends on the chemical properties of the surface material.

#### Soft lithography

The most widely used methods that provide the spatial control over the surface functionalisation with adhesive and cell-repellent molecules are based on soft lithography. In soft lithography, elastomeric (“soft”) polymers, such as polydimethylsiloxan (PDMS), are used to transfer the

---

<sup>7</sup>The tripeptide motive Arginin-Glycin-Aspartate (RGD) is derived from ECM proteins, including fibronectin. The binding sequence is recognised by integrin receptors and mediates cell attachment [231].



---

desired chemical pattern onto the substrate [237]. The elastomer is moulded into a “stamp” by curing the liquid pre-polymer against a structured silicon or glass master that carries the desired micro-pattern. The stamps are then “inked” with a solution of the adhesive molecule, and brought into contact with the substrate. This way, the pattern of the adhesive agent is transferred—printed—to the surface (Fig 2.13). Finally, the surrounding area is passivated to prevent unspecific cell adhesion. This approach is called micro-contact printing ( $\mu$ CP) [238,239]. Alternatively, an array of open micro-channels is moulded into the elastomer, and after placing the structured elastomer onto the surface, the channels are filled with the adhesive agent. This technique is known as microfluidic patterning ( $\mu$ FLP) [240].

These methods enable relatively uncomplicated and cost-effective patterning; however, the resulting pattern is not always homogeneous, and the density of the printed molecules cannot be controlled [236]. Also, the resolution and geometry of the pattern is limited by the mechanical properties of the stamp material. Besides, since a tight contact of the stamp with the surface is required for successful transfer of the adhesive protein, patterning on soft substrates can be complicated.

### Stencil-assisted patterning

Another approach is to micro-pattern specific regions of the surface with the help of a stencil, typically in form of a thin elastomer membrane that is structured with holes of the desired pattern geometry. The stencil is sealed to the substrate to protect the parts surrounding the patterned area from deposition of the adhesive molecules [228, 241–243]. After the adhesion-activating treatment, the stencil can be peeled off and the parts around the patterns backfilled with a passivation agent. Alternatively, cells can also adhere directly into the holes of a stencil deposited on a cell culture substrate, without employing any chemical surface modification [241]. Subsequent to the removal of the stencil, another cell-type can be seeded onto the area that was initially protected from cell adhesion by the stencil to generate patterned co-cultures [244,245].

The advantage of patterning with elastomeric stencils is that no specialised tools or chemistry is required, and the method can be applied on any kind of substrate material. However, the handling of the membranes can be difficult, and the mechanical properties of the stencil material can pose a limit to the pattern geometry.

### Photolithography

In photolithography, the pattern is created by UV illumination through a photomask, or by a laser writing device. Here, the substrate is pre-coated with protein-resistant, photosensitive molecules, and the patterned illumination then selectively alters the surface chemistry and activates the adsorption capacity of the selected (illuminated) regions [246]. This can be achieved for example via photocleavage of the cell-repellent polymer (e.g., PLL-PEG) [247,248]; or by inducing the formation of binding sites for the adhesive agent [249–251]. Photolithographic

methods can yield very homogeneous micro-patterns of any geometry, even in closed systems, such as microfluidic channels or chambers [252]. Furthermore, photolithographic methods provide a better control over the ligand density in the pattern, so that even gradients of the bound proteins can be formed [250]. The disadvantage of photolithographic micro-patterning approaches is the need for relatively complicated photochemistry and specific equipment, such as a deep UV light source, or laser writing devices.

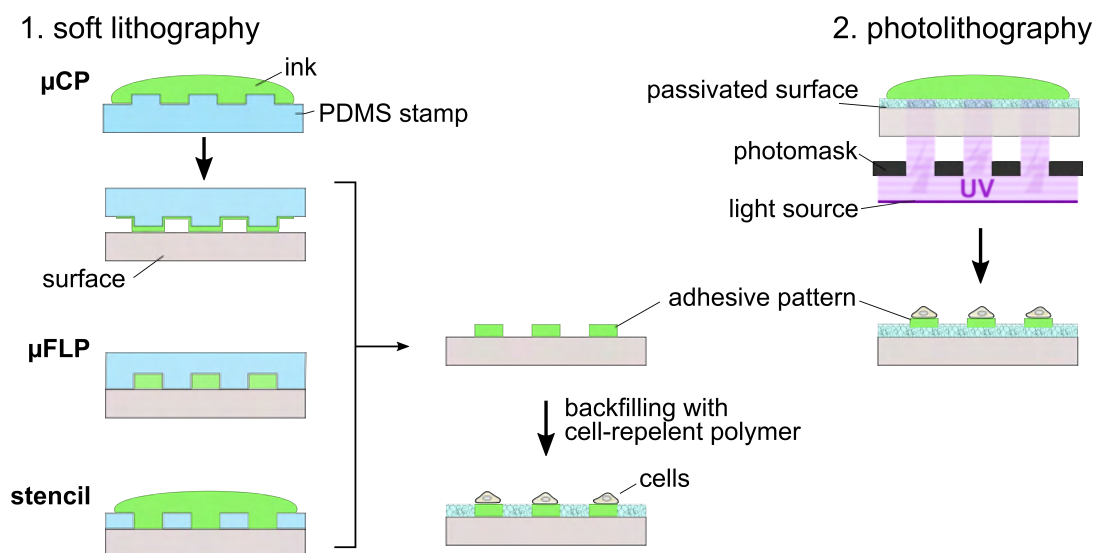


Figure 2.13: Schematic of micro-patterning methods. **1.** Soft lithography utilises a structured elastomer, often PDMS (blue), to transfer a pattern of adhesive molecules (e.g., fibronectin, green) to the selected surface (grey). In micro-contact printing ( $\mu$ CP), a PDMS stamp is inked in a solution of the adhesive agent, which is then printed onto the surface. In microfluidic patterning ( $\mu$ FLP), the adhesive agent is loaded into channels formed between the surface and a PDMS mould. In stencil-assisted patterning, a membrane with holes is sealed to the surface, so that only the areas of the holes are exposed to the adhesive agent. After removal of the PDMS stamp/mould/stencil, the surface regions that surrounds the resulting adhesive pattern can be backfilled with a cell-repellent polymer (e.g., PEG block copolymers) to prevent unspecific cell adhesion. **2.** In photolithographic methods, the desired pattern is transferred to the surface by patterned illumination through a photomask. The light exposure induces binding of the adhesive molecules to a passivated surface, specifically in the illuminated areas.

## Switchable surfaces

Some micro-patterning protocols utilise advanced stimuli-responsive surfaces, whose adhesiveness can be switched on or off in response to external stimuli, such as light, temperature, or chemical agents [253–255]. The dynamic surfaces allow to alter the geometry of the initial patterns in time, and thus to study cell responses to a changing confinement in their micro-environment [256]. Thermally controlled surfaces are also used to detach cultured cell sheets without the need of exposing the cells to an enzymatic treatment [257]. Besides, switchable substrates are useful for multi-patterning of several proteins, or for establishing co-cultures of

---

multiple cell types [258].

## 2.4.2 Micro-engineered 3D environments

In addition to 2D patterned surfaces, engineering of defined 3D micro-environments also finds a wide application in cell research. 3D micro-structuring can confine migrating cells from multiple dimensions, and introduce defined topographic constraints that mimic the physiological ECM structure of the cell micro-environment. Protocols based on soft lithography and photolithography can be applied to prepare 3D micro-structures or micro-environments from biological or synthetic hydrogels; e.g., collagen, or PEG-based polymers [259]. For example, PDMS stamps were used to generate arrays of cells embedded in 3D collagen [230]. Photo-polymerised hydrogels such as PEG-diacrylate (PEG-DA) can be structured with a PDMS mould, similarly as in  $\mu$ FLP, by loading the pre-polymer solution in the space between the mould and the surface prior to the light-induced gelation [228]. Alternatively, UV-responsive hydrogels can be micro-structured by inducing the photo-polymerisation with a patterned illumination, using a photomask, or a laser writing device [260, 261].

Micro-structures of specific geometries from gels of varying rigidity and/or pore size can be fabricated in order to study the cellular responses to the mechanical properties of the ECM; e.g., the contact guidance [262–264]. To impose a 3D confinement, cells can be placed in micro-structured wells [228], grooves [262], or channels [263]; or encapsulated in photo-polymerised gels [265]. Furthermore, not only mechanical confinement, but also other specific cues can be introduced to the cells in the 3D matrix, for example by decorating networks of synthetic gels with peptides that are derived from ECM proteins, mimicking adhesion or cleavage sites [265]. Photolithographic methods also enable generation of biochemical or biomechanical 3D patterns and gradients inside of pre-existing transparent gel structures [261, 266].

### Photo-polymerization of 3D hydrogel micro-structures

In this thesis, a PEG-based hydrogel was photolithographically micro-structured to confine migrating cells within a selected part of a chemotaxis chamber (migration arena, Chapter 4.2). The UV-responsive hydrogel polymerises in presence of a suitable photo-initiator upon an exposure to UV light of a specific wavelength. The photo-initiation of the reaction enables a precise spatial control of the hydrogel polymerisation [265]; e.g., with help of a photomask. The hydrogel backbone of the migration arenas established in this work was formed by norbornene functionalised, 4-arm polyethylene glycol (PEG4norb, 20 kDa), cross-linked by PEG-dithiol (PEG-DT; Fig 2.14). This hydrogel system was chosen because the step-wise mechanism of the thiol-norbornene photo-polymerisation ensures a rapid formation of highly homogeneous networks. The radical polymerisation reaction is triggered by a UV-induced activation of the photoinitiator, which abstracts a hydrogen from the thiol-group of the cross-linker. The result-

ing thiyl-radical propagates across the alkene group of the PEG4norb. Subsequently, a hydrogen from another thiol is abstracted, a thioether linkage is formed, and the thiyl-radical is regenerated. Finally, coupling of the radicals terminates the reaction [267,268]. Finally, coupling of the radicals terminates the reaction [267,268].

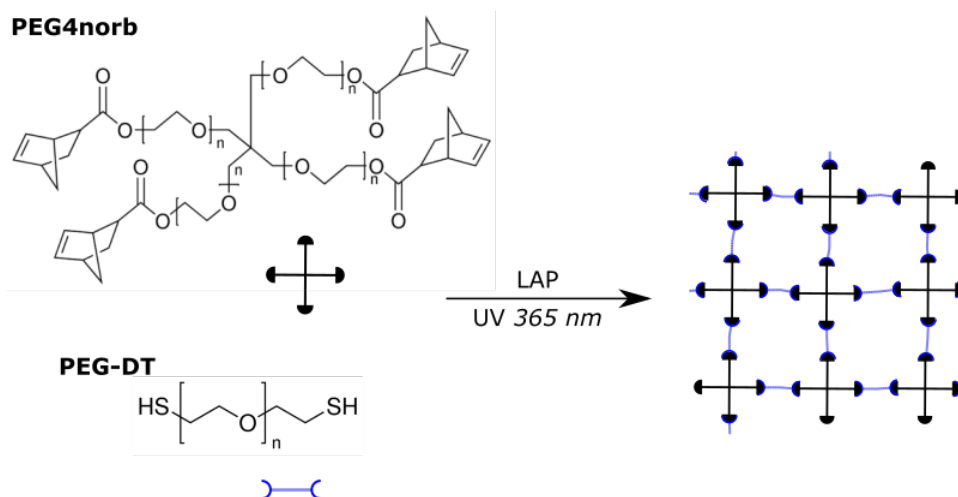


Figure 2.14: Scheme of the PEG4norb/PEG-DT photo-polymerisation and the hydrogel network. The backbone of the hydrogel network is formed by 4-armed PEG-norbonene, cross-linked with PEG-dithiol. The radical polymerisation reaction is induced by UV-illumination in presence of the photo-initiator LAP (lithium phenyl-2,4,6-trimethylbenzoylphosphinate).

Another PEG-based hydrogel used in this work was the polyethylene glycol dimethacrylate (PEG-DMA). PEG-DMA is a bio-compatible, non-degradable, cell-repellent polymer that can be used to prepare precise, micro-scaled environments for controlling cell adhesion and migration. For example, PEG-DMA micro-channels were produced for studying collective cell migration [263], and PEG-DMA micro-structuring was also used for arraying cell cultures [228]. Again, UV light in presence of a photoinitiator induces a radical polymerisation of the hydrogel. The hydrophilic methacrylate groups of the PEG-DMA monomers then form covalent bonds that cross-link the polymer network [260,269].

In the recent years micro-patterning and micro-structuring methods became widely adopted in the field of cell biology and many techniques were developed that are readily available to any standardly equipped biological laboratory. Micro-engineering is used in diverse applications, addressing various aspects of cell behaviour. In this thesis profit was taken from the possibility to restrict cell migration to specific controlled micro-patterns when establishing the end-point chemotaxis assay (see Chapters 1.1.1, and 4).

# 3 Materials and Methods

All materials and instrumentation used in this work and the suppliers are detailed in the Appendix B (List of materials, page 144).

## 3.1 Micro-structuring and micro-patterning

Several methods of micro-structuring and micro-patterning were used in this thesis in order to control the spatial area of cell migration in the chemotaxis chambers of the  $\mu$ -Slide Chemotaxis. This was done to enable a subsequent analysis of the chemotactic behaviour based on the end-point distribution of the cells, in the manner explained in Chapter 1.1.1. The experimental details of the employed methods are described in this chapter. The resulting structures (or patterns) in regard to their application in the chemotaxis assay as well as the suitability of the respective methods for establishing the intended assay will be discussed in detail in Chapter 4.

### 3.1.1 Fabrication of PEG-DMA micro-wells

For a 2D end-point chemotaxis assay, low micro-wells were fabricated from the cell-repellent polymer polyethyleneglycol-dimethacrylate (PEG-DMA, Mn 550, purchased from Sigma-Aldrich) and placed in the gradient area of the chemotaxis chambers to spatially restrict the migration of the chemotaxing cells. The micro-structures were prepared photolithographically, using glass coverslips in the size of the chemotaxis slide (75x25 mm) as a substrate. To maintain a uniform height of the structures, special glass coverslips with elevated edges (LifterSlips) were also employed for the fabrication. The coverslips were cleaned in ultrasonic bath for 2x 5 min in ultra-pure water, and another 5 min in 96% ethanol. The coverslips were then dried with a flow of compressed air, and silanised by an overnight exposure to 3-aminopropyl triethoxysilane vapours in a desiccator. A silanised coverslip was positioned on a quartz photomask, and a smaller LifterSlip (22x25 mm, with 0.03 mm high rims) was placed on top (Fig 3.1). 13  $\mu$ l of PEG-DMA solution with 4 mM lithium phenyl-2,4,6-trimethylbenzoylphosphinate (LAP) was loaded between the coverslips. The polymerisation was initiated by 12 s illumination by 365 nm UV light (10 mW/cm<sup>2</sup>), placing the photomask with the coverslip on a rack fixed 11 cm above a LED lamp KSL70/365 (RappOpto Electronic GmbH). Immediately after the illumination, the LifterSlip was removed and any non-polymerised solution was washed away with PBS. The structures were further washed in a Petri dish with PBS for 10 min. The quality of the

resulting structures was verified optically with a phase-contrast microscope. While doing so, special attention was paid to the integrity of the walls, and to possible unspecific polymerization of the PEG-DMA in the area of the micro-wells. Finally, the coverslip was sprayed with 70 % ethanol, dried by a flow of compressed air, and mounted to the sticky-Slide Chemotaxis (i.e., a bottomless variant of the  $\mu$ -Slide Chemotaxis with a self-adhesive underside) for chemotaxis experiments. The channels of the chemotaxis chambers were then washed with cell culture medium and filled with cell suspension ( $2 \times 10^6$  cells/ml). The cells were allowed to adhere in the micro-wells for 1 h in standard cell culture conditions (37 °C, 5% CO<sub>2</sub>, humidified atmosphere). Then, the channels were washed twice with serum-free medium, and the reservoirs of the chemotaxis chamber were filled with medium containing 0%, or 10% FBS, respectively. Cell migration in the micro-wells was monitored by videomicroscopy, as will be detailed in Section 3.2.6.

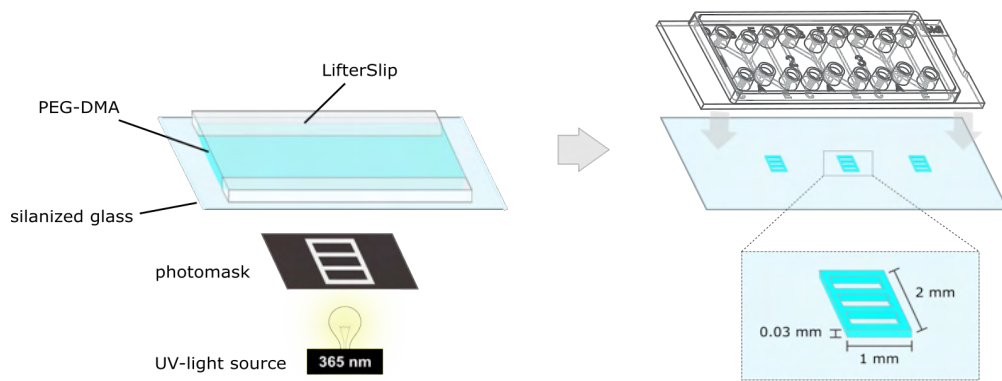


Figure 3.1: **A.** Fabrication of PEG-DMA micro-wells. 3D structures bearing three  $0.8 \times 0.4$  mm wells were fabricated photolithographically on top of a glass coverslip. The pre-polymer solution containing PEG-DMA monomers and the photoinitiator LAP was loaded in the  $30 \mu\text{m}$  high space between the silanised glass coverslip and a LifterSlip. The polymerisation was induced by 12 s illumination with UV light through a suitable photomask. The coverslip was aligned with the photomask in such manner that the three resulting hydrogel structures ( $1 \times 2$  mm apiece) were positioned in place of the gradient areas of the  $\mu$ -Slide Chemotaxis, each structure holding three micro-wells (lower right corner). After washing and drying the coverslip, it was assembled with the sticky-Slide Chemotaxis.

### 3.1.2 Fabrication of fibronectin-patterned surfaces with a silicon stencil

Another method used in this thesis to confine the migrating cells in the chemotaxis chamber was stencil-assisted micro-patterning. Parts of the chemotaxis chamber were selectively patterned with fibronectin (i.e., a molecule that promotes cell adhesion), and the surrounding surface was consecutively passivated with Pluronic F-127. Here, a COP polymer foil (commercially available Coverslips for sticky-Slides, uncoated, ibidi) in the size of the  $\mu$ -Slide Chemotaxis was used as a substrate. Commercially available silicon micro-wells (Culture Insert FulTrack,

ibidi) were used to dispose the fibronectin solution on the selected parts of the substrate. The Culture Insert FulTrack, which contains four round wells of 400  $\mu\text{m}$  in diameter, was cut in four pieces so that the individual wells could be used separately. The wells were then placed on the substrate in positions aligned with the middle of the chemotaxis chambers of the  $\mu$ -Slide Chemotaxis (Fig 3.2). Following the instructions provided by the manufacturer, the wells were filled with PBS and degassed by placing them in a desiccator, from which the air was pumped out, and incubating them in the reduced air pressure atmosphere for 30 min. Afterwards, the PBS was replaced by 5  $\mu\text{l}$  of 1 mg/ml fibronectin solution in PBS. The protein was allowed to physisorb to the surface for 1 h at 37  $^{\circ}\text{C}$ . To prevent evaporation, the substrates were placed in a wet chamber for the incubation period. Then, the solution was aspirated from the wells, and the remaining protein was washed several times with PBS. After removing the wells, the substrate was carefully mounted to the self-adhesive sticky-Slide Chemotaxis, aligning the fibronectin-coated spots with the middle of the chemotaxis chambers.

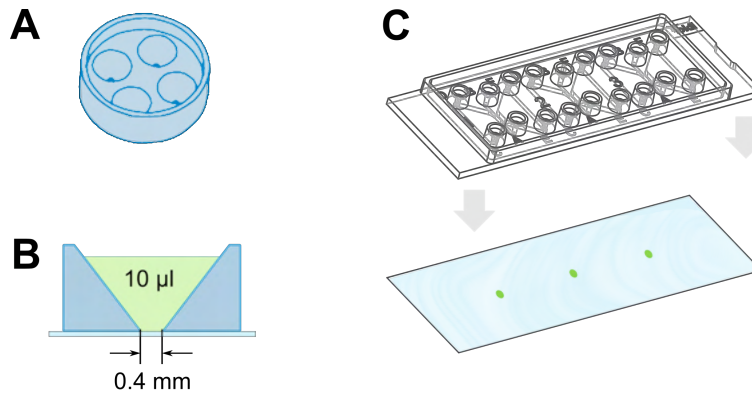


Figure 3.2: Scheme of micro-patterning the adhesive patterns with removable silicon wells. **A.** Culture Insert FulTrack is a removable silicon well-insert for cell culture. One insert bears four micro-wells of 400  $\mu\text{m}$  diameter. **B.** Cross-section of one micro-well placed on a coverslip. One well can hold 10  $\mu\text{l}$  of cell suspension or protein solution (e.g., fibronectin). **C.** For the end-point chemotaxis assay, a polymer foil was patterned with fibronectin (green) and mounted to the sticky-Slide Chemotaxis.

The middle channel of each chamber was then filled with 10  $\mu\text{l}$  Pluronic F-127 (1 mg/ml in PBS), and the slide was incubated for 1 h at room temperature. Before cell experiments, the channels were rinsed several times with PBS and with cell culture medium. HT1080 cells were seeded in the channels at the seeding concentration of  $2 \times 10^6$  cells/ml. The cells were allowed to adhere to the pattern for at least 1 h in standard cell culture conditions (37  $^{\circ}\text{C}$ , 5%  $\text{CO}_2$ , humidified atmosphere), and their adhesion to the patterned area was monitored by phase-contrast microscopy, using EVOS fl inverted microscope (AMG) with a 4x objective. Before a chemotaxis experiment, the unattached cells were washed away with serum-free medium, and the reservoirs of the chemotaxis chamber were filled with medium containing 0%, or 10% FBS, respectively.

### 3.1.3 In-channel micro-patterning

Micro-patterning methods based on photolithography were employed to prepare the cell confining adhesive areas directly inside of an assembled  $\mu$ -Slide Chemotaxis. Two previously published methods based on different chemistries were tested for their applicability in the microfluidic slide. The basic principle is the same for both methods: the patterned substrate is coated beforehand with a thin layer of a hydrophobic polymer that prevents cell adhesion. Then, selected areas of the surface are photolithographically activated—i.e., turned reactive—with the help of a photo-inducible radical initiator, and cell adhesive molecules are grafted to the activated areas of the surface (Fig 3.3).

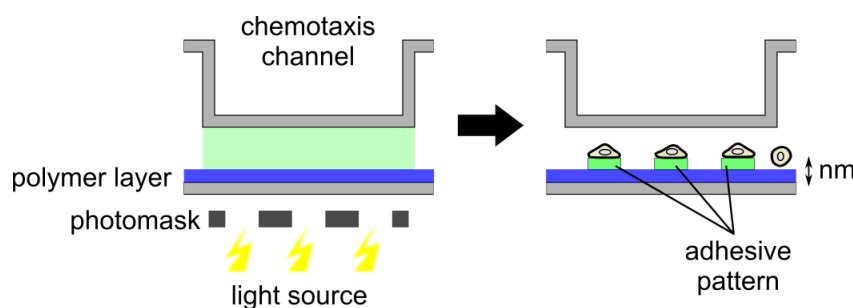


Figure 3.3: Scheme of the photo-induced activation of a passivated surface inside of a chemotaxis channel. Cell adhesion was prevented by a layer of a hydrophobic polymer (depicted in blue) that was grafted on the bottom surface of the chemotaxis chamber. A part of the substrate, defined by patterned illumination through a photomask, was then activated for cell attachment with an adhesion-mediating molecule (green). Note that the scheme is not to scale; the height of the patterned layer depends on the length of the respective polymer chains, but remains on the scale of several nanometres; i.e., below the topographic differences that can be recognised by cells [252].

#### Protein Adsorption by Photobleaching

With the approach introduced by Belisle *et al.* in 2009 [250], fluorescein molecules functionalised with an alkyne-group were immobilised on the selected areas of an inert substrate, and subsequently, cyclic RGD was covalently bound on these pattern with standard click chemistry. For this method, chemotaxis chambers were used that were mounted on polymer coverslips coated with a thin layer of an inert polymer (*BioInert* substrates, ibidi). The channels of the chemotaxis chambers were filled with 10  $\mu$ l of 6-fluorescein-alkyne solution (FAM-6; 1 mg/ml, diluted in PBS). The structured illumination was performed on a microscope system (Zeiss Axiovert 100) with a 20x objective and GFP filter set (both Zeiss). A projector with a built-in metal halide lamp (280 W) was coupled into the light path via the illuminator port at the back of the microscope stand. This set-up enabled projection of a digital photomask with the desired pattern on the substrate, as described in [250]. The focus was set on the bottom of



---

the slide and the substrate was illuminated for 100–200 s. Afterwards, the channel was washed 3x with 30  $\mu\text{l}$  ultra-pure water. The immobilised FAM-6 was visualised by fluorescence microscopy to verify the quality of the pattern. A commercially available click-chemistry reaction kit (Click-iT cell reaction buffer kit, invitrogen) was used to bind azide-functionalised cyclic RGD to the linker (FAM-6). The reaction mix was prepared according to the instructions provided by the manufacturer, containing 5  $\mu\text{M}$  of the cyclic RGD-azide (cyclo[RGDFK(azide)], purchased from Peptides International). The channels of the chemotaxis chamber were filled with the reaction mix and incubated for 1 h in dark at room temperature. The channels were then washed for 10 min with PBS, replacing the washing buffer 3x. In a control experiment, the cyclic RGD-azide was substituted by azide-functionalized fluorescent dye, sulfo-Cyanine-3-azide (5  $\mu\text{M}$  in  $\text{H}_2\text{O}$ ), to enable an optical control of the resulting pattern. Before cell seeding, the channels were washed with cell culture medium. Then, the channels were filled with cell suspension ( $2 \times 10^6$  cells/ml), by rinsing them slowly with  $2 \times 10$   $\mu\text{l}$  of the suspension. The slides with the cells were incubated in cell culture incubator, and the cell adhesion to the patterns was monitored by phase-contrast microscopy.

### Immobilisation of adhesive peptides on photografted PEG-polymers

In 2014, Larsen *et al.* presented a method for protein and cell patterning in closed microfluidic channels [252]. The low volume of the channels poses specific challenges on the patterning reaction, similar to those encountered in the low-volume chemotaxis chambers. In this approach, a cell-repellent, PEG-based polymer, functionalised with reactive groups, is photografted on the polymer surface of the channels [251]. In this thesis, 8-arm polyethylene glycol norbornene (PEG8norb, Fig 3.4) was chosen as the cell-repellent polymer, since it provides more reactive groups compared to other commonly used PEG-based polymers (such as PEG-diacetate, or PEG4norb), thus the adhesive molecules in the activated areas could bind at a relatively high density, possibly resulting in a better attachment of the cells. PEG8norb (purchased from JenKem Technology USA) was grafted on the surface of the  $\mu$ -Slide Chemotaxis by a 30 min exposure to UV light (302 nm UV bench lamp, VWR; 18  $\text{mW}/\text{cm}^2$ ) in presence of the photoinitiator 4-benzoyl benzylamide hydrochloride. The whole chemotaxis chamber (i.e., including the reservoirs) was filled with 140  $\mu\text{l}$  of coating solution containing 7.5  $\mu\text{M}$  PEG8norb, and 4 mM photoinitiator in PBS and the UV lamp was placed 5 cm above the slide, the bottom of the slide facing the lamp. The bottom of the  $\mu$ -Slide Chemotaxis is a cell culture treated polymer foil ('ibiTreat'; i.e., hydrophilic substrate), and the reactive groups of the surface upon illumination in presence of the photoinitiator enable binding of the PEG8norb. After grafting the polymer on the surface of the slide, the chambers were washed with PBS, and the substrate was patterned with RGD peptide. In this step, the binding of the peptide to the reactive norbornene groups of the substrate was induced by the 365 nm UV light, using LAP as the photoreactive agent. The adhesive pattern was applied only in the gradient area of the chemotaxis chambers, therefore only the middle channels were filled with 6  $\mu\text{l}$  of PBS solution

containing 2 mM CRGDS peptide (purchased from Iris Biotech), and 2 mM LAP. The slide was illuminated for 20 s through a quartz photomask with rectangular structures, using the LED lamp KSL70/365, as described in section 3.1.1. Afterwards, the channels were washed with PBS and the functionalised surfaces were kept in PBS until further use. Before cell experiments, the channels were washed by cell culture medium. HT1080 cells were seeded on the patterns by rinsing  $2 \times 10^6$   $\mu\text{l}$  of cell suspension containing  $2 \times 10^6$  cells/ml through the channels. The cells were allowed to adhere in cell culture incubator, and their spreading on the patterned surface was monitored by phase-contrast microscopy.

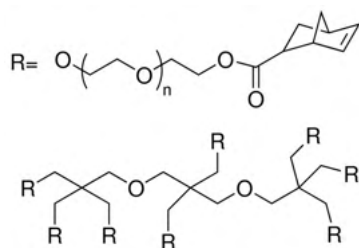


Figure 3.4: Structure of 8-arm PEG-norbornene.

### 3.1.4 Photopolymerisation of PEG-norbornene hydrogel

3D structures—migration arenas—from a porous, cell-repellent PEG-based hydrogel which confined the cells in the gradient area of the chemotaxis chambers were fabricated directly inside of the  $\mu$ -Slide Chemotaxis. A quartz photomask bearing doublets of rectangular structures of varying width (300-500  $\mu\text{m}$ ) was purchased from Compugraphics Jena (Jena, Germany). The structures were set out on the mask with a precise spacing, so that the rectangles border the gradient areas of each chamber of the slide when the  $\mu$ -Slide Chemotaxis is aligned with the mask (Fig 3.5). The middle channel of the chemotaxis chamber was filled with a phosphate buffered saline (PBS)-based pre-polymer solution containing PEG monomers (2-3 mM



Figure 3.5: Quartz photo-mask for fabrication of 3D hydrogel structures. The photomask holds pairs of rectangular structures that frame the gradient area of the chemotaxis chambers when a  $\mu$ -Slide Chemotaxis is placed on the mask and aligned. The slide dimensions (25x75 mm) are outlined on the mask to help achieve a precise alignment. The photomask enables fabrication of structures of varying width and spacing (0.3–0.5 mm/0.1–0.6 mm), resulting in migration arenas of various size. For the chemotaxis assay, the 300  $\mu\text{m}$  wide structures proved to be most suitable, enclosing a 400  $\mu\text{m}$  wide arena between the hydrogel barriers.

---

PEG4norb, Mw 20000, purchased from JenKem Technology USA), the cross-linker (2–6 mM PEG-DT, Sigma-Aldrich), and a photoinitiator (3 mM LAP). The pre-polymer solution was always kept on ice and protected from direct light. The slide was placed on the photomask and the polymerisation was initiated by a 10 s exposure to UV light (365 nm; 10 mW/cm<sup>2</sup> intensity); as described in section 3.1.1. Each of the three chambers of the chemotaxis slide was illuminated separately. Immediately after the illumination of all chambers, the non-polymerised material was removed by washing each of the middle channels 3x with 30  $\mu$ l PBS. After the last washing step, the PBS remained in the channels, and the large reservoirs of the chemotaxis chambers were filled with 65  $\mu$ l PBS each. The quality of the resulting hydrogel structures was assessed optically by phase-contrast microscopy. It was verified that no unspecific polymerization appeared in the vicinity of the illuminated areas, and that the structures have the expected width (responding to the chosen photomask, and the ratio of the cross-linker and the PEG monomers in the pre-polymer solution<sup>1</sup>). The chemotaxis slides with the hydrogel arenas were stored filled with PBS at 4 °C. To prevent evaporation, the slides were closed with the lids provided by the manufacturer, or with a PCR-foil for long-term storage.

## 3.2 Cell-based experiments

Three cell types were used in the experiments presented in this thesis. The human fibrosarcoma cell line HT1080 was employed as a model adherent cell line in the first part of the thesis; i.e., for the development of the end-point chemotaxis assay, and for verification of its functionality (Chapter 4), as its migration and chemotactic behaviour are well characterised. For light-sheet fluorescence microscopy (LSFM) experiments, HT1080 cells transiently labelled with the fluorescent protein LifeAct-GFP2 were used. In another part of this thesis, the chemotaxis assay was applied to study the behaviour of primary epithelial cells—the normal human epithelial keratinocytes, nHEK (Chapter 5).

### 3.2.1 Cell culture

Routine cell culture was performed according to the standard operation procedures implemented in the laboratory. The HT1080 cells (DSMZ, Braunschweig, Germany) were cultured in high glucose Dulbecco's Modified Eagle's Medium (DMEM) supplemented with 10% fetal bovine serum (FBS). The cells were subcultured when reaching 80–90% confluency (3x weekly).

Trypsin/EDTA solution was used to detach the cells from the culture surface: the cells were washed with PBS and treated with trypsin/EDTA for 2 min. The reaction was terminated by addition of FBS-supplemented DMEM, and the cell suspension was centrifuged for 5 min at

---

<sup>1</sup>It was shown previously that the swelling rate of similar rectangular hydrogel structures in microfluidic channels correlates with the cross-linker ratio of the hydrogel [270]. Less cross-linked hydrogels swell more, yielding final structures that are much wider than the responding pattern of the photomask used for their fabrication.

---

200x g. The pellet was resuspended in fresh culture medium at the desired concentration and used in an experiment, or seeded in a new cell culture flask for further culture. The LifeAct-GFP2 HT1080 cells (ibidi, Gräfelfing, Germany) were maintained under the same conditions. The nHEK cells (CellSystems, Troisdorf, Germany) were cultured in DermaLife basal medium supplemented with DermaLife K LifeFactors kit, and Penicillin/Streptomycin. The final component concentrations in the supplemented (complete) DermaLife medium were 5 µg/ml insulin, 6 mM L-glutamine, 1 µM epinephrine, 5 µg/ml apo-transferrin, 100 ng/ml hydrocortisone hemisuccinate, 0.4% bovine pituitary extract, 100 U/ml Penicillin, and 100 µg/ml Streptomycin. For detachment, the cells were treated with trypsin/EDTA for 5 min, and trypsin neutralizing solution was used to terminate the reaction. Only nHEK cells up to passage number 5 were used. All cells were cultured in standard culture flasks (Sarstedt Cell+) in a cell culture incubator (Heracell 150i, ThermoFisher Scientific) at 37 °C in 5% CO<sub>2</sub> humidified atmosphere.

### Coating substrates with fibronectin

For most cell experiments, the surface of the µ-Slide Chemotaxis was coated with fibronectin to promote cell adhesion. 1 mg of fibronectin was diluted in 1 ml of sterile, ultra-pure water for stock solution and stored in aliquots at -20 °C. For coating of the standard µ-Slide Chemotaxis, the stock solution was further diluted in PBS to 70 µg/ml, and 6 µl of the coating solution was loaded in the middle channels of the chemotaxis chambers. When coating only the gradient area of the chemotaxis chambers, the coating area is 0.27 cm<sup>2</sup> per chamber. The slide was incubated for 1 h at 37 °C and the channels were washed 3x with PBS afterwards. After washing, the remaining PBS was aspirated and the channels were allowed to dry completely before seeding the cells. The soft elastomeric substrates used for traction force microscopy experiments were coated with 350 µg/ml fibronectin at the same conditions. For the end-point chemotaxis assay in the slides with 3D hydrogel migration arenas, the concentration of the coating solution was increased to 1 mg/ml due to the smaller volume of the arenas.

### Preparation of collagen type I 3D matrix

Chemotaxis experiments in 3D environment were performed with cells embedded in 1.5 mg/ml bovine collagen type I matrix. The neutralised collagen gel mixture was prepared according to the protocol listed in Table 3.1. If not stated otherwise, the cell suspension contained 12×10<sup>6</sup> cells/ml, which represents 6× the desired final concentration of cells in the gel. The reagents were added in the given order and mixed thoroughly by pipetting the solution several times up and down. The mixture was prepared at room temperature. The collagen mix was filled immediately in the chemotaxis chambers and incubated for 30–60 min at 37 °C in a humid chamber, until gelled.

In control samples in the chemotaxis assays (random, non-directional migration in a uniform, 10% FBS environment), 30 µl of 1×DMEM was replaced by 100% FBS. For fluorescent

Table 3.1: Collagen type I 1.5 mg/ml gel fabrication protocol

component	volume
10× DMEM	20 µl
NaOH 1 M	6 µl
H <sub>2</sub> O	14 µl
NaHCO <sub>3</sub> 7.5%	10 µl
1× DMEM	50 µl
collagen I, 3 mg/ml	150 µl
cell suspension (6×)	50 µl

measurements of gradient formation in the migration arena (Chapter 4.2.2), and in the LSFM chemotaxis chamber (Chapter 6.2), the cell suspension and 1x DMEM were replaced by either PBS or a fluorophore solution.

### 3.2.2 Viability assay

The viability of cells in the migration arenas was determined with a differential live and dead staining with fluorescein diacetate (FDA) and propidium iodide (PI). 5 mg FDA was dissolved in 1 ml acetone for a stock solution. The PI stock solution was prepared by dissolving 2 mg of PI in 1 ml PBS. The FDA and PI stock solutions were stored at -20 °C, and 4 °C, respectively. The live/dead staining solution was prepared by adding 1.6 µl of FDA stock solution, and 10 µl PI stock solution in 1 ml serum-free culture medium (DMEM). Cells embedded in 3D collagen matrix at final concentration 10<sup>6</sup> cells/ml were loaded either in the migration arenas, or in the standard µ-Slide Chemotaxis. After gelation of the collagen matrix, the reservoirs of the chemotaxis chamber were filled with medium containing 0% or 10% FBS and the chambers were incubated at 37 °C and 5% CO<sub>2</sub> in a humid chamber. Three samples were prepared to monitor cell viability at the beginning of the experiment, after 24 h, and 48 h of cultivation. To differentiate the living and dead cells, at the given time-points the medium in the reservoirs was replaced by freshly prepared live/dead staining solution. The chambers were incubated for 5 min at 37 °C, protected from light. Then, fluorescent micrographs of the cells were taken with Nikon Eclipse Ti inverted microscope (Nikon GmbH, Düsseldorf, Germany) equipped with TexRed and FITC filter sets (Nikon), CFI Plan Fluor DL 4x objective (Nikon), and a CCD camera ORCA-Flash 4.0-LT (Hamamatsu Photonics, Hamamatsu City, Japan). The number of all viable and dead cells (stained green and red, respectively) in the migration arena was determined using the *Cell Counter* plugin in the NIH (National Institute of Health) software ImageJ [271, 272]. Approximately 200 cells were counted per arena. Cell viability was then quantified as the percentage of the viable cells in the arena.

---

### 3.2.3 $\mu$ -Slide Chemotaxis assay

The control chemotaxis experiments in the standard  $\mu$ -Slide Chemotaxis were performed according to the protocol provided by the manufacturer, as described previously [62, 211, 273]. For 2D experiments,  $2 \times 10^6$  cells/ml HT1080 were seeded in the channels of the chemotaxis chambers, which were coated with fibronectin beforehand. The slide with the cells was placed in a wet chamber and the cells were allowed to adhere for 1 h in an incubator. For a 3D experiment, HT1080 cells were seeded in the chambers embedded in bovine collagen type I matrix. Fabrication of the collagen gel is described above. After cell adhesion (2D)/collagen gelation (3D), the reservoirs of the chemotaxis chamber were filled with DMEM medium containing 0% or 10% FBS. A phase-contrast video of cell migration was recorded for 24 hours, with 10 min time-lapse interval, as described in section 3.2.6. Trajectories of 35–45 cells in the observation area of each image sequence were tracked manually using the NIH ImageJ *Manual Tracking* plugin. The chemotactic effect was evaluated using the *Chemotaxis and Migration Tool* from ibidi.

### 3.2.4 Migration arena chemotaxis assay

The handling of the  $\mu$ -Slide Chemotaxis equipped with the 3D hydrogel migration arenas (e.g., filling the compartments of the microfluidic chambers with reagents, sealing the chambers with plugs) was performed with several small adjustments according to the manual provided for the standard  $\mu$ -Slide Chemotaxis assay [273].

Before chemotaxis experiments, the slides with the arenas and the culture medium used in the experiment were pre-warmed and degassed by an overnight incubation at 37 °C. The arenas were stored filled with PBS, which was carefully removed from the whole chamber before the experiment. The migration arenas were then coated with fibronectin, or with collagen I (0.3 mg/ml bovine collagen in purified water for 1 h at 37 °C) for 2D or 3D experiments, respectively. Afterwards, the arena was rinsed with PBS. Cells were trypsinised, re-suspended in complete culture media or in collagen gel mixture at a concentration of  $1\text{--}2.5 \times 10^6$  cells/ml, and seeded in the arenas by rinsing  $2 \times 10$   $\mu$ l of cell suspension through the arena channel. To avoid trapping air-bubbles, the channel volume was not aspirated between the rinsing steps. To ensure a homogeneous distribution of the cells in the arena, the cell suspension was not directly injected into the channels, rather applied on top of one of the filling ports of the channel, and then pulled slowly through the channel by removing the same amount from the opposite port with a pipette. After the cell adhesion (2D)/collagen gelation (3D) was completed (30–60 min), the reservoirs were filled with medium containing the respective concentrations of chemoattractant. All filling ports of the chemotaxis chambers were sealed with plugs, and cells in the arena were imaged with phase-contrast microscopy at 4x magnification for 24 h (see Chapter 3.2.6).

In a control experiment, where nHEK proliferation was inhibited (Chapter 5.2.1), the medium

in the arena channel was replaced after the cells attached with a complete medium containing 10  $\mu\text{g}/\text{ml}$  mitomycin C (MMC). The cells were treated with MMC for 3 h at 37  $^{\circ}\text{C}$ . Then, the channel was washed two times with MMC-free medium and the reservoirs were filled with the chemoattractant solutions. In the experiments with EGFR (epithelial growth factor receptor) inhibitors AG-1478 and EGFR antibody 255, the inhibitors were added in the medium (both in the channels and the reservoirs) when the gradient was applied; i.e., with the chemoattractant solutions. The final concentration of AG-1478 and the EGFR antibody in the chemotaxis experiment was 200 nM, and 50 ng/ml, respectively. The inhibitors were used previously at these concentrations to inhibit the chemotactic signalling of EGFR [211].

### 3.2.5 End-point evaluation of chemotaxis in the migration arena assay

The end-point evaluation of chemotaxis was based on comparing cell distribution in the migration arena in the initial state and at a further time-point of the experiment. The chemotactic effect was quantified by the centre of mass displacement in the gradient direction—COMD, where the centre of mass is defined as the spatial average of all cell positions. Only the component along the gradient was considered, here arbitrarily assigned the y-direction, placing the origin of the y-axis on the lower edge of the migration arena (i.e., at the barrier further from the source reservoir). The COMD represents the change in the average position on the y-axis of all cells in the migration arena, and was computed as the difference of the average cell ordinate at the start ( $COMD_{start}$ ) and the end ( $COMD_{end}$ ) of the experiment:

$$COMD = COMD_{end} - COMD_{start} = \left[ \frac{1}{n} \sum_{i=1}^n (y_{i,end}) \right] - \left[ \frac{1}{n} \sum_{i=1}^n (y_{i,start}) \right]$$

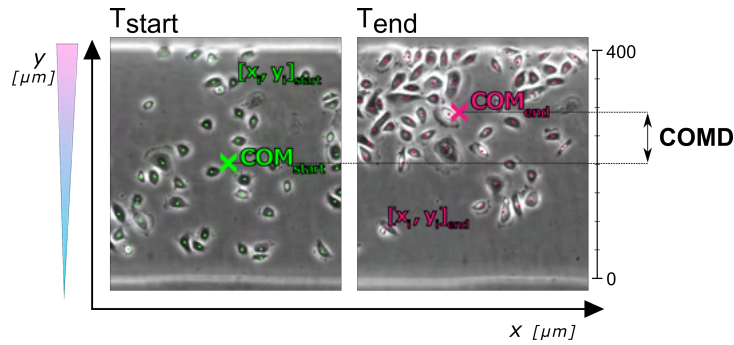


Figure 3.6: End-point evaluation of the chemotactic effect by quantification of the centre of mass displacement. Details of the migration arena with nHEK cells at the start of a chemotaxis experiment (left), and at the end-point; i.e., after 20 hours migration in the gradient of a chemoattractant (right). Spatial positions of all cells in the arena are determined. For computation of the COMD, only the component along the gradient (here assigned the y-direction) is considered. COMD then represents the difference between the average spatial position in the gradient direction of cells at the start and at the end of the experiment.

---

In case of random migration in all directions,  $COMD_{end}$  remains close to  $COMD_{start}$ , and  $COMD \approx 0$ . Directed migration leading to accumulation of cells at one side of the arena results in  $COMD \neq 0$ , indicating a chemotactic effect.

The end-point analysis of the migration arena chemotaxis assay was carried out as follows: two or more micrographs of the cell distribution in the migration arena were taken with a phase-contrast microscope, one at the beginning, other at given time-points of the experiment. The images were cropped to the inner size of the migration arena (area between the hydrogel barriers), and, in the gradient samples, the y-axis origin was set to the chemoattractant-distal side of the arena. The cells ordinates in the experiments with HT1080 cells (Chapter 4) were determined with the help of NIH software ImageJ [271,272] by manual selection of cell positions with the *Cell Counter* plugin, which lists the coordinates of the selected points in the micrographs. For the analysis of the 2D chemotaxis experiments with nHEK cells (Chapter 5), an automated routine was developed for retrieving the cell ordinates with the help of the ImageJ plugin *Analyze Particles*. The micrographs were opened in ImageJ as a stack, cropped to the size of the migration arena, and, if needed, rotated so that the chemoattractant-proximal side of the arena was on the top of the image. Then, the background of the image was subtracted, using the command *Process > Subtract Background*, which is based on the “rolling ball” algorithm [274]. The rolling ball radius was set to 20 pixels (approximately, the radius of a cell body), and the option “light background” was chosen, because the cells appear as dark objects on bright background. Then, the images of the stack were binarised with the *Threshold* plugin, choosing the “Minimum” method [275], setting the threshold to (0, 162), and the option “BlackBackground” to “false”. In next step, the *Process > Binary > Fill Holes* algorithm was applied. The processed images were then analysed with the *Analyze > Analyze Particle* command, which scans the binary images until the edge of an object is found, which is then outlined, and measured. The parameter particle size was set to  $> 100$  pixels, and the circularity to 0.01-1.00. The plugin then rendered a list of cell coordinates, which were used to compute the COMD.

### 3.2.6 Time-lapse microscopy

The cell migration in the chemotaxis assays was recorded by phase-contrast time-lapse microscopy for 24 h with 10 min time interval between frames, if not indicated otherwise. The imaging was performed on an Olympus CKX41 inverted microscope (Olympus Scientific Solutions, Waltham, MA, USA) equipped with a motoric stage (MW Tango, Märzhäuser Wetzlar GmbH, Wetzlar, Germany), a 4x UPlan FLN objective (Olympus), and a CCD camera uEye U3-3480ML-M-GL (IDS, Obersulm, Germany); or on a Nikon Eclipse Ti inverted microscope (Nikon GmbH, Düsseldorf, Germany) with a motorised stage (TI-SH-W), CFI Plan Fluor DL 4x objective (Nikon), and CCD camera ORCA-Flash 4.0-LT (Hamamatsu Photonics, Hamamatsu City, Japan). Both microscopes were equipped with an on-stage incubation system (ibidi GmbH, Munich, Germany) to maintain the cells at 37 °C in a stable 5% CO<sub>2</sub> humidified atmosphere for the whole duration of the experiment. The microscopes were controlled by the



---

Micro-Manager software [276].

### Visualisation of gradient in the migration arena

In order to visualise the development of the chemical gradient in the migration arena, fluorophores of varying molecular size were used to represent the chemoattractants, and their diffusion was monitored over time by fluorescent microscopy. The arena was filled with collagen type I matrix without cells (1.5 mg/ml; see Chapter 3.2.1). To establish the gradient, one of the reservoirs was filled with PBS and the other with the fluorophore solution; i.e., either 1  $\mu$ M Alexa Fluor488 (643 Da) or 0.1 mg/ml FITC-tagged dextran, 40 kDa (both diluted in PBS). The fluorescent signal in the gradient region of the migration arena was observed over time with the Nikon Eclipse Ti microscope equipped with a mercury light source (Intensilight C-HGFIE, Nikon), FITC filter set (Nikon), and a 60x oil-objective (CFI PLAN APOchromat, Nikon). Two rows of nine images across the middle part of the chemotaxis chamber were taken every 30 min, covering the 400  $\mu$ m wide arena, with a step of 50  $\mu$ m between the positions. The centre of the rows was aligned with the centre of the arena. The Z-plane was focused in the middle of the collagen layer, approximately 35  $\mu$ m above the slide surface. Additional micrographs were taken in the fluorophore-containing reservoir, at the extension of each row. Fluorescence intensity was measured in a 10  $\mu$ m<sup>2</sup> area in the centre of each frame using the NIH ImageJ software [271,272]. The measured signal was normalised to the maximal signal of the fluorophore taken in the reservoir at each time point. For control, the background signal was measured in the same chamber before the fluorophore was added to the reservoirs, and in a chamber containing 1  $\mu$ M Alexa Fluor488, or 0.1 mg/ml FITC-tagged dextran in both reservoirs, as well as in the 3D collagen matrix in the arena.

### 3.2.7 Traction Force Microscopy of chemotaxing cells

The traction forces applied by nHEK cells during their migration in chemical gradients were analysed with traction force microscopy. To enable visualisation and measuring of cell forces, the chemotaxis chambers were assembled with a soft, elastomeric substrate with covalently coupled fluorescent beads. The protocol for covalent coupling of beads to a soft elastomer for TFM substrates was based on EDC/NHS (ethyl-dimethyl-aminopropylcarbodiimide and N-hydroxy-succinimide) coupling chemistry and was developed at the Institute of Complex Systems-7, Forschungszentrum Jülich. The elastomeric substrates were fabricated of Sylgard 184 Silicone Elastomere Kit, as described previously [277,278]. The base and cross-linker components were mixed at 60:1 (w/w) ratio to yield substrates of 10 kPa stiffness. The elastomere was degassed, spin-coated (2700 rpm, 7 s) on thin glass coverslips (75x25 mm, thickness 0.08 mm), and cured for 16 h at 60 °C. Then, the elastomeric substrates were silanised. 5% 3-aminopropyl triethoxysilane was hydrolysed in 5% H<sub>2</sub>O in ethanol (pH 4.5–5.5) for 90 min at room temperature before use. Then, it was applied in a thin layer on top of the elastomere (1.5 ml per coverslip), and

---

incubated for 3 min. Afterwards, the substrates were washed thoroughly with 96% ethanol, and dried in vacuum for 30 min. In the meantime, the nanobeads (FluoSpheres Carboxylate, 0.2  $\mu\text{m}$ , crimson) were activated for the coupling reaction. NHS and EDC were dissolved in PBS (pH 6.0) to 200 mg/ml stock solutions. 10  $\mu\text{l}$  of sonicated bead suspension was added to 1 ml reaction mix containing 10  $\mu\text{l}$  SDS (sodium dodecyl sulfate, 10%), 100  $\mu\text{l}$  NHS stock solution, 100  $\mu\text{l}$  EDC stock solution, and PBS. The reaction mix was incubated for 15 min at room temperature. Afterwards, the activated beads were applied on the silanised elastomeric substrates and incubated for 10 min at room temperature. The uncoupled beads were then removed by 3x washing with ultra-pure water. The substrates were dried and carefully assembled with the sticky-Slide Chemotaxis. Before cell experiments, the slides were pre-heated overnight at 37  $^{\circ}\text{C}$ .

The nHEK cells were seeded into the fibronectin-coated TFM/chemotaxis chambers at a low density ( $5 \times 10^5$  cells/ml in complete culture medium) to enable monitoring of individual cells. After the cells adhered (1–2 h), unattached and dead cells were removed by washing the channels 2x with basal medium. Then, the reservoirs were filled with basal culture medium with or without 10 ng/ml TGF $\alpha$ . For the control samples with an uniform concentration of the chemoattractant, the whole chemotaxis chamber was filled with 10 ng/ml TGF $\alpha$  in basal medium. The gradients were established one day before recording the cell migration, and the slides were maintained at the standard cell culture conditions. Imaging of the cells and the fluorescent nanobeads was performed on the Nikon Eclipse Ti microscope with a 60x oil-objective (CFI PLAN Apochromat, Nikon), and TexRed filter set (Nikon) for 60 min, with 1 min interval between frames. The intensity of the excitation light (Intensilight C-HGFIE, Nikon) was regulated with a ND8 density filter in order to prevent a phototoxic damage of the cells. At each time-point, a phase-contrast image of the cell, and a fluorescent image of the respective part of the bead-decorated substrate beneath the cell were taken. At the end of the experiment, the cells were removed by trypsinisation, and a reference image of the beads on the relaxed substrate was taken. The bead displacement was measured and the traction forces computed with a TFM-software developed at the Institute of Complex Systems-7, Forschungszentrum Jülich, as described in [279, 280].

### 3.2.8 Light-sheet Fluorescence Microscopy

Light-sheet fluorescence microscopy was used to visualise the migration of chemotaxing HT1080 cells, stably transfected with the green fluorescent protein LifeAct-TagGFP2. The fluorescent tag labels the F-actin of the cells, allowing a long-time visualisation of the dynamic changes of the cytoskeleton during cell migration. The cell samples were prepared in FEP (fluorinated ethylene propylene) tubes (Bola S1815-04, with the refractive index of 1.338, inner diameter 0.8 mm, and outer diameter 1.6 mm). The tube was cut in 1.5–2 cm long pieces, which were sterilised with 70% ethanol and filled with cells embedded in collagen type I gel mixture. The collagen matrix was prepared according to the protocol listed in Table 3.1. Serum was

---

not added in the chemotaxis samples. The matrix gelled for 30–60 min at 37 °C in a humid chamber. Afterwards, 1-2 mm were cut off on both ends of the FEP tube with the cell sample, to prevent trapping bubbles between the gel matrix and the medium. Alternatively, short rings (3–5 mm) cut from a glass capillary with 2 mm in diameter were placed at both ends of the FEP tube, before loading the collagen mixture. Finally, the FEP tube filled with the polymerised matrix was fixed with parafilm to a 1 ml syringe filled with cell culture medium (DMEM) containing 10% FBS. The other end of the FEP tube was submerged in serum-free medium in a 15 ml falcon tube. The samples were then incubated in an upright position at cell culture conditions overnight to allow the generation of a stable gradient across the whole sample. On the following day, the syringe with the mounted sample was taken out of the falcon tube and placed in the sample holder of a Zeiss Lightsheet Z.1 microscope (ZEISS, Oberkochen, Germany). The sample chamber was filled with sterile, serum-free medium. To visualise the gradient across the sample, the FEP tubes were filled with collagen matrix without cells. The syringe was loaded with 10 µl of AlexaFluor 488 in PBS, and the other end of the sample was submerged in PBS. The fluorescence signal in the collagen matrix was measured 20 hours after mounting the sample to the syringe. A sequence of fluorescent images was taken from the top to the bottom of the FEP tube with a 300 µm step inside of the collagen gel, in ten parallel Z-planes (in 2 µm step). The grey value of each frame was measured with the NIH software ImageJ [271,272].

The LSM experiments were performed at the Institute of Molecular and Cellular Anatomy, RWTH Aachen, with help from Prof. Dr. Reinhard Windoffer, Dr. Volker Buck, and Dr. Sebastian Kant.

### 3.3 Statistical analysis

If not indicated otherwise, the experiments were performed in three or more independent replicates, and data are presented as mean  $\pm$  standard error (SEM). To test for statistical differences, one-way, or two-way ANOVA followed by Dunnett’s multiple comparison test was performed, considering  $p=0.05$  as the level of significance. Graphs and statistical analysis were made in the GraphPad Prism 7 software (GraphPad Software, San Diego, CA, USA). Significantly different results are indicated in the graphs with stars (\*  $p<0.05$ ; \*\*  $p<0.01$ ; \*\*\*  $p<0.001$ ; \*\*\*\*  $p<0.0001$ ). Hairplots representing the path of migrating cells in the chemotactic experiments were generated with the *Chemotaxis and Migration Tool* (ibidi). The software was also used to compute the parameters describing the migration of single cells (FMI, COM, velocity, directness). The force maps and statistics for the TFM experiments were generated by the TFM-software developed at the Institute of Complex Systems-7, Forschungszentrum Jülich, with help of Dr. Ronald Springer and Georg Dreissen. The micrographs shown in the thesis were processed with the NIH ImageJ software [271,272].



## 4 Establishment of a direct end-point chemotaxis assay: Results and Discussion

One focus of this thesis was the development of an end-point method by adapting the chamber of a bridge type chemotaxis assay, as implemented in the  $\mu$ -Slide Chemotaxis, in a way that enables confinement of cell migration to defined patterns in the gradient area. The underlying motivation was to fasten and simplify the evaluation of the chemotactic response of slow moving cells. In the standard  $\mu$ -Slide Chemotaxis it is not possible to evaluate the chemotactic cell behaviour solely from the end-point state of the experiment, as shown in Fig 4.1. This is due to the fact that the cells—initially homogeneously distributed in the gradient area of the chemotaxis chamber—are free to migrate back and forth from the middle channel into the adjacent medium reservoirs. As described in Chapter 2.1, slow moving cells migrate along diffusive trajectories, and the directionality of the movement is demonstrated rather as an overall tendency to follow a preferred direction in a long-term perspective; in contrast to the persistent migration straight towards the chemoattractant source, which is typical for fast moving cells. Besides, it is difficult to prevent cells from escaping into the reservoirs while filling the channel with the cell solution, which results in a number of cells adhering in the proximal area of the reservoirs. These cells then migrate into the channel during the experiment, further biasing the overall end-point distribution in the standard assay. Therefore, the most straightforward way how to enable the end-point evaluation of chemotaxis in such gradient generator is to restrict cell migration to the gradient area; i.e., to the middle channel of the chemotaxis chamber. Confining the cell migration should allow to evaluate the chemotactic response from the end-point of the experiment, based on the change in cell distribution in the restricted adhesive areas resulting from chemically induced directed migration (Fig 1.2).

One option how to restrict the cell adhesion and motility to selected areas of the chemotaxis chamber is to enclose the cells in micro-structured wells or migration arenas from bio-compatible cell-repellent polymers (Chapters 4.1.1, 4.2). Another approach is to selectively functionalise the surface of the chamber with adhesive molecules by 2D micro-patterning techniques (Chapter 4.1.2). There is a multitude of available micro-patterning techniques; the basic principles of the method were described in Chapter 2.4. Several established methods were tested in this thesis to fabricate the intended confinement patterns, either directly inside a closed chemotaxis channel, or in an open system on a substrate that was fixed to the chamber subsequently.

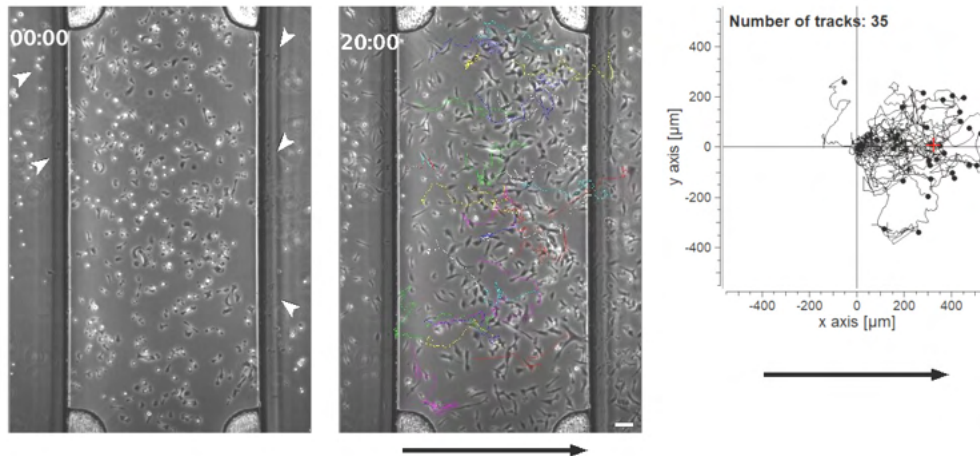


Figure 4.1: Cell distribution in the  $\mu$ -Slide Chemotaxis at the beginning and at the end of an chemotaxis experiment. The experiment was performed following the protocol from the manufacturer, as described in Section 3.2.3. The micrographs show the HT1080 cells after seeding in the middle channel of the standard, unmodified  $\mu$ -Slide Chemotaxis (left). A small portion of the cells adhered also in the adjacent reservoirs (white arrows). The micrograph on the right shows the cell distribution in the same slide after 20 hours of cell migration in a FBS gradient (0% - 10%, from left to right). Scale bar = 100  $\mu\text{m}$ . The coloured lines in the overlay depict the migration paths of 35 randomly selected cells reconstructed by manual tracking. The hairplot shows the migration paths from the experiment, with their starting points set to (0,0). 34 of the tracked cells migrated in direction of the gradient (indicated), towards the 10% FBS. However, this chemotactic effect could not be recognised from the end-point distribution of the cells in the gradient area of the chemotaxis chamber.

The disposable, commercially available chemotaxis chamber  $\mu$ -Slide Chemotaxis was chosen as a suitable tool to generate the long-term stable gradient that is necessary for studying chemotaxis of slow moving cells. The geometry and properties of the chemotaxis assay were described in detail in Chapter 2.3.4. The slide is provided either as a closed chamber with a plasma-treated plastic foil bottom (ibiTreat), or as a open chamber (sticky-Slide Chemotaxis) with a self-adhesive underside that can be assembled with a pre-patterned surface, e.g., a glass microscopic slide. The closed system was used for in-channel micro-patterning and for preparing micro-structures from 3D UV-responsive hydrogel, and the sticky-Slide for 2D assays based on pre-patterned surfaces. However, the low volume and specific geometry of the  $\mu$ -Slide Chemotaxis limited the possibilities of in-channel micro-patterning, and also complicated the positioning of pre-fabricated patterns.

As will be shown in the next chapters, in regard to the labour-intensiveness and success-rate of the fabrication procedure, micro-structuring of spatial barriers from a PEGnorb-based 3D hydrogel inside of the chemotaxis chambers was the most effective and versatile approach to enclose cell migration in the gradient area. The resulting migration arena chemotaxis assay is presented in Chapter 4.2). Other, less successful approaches are briefly described in Chapter 4.1 in order to illustrate the limitations of surface functionalisation in microfluidic chambers.

---

## 4.1 Establishment of a 2D end-point chemotaxis assay: micro-wells and micro-patterns

One approach to fabricate the 2D end-point chemotaxis assay investigated in this thesis was the functionalisation of the surface of the gradient area of the chemotaxis chamber with rectangular or circular adhesion patterns. Three different micro-patterning techniques were tested: selective passivation of a glass surface with the non-adhesive polymer polyethylene glycol dimethylacrylate (PEG-DMA; experimental details described in Section 3.1.1); micro-patterning of fibronectin with the help of removable silicon wells (stencil-assisted patterning; 3.1.2), and in-channel, photo-induced activation of a passivated surface (3.1.3).

### 4.1.1 PEG-DMA micro-wells for 2D chemotaxis assay

Three 30  $\mu\text{m}$  high PEG-DMA structures, each enclosing three micro-wells with the dimensions of 400  $\mu\text{m}$   $\times$  800  $\mu\text{m}$  apiece, were fabricated by photolithography as described in Section 3.1.1. The structures were prepared on top of a silanised glass coverslip the size of a microscopic slide, in such a way that each structure was placed in the gradient area of one of the chemotaxis chambers after mounting the coverslip to the sticky-Slide Chemotaxis. The long side of the rectangular micro-wells in the chemotaxis chamber was aligned with the gradient direction. After mounting the patterned surface to the chemotaxis chambers, the bottom of the micro-

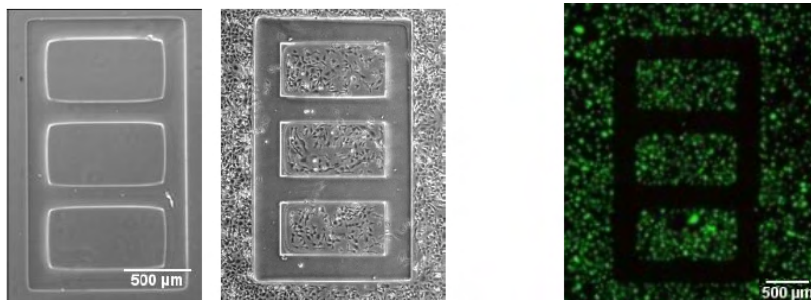


Figure 4.2: PEG-DMA micro-wells. Left: Phase-contrast micrographs of the PEG-DMA structure on a glass coverslip before and after seeding HT1080 cells. Right: PI/FDA staining of HT1080 cells cultivated in presence of the PEG-DMA structure confirmed the bio-compatibility of the polymer. Living cells are stained green, dead cells red. HT1080 cells did not attach to the PEG-DMA passivated surface. Scale bar = 500  $\mu\text{m}$ .

wells was coated with fibronectin to promote cell adhesion. Subsequently, cells loaded into the middle channel of the chemotaxis chamber adhered specifically to the protein patterns; i.e., in the PEG-DMA enclosed micro-wells (Fig 4.2). The application of a chemoattractant gradient then biased the direction of cell migration and the cell mass in the micro-wells accumulated on the side proximal to the source reservoir (Fig 4.3). Thus, the chemotactic response in a micro-well could be identified from the end-point of the experiment and quantified by evaluation of the COMD, as introduced in Chapter 3.2.5.

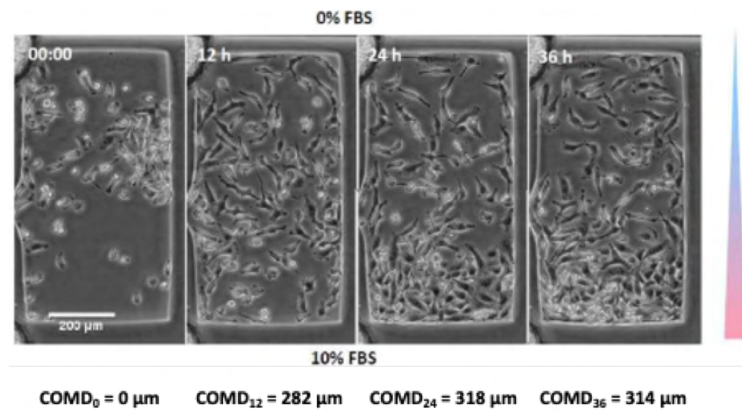


Figure 4.3: The time-lapse sequence of micrographs shows the distribution of HT1080 cells migrating in a gradient of 10% FBS in one of the PEG-DMA micro-wells at the start of the experiment, and after 12 h, 24 h and 36 h. Over time, the centre of mass of the cells shifts in the direction of the increasing concentration of the chemoattractant (downwards). The chemotactic effect was quantified by evaluation of the COMD (3.2.5); aligning the origin of the y axis with the upper rim of the micro-well. Note that the initial cell distribution in the well is not homogeneous (left), because the elevated structure of the PEG-DMA in the bridge area of the chemotaxis chamber complicates the seeding of cells. Scale bar = 200  $\mu\text{m}$ .

This approach has several advantages; for example, the PEG-DMA structures are rigid and mechanically stable and it is possible to store them dry. Besides, the three independent micro-wells situated in each chemotaxis chamber provide for a robust statistical analysis of COMD. However, multiple complications were encountered during the fabrication and experimental procedure. First of all, the fabrication procedure itself is comparatively time-demanding and labour-intensive, as each structure was fabricated independently. Quick handling and extensive washing steps were crucial during the procedure in order to prevent unspecific polymerization of PEG-DMA in areas adjacent to the illuminated surface. Also, mounting of the patterned surface to the sticky-Slide Chemotaxis and aligning the structures precisely to the gradient area of the chemotaxis chambers is complicated. Furthermore, the height of the PEG-DMA structures is about 30  $\mu\text{m}$  due to the fabrication procedure, thus creating a barrier that prevents homogeneous flow of the cell suspension during seeding of the cells in the narrow channel of the chemotaxis chamber (which is 150  $\mu\text{m}$  high in the sticky-Slide Chemotaxis). As result, the initial cell distribution in the arenas was uneven (see Fig 4.3, left micrograph), which could bias the evaluation of the chemotactic response.

#### 4.1.2 Surface functionalisation in the chemotaxis chamber by 2D micro-patterning methods

In order to improve the homogeneity of the initial cell distribution in the 2D end-point chemotaxis assay, flat, adhesive 2D micro-patterns were prepared in the chemotaxis chamber, instead of the elevated micro-wells from PEG-DMA.



## Stencil-assisted patterning

Probably the most straightforward way of preparing adhesive 2D micro-patterns is by defining the pattern with a removable stencil that protects the surface surrounding the pattern. The exposed area of the pattern is incubated with an adhesive molecule (e.g., fibronectin), and subsequently, after removal of the stencil, the surrounding surface is passivated with a hydrophobic agent to prevent unspecific cell adhesion. A removable silicon well, the Culture Insert FulTrack from ibidi (disposable silicone well of 400  $\mu\text{m}$  diameter, Fig 3.2A,B), was used here to yield such selective coating with fibronectin. The removable wells were placed on the substrate and filled with fibronectin solution, as described in Chapter 3.1.2. The wells were positioned on the foil in such way that, after assembly with the sticky-Slide Chemotaxis, each fibronectin pattern was in the centre of one chemotaxis chamber. In a second step, the area surrounding the adhesive spots was passivated with pluronic to prevent unspecific cell adhesion outside the pattern. However, since the removable wells were positioned on the substrate manually, achieving a precise alignment of the pattern and the chemotaxis chambers was problematic (Fig 4.4A), and the success rate of the fabrication procedure was low ( $< 30\%$ ).

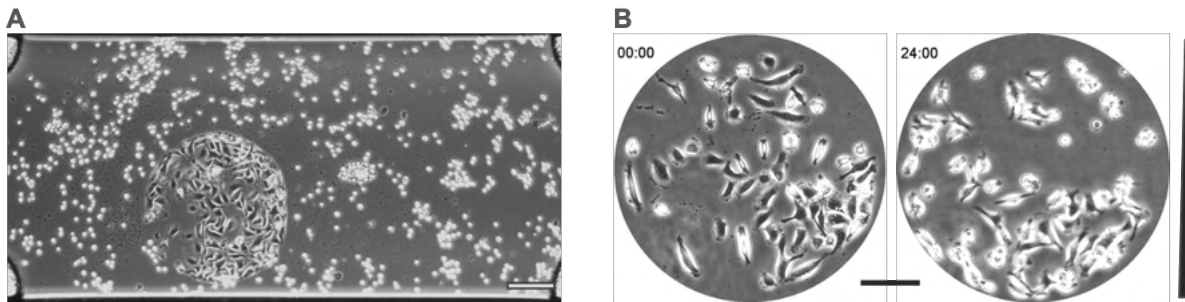


Figure 4.4: Cell adhesion and chemotaxis on round fibronectin patterns. **A.** The micrograph of the patterned chemotaxis chamber shows HT1080 cells adhering to the fibronectin coated area, which was defined by the silicon micro-well (400  $\mu\text{m}$  diameter; the adhered cells appear as dark and prolonged, spindle-shaped). The area surrounding the round pattern was passivated with pluronic, which prevented unspecific cell adhesion. The unattached cells (small, rounded bright dots) were washed away before the chemotaxis experiment. As demonstrated, an alignment of the pattern with the centre of the chemotaxis chamber was difficult to achieve. **B.** The detail of the chemotaxis chamber shows the cell distribution on the fibronectin pattern at the beginning and at the end of an chemotaxis experiment. The suspension of HT1080 cells was loaded in the patterned chemotaxis chamber and after cell adhesion to the pattern and removal of the unattached cells, the reservoirs of the chemotaxis chamber were filled with cell culture medium containing 0%, or 10% FBS, respectively. The direction of the gradient is indicated. Over the duration of the experiment (24 h), the cells accumulated in the part of the patterned area proximal to the chemoattractant source. Scale bars = 100  $\mu\text{m}$ .

---

## Photolithographic in-channel micro-patterning on passivated surfaces

Photolithography is a powerful means to prepare precisely defined micro-patterns. To prevent problems with aligning the adhesive patterns with the chemotaxis chambers, micro-patterning methods were applied that enable light-induced activation of passivated, non-adhesive substrates directly inside of a closed microfluidic channel. In this process, the bottom surface of the chemotaxis chamber was first chemically modified with a hydrophilic, cell-repellent polymer. Then, the passivated substrate was selectively activated by light-induced functionalisation with reactive groups, using a suitable photomask to transfer the micro-pattern on the substrate. Subsequently, the substrate was incubated with an adhesive molecule that selectively binds to the activated pattern (as described in Chapter 3.1.3, Fig 3.3).

Two methods based on this principle were tested, each employing a different chemistry. The experimental details are described in Chapter 3.1.3. The first method was based on photo-immobilisation of adhesive proteins on a polymer photografted on the bottom of the chemotaxis channel [251]. This method uses grafting of a cell-repellent polymer functionalised with reactive groups to a plasma treated surface inside a closed channel [252]. Exposure to UV light in presence of a photoinitiator induced formation of free radicals both on the plasma-treated surface and also on the polymer, which created a non-adhesive polymer layer by covalent links. In the same way, adhesive molecules—e.g., the adhesion-mediating peptide RGD—were subsequently bound to the remaining reactive groups on the polymer, using patterned UV exposure to restrict the coupling to defined areas.

Another tested method was protein adsorption by photobleaching [250]. For this method, chemotaxis chambers were assembled with a cell-repellent surface (*BioInert* substrate, ibidi) that prevented cell adhesion. Then, a defined micro-pattern of reactive groups was created on the surface by light-induced adsorption of alkyne-functionalised fluorescein (FAM-6). Subsequently, a commercial click chemistry reaction kit was used to bind a cyclic form of the adhesive peptide RGD functionalised with an azide group to the pattern, as described in Materials and Methods, Section 3.1.3.

However, both of the tested methods generated only faint patterns of adhesive molecules in the bridge area that did not support cell adhesion sufficiently. The morphology and motility of cells that were able to adhere to the patterned surface was clearly affected by a too low density of adhesion sites (Fig 4.5).

This only occurred while micro-patterning inside the closed chemotaxis chamber. In open systems, such as a culture dish, or in microfluidic channels with larger volumes, it was possible to prepare micro-patterns that were recognised by cells. They adhered and showed normal morphology and motility. Therefore, it seems that the specific geometry of the  $\mu$ -Slide Chemotaxis (the chamber sections adjacent to the middle channels are divided by rims that could cause light scattering during photolithography) and low volume of the gradient area (140 nl in the closed variant of the slide, and 300 nl in the self-adhesive variant) thwarted the fabrication of cell migration confining micro-patterns inside of the bridge channel.

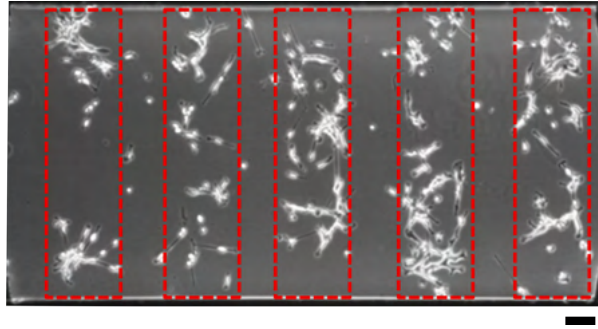


Figure 4.5: A micrograph of the gradient area of a chemotaxis chamber show HT1080 cells attached to a micro-pattern of RGD peptide on a PEG8norb passivated surface. The patterned area is outlined in red. The abnormal morphology and uneven distribution of the cells indicates poor adhesion on the pattern. Scale bar = 100  $\mu\text{m}$ .

## 4.2 2D/3D migration arena enclosed by a cell repellent 3D hydrogel<sup>1</sup>

The aim of the work presented in this chapter was to produce hydrogel barriers that would function as a membrane that prevents the cells in the gradient area of a chemotaxis chamber from migrating into the medium reservoirs, but, at the same time, does not hinder the diffusion of the chemoattractant and the formation of the gradient across the bridge area. A PEG-based hydrogel was employed, which could be micro-structured by photolithography directly inside of the chemotaxis chamber, to fabricate the 3D barriers that separated the middle channel from the reservoirs, as depicted in Figure 4.6.

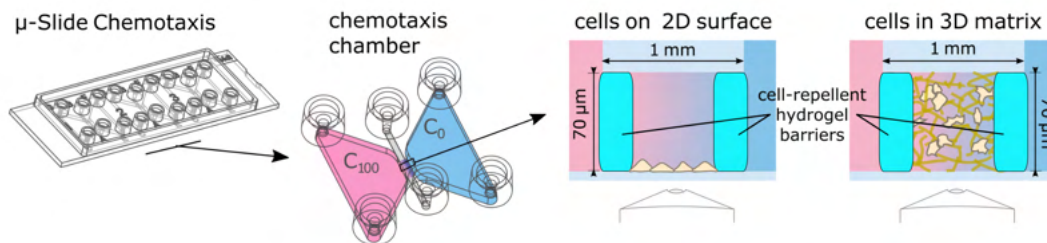


Figure 4.6: Scheme of the hydrogel-enclosed migration arena in the  $\mu$ -Slide Chemotaxis. The 3D hydrogel barriers were placed between the reservoirs and the bridge area of the chemotaxis chamber. In the resulting middle channel the cells could be seeded either in 2D, or embedded in a 3D matrix. The figure was adapted from [281] under the terms of the Creative Commons Attribution License.

The cell-confining migration arena is here represented by the middle channel of the chamber, enclosed by the hydrogel structures. The 3D barriers span along the whole height of the channel and thus enable seeding of the cells in the arena both in 2D, or embedded in a 3D matrix. In this

<sup>1</sup>Part of this chapter and figures are adopted from Tomasova *et al.*, 2019 [281].

set-up, the cell migration is confined only in the direction parallel to the gradient. The cells are free to migrate along the length of the migration arena and beyond the gradient area towards the filling ports of the chemotaxis chamber. However, in order to evaluate the chemotactic behaviour, it is safe to neglect the migration perpendicular to the gradient.<sup>2</sup>

The functionality of this set-up was verified in cell experiments presented in Section 4.2.3. As depicted in the scheme in Fig 4.7, the chemotaxis effect could be detected in the arena as an accumulation of the cells at one of the barriers. In order to quantify this effect, the COMD (centre of mass displacement) was introduced, as defined in Chapter 3.2.5.

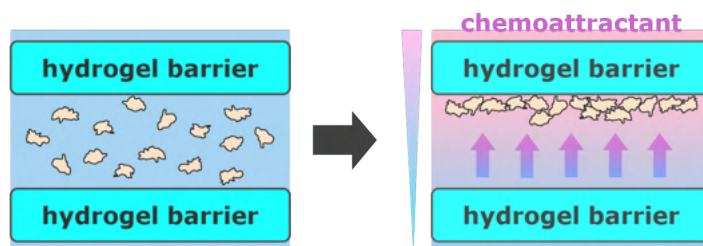


Figure 4.7: Scheme of cell distribution in the migration arena assay at the beginning and at the end of a chemotaxis experiment. Initially, cells are distributed homogeneously in the migration arena. Chemotactic response to a gradient of a chemoattractant leads over time to accumulation of cells at one side of the arena. The chemotactic effect can be identified from the end-point of the experiment, based on the displacement of the cell mass. The figure was adapted from [281] under the terms of the Creative Commons Attribution License.

#### 4.2.1 Fabrication of barriers from a 3D PEG-based hydrogel

The hydrogel barriers framing the migration arena were fabricated by standard photolithography directly inside the chemotaxis chambers (Fig 4.8). The experimental procedure is described in further detail in Materials and Methods, Section 3.1.4. The rectangular structures—barriers—were placed along the border of the cross-section of the reservoirs and the middle channel of the chemotaxis chamber (2 mm), filling the whole height of the channel (i.e., 70  $\mu\text{m}$ ). The width of each barrier was 300  $\mu\text{m}$ , enclosing a 400  $\mu\text{m}$  wide arena. Migration arena of this width could accommodate a sufficient number of cells for a statistically relevant analysis of chemotaxis (typically, when the cells are seeded in an optimal density, the arena holds 100-200 cells). Fabrication of a wider arena was not possible, since barriers thinner than 300  $\mu\text{m}$  were unstable, prone to bending or rupture.

The composition of the pre-polymer solution was optimised to yield stable 3D hydrogel microstructures. The mechanical stability of the barriers depended on the stiffness of the hydrogel, which is related to the concentration of the PEG4norb monomers in the pre-polymer solution,

<sup>2</sup>Previous detailed analysis of cell migration in the standard  $\mu$ -Slide Chemotaxis assay showed that cell motility and displacement of the cell mass in the direction perpendicular to the gradient is not affected by the chemoattractant [38,39,211].

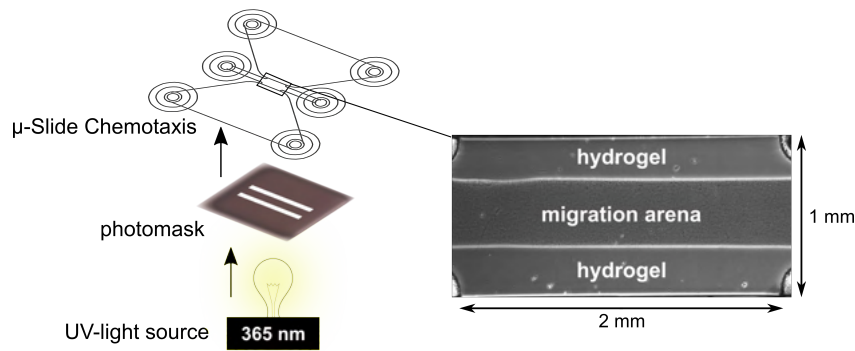


Figure 4.8: Schematic of fabrication of the migration arena. The hydrogel barriers that form the migration arena were micro-structured photolithographically directly inside of the chemotaxis chamber, as described in Chapter 3.1.4. The pre-polymer solution of the hydrogel was loaded into the middle channels of the  $\mu$ -Slide Chemotaxis chambers. The slide was then placed on a quartz photomask and aligned with the rectangular pattern of the barriers. Hydrogel polymerisation was induced by short illumination with UV light (365 nm) through the photomask. Non-polymerised hydrogel was washed away and the arena could be filled with cell solution for a 2D chemotaxis experiment, or with a 3D matrix containing cells (e.g., collagen gel).

and to the ratio of the monomers and the cross-linker [270]. Barriers fabricated from too soft hydrogel (i.e.,  $<3$  mM PEG<sub>4</sub>norb, cross-linker ratio  $<1$ ) tended to swell and bend, or split. With increasing polymer concentration and cross-linking, the gel rigidity grows; however, too high PEG<sub>4</sub>norb concentration ( $>3$  mM) led to an unspecific polymerisation between the barriers in the chemotaxis chamber, which blocked the migration arena channel. Pre-polymer solution containing 3 mM PEG<sub>4</sub>norb in 1:1 ratio with the cross-linker was optimal for fabrication of spatially defined and stable micro-structures inside of the chamber. The densely cross-linked network (the pore size on the scale of several nanometres [66]) and non-adhesive character of the resulting hydrogel prevented cells from migrating into the gel, confining them in the migration arena. The slides with the hydrogel-framed migration arenas filled with PBS could be stored for several months at 4° C.

#### 4.2.2 Visualisation of gradient formation in the migration arena

To verify that a stable and linear gradient was formed and sustained across the migration arena, the concentration profile of a substance diffusing from the source reservoir was visualised over a long-term time period in arenas filled with 3D collagen matrix, using fluorescent dyes to simulate the chemoattractant. Two fluorophores of a different size were used, AlexaFluor 488 (643 Da), and FITC-labelled 40 kDa dextran (FITC-dextran) to represent the diffusion of small and larger molecules, respectively. Cells in their physiological environment are exposed to chemical agents of varying size; most of the motogenic growth factors are typically small polypeptides with a molecular weight below 30 kDa [30,282]. The fluorescent dye was loaded in one of the reservoirs of the chemotaxis chamber, and the fluorescence intensity was measured

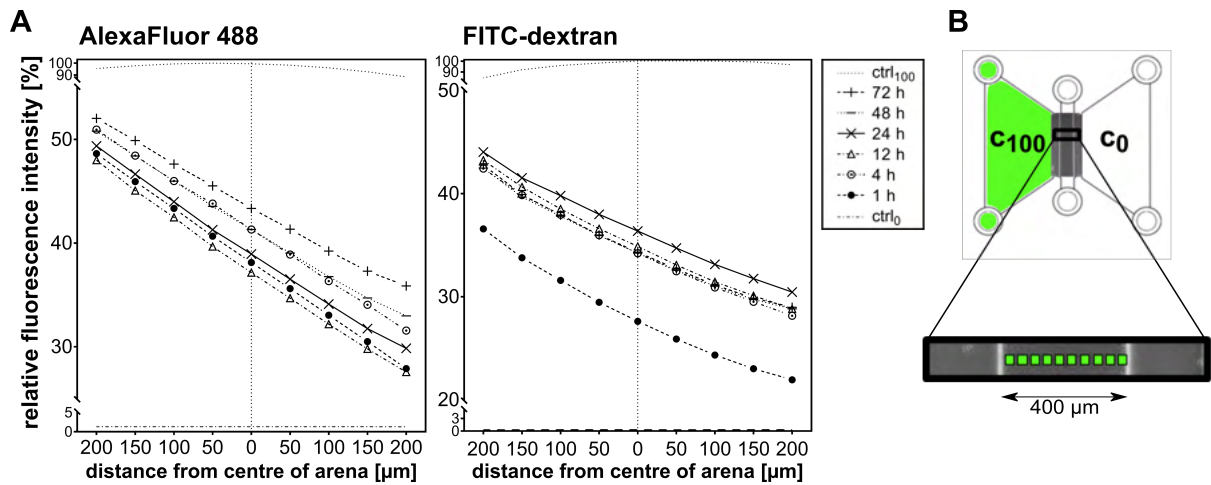


Figure 4.9: Visualisation of the gradient in the 3D migration arena assay. **A.** The concentration profiles of Alexa Fluor 488 (643 Da; left) and FITC-dextran (40 kDa; right) are represented by the fluorescence intensity, which was measured at nine positions across the migration arena (indicated in green in the scheme in **B**), 30  $\mu\text{m}$  above the bottom of the chamber; i.e., inside of the 3D collagen gel that fills the migration arena. The graphs show that a long-term stable, linear gradient was formed, and sustained up to 72 hours. Control measurements  $\text{ctrl}_0$  and  $\text{ctrl}_{100}$  were performed in absence of the fluorophore, or in a chamber uniformly filled with the maximal fluorophore concentration, respectively. Graphs show representative results of three experiments. Due to the fluctuations in the intensity of the illumination source (mercury lamp) between experiments, the absolute values of the measured fluorescence signal vary between the replicates. However, the data show a stable trend that is demonstrated in the shown graphs. Origin of the x-axis represents the centre of the migration arena. Part of the figure was adapted from [281] under the terms of the Creative Commons Attribution License.

at several points across the migration arena (Fig 4.9B) over a 72 hours time-period with a fluorescence microscope (see Section 3.2.6 for experimental details). The results shown in Fig 4.9 indicate that a linear gradient was formed within several hours across the arena and remained stable over the whole duration of the experiment. The initial phase of gradient formation of FITC-dextran was slower when compared to AlexaFluor 488, but the gradient of the larger molecule also reached a linear state by 4 h after the start of the experiment. The linearity of the detected fluorescence intensity signal was verified in a separate experiment.

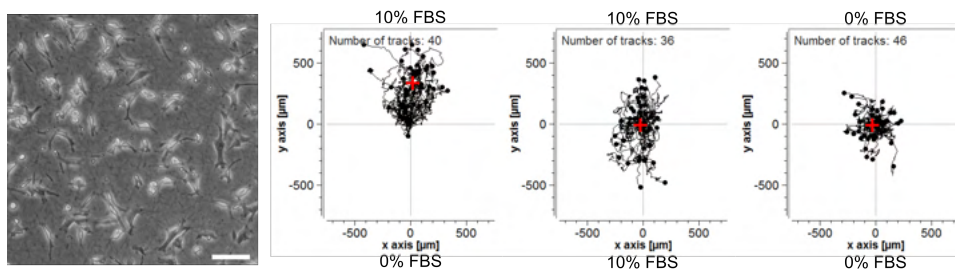
### 4.2.3 Validation of the migration arena chemotaxis assay on the example of HT1080 chemotaxis in a FBS gradient

In order to validate the functionality of the end-point chemotaxis assay, the migration arena assay was employed to examine the chemotaxis of HT1080 cells towards FBS. Chemotaxis experiments were performed either in 3D (with cells embedded in a collagen I matrix), or in 2D (on a fibronectin-coated surface), as described in Chapter 3.2.4. The chemotactic effect was evaluated from the end-point state of the experiment and quantified as COMD (introduced in

Chapter 3.2.5). The results obtained with the end-point analysis were compared with that of the manual tracking, and with results obtained in the standard  $\mu$ -Slide Chemotaxis assay. As control, non-directional cell migration in uniform concentrations of 10% or 0% FBS was also studied.

The previously described chemotactic behaviour of the model cell line was first confirmed by performing the standard  $\mu$ -Slide Chemotaxis assay, following the protocol provided by the manufacturer (see Chapter 3.2.3 for experimental details). The cell migration in the gradient of FBS was analysed both in 2D on fibronectin coated substrate, and in 3D in a collagen type I matrix. The coating parameters and preparation of the 3D matrix are detailed in Chapter 3.2.1. The results of the control experiment are presented in the Fig 4.10.

#### HT1080 in 3D collagen matrix



#### HT1080 on 2D fibronectin-coated surface

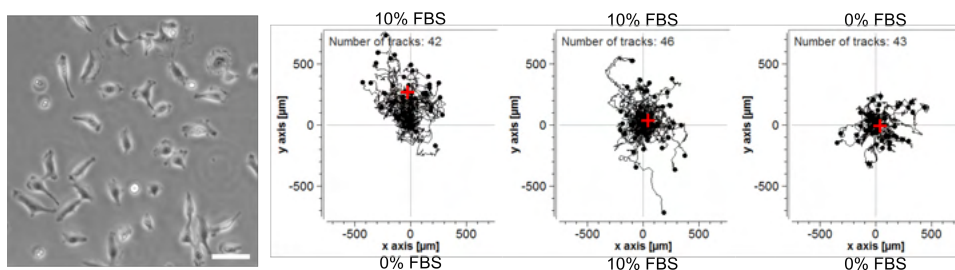


Figure 4.10: Chemotaxis of HT1080 cell in a gradient of fetal bovine serum in the standard  $\mu$ -Slide Chemotaxis assay. The micrograph and the hairplots in the upper row represent HT1080 migration in a 3D collagen I matrix. The lower row of images represents the locomotion of HT1080 in 2D, on a fibronectin-coated surface. Scale bars = 100  $\mu$ m. The hairplots show trajectories of cells that migrated in 0-10% gradients of fetal bovine serum (FBS) for 24 hours, or in homogeneous concentrations of 10% FBS and 0% FBS, from left to right. While cells exposed to a gradient of FBS migrate predominantly in the direction of the increasing FBS concentration, the directions of the cell paths in the uniform conditions are random. The longer migration paths of HT1080 in 10% FBS respective to 0% FBS indicate the chemokinetic effect of FBS. The cell migration was monitored in the  $\mu$ -Slide Chemotaxis assay via videomicroscopy with a 10 min time-lapse interval for 24 hours, and the trajectories were reconstructed by manual tracking of 30-40 cells per sample throughout the entire time-lapse recording. The dots in the hairplots represent the end-point of each cell, and the red cross the centre of the cell mass at the end of the experiment. The figure show representative results of at least three independent experiments.

## Verification of the bio-compatibility of the 3D hydrogel by live and dead cell staining

Before analysing the HT1080 chemotaxis in the migration arena assay, the effect of the hydrogel barriers on cell survival was investigated. The bio-compatibility of the 3D hydrogel was verified by examining cell viability in 3D migration arenas by differential live and dead staining with fluorescein diacetate (FDA) and propidium iodide (PI), as described in Chapter 3.2.2. The method is based on metabolisation of FDA into a green fluorescent metabolite—fluorescein—by living cells. Thus, living cells could be identified by the green fluorescent signal. In contrast, the red fluorophore PI is a DNA-binding molecule that cannot pass the intact membranes of living cells and enters only into dead cells. Figure 4.11 shows merged fluorescent micrographs of the live (green), and dead (red) cells in the migration arenas at the beginning of the experiment, and after 24 and 48 hours of cell migration. The results of the viability analysis presented in the graph in Figure 4.11 confirm that the 3D hydrogel does not affect survival of HT1080 cells in the arenas when compared to cells migrating in a 3D collagen matrix within a standard  $\mu$ -Slide Chemotaxis (ctrl).

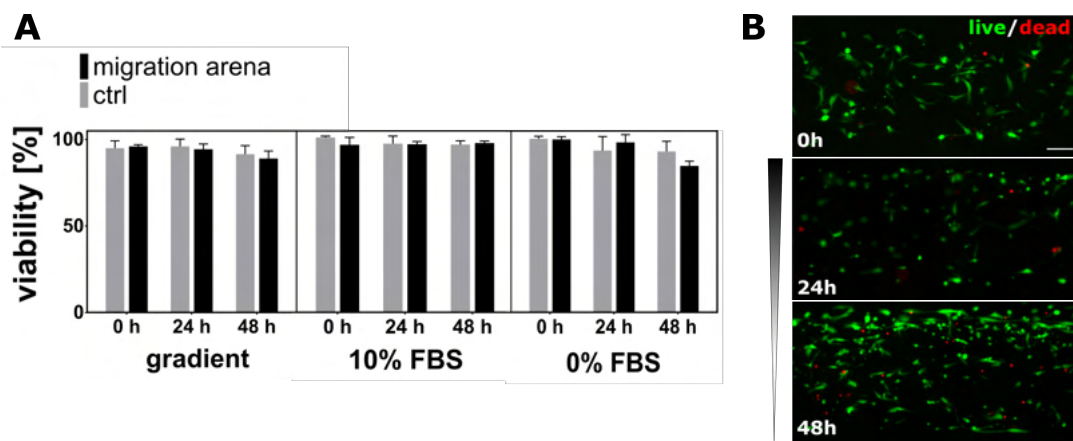


Figure 4.11: Cell viability in the 3D migration arena assay. **A.** Viability of HT1080 cells embedded in a 3D collagen matrix in the migration arena (black bars), and in standard  $\mu$ -Slide Chemotaxis (ctrl; grey bars), in gradual or uniform concentration of FBS was evaluated with the FDA/PI live and dead staining. The bars represent the mean rate of viable cells + SD ( $n=3$ ). In average, 200 cells per arena were analyzed. **B.** Merged fluorescent images show an example of live (green) and dead (red) staining of the HT1080 cells in the migration arena in a gradient of FBS. The direction of the gradient is indicated. Scale bar = 100  $\mu$ m. The figure was reprinted from [281] under the terms of the Creative Commons Attribution License.

The viability was examined in a gradient of 10% FBS, and in uniform concentrations of 10% or 0% FBS. The viability in the serum-free conditions (0% FBS) decreases after 48 hours incubation, but there is no significant difference between the survival in the migration arenas and the control, unmodified  $\mu$ -Slide Chemotaxis.



---

## Stabilisation of the 3D matrix in the migration arena by collagen coating

Studying migration and chemotaxis of the fibroblast-like HT1080 cells is most relevant in a 3D environment, as these cells move through 3D tissues *in vivo*, secreting matrix metalloproteases (MMPs) to degrade the surrounding matrix. Therefore, the cells were embedded in a 3D matrix of bovine collagen I and their chemotactic response to a gradient of fetal bovine serum (FBS) was evaluated by the end-point analysis in the migration arena chemotaxis assay. As the cells moved through the 3D matrix along the collagen fibres, they exerted traction forces on the fibres that resulted in a detachment of the matrix from the hydrogel barriers (Fig 4.12, left panel).

This complication occurred due to the non-adhesive properties of the hydrogel barriers that do not provide any attachment spots for stabilizing the collagen matrix in the arena. In order to steady the collagen matrix in the migration arena, the channel was pre-coated with soluble collagen I before the experiment. The treatment improved the stability of the 3D collagen and prevented the matrix from shrinking and detaching from the channel surface and the barriers (Fig 4.12, right panel).

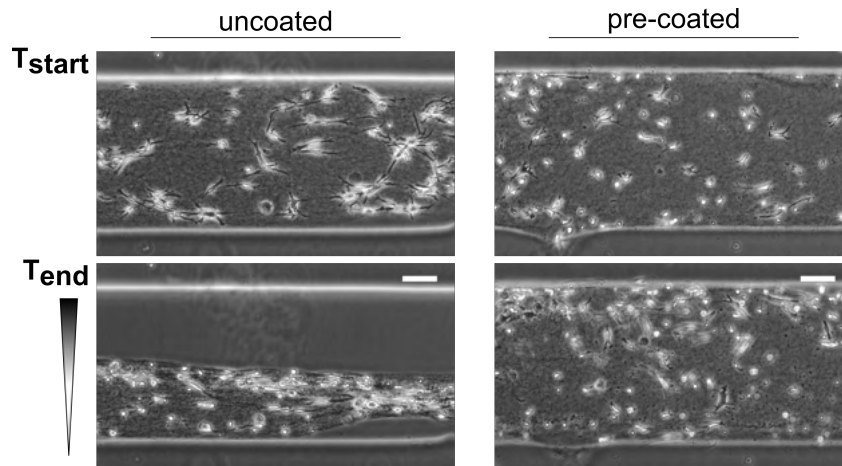


Figure 4.12: Stabilisation of 3D collagen matrix in the migration arena. Due to the non-adhesive properties of the 3D hydrogel, the collagen matrix shrinks in result of the forces applied on the collagen fibres by the migrating cells (left panel). Pre-coating of the arena with soluble collagen stabilised the matrix in the channel (right panel).  $T_{end} = 24$  h; scale bar = 100  $\mu$ m.

## HT1080 chemotaxis in 3D collagen matrix

The chemotactic effect was investigated with cells embedded in a 3D collagen matrix that was exposed to a gradient of 0-10% FBS, and in uniform concentrations of 10% and 0% FBS, by evaluation of the changes of cell distribution after 24 hours of cell migration. Micrographs presented in Figure 4.13 show the cell distribution in the arenas at the end-point of the experiment.

As shown in the left micrograph, the cells accumulated at the upper barrier in response to the gradient of FBS. In contrast, cells in chemically uniform environment remained homogeneously

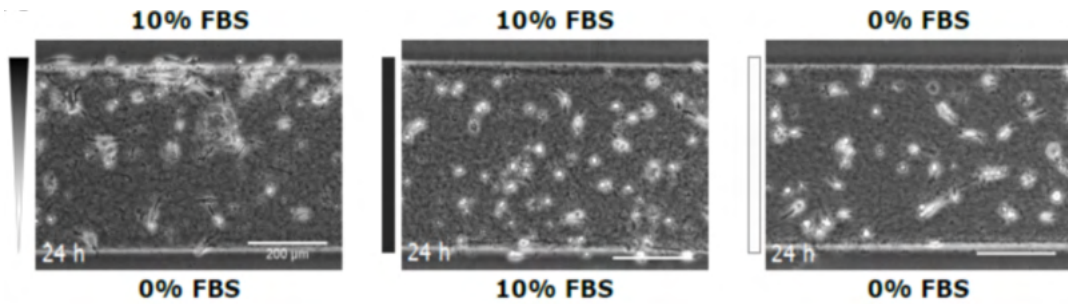


Figure 4.13: Chemotaxis of HT1080 in a 3D migration arena assay. The micrographs show the cell distribution in the 3D migration arena at the end-point of the experiment; i.e., after 24 hours of migration in a gradient of 10% FBS (left), or in a uniform environment of 10% FBS (middle), or 0% FBS (right). The chemotactic effect of the FBS gradient leads to a non-homogeneous cell distribution at the end-point of the experiment. Scale bar = 200  $\mu\text{m}$ . The figure was adapted from [281] under the terms of the Creative Commons Attribution License.

distributed in the arenas. The migration of cells in the migration arena was recorded for the whole time of the experiment (24 hours), with a 10 min time-lapse interval, and the first and last frame of the sequence were employed to compute the COMD, as described in Section 3.2.5. The end-point analysis of the COMD correctly identified the expected chemotactic response to the FBS gradient (Fig 4.14): the COMD in the gradient (51  $\mu\text{m}$ ) was significantly higher than the COMD in uniform environment ( $< 2 \mu\text{m}$ ).

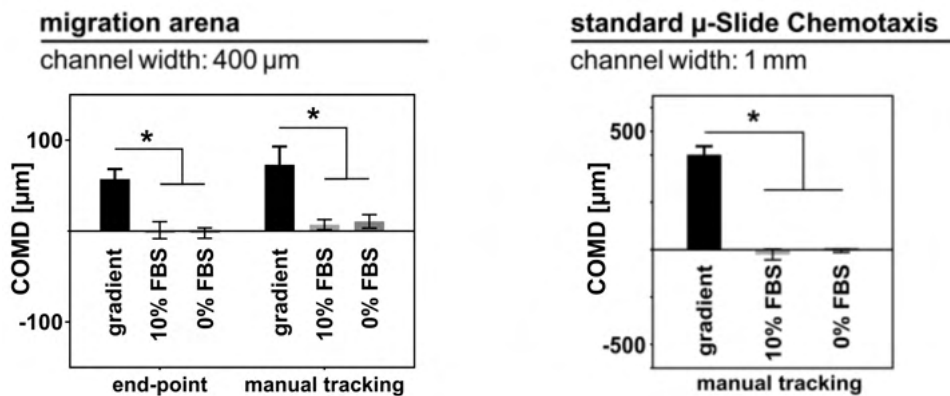


Figure 4.14: Analysis of chemotaxis in a 3D migration arena assay with a gradient of 10% FBS, and in uniform concentrations of 10% and 0% FBS. The chemotactic effect represented by the COMD was evaluated in the migration arena from the end-point cell distribution, and by manual tracking of 30-40 cells in each arena (left graph). All cells in the arena (100-200) were included in the end-point analysis. The graph in the right side of the figure shows the results of a control experiment that was performed under the same conditions in the standard  $\mu$ -Slide Chemotaxis assay. The bars show the mean COMD  $\pm$  SEM ( $n=3$ ). \* indicates significantly different means (ANOVA analysis followed by Dunnett test;  $p<0.05$ ). The figure was adapted from [281] under the terms of the Creative Commons Attribution License.

---

To verify the results of the end-point analysis, migration trajectories of 30-40 cells in each arena were tracked manually, and the centre of mass displacement was evaluated with the Chemotaxis and Migration Tool software (ibidi) that is standardly used for analysis of the cell trajectories in the  $\mu$ -Slide Chemotaxis assay. For a further control, the experiment was repeated under the same conditions in the standard  $\mu$ -Slide Chemotaxis assay. The results are shown in the right graph in Figure 4.14. Due to the different width of the cell migration area in the migration arena assay and the standard  $\mu$ -Slide Chemotaxis assay, the absolute values of the COMD differ, but the trend show the same result; i.e., that the gradient of FBS induces chemotaxis of HT1080 cells in 3D environment; and that such chemotactic effect is not present in the control samples with uniform concentrations of FBS. For the manual tracking, only viable, motile cells were selected.

In the samples with the FBS gradient three scenarios of cell behaviour were observed in the migration arena when the cells reached the hydrogel barrier: 1) attempt to persist in forward migration, that resulted in sliding motion along the barrier; 2) arrest of migration; the cells stalling at the barrier; 3) change of the direction—in such case, the cell migrated back from the densely inhabited area at the barrier towards the centre of the migration arena, until the chemotactic stimuli prevailed again, and the cell turned back towards the barrier.<sup>3</sup>

#### HT1080 chemotaxis in 2D on a fibronectin coated surface

Further, chemotaxis of HT1080 in 2D conditions was investigated. This was done in order to verify that the end-point assay is suitable for examining cell migration in 2D as well, and could be therefore employed for studying chemotactic behaviour of basal keratinocytes, which is the next objective of this thesis.

For 2D experiments, the migration arenas were coated with fibronectin in order to improve the attachment and migration of HT1080 cells. The experiments were performed under the same conditions as in 3D. Again, the chemotactic effect of 0-10% FBS was compared with random cell migration in an uniform environment of 10% and 0% FBS (Fig 4.15).

The end-point analysis of the COMD was verified by the analytical method employing the manual tracking and the results were compared with results of an analogous experiment carried out with the standard  $\mu$ -Slide Chemotaxis assay. The graphs in Figure 4.15 demonstrate similar trends as observed in the 3D chemotaxis experiment, clearly showing the chemotactic response of cells exposed to the gradient, and random migration of cells in a chemically homogeneous environment. As to the control experiments in the uniform conditions, the 10% FBS induced random cell motility (chemokinesis), which resulted in a larger scatter of the COMD values, compared to 0% FBS samples. The higher results of manual tracking (when compared to the end-point analysis) could be explained by an observer bias: for the manual tracking only

---

<sup>3</sup>The latter observation demonstrates that micro-structuring of the 3D hydrogel inside of the chemotaxis chamber could provide an interesting tool for studying the relation of cell migratory response to chemical and mechanical stimuli.

motile cells are selected, whereas the end-point analysis reflects all cells in the arena, including immobile or dead cells.

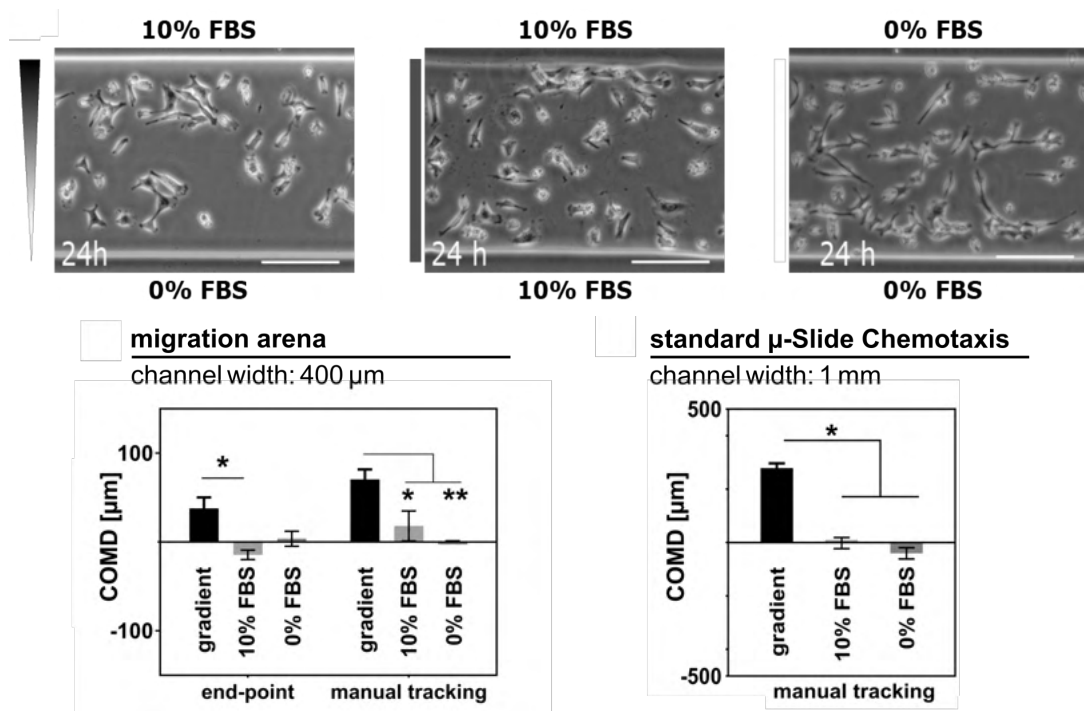


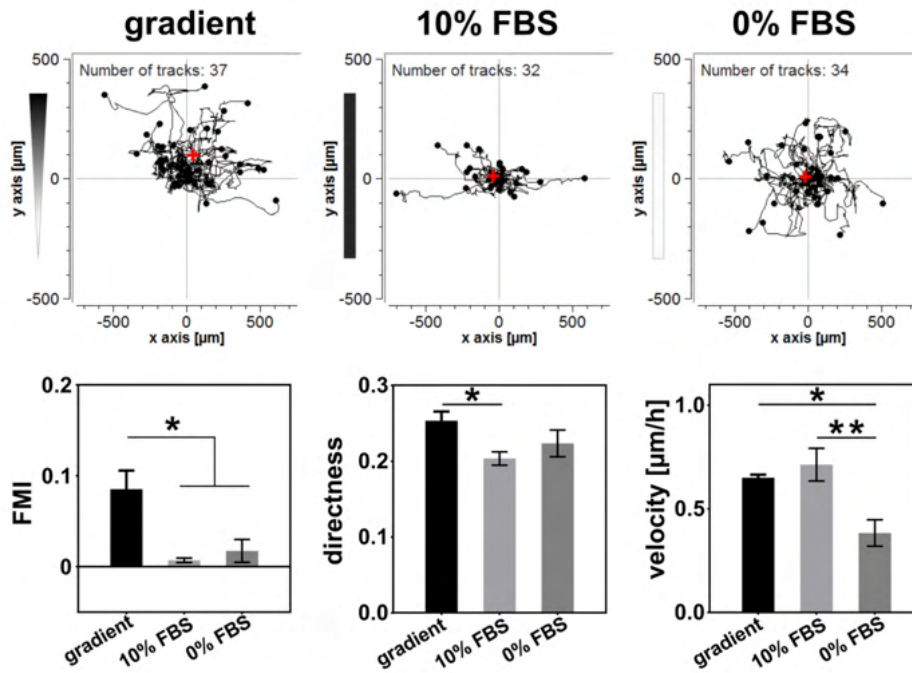
Figure 4.15: Chemotaxis of HT1080 in the 2D migration arena assay. Micrographs show the cell distribution in 2D migration arenas after 24 hours of migration in a 0-10% gradient of FBS (left), or in an uniform environment of 10% FBS (middle), or 0% FBS (right). The chemotactic effect of the FBS gradient leads to an uneven cell distribution at the end-point of the experiment. Scale bar = 200 μm. The left graph shows the COMD of HT1080 cell migrating for 24 hours in a gradient (black bars), or in uniform concentrations of FBS (grey bars) in 2D migration arenas. The chemotactic effect was evaluated from the end-point cell distribution in the arena. All cells in the arena (100-200) were included in the end-point analysis. Besides, 30-40 cells in each arena were tracked manually and the COMD was evaluated based on the trajectories (left graph). Results of a control experiment carried out in the standard μ-Slide Chemotaxis assay, are shown in the graph on the right. The bars represent the mean COMD ± SEM (n=3). \* indicates significantly different means (ANOVA analysis followed by Dunnett test; p<0.05). The figure was adopted from [281] under the terms of the Creative Commons Attribution License.

---

## Analysis of single cell migration trajectories in the arena assay

In the 2D and 3D HT1080 chemotaxis experiments, the trajectories of individual cells moving in the migration arena were reconstructed in order to verify the results of the end-point analysis by another, standardly used analytical method. The migration trajectories were further analysed to characterise the motility of cells confined in the arenas on a single-cell level. The hairplots in Figure 4.16 demonstrate the trajectories of HT1080 cell migrating in the 3D or 2D migration arenas. Besides, parameters describing cell migration, such as forward migration indices (FMI), directness, and velocity were computed from the trajectories with the Chemotaxis and Migration Tool (the parameters are described in detail in Chapter 2.3.5). The cell trajectories were deformed along the x-axis, as a result of the confinement of the migration in y-direction in the arenas. The FMI, representing the tendency of cells to migrate in the direction of the gradient (i.e., the chemotactic effect), showed the same result as the analysis of COMD. The directness represents the persistence of cell movement along a straight path, regardless of the gradient direction. Exposure to the gradient slightly increased the tendency to pursue the locomotion in one set direction. In contrast, randomly migrating cells in the uniform 10% concentration of FBS changed the direction more frequently. They also moved faster than cells in serum-free conditions. The velocity that increased with the overall concentration of FBS in the system corresponds with the chemokinetic activity of FBS, that was observed previously in the standard  $\mu$ -Slide Chemotaxis assay as well (Fig 4.10; and [39]).

## 3D collagen matrix



## 2D fibronectin coating

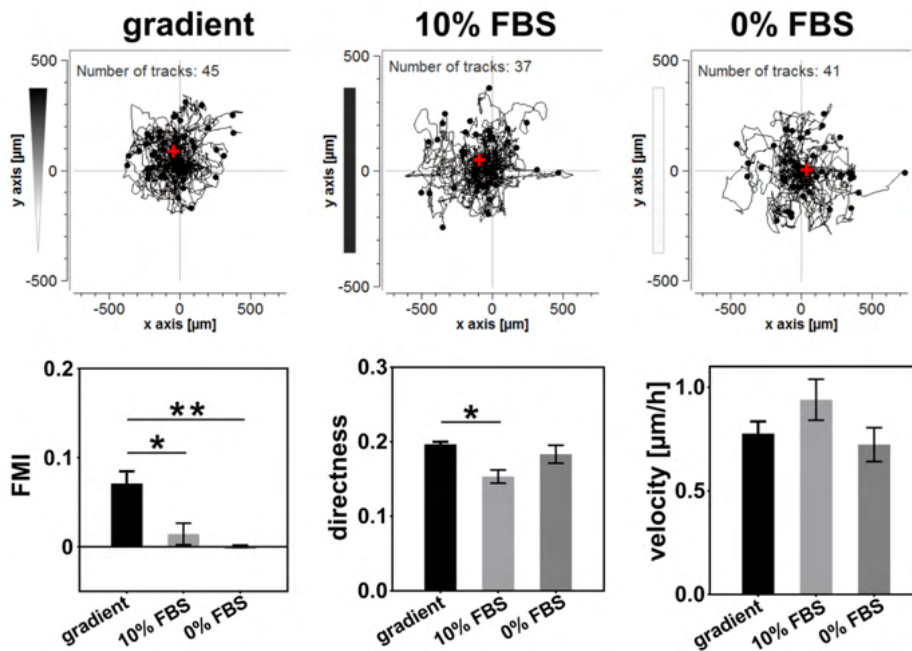


Figure 4.16: Analysis of cell trajectories in the 3D and 2D migration arena assay. Individual trajectories were retrieved by manual tracking of HT1080 cells migrating for 24 hours in a gradient or uniform concentrations of FBS in the migration arena assay, either in a 3D collagen matrix, or in 2D on a fibronectin coated surface. The hairplots show representative results of three independent replicates. The red crosses indicate the centre of mass of the end-points of the tracked cells. Numbers of analysed cells are indicated. Based on the trajectories, further parameters describing cell migration, FMI, directness, and velocity (as defined in Chapter 2.3.5) were evaluated with the Chemotaxis and Migration Tool. The bar graphs show the mean of three independent experiments  $\pm$  SEM; \* indicates significantly different results (ANOVA analysis followed by Dunnett test;  $p < 0.05$ ). The figure was adopted from [281] under the terms of the Creative Commons Attribution License.

---

## 4.3 Discussion

The first objective of this work addressed in this chapter was the development of an end-point method for analysing chemotaxis of slow-moving cells based on the  $\mu$ -Slide Chemotaxis assay.

First, the options of modifying the gradient area of the  $\mu$ -Slide Chemotaxis with advanced UV-responsive materials and methods of chemical surface modifications were investigated. Based on the results of these investigations, the migration arena assay from PEGnorb hydrogel was established. It proved to be a suitable platform for studying chemotaxis both in a 2D and 3D environment, and a fast and simple method for quantifying the chemotactic effect was introduced. Finally, the functionality of the modified chemotaxis assay and the analytical method based on the end-point of the migratory response was verified on the model example of HT1080 chemotaxis.

### 4.3.1 Limitations regarding chemical functionalisations in the gradient area of the $\mu$ -Slide Chemotaxis

The methods that were employed to modify the gradient area with a pattern restricting the cell migration can be categorised from two different perspectives:

1. in respect to the principle of cell confinement; the area of cell migration being defined by:
  - spatial barriers from a non-adhesive polymer that were micro-structured on a cell-adhesive substrate, enclosing cell migration arenas or micro-wells
  - patches of adhesive molecules micro-patterned on a passivated, cell-repellent substrate;
2. in respect to the fabrication procedure; the patterns were prepared:
  - directly inside of a closed chemotaxis channel, by photolithographic methods
  - in an open system, on a substrate that was subsequently mounted to the sticky-Slide Chemotaxis;

To the first point: confining cell migration between three-dimensional non-adhesive micro-structures allowed for a specific cell attachment and yielded better results than the 2D micro-patterning. It was not possible to manufacture adhesive patterns providing adhesion sites of a satisfactory density to efficiently support cell attachment with the tested micro-patterning methods; especially not when the patterns were prepared directly inside the closed channel. The specific geometry and particularly the low volume of the bridge area of the chemotaxis channel (140 nl) thwarted the efficiency of in-channel micro-patterning, resulting in blurred patterns and, if any, only a weak attachment of cells that did not permit efficient locomotion. Optimizing the chemistries of the micro-patterning methods such as varying the passivation agents or the adhesive molecules (e.g., substituting the linear RGD with fibronectin, or a cyclic form of

---

the peptide that has a higher affinity to integrin receptors [283]), or increasing the reaction volume by refilling the chemotaxis chamber during the reaction time in order to improve the material exchange did not sufficiently improve cell attachment. Besides, it is possible that light is reflected from the top surface of the channel or the rims of the adjacent reservoirs during photolithography, and disturbs the in-channel micro-patterning. In contrast to the 2D micro-patterns, cell attachment inside of the areas defined by the 3D micro-structures (i.e., migration arenas enclosed by the 3D PEG4norb hydrogel, and PEG-DMA micro-wells) was not affected. The morphology and migration of the cells was normal, comparable to cells in culture or in the standard  $\mu$ -Slide Chemotaxis assay.

In respect to the second point; i.e., fabrication of the confinement patterns directly inside of the chemotaxis chamber, or assembly of the chamber with a pre-patterned substrate: the latter approach turned out to be inapt due to the need of a precise positioning of the pattern inside the gradient area of the chemotaxis chamber. Because the patterned substrates were fixed manually to the sticky-Slide Chemotaxis, achieving a perfect alignment was challenging, and the success rate unsatisfactory (< 30%).

As stated above, in-channel micro-patterning also did not yield the desired results. Thus, the remaining and most effective approach was the in-channel micro-structuring of 3D barriers from PEG4norb-based hydrogel. Besides, the resulting migration arena has the notable advantage that it can accommodate both cells seeded directly on the surface (in 2D), or embedded in a 3D matrix; thus providing for a more versatile end-point chemotaxis assay. The light-induced polymerisation and micro-structuring of the thiol-ene cross-linked PEG4norb hydrogel is a well established method [265, 284, 285]. The hydrogel, cross-linked with a cell-degradable peptides and decorated with the adhesion peptide RGD, was previously used as a synthetic ECM for studying the migration of cells encapsulated in a precisely defined 3D environments [19, 66, 270, 286]. Such set-up; i.e., utilizing a peptide-decorated PEG4norb hydrogel as a cell-degradable synthetic matrix, in combination with the possibility of micro-structuring the hydrogel inside of the chemotaxis chamber offers for an intriguing tool for studying further aspects of chemically directed cell migration in defined 3D micro-environments.

### 4.3.2 Migration arena chemotaxis assay

Modification of the  $\mu$ -Slide Chemotaxis with the hydrogel barriers enabled the end-point evaluation of chemotaxis, and at the same time, the characteristic qualities of the standard assay were not corrupted by the micro-structures. Most importantly, it was verified that the barriers did not hinder the formation of the gradient. Comparable to the standard chemotaxis chamber [211], a linear gradient was formed in the migration arenas within few hours, and remained stable over more than 48 hours (Fig 4.9). This makes the assay optimal for investigating the chemotactic behaviour of slow moving cells.

Another important feature of the assay is the accessibility of cells for an optical control during the whole time of the experiment. The lack of the optical control is one of the most



---

reproached drawbacks of other end-point migration assays; e.g., the Boyden chamber type of assays [40, 187]. The geometry of the  $\mu$ -Slide Chemotaxis chamber enables visualisation of the cells in the low (70  $\mu\text{m}$ ) bridge area with a high imaging quality, even in case of cells embedded in a 3D matrix. This also made it possible to verify that the confinement between the hydrogel barriers does not affect cell viability by fluorescent labelling of living and dead cells directly inside of the migration arena (Fig 4.11).

### End-point based approach for evaluation of the chemotactic response

By confining the cells in the arenas, evaluation and quantification of the chemotactic effect from the end-point state of the experiment was made possible. The end-point analysis substantially accelerated the evaluation of the assay, in comparison to the usually employed manual reconstruction of the complete cell migration trajectories that is required by the standard  $\mu$ -Slide Chemotaxis assay; thus providing for an increased experimental throughput.

For illustration, the end-point analysis of one migration arena requires evaluation of the cell distribution at the start and at the end of the experiment (i.e., two micrographs). If the image quality allows to automatise the recognition of cell bodies, the analysis can be carried out virtually within few seconds. If the cell coordinates have to be determined manually, positions of approximately 100-200 cells (the typical number of cells in one migration arena) have to be marked in the two micrographs, resulting in 400 “mouse-clicks”. This can be done in several minutes. In the standard  $\mu$ -Slide Chemotaxis assay, cell migration of slow moving cells is recorded for several hours, with a time-lapse interval of 5-10 minutes. A typical video-sequence of HT1080 chemotaxis is recorded for 24 hours with a 10 min time-lapse interval, resulting in 145 frames. In order to reconstruct the complete migration trajectories and to obtain a statistically relevant result, 30-40 cells per sample are tracked through the whole time-lapse sequence, representing more than 5000 “mouse-clicks”; the analysis of one sample typically taking 30-45 min.

To analyse the chemotaxis of HT1080 cells in 2D and 3D, a data set that consisted of 18 independent samples was generated (Figs 4.14, 4.15).<sup>4</sup> With the end-point analysis, such data-set can be processed within several hours. In contrast, reconstruction of all cell trajectories needed to evaluate the whole data-set with manual tracking would take several days. Therefore, the end-point analysis could considerably facilitate chemotaxis studies that cover a larger number of samples, such as clinical testing, or screening for chemoattractants or inhibitors of chemotaxis.

Moreover, the end-point analysis can be further simplified by fluorescent labelling of cell nuclei for more stable automatic detection of cells. Also, if the cells after seeding are homogeneously distributed around the centre of the arena in a reproducible way, the  $COMD_{start}$  can be considered constant. The chemotactic effect can then be evaluated solely from the end-point state of the experiment, assuming  $COMD_{end} = COMD$ . The homogeneity of the cell seeding

---

<sup>4</sup>In each experiment, three 2D samples and three 3D samples were evaluated (0-10% FBS, 0% FBS, and 10% FBS), and all experiments were repeated three times.

---

depends on multiple factors including cell density, quality of surface coating, or cell type; however, in our experiments, the centre of the total cell mass was usually superimposed with the centre of the arena ( $\pm 3\%$  of the arena width). Actually, the hydrogel barriers, representing a mechanical barrier between the bridge channel and the reservoirs of the chemotaxis chamber, facilitated a regular flow of the cell suspension during seeding, resulting in more stable uniformity of the cell distribution relative to the standard chemotaxis chamber, where the cell suspension often spill into the reservoirs (Fig 4.1).

The results of the HT1080 chemotaxis analysis showed that in order to correctly identify the chemotactic effect, the time-saving end-point evaluation can be safely used to replace the challenging analysis of single cell migration paths. The results were verified by manual tracking of the cells in the migration arena, and by comparing them with results obtained in the standard  $\mu$ -Slide Chemotaxis assay. Overall, the outcome of the compared methods corresponded with the results of previous studies of HT1080 chemotaxis [39].

Nevertheless, it should be noted that the end-point evaluation is based on the whole population of cells in the migration arena. Comparison of the two analytical methods (end-point, and manual tracking) in the 2D HT1080 chemotaxis experiment (Fig 4.15, left graph) showed higher statistical significance of the manual tracking of cells in the migration arena, although the number of analysed cells is higher in the end-point approach ( $n=100-200$ ; while  $n=40$  for manual tracking). This could be caused by the observer bias that is implemented in the manual tracking analysis, selecting only complete tracks of cells for evaluation (i.e., cells that migrate throughout the whole duration of the experiment), whereas immobile cells, or cells that died during the experiment were not tracked. Yet, such cells are still included in the end-point analysis that evaluates the migratory behaviour of the entire population as a whole. In the experiments presented in this chapter, the bias caused by this effect was only notable in the analysis of HT1080 migration in 2D in the serum-free environment (0% FBS); i.e., conditions under which the subpopulation of immobile and dead cells represented a larger fraction of the population compared to the other analysed samples. In the experiments under different conditions, the share of non-motile cells on the overall migratory behaviour of the population did not significantly affect the result. A study of Friedl *et al.* [42] from 1993 comparing several analytical methods of leukocyte migration showed that under certain conditions, the analysis of manually reconstructed migration paths was more sensitive than evaluation of the end-point COMD of the whole population. As noted above, the advantage of the migration arena chemotaxis assay is that the cells are accessible for real-time monitoring, providing for a control of the viability and overall behaviour of the cells in the population; and, if needed, the individual cell trajectories can be reconstructed in order to analyse the migration of single cells in the arena in detail (Fig 4.16). Yet again, in such case, it has to be accounted for the effect of the confinement imposed by the hydrogel barriers that limits the distance travelled in the gradient direction, and leads to a deformation of the migration paths along the x-axis (i.e., in

---

the direction perpendicular to the gradient).

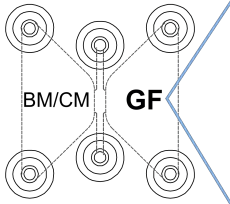
Therefore, the choice of the experimental tool and the analytical method should be suited to the scientific question of each particular study. For analysing the parameters of single cell migration, the standard  $\mu$ -Slide Chemotaxis assay, permitting unconfined locomotion in all directions, is an optimal tool. However, taken together, the experiments presented in Section 4.2.3 verified that the migration arena chemotaxis assay, employing the time-saving end-point analysis, is a suitable approach for identification of a chemotactic effect in cell populations; thus providing an optimal platform for studying chemotaxis of slow moving cells with an increased experimental throughput.



# 5 Chemotaxis of primary keratinocytes: Results and Discussion <sup>1</sup>

In order to identify a chemoattractant and the optimal gradient parameters to stimulate directed migration of KCs, the migration arena chemotaxis assay described in Chapter 4.2 was employed to investigate the chemoattractant capacity of several growth factors (GFs) toward normal human epidermal keratinocytes (nHEK). For these experiments, five agents were selected that were previously described as potent motogens of keratinocytes: EGF, TGF $\beta$ -1, TGF $\alpha$ , insulin, and BPE (bovine pituitary extract) [69,71,75–79].

*In vivo*, keratinocytes migrate into the wound bed along the basal membrane; thus, in 2D-like conditions. Therefore, the chemotaxis of nHEK cells was examined in 2D; in migration arenas pre-coated with fibronectin. nHEK cells were cultivated in a medium for epithelial cells, supplied with additives improving the cell growth; including insulin, BPE, and other GFs (the exact composition of the complete medium is described in Chapter 3.2). The nHEK chemotactic response was investigated on the background of either complete medium (CM), or basal medium without additives (BM). Each of the five examined agents was applied in three different maximal gradient concentrations. The gradients started from zero concentration; i.e., one of the reservoirs of the chemotaxis chamber was filled with the agent solution of given concentration; while the other reservoir and the cell containing arena were filled with the background medium (Fig 5.1). Exceptions were the gradients of insulin and BPE in CM, since



	basal medium			complete medium		
<b>EGF</b> [ng/ml]	1	10	100	1	10	100
<b>TGF<math>\beta</math></b> [ng/ml]	1	10	100	1	10	100
<b>TGF<math>\alpha</math></b> [ng/ml]	1	10	100	1	10	100
<b>insulin</b> [ $\mu$ g/ml]	0,5	5	50	-		
<b>BPE</b> [%]	0,4	4	20			
-	ctrl BM			ctrl CM		

Figure 5.1: GF-induced nHEK chemotaxis: scheme of the experimental set-up. To establish the gradient, one reservoir of the chemotaxis chamber was filled with medium (basal or complete, BM or CM), and the other reservoir with GF solution in the respective medium. GFs were applied in the concentrations listed in the table. In control samples (ctrl), both reservoirs were filled with BM or CM, respectively.

<sup>1</sup>Part of this chapter and figures are adopted from Tomasova *et al.*, 2019 [281].

---

these factors are already present in low concentration in the background medium.

The experimental procedures and materials are described in detail in Section 3.2.

## 5.1 Effect of growth factors on nHEK migration—time development of the chemotactic response

First, it was necessary to determine the optimal duration of the experiment for the end-point analysis. For that purpose, migration of nHEKs exposed to the GF gradients in the migration arena was recorded by time-lapse microscopy for 24 h with 1 h interval (see Sections 3.2.4 - 3.2.6 for experimental details), and COMD was computed for each frame of the sequence (Fig 5.4).

The nHEK cells showed a relatively stable circular shape with easy detectable integral edges, which made it possible to automatise the determination of their coordinates in the migration arena with the help of the ImageJ plug-in *Analyse Particles*. An automated image processing routine was established for this purpose, as described in Chapter 3.2.5. The required image processing steps are illustrated in Fig 5.2A. The accuracy of the automated approach was verified by comparison with COMD computed from values of cell ordinates that were retrieved manually (Fig 5.2B). This approach enabled rapid processing of the voluminous sample set (28 samples  $\times$  24 frames  $\times$  3 replicates resulted in more than 2000 analysed micrographs (see Fig 5.1)).

The obtained data show that in the samples where a positive chemotactic response was detected, the COMD increased gradually in the first several hours and after reaching the maximum, it remained stable for the remaining time of the experiment. The duration of the initial period depended on the agent, and the slope of the gradient (Fig. 5.4). For example, EGF induced chemotaxis most potently in BM at the concentration of 10 ng/ml, and the respective COMD reached the maximal values faster, when compared to the other tested gradients of EGF. In contrast, there is no significant difference in the time course of the chemotactic response in TGF $\alpha$  gradients. In all positive samples the COMD value reached its plateau by 10–15 h after the beginning of the experiment. Therefore, 20 h was chosen as a suitable and reliable end-point for the nHEK chemotaxis experiments. The distribution of cells in the migration arenas at this time-point is depicted in Fig 5.3.

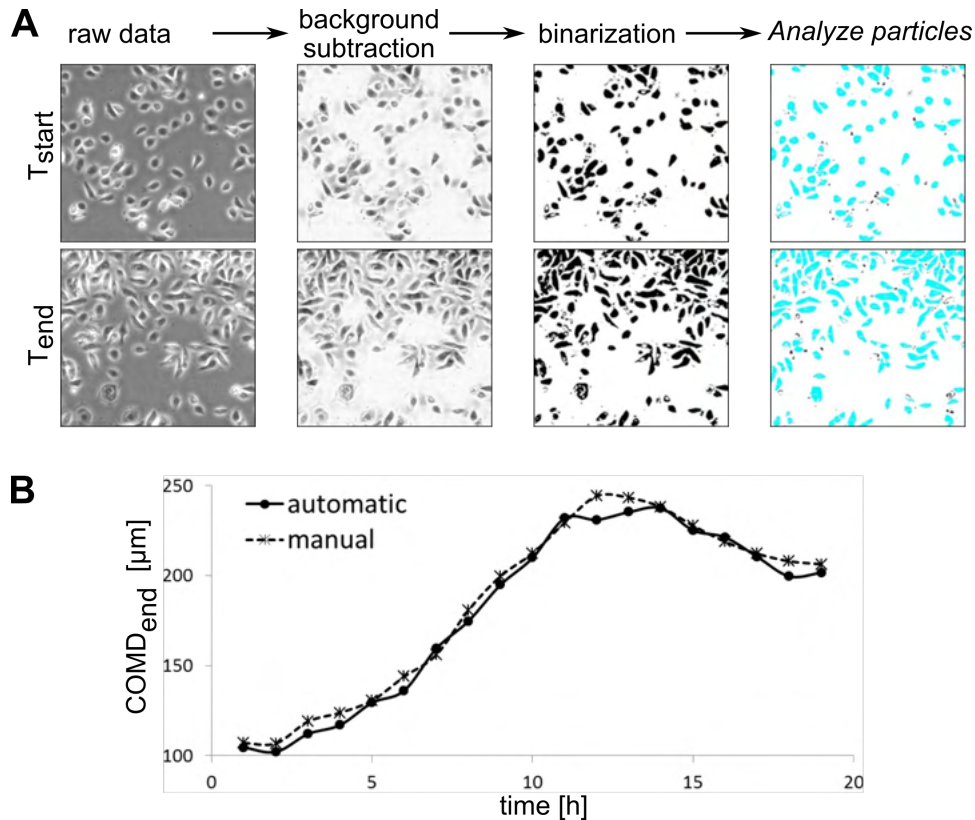


Figure 5.2: Automated end-point analysis of the migration arena assay. **A.** Work-flow of the image processing. The automatic end-point analysis with the ImageJ Particle Analyser requires processing of the raw phase-contrast data in order to provide a binary image. The micrographs represent a detail of a migration arena with nHEK cells at the start of a chemotaxis experiment (upper row), and after 20 hours of migration in a chemoattractant gradient (lower row). The phase contrast micrographs were transformed with the ImageJ software by subtracting the background and thresholding (binarisation). The last images in the row show the cell bodies that were automatically recognised by the *Analyse Particles* command (blue). **B.** Comparison of the automatic and manual end-point analysis of COMD of nHEK cells. Time-development of the average cell position in the gradient direction (COMD<sub>end</sub>) is shown in the graph. Migration of nHEK cells in a gradient of a chemoattractant was recorded for 20 hours with 1 hour time-lapse interval, and the COMD<sub>end</sub> was determined for each frame of the video-sequence by the automatic analysis using the ImageJ *Analyse Particles* command (dots connected by a full line), or by manual detection of cells (asterisks connected by a dotted line). The automatic particle recognition yielded the same results as the manual detection of cell bodies in the end-point micrograph of a migration arena. At very high cell densities that can occur due to the accumulation of cells at the hydrogel barrier, the particle recognition is less accurate, since multiple cell bodies could merge in bigger clusters that are recognised as a single particle (this effect can be observed in the graph as the COMD<sub>end</sub> peaks at 12-14 hours). However, the deviation from the results retrieved by manual cell selection is minimal. The decrease of the COMD<sub>end</sub> towards the end of the experiment ( $t > 12$  h) that was measured both with manual, and automated analysis results from proliferation of the accumulated cells (as the cell mass grows, it spreads back towards the centre of the channel).

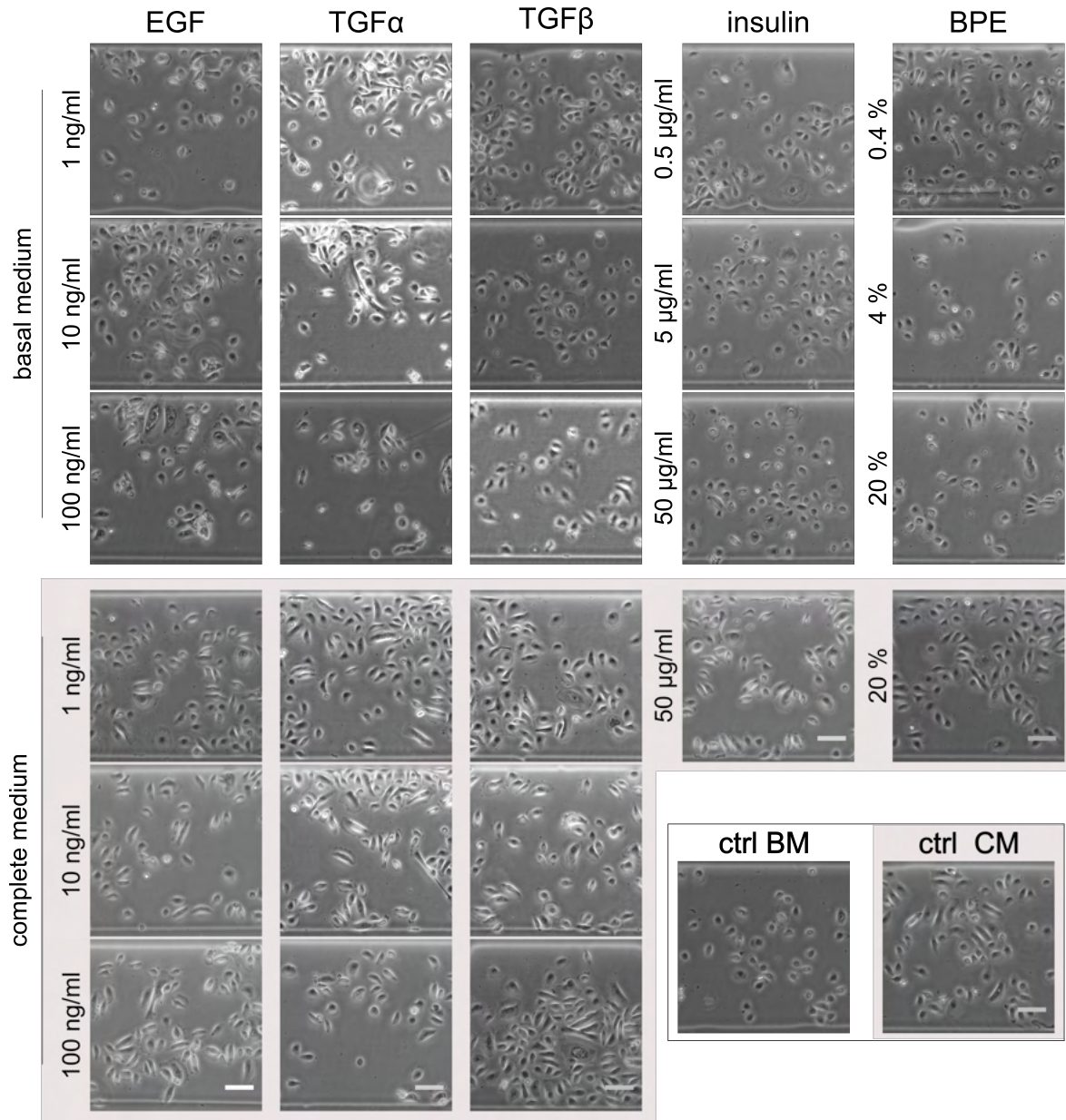


Figure 5.3: EGF, TGF $\alpha$ , and BPE, but not insulin, or TGF $\beta$  induce chemotaxis of nHEK. Micrographs show the nHEK distribution in the migration arena at the end-point of the experiment; i.e., after 20 h after cell migration in the gradient. Chemoattractant is placed in the upper reservoir. Cell accumulation at the upper side of the arena indicate chemotactic effect of the respective GF. The maximal concentration of GFs is indicated. The presented micrographs are representative examples of four biological replicates. Scale bars represent 100  $\mu$ m and apply to all micrographs.



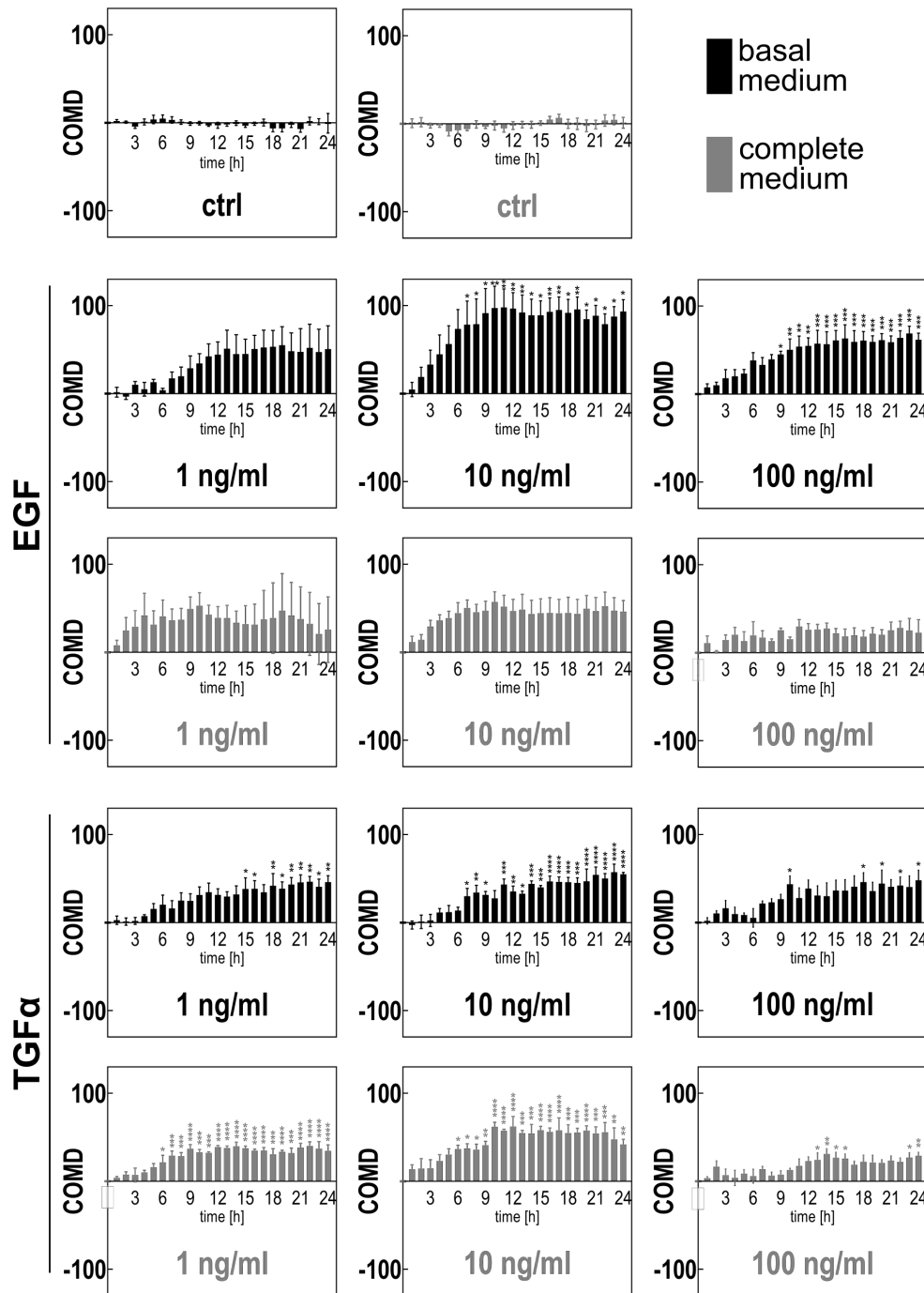


Figure 5.4: Time-lapse analysis of nHEK chemotaxis: EGF and TGF $\alpha$ . Cell migration in fibronectin coated arenas in gradients of several GF on the background of basal (BM; black bars) or complete medium (CM; grey bars) was recorded for 24 h with 1 h time-lapse interval. To identify the time of the best chemotactic response, the COMD was determined by end-point analysis of every time-lapse frame. The bar graphs show mean COMD  $\pm$  SEM (n=3); all graphs are scaled identically. Maximal concentrations of gradients are indicated in the graphs. Data were analysed with ANOVA test followed by Dunnett's multiple comparisons test ( $t_0$  vs.  $t_n$ ); stars indicate means significantly different from  $t_0$ . The figure was adapted from [281] under the terms of the Creative Commons Attribution License.

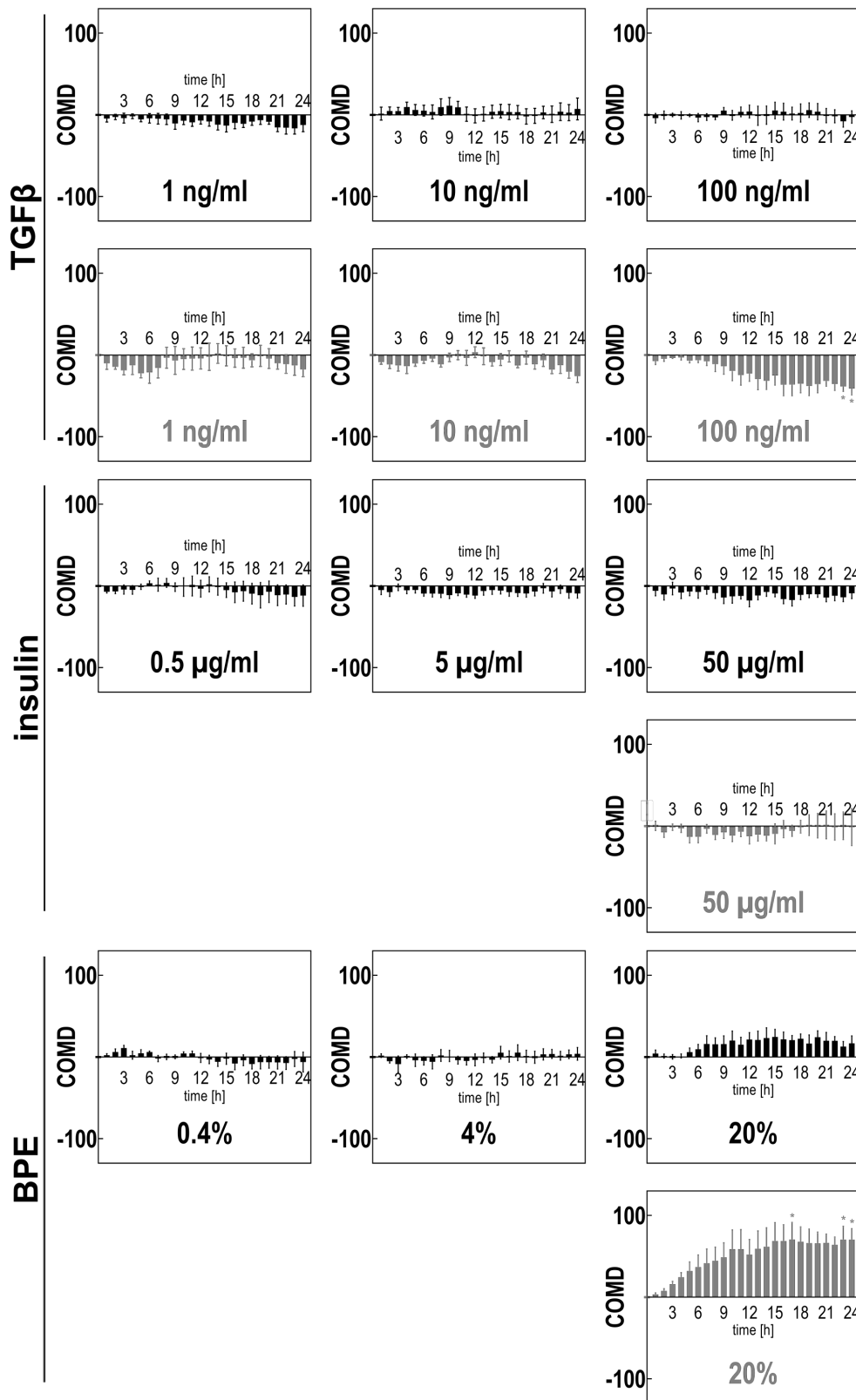
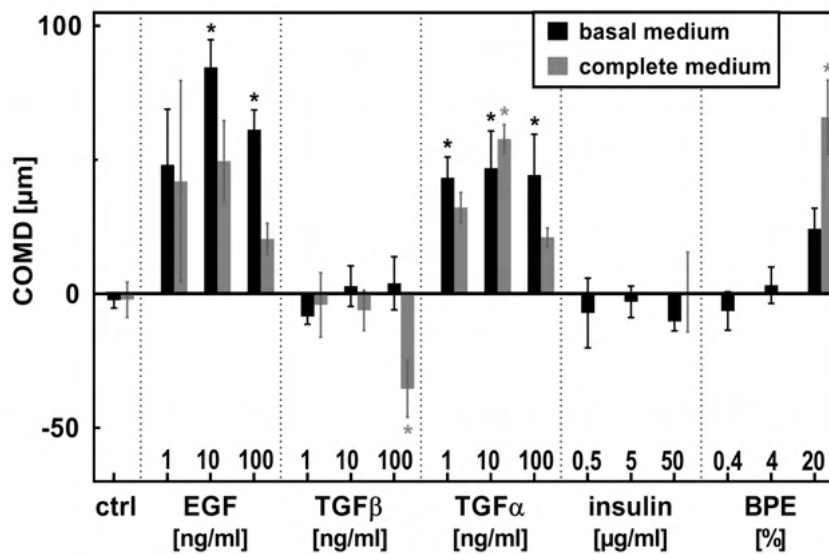


Figure 5.5: Time-lapse analysis of nHEK chemotaxis in gradients of TGF $\beta$ , insulin, and BPE. Mean COMD  $\pm$  SEM (n=3); all graphs are scaled identically. ANOVA test was followed by Dunnett's multiple comparisons test ( $t_0$  vs.  $t_n$ ); stars indicate means significantly different from  $t_0$ . The figure was adapted from [281] under the terms of the Creative Commons Attribution License.

## 5.2 TGF $\alpha$ , EGF, and BPE induce chemotaxis of nHEKs

The chemotactic behaviour of nHEK cells migrating in the presence of GF gradients was evaluated from the cell distribution in the migration arena from the micrographs taken 20 h after addition of the GFs (Fig 5.3). The accumulation of cells on the chemoattractant side of the arena in the gradient of the chemotactically active agents was easily detectable by eye. In contrast, cells of the control sample (ctrl) migrating in absence of GFs gradient were distributed uniformly in the arenas, as were also the cells exposed to gradients of chemotactically inactive GFs. The measured chemotactic effect represented by COMD is presented in Fig 5.6. Positive chemotaxis of nHEK cells was induced by EGF, TGF $\alpha$ , and BPE. The EGF-induced chemotactic response was concentration-dependent; steeper EGF gradients stimulated chemotaxis more effectively. Besides, the chemotactic effect was weaker in CM. TGF $\alpha$  stimulated chemotaxis in



COMD SEM [μm]	ctrl	EGF [ng/ml]			TGF $\beta$ [ng/ml]			TGF $\alpha$ [ng/ml]			insulin [μg/ml]			BPE [%]		
	-	1	10	100	1	10	100	1	10	100	0.5	5	50	0.4	4	20
BM	-2	48	85	61	-8	3	4	43	47	44	-7	-3	-10	-6	3	24
	3	18	9	6	3	7	9	7	12	13	11	5	3	6	6	7
CM	-2	42	50	20	-4	-6	-36	32	58	21				1		66
	6	31	14	5	10	6	9	5	4	3				12		12

Figure 5.6: GF-induced chemotaxis of nHEK cells. Chemotactic response of nHEK cells to gradients of EGF, TGF $\alpha$ , TGF $\beta$ , insulin and BPE was evaluated in the migration arena assay from the end-point cell distribution after 20 hours of migration. The maximal concentration of each gradient is indicated in the graph. All gradients start from zero, with the exception of insulin and BPE, which were contained already at low concentrations in complete medium (0.4% BPE, 5  $\mu$ g/ml insulin). In the basal medium, the gradients of these factors also started from zero. The bar graph show the mean COMD  $\pm$  SEM (n=4); \* indicate means significantly different from control (ANOVA followed by Dunnett's test; p<0.05). Mean COMD  $\pm$  SEM is also listed in a table. The figure was adapted from [281] under the terms of the Creative Commons Attribution License.

---

a comparable manner in all tested concentrations, both on the background of BM and CM. The GFs mixture BPE showed chemotactic activity in CM at 20% concentration; however, no cell response was observed at lower BPE concentrations or in BM. No chemotactic activity of insulin or TGF $\beta$  was detected, apart from a surprising negative chemotactic effect of the steepest gradient of TGF $\beta$  in CM.

### 5.2.1 Cell proliferation does not bias the measured chemotaxis effect

Common problem of end-point migration assays is how to distinguish the effect of cell motility from cell proliferation. These processes are tightly interconnected in cells and many growth factors responsible for activation of cell migration also stimulate cell growth [51,287]. Therefore, an increased proliferation of cells exposed to the chemical agent has to be taken in account. Furthermore, cell proliferation could bias the chemotactic effect; or, in fact, the accumulation of cells on the chemoattractant side of the migration arena at the end-point of the experiment could be solely a result of the GF-induced proliferation. For that reason, a control chemotaxis experiment was performed in the presence of the cell growth inhibitor mitomycin C (MMC). Mitomycin C, also used in anti-tumour therapy, is a DNA cross-linker, and it is cytotoxic in higher concentrations [288]. However, in an optimal concentration it prevents cell doubling independently from cell motility and is therefore often applied as the anti-proliferative drug of choice in migration assays (e.g., wound healing assay), in order to separate the proliferation effect from migration [289–292].

To optimise the MMC treatment for nHEK cells, a 24 hours time-lapse video of cells migrating on a fibronectin-coated surface was recorded, and the proliferation and viability of cells treated with either 10  $\mu\text{g/ml}$ , or 50  $\mu\text{g/ml}$  MMC for the whole time of the experiment, or pre-treated with the drug for 3 hours before the experiment was compared optically. Samples treated for longer than three hours or with the higher drug concentration showed increased mortality and impaired motility (Fig 5.7). Cells pre-treated for 3 hour with 10  $\mu\text{g/ml}$  MMC behaved comparably to control cells migrating in hunger (basal) medium (BM), and proliferated less than the cells of another control sample, growing in the complete medium (CM). Therefore, for the chemotaxis experiments, the cells were seeded in the fibronectin-coated migration arenas and after cell attachment the samples were incubated for three hours with 10  $\mu\text{g/ml}$  MMC. Then, the channel of the migration arena was washed with MMC-free medium and the reservoirs of the chamber were filled with the respective chemoattractant solutions to induce chemotaxis.

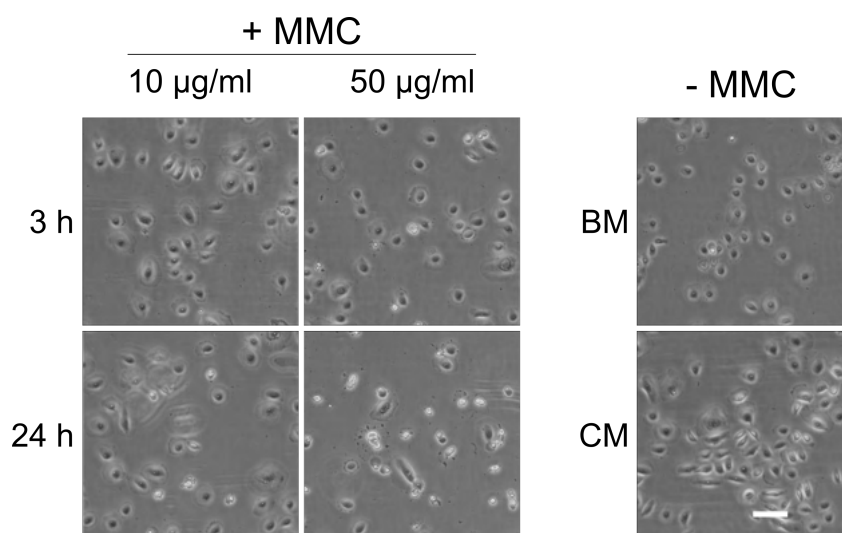


Figure 5.7: Inhibition of cell proliferation—optimisation of MMC treatment. nHEK cells were seeded in fibronectin coated channels and treated with mitomycin C, either 3 h prior to the experiment, or exposed to the drug for the whole time of the experiment; i.e., for 24 hours. Micrographs show the cell morphology and density at the end-point of the experiment. Adhered cells with normal morphology appear on the micrographs as dark with bright edges, whereas dead or improperly adhered cells can be distinguished as bright, small, round dots. In the right panel are shown the control cells growing in MMC-free, complete or basal (hunger) media. Scale bar = 100  $\mu\text{m}$  applies to all micrographs.

No significant difference between the chemotaxis of normally proliferating and MMC-treated cells was observed (Fig 5.8). Therefore, it can be assumed that the accumulation observed in the previous experiment indeed resulted from GF-induced directed locomotion. MMC treatment was also applied on samples that showed different chemotactic response in basal and complete medium; i.e., EGF and BPE (see Fig 5.6). The motivation for these experiments was the hypothesis that the cell growth is differentially stimulated in BM and CM, and such unlike growth could result in the observed discrepancy in the chemotactic behaviour. However, the inhibition of cell growth did not significantly affect the COMD in either medium in respect to normally proliferating cells (Fig 5.8). For example, if the response of MMC-treated cells (grey bars) is compared to the gradient of 100 ng/ml EGF, it shows that directed migration is induced only in the basal medium.

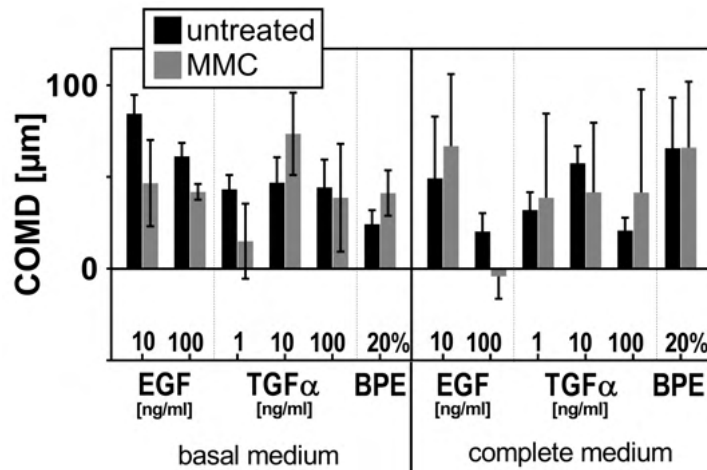


Figure 5.8: Chemotaxis of MMC-treated cells. Proliferation does not affect directed migration of nHEKs in the migration arena. Cells were pre-treated for 3 h with 10  $\mu\text{g}/\text{ml}$  MMC before applying the gradients that induced chemotaxis in the previous experiments. Besides, effect of cell proliferation was investigated in those samples where differential response to a GF gradient was observed in basal, and complete medium. The bars represent the mean COMD  $\pm$  SEM ( $n=3$ ). No significant differences were between COMD of normally proliferating (black bars), and MMC-treated cells (grey bars). The figure was adopted from [281] under the terms of the Creative Commons Attribution License.

## 5.2.2 Interplay of signals: chemotactic response to gradients of mixed GFs

*In vivo*, cells are exposed to multiple signals at once. Chemotactic activity of GFs *in vitro* can be affected by the presence of another substance—combination of two and more GFs can lead to amplification, or attenuation of the chemotactic response [293]. Therefore, chemotaxis was investigated in nHEK cells that were exposed to gradients of combined growth factors. Gradients of pairs of GFs, and of all factors mixed together (“all”) were applied in BM, and the COMD was compared with the previously measured chemotactic effect of single GFs (Fig 5.9). The results showed that insulin significantly reduced the EGF-stimulated chemotaxis; similar effect had also TGF $\beta$ . The chemotactic activity of TGF $\alpha$  was not significantly affected by addition of other GFs. Surprisingly, although none of these factors showed any chemotactic activity in BM on itself, combination of TGF $\beta$  and insulin induced a negative chemotaxis effect, similar to the effect of TGF $\beta$  in CM described above.

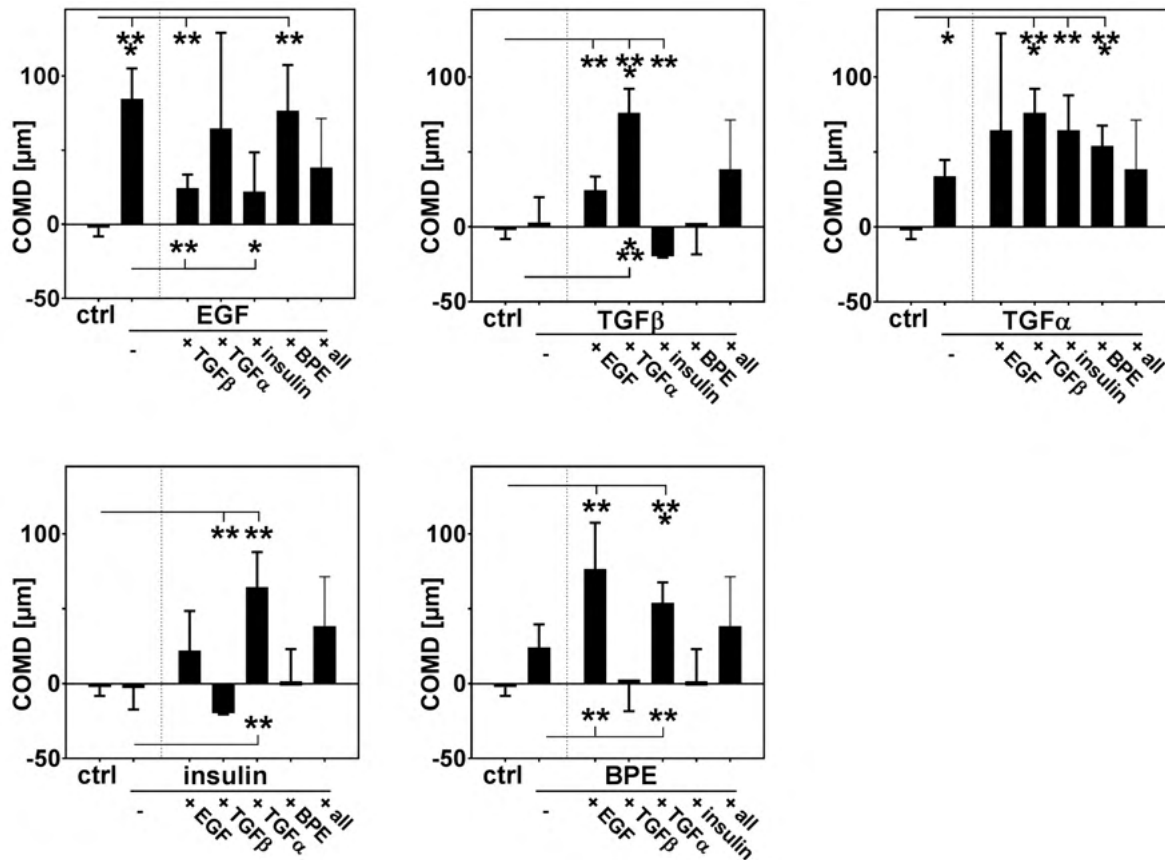


Figure 5.9: Effect of gradients of combined GFs on nHEK chemotaxis. COMD of nHEK cells exposed to gradients of two and more combined GFs was measured in the migration arena assay and compared with chemotactic response to gradient of single GFs. Bar graphs show COMD  $\pm$  SEM,  $n=4$ . Statistical analysis was performed by ANOVA followed by Dunnett's test;  $p<0,05$ . The first bar in each graph represents the COMD of randomly migrating nHEKs in BM (ctrl), the second bar the COMD of cells exposed to a single gradient of the indicated GF. The maximal concentrations of the gradients were 10 ng/ml for EGF, TGF $\beta$ , and TGF $\alpha$ , 5  $\mu$ g/ml insulin, and 20 % BPE. The figure was adopted from [281] under the terms of the Creative Commons Attribution License.

### 5.2.3 Specificity of the EGF- and TGF $\alpha$ -induced chemotactic response - inhibitor test

The experiments described above identified TGF $\alpha$  and EGF as potent chemoattractants of primary keratinocytes. These structurally similar polypeptides are members of the EGF family of growth factors, and are ligands of the EGFR (epithelial growth factor receptor). EGFR is a receptor tyrosine kinase (RTK) that dimerises upon binding its ligand, and transduces the signal into the cell by triggering a cascade of phosphorylation of diverse factors. EGFR signal transduction pathway is involved in the coordination of several vital processes in epithelial cells, including cell motility [294]. In order to verify the specificity of the observed chemotactic response, it was further investigated how inhibition of EGFR signalling affects the EGF-

and TGF $\alpha$ -induced chemotaxis. The EGFR inhibitor tyrphostin (AG-1478) or EGFR-specific antibody 255 were added into the medium in the chemotaxis experiment, as described in Chapter 3.2.4. The chemotactic response of nHEK cells in presence of the inhibitors and EGF or TGF $\alpha$  gradients in BM was measured in the migration arena chemotaxis assay. Tyrphostin is an inhibitor of the intracellular tyrosine-kinase activity of the receptor, while the EGFR antibody blocks the extracellular part of EGFR and prevents its interaction with the ligand. The results of the experiment are shown in Figure 5.10. TGF $\alpha$ -induced chemotaxis was impaired by both inhibitors. Tyrphostin also reduced the EGF-induced chemotactic effect, although the result was not statistically significant. The EGFR antibody at the employed concentration did not affect EGF-induced chemotaxis. In previous experiments, a chemotactic effect of BPE in CM was also detected. Since BPE is an undefined mixture of GFs, presumably also containing EGFR ligands, it was also tested if the BPE-induced chemotaxis is—at least partially—EGFR dependent. Indeed, a similar trend could be observed in the result as for EGF, however, the difference in COMD of tyrphostin-treated and control cells were not statistically significant.

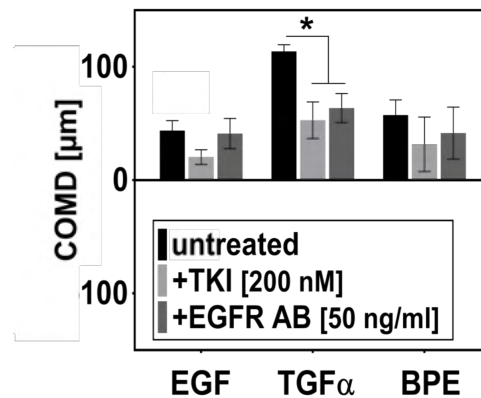


Figure 5.10: EGF- and TGF $\alpha$  - induced chemotaxis is EGFR dependent. Signals from both EGF and TGF $\alpha$  are transferred into the cell by EGFR. Cell chemotaxing in gradients of EGF, TGF $\alpha$  , and BPE were treated by EGFR inhibitors (EGFR antibody, EGFR AB; and tyrosine kinase inhibitor tyrphostin AG-1478, TKI), and the COMD was evaluated after 20 h. Mean COMD  $\pm$  SEM (n=4); \* indicate means significantly different from control (ANOVA followed by Dunnett's test; p<0.05). The figure was adopted from [281] under the terms of the Creative Commons Attribution License.



---

## 5.3 Discussion

Migration of epithelial cells plays a crucial role in wound healing and related pathologies. Therefore, its activation and mechanisms of its guidance were thoroughly studied in the past. Many signals were identified to affect KCs behaviour, involving both mechanical and chemical stimuli, originating from wound-related cells and ECM components. Signal transduction pathway of EGFR, a membrane receptor highly expressed by epithelial cells, is one of the best studied signalling pathways. The chemokinetic effect of several wound-related GFs was described, including EGFR ligands EGF and TGF $\alpha$ . Because it is apparent that the KCs are navigated into the wound bed by GF-induced chemotaxis, multiple studies concentrated on uncovering the chemoattractants of these cells. However, the choice of experimental methods (mostly, Boyden, or transwell assay) did not reflect the need of exposing the slow moving cells to a long-term stable gradient in order to reliably discern between chemokinesis and proper chemotaxis. Therefore, the results remain inconclusive.

By employing the migration arena assay, it was possible to reliably identify GF-induced chemotaxis of primary keratinocytes, and the fast end-point analysis approach enabled investigation of the chemotactic behaviour of nHEKs in multiple chemical gradients. The chemotactic effect of five motogens was analysed: EGF, TGF $\alpha$ , TGF $\beta$ , insulin and BPE, applied in gradients of varying steepness, on the background of basal and complete media. Further experiments examined whether cell proliferation affects the chemotactic behaviour, and the cell response to gradients of combined GFs was studied, too.

The results of this work confirmed the potency of EGF family growth factors to induce directed migration of KCs (Fig 5.6). The motogenic activity of EGF and TGF $\alpha$  on epithelial cells and its important role in the wound healing process was reported previously by numerous studies [68, 71, 75–77, 79, 209, 295–297]. The inhibitor assay confirmed the specificity of the TGF $\alpha$ -induced response, showing that the effect is EGFR-dependent (Fig 5.10). Surprisingly, similar blocking effect was not detected for the EGF-induced chemotaxis. It is possible that the chosen concentration of the EGFR antibody was too low to ensure complete blocking of the EGF signalling. Previously, the inhibitors applied at the same concentrations were shown to perturb the EGF-mediated chemotaxis of breast cancer cells MDA-MB-231 in 3D collagen [211]. It was also reported that the kinetics and affinity of EGF binding to EGFR varies greatly in different cell types [298], and various cell lines show distinct sensitivity to inhibitors of EGFR-dependent cell growth [299]. Thus, it is possible that higher concentrations of the inhibitors are needed to block the EGF signalling in keratinocytes, than in MDA-MB-231 cells.

EGFR signalling activates several cell processes, including cell proliferation and motility; and is vital for effective healing of wounds [294]. Furthermore, inhibition of EGFR *in vivo* leads to significant delay in wound closure [300,301]. However, the results presented in this thesis showed several differences in the way how EGF and TGF $\alpha$  stimulate nHEK chemotaxis. For example, EGF-induced response was dose-dependent, and significantly reduced on the back-

---

ground of CM (Fig 5.6). Besides, the response of the factors to the inhibitor tyrphostin and the EGFR-antibody was also unlike (Fig 5.10). In spite of the structural similarity of EGF and TGF $\alpha$  [297, 302, 303], the two factors were described to activate EGFR in distinct ways, and to trigger different downstream signals [76, 295, 304, 305]. EGFR, also named ErbB-1,<sup>2</sup> is a transmembrane receptor with intracellular tyrosine-kinase activity (RTK). Binding of a ligand leads to dimerisation of the receptor, and phosphorylation of its intracellular domains. EGFR can form homodimers or heterodimers (with other related receptors of the ErbB family) that propagate the downstream signal transduction in distinct ways [306]. The function selectivity of EGF and TGF $\alpha$  is attributed to their different preference to the receptor dimers; i.e., distinct EGFR heterodimers are formed upon binding the ligands [307]. Therefore, the differences in the chemotactic response, and sensitivity to the EGFR inhibition observed here could be another manifestation of this phenomenon.

Intriguing is also the unlike chemotactic behaviour of nHEKs in basal and complete medium. Next to EGF, cells in gradients of BPE and TGF $\beta$  also reacted differently in BM and CM (Fig 5.6). The hypothesis that the increased cell proliferation in complete medium could mask or bias the effect of directed migration was, however, incorrect. The result of a control experiment in which the cell growth was inhibited with MMC did not show any significant difference between the chemotactic response of normally proliferating and MMC-treated cells in either media (Fig 5.8). Therefore, it is likely that some factor present in the background medium (e.g., insulin, or BPE, which are both contained in the CM) biases the chemotactic effect rather by affecting the cell migratory behaviour than the cell growth.

Insulin has been previously reported as a potent promoter of keratinocyte migration and proliferation [51, 75, 308]. It is possible that the insulin-induced random migration (chemokinesis) interferes with the effect of the directed motion in the migration arena assay. Indeed, in the experiment analysing chemotactic behaviour of nHEK cells exposed to the gradients of combined GFs, insulin decreased the EGF-induced chemotactic response (Fig 5.9). The same effect on EGF-induced chemotaxis had TGF $\beta$ . Furthermore, combination of insulin and TGF $\beta$  induced negative chemotactic response in BM, although none of these factors alone induced directed migration of nHEKs in BM. However, the gradient of TGF $\beta$  in CM (i.e., in the presence of low concentration of insulin in the background), also resulted in negative chemotaxis. The role of TGF $\beta$  in epithelial cell behaviour still remains rather unexplained; conflicting reports on the TGF $\beta$  effect on keratinocytes span from stimulation of cell migration, to the terminal differentiation of the cells [30, 68, 78, 309–311]. Nevertheless, to my knowledge, no previous studies can explain the observed negative chemotactic activity of TGF $\beta$  in combination with insulin.

All these results taken together demonstrate that GFs affect cell migration in distinct ways, and that the interplay of signalling of the respective GFs can both mask, or enhance chemo-

---

<sup>2</sup>The name is derived from the homologous viral oncogene, the erythroblastic leukaemia viral oncogene. The ErbB receptor family comprises in humans of four members; EGFR (ErbB-1), and HER2-4 (ErbB2-4) [306].

---

tactic response. This has to be acknowledged in *in vivo* studies. Also, these results suggest that testing chemotaxis *in vitro* on the background of basal medium can improve the assay sensitivity. This conclusion support recent findings of Biswenger *et al.* [211] that show that the standard  $\mu$ -Slide Chemotaxis assay is more sensitive when EGF-induced chemotaxis of cancer cells MDA-MB-231 is investigated in a defined, serum-free medium.

To conclude, the results of the experiments presented in this chapter show that directed migration of primary keratinocytes can be induced independently of mechanical stimuli, and confirm the chemotactic activity of the EGFR ligands EGF and TGF $\alpha$  towards these cells. The quantitative measurements of the chemotactic response parameters, such as chemoattractant concentration, and time progression of cell response, provide a basis for establishment of a chemotaxis model for studying the directed migration of epithelial cells. Further characterisation of the behaviour of chemotaxing KCs and investigation of their responsiveness to various stimuli during a chemically guided migration could contribute to a better understanding of KCs regulation in wound healing and mechanisms underlying skin reepithelisation.



# 6 Combined assays for studying single cell behaviour in response to chemical gradients with advanced microscopy techniques:

## Results and Discussion

In this chapter, experimental procedures are outlined that enable an in-depth investigation of slow moving cells migrating in long-term chemical gradients, using advanced microscopy techniques. The population based analysis of chemotactic response with the end-point chemotaxis assay that was presented in the previous chapters enables the identification of parameters that induce a chemotactic response. These findings provided the fundamental information needed for a follow-up detailed analysis of the migratory behaviour on single cell level. In this part of the work, the focus was set on the development of chemotaxis tools suited for two advanced imaging methods; the traction force microscopy (TFM), and the light-sheet fluorescence microscopy (LSFM). Where applicable, preliminary experiments were performed to compare the behaviour of slow moving cells in chemotactic, and chemokinetic conditions. At the end of the chapter, the developed experimental procedures and limitations regarding the employed techniques will be discussed, outlining further aims and possible applications of the chemotaxis tools.

### 6.1 Chemotaxis chamber for Traction Force Microscopy

In order to measure the traction forces of slow moving cells responding to a chemical gradient, a chemotaxis chamber (sticky-Slide Chemotaxis) was equipped with a soft, elastic substrate decorated with fluorescent nano-beads (Fig 6.1). The beads serve as markers of displacement of the substrate surface that occurs as a result of the applied cell forces. Based on the displacement of the beads, the traction forces can be estimated. The goal of this work was to optimise the fabrication of the TFM-substrates for an assembly with the chemotaxis chamber. The resulting TFM/chemotaxis tool was then employed for observing the forces of normal human epithelial keratinocytes (nHEK) in a gradient, or in an uniform concentration of a chemoattractant.

### 6.1.1 Fabrication of the TFM/chemotaxis chamber

To prepare the TFM substrate, a glass coverslip was overlaid with a soft polydimethoxysilan (PDMS) elastomer. By altering the ratio of the cross-linker to the polymer, the stiffness of the elastomer can be defined. The rigidity of the substrate was chosen in respect to the cell type under study and the typical amplitude of forces that they impose on the substrate. For the experiments with the keratinocytes, substrates of 10 kPa were utilised. The chosen stiffness is close to the Young's modulus of a basal membrane; i.e., mimics the natural habitat of keratinocytes [312]. An 80  $\mu\text{m}$  high layer of PDMS was grafted by spin-coating on a glass coverslip of the size of the chemotaxis slide, as described in Chapter 3.2.7. The method parameters were optimised to generate a perfectly flat surface. This was important in order to ensure a conformal contact with the chemotaxis chamber, since a buckled elastomer surface could lead to leakage of the reservoirs, or blocking of the narrow chemotaxis channel. Besides, for successful measurement of the beads displacement, it is required that the beads on the substrate surface are in one focus plane.

After curing the PDMS-coated substrates, fluorescent nanobeads were covalently coupled to the top of the elastomer, following a protocol based on EDC/NHS (ethyl-dimethyl-aminopyrlocarbodiimide and N-hydroxy-succinimide) coupling chemistry. The experimental details are described in Chapter 3.2.7. Finally, the bead-decorated TFM substrate was carefully assembled with the sticky-Slide Chemotaxis chamber (Fig 6.1A).

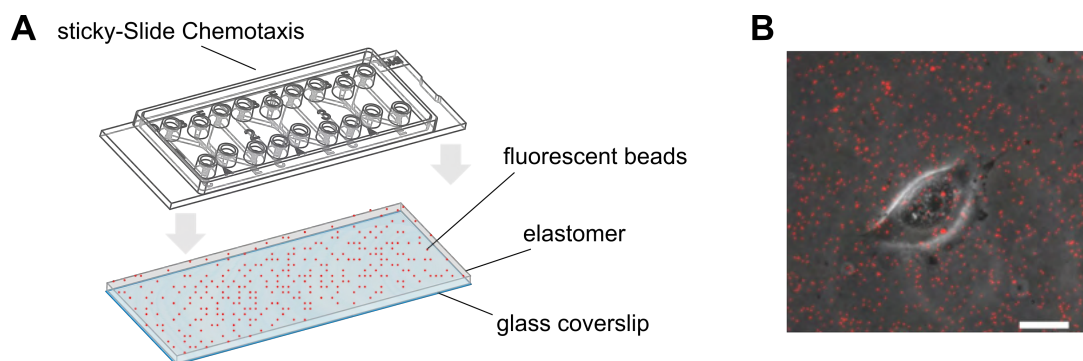


Figure 6.1: **A.** Scheme of the chemotaxis slide with a TFM-substrate. A layer of a soft PDMS elastomer was spincoated on a glass coverslip. Subsequently, the substrate was silanised and crimson fluorescent beads were covalently coupled to the surface, utilising the EDC/NHS chemistry. The sticky-Slide Chemotaxis chamber was mounted to the substrate. **B.** The merged image shows a phase -contrast micrograph of a nHEK cell in the chemotaxis channel, migrating over the TFM substrate (fluorescent beads in red). Scale bar = 10  $\mu\text{m}$ .

---

## 6.1.2 Traction forces of keratinocytes during chemotaxis and chemokinesis

nHEK cells were loaded in a fibronectin-coated channel of the TFM/chemotaxis chamber in a low density to enable observation of individual cell bodies. A chemical gradient was generated by filling the reservoirs of the chemotaxis chamber with chemoattractant solutions of different concentration (0 and 10 ng/ml TGF $\alpha$ , respectively). The cell forces were measured after several hours of cell migration in the established gradient, as described in Chapter 3.2.7. The cells and the related beads displacement on the stressed surface were recorded by time-lapse fluorescence microscopy for 60 min. Afterwards, the cells were removed from the substrate by trypsinisation, and reference images of bead distributions on relaxed substrates were taken.

### Cell morphology and spatio-temporal distribution of forces

In a set of preliminary experiments, the traction forces were analysed for 26 cells exposed to a gradient of TGF $\alpha$ ,<sup>1</sup> and for 24 cells in an uniform concentration of the chemoattractant. These conditions represent chemotactic, and chemokinetic environments, respectively. In the gradient, 70% of the cells polarised in the direction towards the increasing concentration of the chemoattractant; whereas the cells in the uniform environment migrated randomly in all directions, or were changing the course over the duration of the experiment. Cells with two distinct morphologies could be detected: fan-shaped cells (as the cell depicted in Fig 6.1B); or prolonged, tear-shaped cells, with a ruffling lamellipodium at the front, and a long uropod. These are typical shapes of migrating keratinocytes, where the fan-like morphology is characteristic for cells that move persistently in one set direction, whereas the prolonged shape indicates cells that are in course of re-polarising and changing the direction of migration [313]. Consistently, the fraction of the fan-shaped cells was larger in the chemotactic conditions (62%) compared to the chemically uniform environment (21%; Fig 6.2A).

The distribution of the applied traction forces depended on the cell shape: in the fan-shaped cells, two focal regions of force generation were observed, one under each flank of the fan, both directed towards the centre of the cell (Fig 6.2B). In the prolonged cells, the forces appeared mainly under the front lamellipodium, aiming inward; with a second focal at the rear of the cell. Similar distribution of cell forces was observed previously in fibroblasts; i.e., cells that also have a prolonged morphology [85]. Thus, in the fan-shaped cells, the principal traction vector is orthogonal to the direction of movement; whereas in the tear-shaped cells, it is parallel with the cell polarisation axis (Fig 6.2B).

---

<sup>1</sup>TGF $\alpha$  has a chemotactic activity towards nHEK cells, as showed the results of the analysis of nHEK chemotaxis presented in Chapter 5.

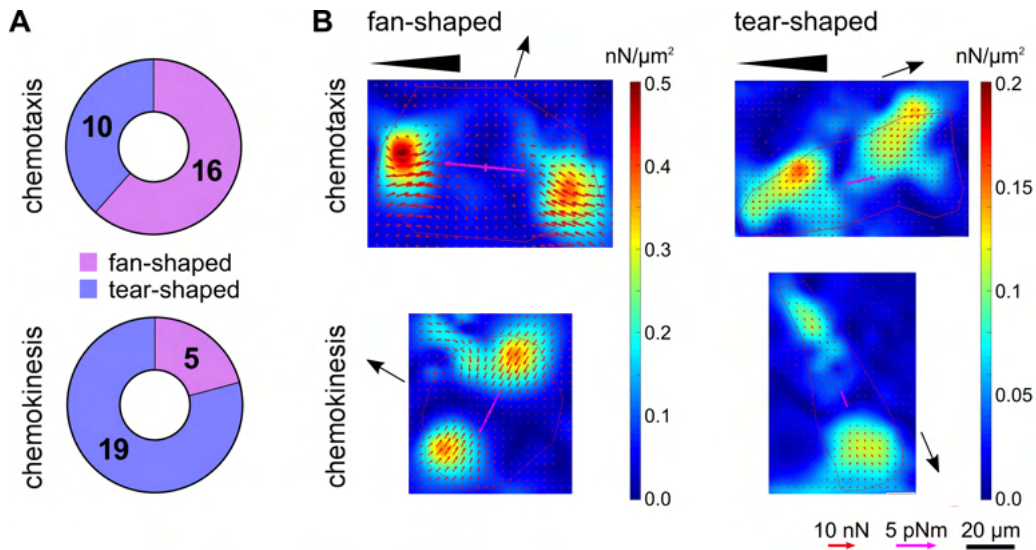


Figure 6.2: Cell morphology and distribution of forces. **A.** The cells observed in the TFM/chemotaxis chambers were either fan-shaped and persistently migrating, or prolonged (tear-shaped) and less motile. In the chemotactic conditions, more cells showed the fan-shaped morphology, than in the uniform concentration of the chemoattractant (chemokinesis). **B.** The heat-maps show the traction forces generated by the fan-shaped cells (left panel), and the prolonged cells (right panel), either in a gradient of TGF $\alpha$  (upper row; the direction of the gradient is indicated by the black triangles), or in uniform conditions (lower row). The black arrows indicate the direction of cell migration; red arrows represent the traction forces; force dipole as defined in [277] is depicted in magenta.

However, the analysis of the distribution and magnitude of the forces did not show any statistically significant differences in gradient and in uniform concentration of TGF $\alpha$ . The graphs in Figure 6.3 show an expectable larger variance of the forces in the randomly migrating cells. Also, the magnitude of mean forces generated by the chemotaxing cells remained constant over the time of the experiment, whereas in the cells undergoing chemokinesis, the mean of the contractile forces as well as its standard deviation slightly increased over time (Fig 6.3B).



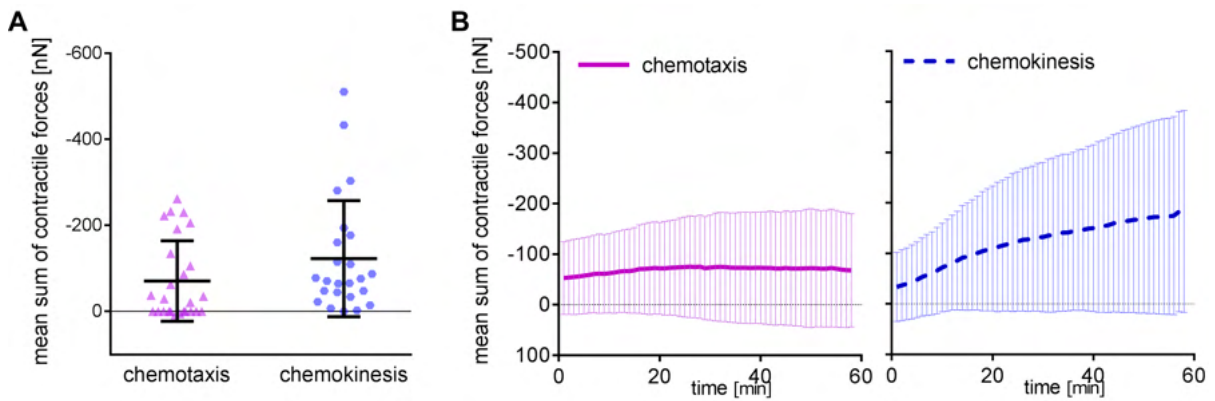


Figure 6.3: Contractile forces generated by nHEK cells in chemotaxis and chemokinesis. Cells in a gradient (chemotaxis, magenta), and in a uniform concentration of  $\text{TGF}\alpha$  (chemokinesis, blue) migrating in the TFM/chemotaxis chamber were recorded for 60 min with an 1 min time-lapse interval. Afterwards, the cells were trypsinised and a reference image of the relaxed TFM substrate was taken. The bead displacement was measured, and the traction forces were computed as detailed in Section 3.2.7. **A.** The graph shows mean sum of cell forces over the whole duration of the experiment,  $\pm$  SD. The triangles and bullets represent mean sum of contractile forces of single cells in a gradient or an uniform environment, respectively. **B.** The graphs on right show the development of the mean forces of all observed cells over time,  $\pm$  SD. The traction forces were analysed for 26 single cells exposed to a chemical gradient (*chemotaxis*), and for 24 cells migrating through a chemically uniform environment (*chemokinesis*).

---

## 6.2 Chemotaxis set-up for Light-sheet Fluorescence Microscopy

Given the decreased illumination stress imposed on the cells under study, and a good optical sectioning capacity, the Light-sheet Fluorescence Microscopy (LSFM) is a suitable imaging method for a long-term visualisation of fluorescently labelled slow moving cells within a 3D environment. Here, a protocol was established to apply a gradient on LSFM samples using the commercial Zeiss Lightsheet Z.1 microscope. In this platform, the sample holder is located on the top of the imaging chamber. The specimen is placed vertically in a medium-filled sample chamber and illuminated from side with the laser light-sheet; i.e., orthogonally from the direction of signal detection. Typically, the tissue sample is embedded in a cylinder of a soft transparent 3D gel; e.g., agarose, which is extruded from a glass capillary that hangs from the sample holder from above the chamber. Alternatively, it is also possible to place a low-volume syringe in the sample holder.

To enable a detailed investigation of the spatio-temporal chemotactic behaviour of the fibrosarcoma cells HT1080 in a 3D collagen matrix, a special sample container— a LSFM chemotaxis chamber—was constructed. The intention was to isolate the sample from the immersion medium, in order to maintain a defined chemical environment (i.e., the chemoattractant gradient) across the sample. For that purpose, tubes from fluorinated ethylene propylene (FEP) were used. The material was chosen for its refractive index which is similar to the one of water; thus, the FEP tubes submerged in the medium-filled sample chamber are virtually invisible and do not disturb the illumination and detection of the enclosed sample.

### 6.2.1 FEP chamber for generation of a chemical gradient

An experimental procedure was established for generating a long-term stable chemical gradient across a LSFM sample inside of the FEP container. The sample preparation and experimental details are described in detail in Chapter 3.2.8. The collagen matrix embedding the studied cells was loaded in the FEP tubes, and after polymerisation of the matrix, one end of the FEP tube was fixed to a syringe containing a chemoattractant solution (10 % FBS). Then, the other end of the tube was submerged in a vessel filled with chemoattractant-free medium (Fig 6.4A). This way, the FEP tube represented a low volume bridge between two vast reservoirs, in which a stable, diffusion-based gradient was formed within several hours (see Chapter 2.3.1).

In order to verify the stability of the gradient formed across the samples in the FEP tubes, the tubes were loaded with collagen matrix, and the source reservoir (i.e., the syringe) was filled with a fluorophore solution. The fluorophore was allowed to diffuse into the sample for 20 h. Afterwards, the fluorescence signal was measured at multiple positions across the sample. The graph in Fig 6.4C shows that a linear gradient was generated across the FEP container.

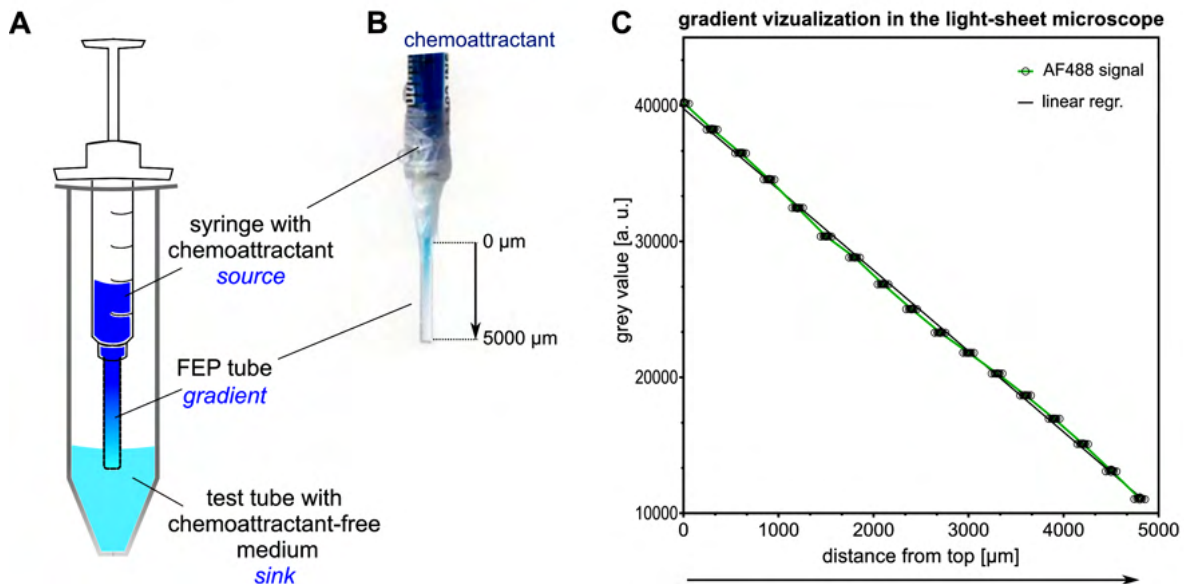


Figure 6.4: Visualisation of the gradient formed across a 3D collagen sample in the FEP tube. **A.** Schematic of the experimental set-up. The FEP tube with the sample embedded in a 3D matrix was fixed to a syringe filled with a chemoattractant (source reservoir). The other end of the sample was submerged in a chemoattractant-free medium (sink reservoir). Due to the diffusion between the reservoirs, a linear gradient was generated across the FEP tube. **B.** The photograph depicts the gradient formed across the sample visualised with a blue food colouring. **C.** The graph shows the gradient of AlexaFluor 488 visualised by the light-sheet fluorescence microscopy. The source syringe was filled with 10  $\mu\text{M}$  solution of the fluorophore and the fluorescence signal in the 3D collagen matrix in the FEP tube was measured 20 hours after fixing the tube to the syringe. A sequence of fluorescent images was taken from the top of the FEP tube to the bottom of the sample with a 300  $\mu\text{m}$  interval inside of the collagen gel, in ten parallel Z-planes (with 2  $\mu\text{m}$  step). The grey value of each frame was measured with the ImageJ software. The grey values of different Z-planes are depicted as staggered circles; the green line connects the mean grey values of the Z-stack. The black line represents the linear regression of the data.

The FEP tubes with cells embedded in collagen I matrix were incubated in the gradient set-up for 20 hours in a cell culture incubator to ensure that the gradient was established over the whole sample before starting the LSFM experiment. Then, the syringe with the FEP tube was mounted into the LSFM sample holder and the tube was submerged into the medium-containing LSFM chamber, which at that point represented the sink reservoir of the chemotaxis chamber. For visualising cell behaviour in the FEP containers a HT1080 cell line was used, being transiently labelled with the fluorescent protein LifeAct-GFP2. The fluorescent signal linked to the actin cytoskeleton was detectable inside of the FEP tube, qualifying FEP to be a suitable material which does not compromise the imaging quality of the method (Fig 6.5).

However, several complications were experienced when establishing the LSFM chemotaxis probes. First of all, the 3D collagen matrix within the FEP tubes was unstable and tended to

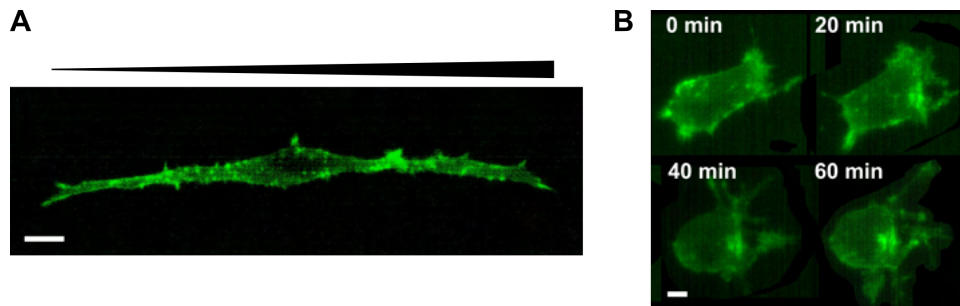


Figure 6.5: LifeAct-GFP2 HT1080 cells in 3D collagen matrix. **A.** The micrograph shows a maximal projection of a LifeAct-GFP2 HT1080 cell embedded in collagen matrix in the FEP chemotaxis chamber, visualised by LSM. Actin cytoskeleton is depicted in green, scale bar = 10  $\mu\text{m}$ . **B.** Time-lapse sequence of a HT1080 cell moving through the matrix by cyclically contracting the rear end (20 min), and protruding filopodia at the front (60 min). Scale bar = 10  $\mu\text{m}$ .

shrink. FEP is a highly inert, non-adhesive material. Therefore, the cell-containing collagen pillar could not attach to its surface. Rather, the collagen matrix floated in the tube, as a net with free ends. Therefore, as a result of the traction forces applied by the cells on the collagen fibres, the gel shrank as the fibres were pulled under the cell bodies. Thus, the cells were unable to effectively migrate; they extracted long branched filopodia along the collagen fibres, but since the fibres were not stabilised, the traction forces could not be transformed into propulsion (Fig 6.6A). Instead, the cells eventually pulled the collagen network into a shrunk bundle that was floating in the middle of the tube (Fig 6.6B).

A possible solution to this problem was providing an anchorage for the collagen pillar by placing short pieces of a glass capillary at the ends of the FEP tube. The stabilisation of the collagen network at the ends of the tubes was sufficient to provide a stable matrix for the cell migration (Fig 6.6C).

Furthermore, the locomotion and viability of the cells enclosed in the FEP tubes was in general impaired. The decreased cell survival was presumably caused by ineffective oxygen diffusion in the sample container, resulting in hypoxic stress to the cells. The aeration of the sample could be improved by penetrating the ends parts of the FEP container with small “ventilation gaps”. Thereby, the survival of cells was partially recovered. Nevertheless, this only enabled observation of the migration in a small number of cells in the vicinity of the gaps. For a more profound analysis of the cell behaviour within the gradient conditions further optimisations of the experimental procedure would be beneficial.

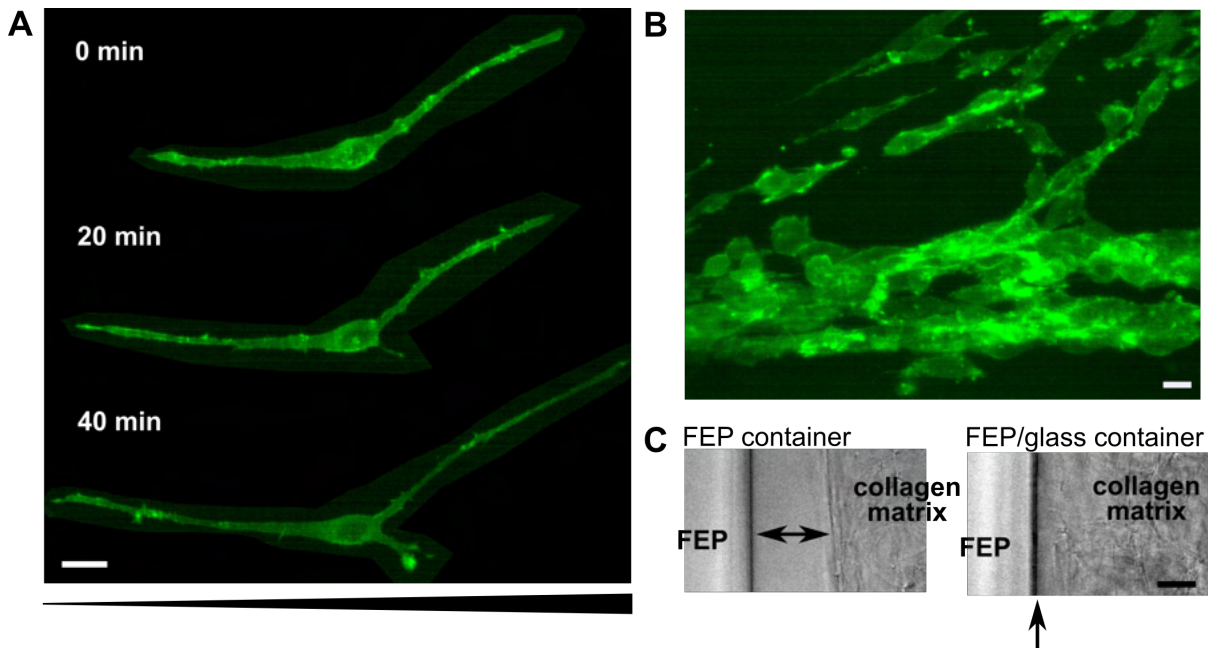


Figure 6.6: Stabilisation of the collagen matrix in the FEP container. **A.** In the seminal experiments the cells protracted long, thin filopodia, mostly aligned with the gradient direction, but were unable to move through the matrix; as the cell depicted in the time-lapse sequence. **B.** The micrograph shows the LifeAct-GFP2 HT1080 that pulled the fibres of the collagen matrix creating a thin pillar inside of the FEP container. **C.** The micrograph on left shows the collagen matrix floating freely in the FEP container. On right, the matrix was stabilised in the container by placing pieces of glass capillaries at the end of the FEP tube, which provided the necessary anchorage for the collagen fibres. All scale bars represent 10  $\mu\text{m}$ .

## 6.3 Discussion

### 6.3.1 TFM/chemotaxis assay

#### On the fabrication of the TFM substrates

In this part of this study, the fabrication protocol for TFM substrates was optimised to yield a substrate suitable for the chemotaxis tool. For that purpose, a glass coverslip was spin-coated with a soft PDMS elastomer, and subsequently fluorescent beads were covalently coupled to the surface. The combination of these two methods guaranteed the formation of an elastomeric layer with a perfectly flat surface that did not bend at the bottom of the chemotaxis chamber, and all beads below the migrating cell being in one focal plane. Other methods that are routinely used to decorate the elastomeric substrates for TFM with the fluorescent beads include physisorption of the beads to the surface, or embedding the beads in the upper layer of the elastomer. They can be either in a random pattern by simple mixing the beads with the pre-polymerised elastomer, or in a regular grid, using a structured wafer (i.e., soft lithography). Alternatively, a regular pattern of micro-structures (e.g., micro-pillars) can be employed to monitor the deformations of the substrate [87]. In contrast to these methods, coupling the beads covalently to the elastomeric

---

substrate has several advantages. First being that all coupled beads are in one microscopic focal plane on top of the substrate, rather than embedded within the elastomer—which facilitates the imaging of the beads and subsequent measurement of their displacement fields, and traction forces. Besides, the fabrication protocol is significantly simpler than protocols based on soft lithography. In contrast to physisorption, covalently coupled beads are firmly fixed to the substrate, and thus can not be removed and digested by cells, which is what often happens with physisorbed beads. The stability of the covalent bonding also simplifies the manipulation with the substrates during the assembly of the TFM/chemotaxis chamber.

### On the analysis of the forces generated by chemotaxing nHEK cells

In this study, the TFM/chemotaxis chambers were applied to examine the traction forces of nHEK cells in respect to gradual, or homogeneous chemical conditions. The preliminary data showed that the cells retain morphologies and distribution of forces that are consistent with previously published results on traction forces exerted by these cells in uniform chemical environments [313]. However, no significant changes were observed in the forces of cells that were exposed to a chemotactic cue.

A previous analysis of traction forces in chemotaxing fast moving cells showed that the effect of the chemically imposed directionality on force generation depends on the mechanical properties of the substrates [88]. Thus, it would be interesting to investigate in further TFM/chemotaxis experiments, whether the relation of the forces and the direction of the migration in slow moving cells is affected in a similar manner by modulating the rigidity of the substrate. Such experiments that expose the cells to precisely controlled, both chemical and mechanical cues could contribute to our understanding of the interplay between the properties of the ECM and cytoskeletal architecture, and the related cell forces. While the complexity of *in vivo* environments induces a large variability in the cell behaviour, an assay combining several precisely tunable parameters would make it possible to determine the effect of each specific environmental cue on cell behaviour, which is necessary in order to build a complete picture of the cell-ECM interactions [314].

In the experiments presented in this thesis, the exposure of cells to a chemotactic stimuli led to inducement of a persistent polarisation and migration in a larger fraction of cells, when compared to samples where TGF $\alpha$  was applied uniformly. Thus, the TFM/chemotaxis chamber could be used as an *in vitro* tool to define the chemical parameters of the environment in order to impose a persistent polarisation in a pre-determined direction, and to unify the course of migration in the studied cells. Furthermore, the microfluidic chamber could be further combined with a substrate functionalised with adhesive surface patterns, in order to control the topological cues, and the density of cell-matrix adhesions (i.e., the loci of mechanotransduction [84]).

---

### 6.3.2 Light-sheet microscopy

In order to study the long-term dynamics of directional cell migration using the LSFM, a protocol for sample preparation was developed in this thesis that makes it possible to expose the studied cells or tissues to a long-term stable chemical gradient. Visualisation of diffusion of a fluorescent dye through the matrix confirmed that using the presented technique, a linear gradient was generated over the sample (Fig 6.4). To construct the chemotaxis chambers for LSFM, FEP tubes were employed as a material that is index matched to the surrounding liquid and allows observing the sample. In agreement with previously reported studies that utilised FEP tubes for mounting LSFM samples [95,98,99], FEP proved to be an apposite material for that purpose, enabling to enclose the sample and isolate it from the surrounding environment, yet not disturbing the imaging quality of LSFM.

However, two major complications arose in this experimental set-up. First, being a highly inert and non-adhesive material, the FEP could not provide any anchorage for the collagen matrix with the cells of interest embedded. Due to the interaction between the cells and the matrix, and the forces applied by the migrating cells on the collagen fibres, the matrix network needs to be stabilised inside of the chemotaxis chamber, so that an effective cell migration through the gel is enabled.<sup>2</sup> In the other published works on FEP tubes utilised as sample holders for LSFM, only immobile samples (i.e., plant seedlings [98,99], or zebrafish embryos [95]) embedded in a stub of solid agarose were studied. For the purpose of examining cell migration through a matrix that interacts with the cells, the non-adhesive nature of the FEP tube poses a difficulty. It was possible to overcome this problem by stabilising the matrix with glass extensions of the FEP chemotaxis chamber that provided the necessary anchorage of the collagen network; however such solution also substantially complicated the sample preparation procedure. Besides, the low oxygen permeability of the FEP/glass chemotaxis chamber resulted in an overall low viability of the cells, presumably due to the imposed hypoxic stress. Ovecká *et al.* presented an “open sample system” that permits the aeration of the samples of later developmental stages of plant seedlings [98]. However, in the chemotaxis set-up developed in this thesis, the attempts of improving the gas exchange in the chamber must not compromise the integrity of the chemical gradient across the sample. This proved to be a major complication for this work. In the preliminary tests, commercially available FEP tubes with rather thick walls (0.8 mm) were used. Using tubes or chambers fabricated from thinner layers of FEP, or other material with higher oxygen permeability, could improve the gas exchange in the chemotaxis chamber, not compromising cell viability.

---

<sup>2</sup>Similar problem with instability of the collagen matrix was encountered also in the end-point chemotaxis assay with the hydrogel migration arena presented in Chapter 4.2; see Figure 4.12.





## 7 Conclusions and outlook

In this thesis, a novel analytical tool for studying chemotaxis of slow-moving cells was established. The basic idea of restricting the cell migration to a specific part of a microfluidic gradient generator has proved suitable to enable a read-out based on the end-point state of the experiment. The presented experiments show that this approach leads to a substantial simplification of the evaluation process, compared to the existing assays. The evaluation of the chemotaxis behaviour in the end-point assay is fast and effortless, making the platform well suited for large-scaled studies, such as drug screening. This was demonstrated in the study of the role of growth factors in the directed migration of epithelial cells. At the same time, the assay profits from the features of the chosen gradient generator, which is tailored to provide reliable data regarding the migration of both fast and slow moving cells, generating a long term stable, well defined gradient, and allowing a microscopic observation of the cells. In future, the availability of such an assay could contribute to a faster deciphering of the signalling events related to cell migration and chemotaxis, with the ultimate goal of developing new therapeutic strategies in fields such as wound healing or cancer treatment.

When establishing the end-point assay, limitations were encountered posed by the low volume and specific geometry of the microfluidic chemotaxis chamber, which are crucial characteristics for the correct function of the tool. At the end, the photolithographical fabrication of hydrogel barriers, or “membranes”, which enclosed cells in a migration arena inside of the gradient region of the microfluidic chamber, proved to be an appropriate strategy for achieving the first goal of this thesis. The remaining drawback of this approach is the necessity to keep the chemotaxis chambers stored wet to sustain the hydrogel structures intact. However, this is compensated by the functionality, relative ease of fabrication, and the application versatility that this set-up provides. Micro-structuring of the PEG4norb hydrogel in the chemotaxis chamber does not require any specialised equipment than an illumination source and a photomask, and can be performed in any standard cell biology laboratory. The 3D character of the confining arena makes the platform suitable for investigation of cells in both 2D or 3D environment. This provides the user with a highly versatile tool for cell migration studies, which can be prepared by modification of a commercially available chemotaxis chamber.

In contrast to the standard bridge chemotaxis assays, the modified, end-point assay provides information on the chemotactic behaviour of the whole cell population, rather than single cells [39,40,185,186]. One might argue that the analysis of trajectories of individual cells delivers

---

a more detailed information on cell locomotion, especially where general migration parameters are concerned, such as velocity, or directness of cell paths [39, 42]. However, the results of the presented work show that the end-point assay provides reliable data on the chemotactic behaviour. Unlike another widely used end-point migration assay, the Boyden/transwell assay, it can clearly discern between a chemotactic response (i.e., directed migration), and chemokinesis (i.e., increase in random motility).

The capacity and relevance of the novel, population-based assay were demonstrated on the study of the chemotactic behaviour of human keratinocytes in response to gradients of various growth factors. The end-point approach made it possible to process a large data set, providing an insight into the signalling events responsible for the directional response of these cells. The effect of five various motogens was studied, all of them being previously reported to prompt chemotaxis in epithelial cells [69, 71, 75–79]. The main goal of this work was to determine the most potent conditions to induce directed migration in the nHEK cells, in order to establish a chemotaxis model for epithelial cells that could be applied in further migration studies. In these experiments, where the cells in contrast to the previous studies were exposed to defined and long lasting gradients, the chemotactic potency of the EGFR ligands EGF and TGF $\alpha$  was confirmed. The other agents, however, did not induce a directional response in the cells, or even attenuated the effect of the identified chemoattractants (e.g., insulin; Chapter 5.2.2). These results suggest a complex interplay of the signals. After identifying the suitable parameters to actuate chemotaxis in nHEKs, the end-point assay was further employed to investigate the underlying signalling events more closely in an experiment where the EGFR signalling was perturbed by inhibitors (Chapter 5.2.3). The results of this experiment confirmed the involvement of the RTK receptor EGFR in the nHEK chemotactic response, and insinuated a disparity in TGF $\alpha$  and EGF signalling.

Along these lines, the end-point assay can be in future applied to identify specific chemoattractants of various cell types, and then subsequently for the study of the interplay of the signalling agents, in the direction of a more complex understanding of the molecular events that underlay cell migration in general (i.e., not only chemotaxis). As such, given its simple read-out, the assay could find application as a simple migration (2D) or invasion (3D) assay for cells whose chemoattractants have already been identified, as was demonstrated in the experiment with the EGFR inhibitors in this study. Here, the gradient only served as a mean to prompt the directional response leading to the accumulation of the cells on one side of the migration arena ( $COMD \neq 0$ ), which is an easily discernible sign of both gradient sensing, and a non-impaired motility. Perturbation of cell migration by a tested agent (e.g., an anti-migratory drug) would naturally result in distortion of the observed chemotactic effect, and could be identified from the distinct cell distribution ( $COMD \approx 0$ ). Although it is not possible to discern from the end-point state of such experiment whether motility in general, or only gradient sensing (i.e., the directional response) was impaired, this could be determined by

---

recording the cell behaviour in the migration arena over time, as the cells in the chemotaxis chamber are accessible for microscopic observation during the whole duration of the experiment. This was also demonstrated in the experiments evaluating the time-dependence of the nHEK chemotactic response (Figures 5.4, 5.5). As already mentioned, this is a significant advantage to the other existing end-point migration assays (e.g., Boyden/transwell). Such migration assay could find a wide user base in drug development, especially in the 3D set-up; i.e., as an invasion assay. The invasive capacity of cancer cells is the key hallmark of aggressive metastatic tumours; invasion and metastasis being responsible for more than 90 % of mortality in solid cancers. For that reason, the underlying migratory machinery came to the focus of the field in the recent years, aiming towards new complementary anticancer therapies targeting specifically metastatic and invasive cells (so called “*migrastatics*”, in contrast to cytotoxic and anti-proliferative drugs [315–317]). However, this endeavour has been in most cases hampered by the lack of readily available, robust, end-point invasion assays that would allow a direct observation of the migrating cells [318,319].

As described above, the population based chemotaxis assay can provide the necessary basis (i.e., identification of chemotaxis-inducing conditions) for a further, in-depth investigation of chemotactic behaviour on a single cell level. Once a model of directed migration is established for the cell type of interest, further questions might arise regarding the guided migration, like: What is happening on the subcellular level, what are the similarities and discrepancies in the processes that underlay cell migration in response to a chemically uniform or gradual environment (e.g., in regard to dynamics of cytoskeleton, traction force generation, distribution of signalling molecules)? How do cells react to, and interpret the manifold guidance cues; i.e., what is the interplay between chemical and mechanical signals that a cell migrating through any physiological environment is simultaneously exposed to? To provide the means to address such questions, the next aim of this thesis was to construct tools that could couple investigation of chemotaxis with other parameters, using advanced imaging methods such as traction force microscopy, or laser sheet fluorescence microscopy. In this part of the thesis, a chemotaxis chamber combined with a substrate for traction force microscopy was introduced. With this tool, a suitable chemoattractant gradient could be applied to actuate the directed migration of the studied cells, while measuring their traction forces (Chapter 6.1). Although the preliminary experiments with nHEK cells did not reveal any difference in the force generation in directly and randomly migrating cells, literature suggests that there are differences in forces generated by fast moving cells in response to changes in the chemical environment in relation to the stiffness of the substrate [88]. It would be interesting to further investigate if this phenomenon is specific for fast migrating cells, or is under some conditions discernible also in slow moving cells.

Since the substrate stiffness of the TFM/chemotaxis chamber can be tuned, and the method can be combined with fluorescent labelling of subcellular structures, the tool represents a plat-

---

form where the dynamics of tension forces and cytoskeletal architecture during cell migration can be observed and measured in a precisely, both chemically and mechanically defined environment. This makes it possible to determine the cell response to each specific parameter. On another note, the possibility to impose a unite direction of polarisation in the analysed cells in the TFM/chemotaxis chamber, potentially by additionally micro-patterning the substrate with defined adhesive patches, could help to simplify and automatise the analysis of cell behaviour.

To enable studying cellular processes in chemotaxing cells over long time periods in 3D environments without exposing the cells to a high illumination stress, a possible experimental set-up for LSFM was outlined. A chemotaxis chamber was constructed that generates a stable linear gradient, while the sample can be imaged with the commercial LSFM system from Zeiss. However, a remaining challenge is to find a suitable strategy to improve the oxygenation of the chamber. Then, a LSFM/chemotaxis chamber would make it possible to study the dynamics of the cytoskeletal compartments of chemotaxing cells, and the ECM-matrix interactions. Furthermore, the intracellular signalling pathways that participate in the chemotactic stimuli transduction and the subsequent long-term directional response in living cells could be investigated. Next to studying single cell migration in 3D environments, a set-up exposing a LSFM sample to a chemical gradient could find its application also in many other fields of biological research that operate with larger living samples, such as organoids, or even whole organisms, since gradual chemical cues play an important role in many cellular processes (e.g., embryonic development).

To conclude, the analytical tool introduced in this work provides a versatile platform for high-throughput investigation of cell chemotaxis in both fast and slow moving cells; thus, offering a mean for drug screening and clinical testing of therapeutics targeting the migratory apparatus of cells, and in general for gathering the knowledge-base towards comprehension of the chemically stimulated processes underlying cell migration. The performed experiments help to gain an insight into the chemical guidance of epithelial cells, a crucial player in wound healing and related pathologies. The results further affirmed the importance of studying cell behaviour in precisely defined environments, using tools that are tailored to the specific migration strategies of given cell types.

# Bibliography

- [1] T. Mitchison and L. Cramer, “Actin-Based Cell Motility and Cell Locomotion,” *Cell*, vol. 84, no. 3, pp. 371–379, 1996.
- [2] A. J. Ridley, M. A. Schwartz, K. Burridge, R. A. Firtel, M. H. Ginsberg, G. Borisy, J. T. Parsons, and A. R. Horwitz, “Cell Migration: Integrating Signals from Front to Back,” *Science*, vol. 302, no. 5651, pp. 1704–1709, 2003.
- [3] M. Sarris and M. Sixt, “Navigating in tissue mazes: Chemoattractant interpretation in complex environments,” *Current Opinion in Cell Biology*, vol. 36, pp. 93–102, 2015.
- [4] Y. Artemenko, L. Axiotakis, J. Borleis, P. A. Iglesias, and P. N. Devreotes, “Chemical and mechanical stimuli act on common signal transduction and cytoskeletal networks,” *Proceedings of the National Academy of Sciences of the United States of America*, vol. 113, no. 47, pp. E7500–E7509, 2016.
- [5] D. Lauffenburger and F. Horwitz, “Cell migration: a physically integrated molecular process,” *Cell*, vol. 84, no. 3, pp. 359–369, 1996.
- [6] P. Friedl, K. S. Zänker, and E. B. Bröcker, “Cell migration strategies in 3-D extracellular matrix: Differences in morphology, cell matrix interactions, and integrin function,” *Microscopy Research and Technique*, vol. 43, no. 5, pp. 369–378, 1998.
- [7] X. Trepap, Z. Chen, and K. Jacobson, “Cell migration,” *Comprehensive Physiology*, vol. 2, no. 4, pp. 2369–2392, 2012.
- [8] K. Wolf and P. Friedl, “Extracellular matrix determinants of proteolytic and non-proteolytic cell migration,” *Trends in Cell Biology*, vol. 21, no. 12, pp. 736–744, 2011.
- [9] G. Charras and E. Sahai, “Physical influences of the extracellular environment on cell migration,” *Nature Reviews Molecular Cell Biology*, vol. 15, no. 12, pp. 813–824, 2014.
- [10] A. D. Doyle and K. M. Yamada, “Mechanosensing via cell-matrix adhesions in 3D microenvironments,” *Experimental Cell Research*, vol. 343, no. 1, pp. 60–66, 2016.
- [11] C. D. Paul, W.-C. Hung, D. Wirtz, and K. Konstantopoulos, “Engineered Models of Confined Cell Migration,” *Annual Review of Biomedical Engineering*, vol. 18, no. 1, pp. 159–180, 2016.
- [12] T. Lämmermann, B. L. Bader, S. J. Monkley, T. Worbs, R. Wedlich-Söldner, K. Hirsch, M. Keller, R. Förster, D. R. Critchley, R. Fässler, and M. Sixt, “Rapid leukocyte migration by integrin-independent flowing and squeezing,” *Nature*, vol. 453, no. 7191, pp. 51–55, 2008.
- [13] P. Friedl and K. Wolf, “Proteolytic interstitial cell migration: A five-step process,” *Cancer and Metastasis Reviews*, vol. 28, no. 1-2, pp. 129–135, 2009.
- [14] P. Friedl and K. Wolf, “Plasticity of cell migration: A multiscale tuning model,” *Journal of Cell Biology*, vol. 188, no. 1, pp. 11–19, 2010.
- [15] K. Wolf, M. Lindert, M. Krause, S. Alexander, J. te Riet, A. L. Willis, R. M. Hoffman, C. G. Figdor, S. J. Weiss, and P. Friedl, “Physical limits of cell migration: Control by ECM space and nuclear deformation and tuning by proteolysis and traction force,” *Journal of Cell Biology*, vol. 201, no. 7, pp. 1069–1084, 2013.

- 
- [16] R. Bzymek, M. Horsthemke, K. Isfort, S. Mohr, K. Tjaden, C. Müller-Tidow, M. Thomann, T. Schwerdtle, M. Bähler, A. Schwab, and P. J. Hanley, “Real-time two- and three-dimensional imaging of monocyte motility and navigation on planar surfaces and in collagen matrices: Roles of Rho,” *Scientific Reports*, vol. 6, no. 1, p. 25016, 2016.
- [17] J. Condeelis and J. E. Segall, “Intravital imaging of cell movement in tumours,” *Nature Reviews Cancer*, vol. 3, no. 12, pp. 921–930, 2003.
- [18] W. J. Polacheck, I. K. Zervantonakis, and R. D. Kamm, “Tumor cell migration in complex microenvironments,” *Cellular and Molecular Life Sciences*, vol. 70, no. 8, pp. 1335–1356, 2013.
- [19] S. P. Singh, M. P. Schwartz, E. Y. Tokuda, Y. Luo, R. E. Rogers, M. Fujita, N. G. Ahn, and K. S. Anseth, “A synthetic modular approach for modeling the role of the 3D microenvironment in tumor progression,” *Scientific Reports*, vol. 5, p. 17814, 2015.
- [20] K. A. Kyburz and K. S. Anseth, “Three-dimensional hMSC motility within peptide-functionalized PEG-based hydrogels of varying adhesivity and crosslinking density,” *Acta Biomaterialia*, vol. 9, no. 5, pp. 6381–6392, 2013.
- [21] C. F. Buchanan, E. E. Voigt, C. S. Szot, J. W. Freeman, P. P. Vlachos, and M. N. Rylander, “Three-Dimensional Microfluidic Collagen Hydrogels for Investigating Flow-Mediated Tumor-Endothelial Signaling and Vascular Organization,” *Tissue Engineering Part C: Methods*, vol. 20, no. 1, pp. 64–75, 2014.
- [22] M. Kyung, M. H. Rich, J. Lee, and H. Kong, “A bio-inspired , microchanneled hydrogel with controlled spacing of cell adhesion ligands regulates 3D spatial organization of cells and tissue,” *Biomaterials*, vol. 58, pp. 26–34, 2015.
- [23] M. B. Browning, B. Russell, J. Rivera, M. Höök, and E. M. Cosgriff-Hernandez, “Bioactive hydrogels with enhanced initial and sustained cell interactions,” *Biomacromolecules*, vol. 14, pp. 2225–2233, 2013.
- [24] H. U. Keller, P. C. Wilkinson, M. Abercrombie, E. L. Becker, J. G. Hirsch, M. E. Miller, R. W. Scott, and S. H. Zigmond, “A proposal for the definition of terms related to locomotion of leukocytes and other cells,” *Bulletin of the World Health Organization*, vol. 58, no. 3, pp. 505–509, 1980.
- [25] J. Condeelis, R. H. Singer, and J. E. Segall, “The Great Escape: When Cancer Cells Hijack the Genes for Chemotaxis and Motility,” *Annual Review of Cell and Developmental Biology*, vol. 21, no. 1, pp. 695–718, 2005.
- [26] T. F. Deuel, R. S. Kawahara, T. A. Mustoe, and a. F. Pierce, “Growth factors and wound healing: platelet-derived growth factor as a model cytokine.” *Annual Review of Medicine*, vol. 42, no. 1, pp. 567–584, 1991.
- [27] A. J. Singer and R. A. Clark, “Cutaneous Wound Healing,” *New England Journal of Medicine*, vol. 341, no. 10, pp. 738–746, 1999.
- [28] N. J. Protopsaltis, W. Liang, E. Nudleman, and N. Ferrara, “Interleukin-22 promotes tumor angiogenesis,” *Angiogenesis*, vol. 22, no. 2, pp. 311–323, 2019.
- [29] P. Martin and R. Nunan, “Cellular and molecular mechanisms of repair in acute and chronic wound healing,” *British Journal of Dermatology*, vol. 173, no. 2, pp. 370–378, 2015.
- [30] A. T. Grazul-Bilska, M. L. Johnson, J. J. Bilski, D. A. Redmer, L. P. Reynolds, A. Abdullah, and K. M. Abdullah, “Wound healing: The role of growth factors,” *Drugs of Today*, vol. 39, no. 10, pp. 787–800, 2003.
- [31] A. Shellard and R. Mayor, “Chemotaxis during neural crest migration,” *Seminars in Cell and Developmental Biology*, vol. 55, pp. 111–118, 2016.

- 
- [32] B. Moser and K. Willmann, "Chemokines: Role in inflammation and immune surveillance," *Annals of the Rheumatic Diseases*, vol. 63, no. 2, pp. 84–89, 2004.
- [33] J. E. Bear and J. M. Haugh, "Directed migration of mesenchymal cells: where signaling and the cytoskeleton meet.," *Current Opinion in Cell Biology*, vol. 30, pp. 74–82, 2014.
- [34] P. J. M. Van Haastert and P. N. Devreotes, "Chemotaxis: signalling the way forward," *Nature Reviews Molecular Cell Biology*, vol. 5, no. 8, pp. 626–634, 2004.
- [35] L. Stephens, L. Milne, and P. Hawkins, "Moving towards a Better Understanding of Chemotaxis," *Current Biology*, vol. 18, no. 11, pp. 485–494, 2008.
- [36] S. H. Zigmond and J. G. Hirsch, "Leukocyte locomotion and chemotaxis. New methods for evaluation, and demonstration of a cell-derived chemotactic factor.," *The Journal of Experimental Medicine*, vol. 137, no. 2, pp. 387–410, 1973.
- [37] M. H. Gail and C. W. Boone, "The Locomotion of Mouse Fibroblasts in Tissue Culture," *Biophysical Journal*, vol. 10, no. 10, pp. 980–993, 1970.
- [38] R. Zantl and E. Horn, "Chemotaxis of slow migrating mammalian cells analysed by video microscopy," *Methods in Molecular Biology*, vol. 769, pp. 191–203, 2011.
- [39] P. Zengel, A. Nguyen-Hoang, C. Schildhammer, R. Zantl, V. Kahl, and E. Horn, " $\mu$ -Slide Chemotaxis: a new chamber for long-term chemotaxis studies.," *BMC Cell Biology*, vol. 12, no. 21, pp. 1–14, 2011.
- [40] S. H. Zigmond, "Ability of polymorphonuclear leukocytes to orient in gradients of chemotactic factors," *Journal of Cell Biology*, vol. 75, no. 2, pp. 606–616, 1977.
- [41] I. Barkefors, S. Thorslund, F. Nikolajeff, and J. Kreuger, "A fluidic device to study directional angiogenesis in complex tissue and organ culture models," *Lab on a Chip*, vol. 9, no. 4, pp. 529–535, 2009.
- [42] P. Friedl, P. B. Noble, and K. S. Zänker, "Lymphocyte locomotion in three-dimensional collagen gels comparison of three quantitative methods for analysing cell trajectories," *Journal of Immunological Methods*, vol. 165, no. 2, pp. 157–165, 1993.
- [43] E. Meijering, I. Smal, and G. Danuser, "Tracking in molecular bioimaging," *IEEE Signal Processing Magazine*, vol. 23, no. 3, pp. 46–53, 2006.
- [44] E. T. Roussos, J. S. Condeelis, and A. Patsialou, "Chemotaxis in cancer," *Nature Reviews Cancer*, vol. 11, no. 8, pp. 573–587, 2011.
- [45] S. Goswami, W. Wang, J. B. Wyckoff, and J. S. Condeelis, "Breast Cancer Cells Isolated by Chemotaxis from Primary Tumors Show Increased Survival and Resistance to Chemotherapy," *Cancer Research*, vol. 64, pp. 7664–7667, 2004.
- [46] J. M. Birmingham, J. V. Busik, F. M. Hansen-Smith, and J. I. Fenton, "Novel mechanism for obesity-induced colon cancer progression," *Carcinogenesis*, vol. 30, no. 4, pp. 690–697, 2009.
- [47] S. A. Eming, P. Martin, and M. Tomic-Canic, "Wound repair and regeneration: mechanisms, signaling, and translation.," *Science Translational Medicine*, vol. 6, no. 265, p. 265sr6, 2014.
- [48] I. Pastar, O. Stojadinovic, N. C. Yin, H. Ramirez, A. G. Nusbaum, A. Sawaya, S. B. Patel, L. Khalid, R. R. Isseroff, and M. Tomic-Canic, "Epithelialization in Wound Healing: A Comprehensive Review," *Advances in Wound Care*, vol. 3, no. 7, pp. 445–464, 2014.
- [49] G. Kirfel and V. Herzog, "Migration of epidermal keratinocytes: Mechanisms, regulation, and biological significance," *Protoplasma*, vol. 223, no. 2-4, pp. 67–78, 2004.
- [50] F. Grinnell, "Wound repair, keratinocyte activation and integrin modulation," *Journal of Cell Science*, vol. 101, no. 1, pp. 1–5, 1992.

- 
- [51] M. A. Seeger and A. S. Paller, "The Roles of Growth Factors in Keratinocyte Migration," *Advances in Wound Care*, vol. 4, no. 4, pp. 213–224, 2015.
- [52] S. Werner, K. G. Peters, M. T. Longaker, F. Fuller-Pace, M. J. Banda, and L. T. Williams, "Large induction of keratinocyte growth factor expression in the dermis during wound healing," *Proceedings of the National Academy of Sciences of the United States of America*, vol. 89, no. 15, pp. 6896–6900, 1992.
- [53] R. A. Clark, J. M. Lanigan, P. DellaPelle, E. Manseau, H. F. Dvorak, and R. B. Colvin, "Fibronectin and fibrin provide a provisional matrix for epidermal cell migration during wound reepithelialization," *Journal of Investigative Dermatology*, vol. 79, no. 5, pp. 264–269, 1982.
- [54] H. Seppa, G. Grotendorst, S. Seppa, E. Schiffmann, and G. R. Martin, "Platelet-derived growth factor is chemotactic for fibroblasts," *Journal of Cell Biology*, vol. 92, no. 2, pp. 584–588, 1982.
- [55] G. Kirfel, A. Rigort, B. Borm, C. Schulte, and V. Herzog, "Structural and compositional analysis of the keratinocyte migration track," *Cell Motility and the Cytoskeleton*, vol. 55, no. 1, pp. 1–13, 2003.
- [56] J. K. Klarlund and E. R. Block, "Free edges in epithelia as cues for motility," *Cell Adhesion and Migration*, vol. 5, no. 2, pp. 106–110, 2011.
- [57] E. R. Block, M. A. Tolino, J. S. Lozano, K. L. Lathrop, R. S. Sullenberger, A. R. Mazie, and J. K. Klarlund, "Free edges in epithelial cell sheets stimulate epidermal growth factor receptor signaling," *Molecular Biology of the Cell*, vol. 21, no. 13, pp. 2172–2181, 2010.
- [58] P. Friedl and D. Gilmour, "Collective cell migration in morphogenesis, regeneration and cancer," *Nature Reviews Molecular Cell Biology*, vol. 10, no. 7, pp. 445–457, 2009.
- [59] N. Martinet, L. A. Harne, and G. R. Grotendorst, "Identification and Characterization of Chemoattractants for Epidermal Cells," *Journal of Investigative Dermatology*, vol. 90, no. 2, pp. 122–126, 1988.
- [60] H. A. Navsaria, S. R. Myers, I. M. Leigh, and I. A. McKay, "Culturing skin in vitro for wound therapy," *Trends in Biotechnology*, vol. 13, no. 3, pp. 91–100, 1995.
- [61] A. Gröne, "Keratinocytes and cytokines," *Veterinary Immunology and Immunopathology*, vol. 88, no. 1-2, pp. 1–12, 2002.
- [62] Ibidi, "Appl. Note 24: Chemotaxis of HT-1080 cells in 2D and 3D," 2015.
- [63] K. Wolf, I. Mazo, H. Leung, K. Engelke, U. H. von Andrian, E. I. Deryugina, A. Y. Strongin, E.-B. Bröcker, and P. Friedl, "Compensation mechanism in tumor cell migration: mesenchymal-amoeboid transition after blocking of pericellular proteolysis," *The Journal of Cell Biology*, vol. 160, no. 2, pp. 267–277, 2003.
- [64] V. Niggli, M. Schmid, and A. Nievergelt, "Differential roles of Rho-kinase and myosin light chain kinase in regulating shape, adhesion, and migration of HT1080 fibrosarcoma cells," *Biochemical and Biophysical Research Communications*, vol. 343, no. 2, pp. 602–608, 2006.
- [65] J. C. Hoffmann and J. L. West, "Three-dimensional photolithographic micropatterning: a novel tool to probe the complexities of cell migration," *Integrative Biology*, vol. 5, pp. 817–27, 2013.
- [66] M. P. Schwartz, B. D. Fairbanks, R. E. Rogers, R. Rangarajan, M. H. Zaman, and K. S. Anseth, "A synthetic strategy for mimicking the extracellular matrix provides new insight about tumor cell migration," *Integrative Biology*, vol. 2, no. 1, pp. 32–40, 2010.
- [67] G. Michel, L. Kemény, R. U. Peter, A. Beetz, C. Ried, P. Arenberger, and T. Ruzicka, "Interleukin-8 receptor-mediated chemotaxis of normal human epidermal cells," *FEBS Letters*, vol. 305, no. 3, pp. 241–243, 1992.



- 
- [68] J. L. Andresen and N. Ehlers, "Chemotaxis of human keratocytes is increased by platelet-derived growth factor-BB, epidermal growth factor, transforming growth factor-alpha, acidic fibroblast growth factor, insulin-like growth factor-I, and transforming growth factor-beta," *Current Eye Research*, vol. 17, no. 1, pp. 79–87, 1998.
- [69] R. Gyulai, J. Hunyadi, A. Kenderessy-Szabo, L. Kemeny, and A. Dobozy, "Chemotaxis of freshly separated and cultured human keratinocytes," *Clinical and Experimental Dermatology*, vol. 19, no. 4, pp. 309–311, 1994.
- [70] D. N. Sauder, F. W. Orr, S. Matic, D. Stetsko, K. P. Parker, R. Chizzonite, and P. L. Kilian, "Human interleukin-1 alpha is chemotactic for normal human keratinocytes," *Immunology Letters*, vol. 22, no. 2, pp. 123–127, 1989.
- [71] E. Ho and L. Dagnino, "Epidermal growth factor induction of front-rear polarity and migration in keratinocytes is mediated by integrin-linked kinase and ELMO2," *Molecular Biology of the Cell*, vol. 23, no. 3, pp. 492–502, 2012.
- [72] E. P. Brennan, X.-H. Tang, A. M. Stewart-Akers, L. J. Gudas, and S. F. Badylak, "Chemoattractant activity of degradation products of fetal and adult skin extracellular matrix for keratinocyte progenitor cells," *Journal of Tissue Engineering and Regenerative Medicine*, vol. 2, no. 8, pp. 491–498, 2008.
- [73] A. I. Chernyavsky, J. Arredondo, L. M. Marubio, and S. A. Grando, "Differential regulation of keratinocyte chemokinesis and chemotaxis through distinct nicotinic receptor subtypes," *Journal of Cell Science*, vol. 117, no. Pt 23, pp. 5665–5679, 2004.
- [74] G. Kirfel, B. Borm, A. Rigort, and V. Herzog, "The secretory beta-amyloid precursor protein is a motogen for human epidermal keratinocytes," *European Journal of Cell Biology*, vol. 81, no. 12, pp. 664–76, 2002.
- [75] Y. Li, J. Fan, M. Chen, W. Li, and D. T. Woodley, "Transforming Growth Factor-Alpha: A Major Human Serum Factor that Promotes Human Keratinocyte Migration," *Journal of Investigative Dermatology*, vol. 126, no. 9, pp. 2096–2105, 2006.
- [76] D. Cha, P. O'Brien, E. A. O'Toole, D. T. Woodley, and L. G. Hudson, "Enhanced modulation of keratinocyte motility by transforming growth factor- $\alpha$  (TGF- $\alpha$ ) relative to epidermal growth factor (EGF)," *Journal of Investigative Dermatology*, vol. 106, no. 4, pp. 590–597, 1996.
- [77] Y. Barrandon and H. Green, "Cell migration is essential for sustained growth of keratinocyte colonies: the roles of TGF-a and EGF," *Cell*, vol. 50, pp. 1131–1137, 1987.
- [78] N. E. Wikner, K. A. Persichitte, J. B. Baskin, L. D. Nielsen, and R. A. Clark, "Transforming Growth Factor- $\beta$  Stimulates the Expression of Fibronectin by Human Keratinocytes," *Journal of Investigative Dermatology*, vol. 91, pp. 207–212, 1988.
- [79] W. Li, G. Henry, J. Fan, B. Bandyopadhyay, K. Pang, W. Garner, M. Chen, and D. T. Woodley, "Signals that initiate, augment, and provide directionality for human keratinocyte motility," *The Journal of Investigative Dermatology*, vol. 123, no. 4, pp. 622–633, 2004.
- [80] T. Oliver, J. Lee, and K. Jacobson, "Forces exerted by locomoting cells," *Seminars in Cell and Developmental Biology*, vol. 5, no. 3, pp. 139–147, 1994.
- [81] S. C. Kuo and D. A. Lauffenburger, "Relationship between receptor/ligand binding affinity and adhesion strength," *Biophysical Journal*, vol. 65, no. 5, pp. 2191–2200, 1993.
- [82] C.-M. M. Lo, H.-B. B. Wang, M. Dembo, and Y.-L. Wang, "Cell Movement Is Guided by the Rigidity of the Substrate," *Biophysical Journal*, vol. 79, no. 1, pp. 144–152, 2000.
- [83] S. V. Plotnikov, A. M. Pasapera, B. Sabass, and C. M. Waterman, "Force fluctuations within focal adhesions mediate ECM-rigidity sensing to guide directed cell migration," *Cell*, vol. 151, no. 7, pp. 1513–1527, 2012.

- 
- [84] U. S. Schwarz and M. L. Gardel, “United we stand – integrating the actin cytoskeleton and cell–matrix adhesions in cellular mechanotransduction,” *Journal of Cell Science*, vol. 125, pp. 3051–3060, 2012.
- [85] M. Dembo and Y. L. Wang, “Stresses at the cell-to-substrate interface during locomotion of fibroblasts,” *Biophysical Journal*, vol. 76, no. 4, pp. 2307–2316, 1999.
- [86] N. Q. Balaban, U. S. Schwarz, D. Riveline, P. Goichberg, G. Tzur, I. Sabanay, D. Mahalu, S. Safran, A. Bershadsky, L. Addadi, and B. Geiger, “Force and focal adhesion assembly: A close relationship studied using elastic micropatterned substrates,” *Nature Cell Biology*, vol. 3, no. 5, pp. 466–472, 2001.
- [87] O. du Roure, A. Saez, A. Buguin, R. H. Austin, P. Chavrier, P. Silberzan, and B. Ladoux, “Force mapping in epithelial cell migration,” *Proceedings of the National Academy of Sciences*, vol. 102, no. 7, pp. 2390–2395, 2005.
- [88] R. A. Jannat, M. Dembo, and D. A. Hammer, “Traction forces of neutrophils migrating on compliant substrates,” *Biophysical Journal*, vol. 101, no. 3, pp. 575–84, 2011.
- [89] J. P. Rieu, C. Barentin, S. Sawai, Y. Maeda, and Y. Sawada, “Cell movements and mechanical force distribution during the migration of Dictyostelium slugs,” *Journal of Biological Physics*, vol. 30, no. 4, pp. 345–364, 2004.
- [90] A. K. Harris, P. Wild, and D. Stopak, “Silicone rubber substrata: a new wrinkle in the study of cell locomotion,” *Science*, vol. 208, no. 4440, pp. 177–9, 1980.
- [91] B. Sabass, M. L. Gardel, C. M. Waterman, and U. S. Schwarz, “High resolution traction force microscopy based on experimental and computational advances,” *Biophysical Journal*, vol. 94, no. 1, pp. 207–220, 2008.
- [92] J. Huisken, J. Swoger, F. Del Bene, J. Wittbrodt, and E. H. K. Stelzer, “Optical sectioning deep inside live embryos by selective plane illumination microscopy,” *Science*, vol. 305, no. 5686, pp. 1007–9, 2004.
- [93] J. Doerr, M. K. Schwarz, D. Wiedermann, A. Leinhaas, A. Jakobs, F. Schloen, I. Schwarz, M. Diedenhofen, N. C. Braun, P. Koch, D. A. Peterson, U. Kubitscheck, M. Hoehn, and O. Brüstle, “Whole-brain 3D mapping of human neural transplant innervation,” *Nature Communications*, vol. 8, p. 14162, 2017.
- [94] J. G. Ritter, R. Veith, A. Veenendaal, J. P. Siebrasse, and U. Kubitscheck, “Light sheet microscopy for single molecule tracking in living tissue,” *PloS One*, vol. 5, no. 7, p. e11639, 2010.
- [95] A. Kaufmann, M. Mickoleit, M. Weber, and J. Huisken, “Multilayer mounting enables long-term imaging of zebrafish development in a light sheet microscope,” *Development*, vol. 139, no. 17, pp. 3242–3247, 2012.
- [96] P. A. Santi, “Light sheet fluorescence microscopy: A review,” *Journal of Histochemistry and Cytochemistry*, vol. 59, no. 2, pp. 129–138, 2011.
- [97] Chemours™, “Teflon™ FEP product website.” [https://www.chemours.com/Teflon-Industrial/en-US/products/product\\_by\\_name/teflon\\_fep/index.html](https://www.chemours.com/Teflon-Industrial/en-US/products/product_by_name/teflon_fep/index.html); accessed: 5.11.2018.
- [98] M. Ovečka, L. Vaškebová, G. Komis, I. Luptovčiak, A. Smertenko, J. Šamaj, M. Ovec, L. Va, G. Komis, I. Luptovc, and A. Smertenko, “Preparation of plants for developmental and cellular imaging by light-sheet microscopy,” *Nature Protocols*, vol. 10, no. 8, pp. 1234–1247, 2015.
- [99] M. A. de Luis Balaguer, M. Ramos-Pezzotti, M. B. Rahhal, C. E. Melvin, E. Johannes, T. J. Horn, and R. Sozzani, “Multi-sample Arabidopsis Growth and Imaging Chamber (MAGIC) for long term imaging in the ZEISS Lightsheet Z.1,” *Developmental Biology*, vol. 419, no. 1, pp. 19–25, 2016.

- 
- [100] C. Dobbel, *Antony van Leeuwenhoek and his "Little animals"*. New York: Harcourt, Brace and company, 1932.
- [101] D. Bray, *Cell Movements : From Molecules to Motility*. New York: Garland Publishing, 2nd ed., 2001.
- [102] H. C. Berg, "Motile behavior of bacteria," *Physics Today*, vol. 53, no. 1, pp. 24–29, 2000.
- [103] G. Drews, "Contributions of Theodor Wilhelm Engelmann on phototaxis, chemotaxis, and photosynthesis," *Photosynthesis Research*, vol. 83, no. 1, pp. 25–34, 2005.
- [104] H. C. Berg, "Chemotaxis in bacteria," *Annual Review of Biophysics and Bioengineering*, vol. 4, no. 7, pp. 119–136, 1975.
- [105] S. Cerezales, S. Boryshpolets, and M. Eisenbach, "Behavioral mechanisms of mammalian sperm guidance," *Asian Journal of Andrology*, vol. 17, no. 4, pp. 628–632, 2015.
- [106] G. L. Garcia and C. A. Parent, "Signal relay during chemotaxis," *Journal of Microscopy*, vol. 231, no. 3, pp. 529–534, 2008.
- [107] F. Sánchez-Madrid and M. A. Del Pozo, "Leukocyte polarization in cell migration and immune interactions," *EMBO Journal*, vol. 18, no. 3, pp. 501–511, 1999.
- [108] Hohmann and Deghani, "The Cytoskeleton—A Complex Interacting Meshwork," *Cells*, vol. 8, no. 4, p. 362, 2019.
- [109] Y.-L. Shih and L. Rothfield, "The bacterial cytoskeleton," *Microbiology and Molecular Biology Reviews*, vol. 70, no. 3, pp. 729–754, 2006.
- [110] J. V. Small, K. Rottner, I. Kaverina, and K. I. Anderson, "Assembling an actin cytoskeleton for cell attachment and movement," *Biochimica et Biophysica Acta - Molecular Cell Research*, vol. 1404, no. 3, pp. 271–281, 1998.
- [111] C. S. Izzard and L. R. Lochner, "Formation of cell-to-substrate contacts during fibroblast motility: an interference-reflexion study.," *Journal of Cell Science*, vol. 42, no. 1, pp. 81–116, 1980.
- [112] S. Lee and S. Kumar, "Actomyosin stress fiber mechanosensing in 2D and 3D," *F1000Research*, vol. 5, pp. 2261–2272, 2016.
- [113] B. Geiger, J. P. Spatz, and A. D. Bershadsky, "Environmental sensing through focal adhesions," *Nature Reviews Molecular Cell Biology*, vol. 10, no. 1, pp. 21–33, 2009.
- [114] T. D. Pollard, "Polymerization of ADP-Actin," *Journal of Cell Biology*, vol. 99, pp. 769–777, 1984.
- [115] Y. L. Wang, "Exchange of actin subunits at the leading edge of living fibroblasts: Possible role of treadmilling," *Journal of Cell Biology*, vol. 101, no. 2, pp. 597–602, 1985.
- [116] T. D. Pollard and G. G. Borisy, "Cellular motility driven by assembly and disassembly of actin filaments," *Cell*, vol. 112, no. 4, pp. 453–465, 2003.
- [117] T. D. Pollard, "Actin and actin-binding proteins," *Cold Spring Harbor Perspectives in Biology*, vol. 8, no. 8, 2016.
- [118] S. J. Heasman and A. J. Ridley, "Mammalian Rho GTPases: new insights into their functions from in vivo studies.," *Nature Reviews Molecular Cell Biology*, vol. 9, pp. 690–701, 2008.
- [119] L. Van Aelst and C. D'Souza-Schorey, "Rho GTPases and signaling networks," *Genes & Development*, vol. 11, no. 18, pp. 2295–2322, 1997.
- [120] A. J. Ridley, H. F. Paterson, C. L. Johnston, D. Diekmann, and A. Hall, "The small GTP-binding protein rac regulates growth factor-induced membrane ruffling," *Cell*, vol. 70, no. 3, pp. 401–410, 1992.

- 
- [121] C. D. Nobes and A. Hall, "Rho, rac, and cdc42 GTPases regulate the assembly of multi-molecular focal complexes associated with actin stress fibers, lamellipodia, and filopodia.," *Cell*, vol. 81, no. 1, pp. 53–62, 1995.
- [122] A. J. Ridley and A. Hall, "The small GTP-binding protein rho regulates the assembly of focal adhesions and actin stress fibers in response to growth factors," *Cell*, vol. 70, no. 3, pp. 389–399, 1992.
- [123] A. J. Ridley, "Rho GTPases and cell migration.," *Journal of Cell Science*, vol. 114, no. 15, pp. 2713–2722, 2001.
- [124] E. F. Woodham and L. M. Machesky, "Polarised cell migration: Intrinsic and extrinsic drivers," *Current Opinion in Cell Biology*, vol. 30, no. 1, pp. 25–32, 2014.
- [125] E. E. Evers, G. C. Zondag, A. Malliri, L. S. Price, J. P. ten Klooster, R. A. van der Kammen, and J. G. Collard, "Rho family proteins in cell adhesion and cell migration.," *European Journal of Cancer*, vol. 36, no. 10, pp. 1269–74, 2000.
- [126] M. Machacek, L. Hodgson, C. Welch, H. Elliott, O. Pertz, P. Nalbant, A. Abell, G. L. Johnson, K. M. Hahn, and G. Danuser, "Coordination of Rho GTPase activities during cell protrusion," *Nature*, vol. 461, no. 7260, pp. 99–103, 2009.
- [127] L. G. Tilney, E. M. Bonder, and D. J. DeRosier, "Actin filaments elongate from their membrane-associated ends," *Journal of Cell Biology*, vol. 90, no. 2, pp. 485–494, 1981.
- [128] K. Burridge, "Focal Adhesions: Transmembrane Junctions Between The Extracellular Matrix And The Cytoskeleton," *Annual Review of Cell and Developmental Biology*, vol. 4, no. 1, pp. 487–525, 1988.
- [129] P. Friedl and E. B. Bröcker, "The biology of cell locomotion within three-dimensional extracellular matrix.," *Cellular and Molecular Life Sciences*, vol. 57, no. 1, pp. 41–64, 2000.
- [130] S. Pellegrin and H. Mellor, "Actin stress fibres," *Journal of Cell Science*, vol. 120, no. 20, pp. 3491–3499, 2007.
- [131] S. Kumar, I. Z. Maxwell, A. Heisterkamp, T. R. Polte, T. P. Lele, M. Salanga, E. Mazur, and D. E. Ingber, "Viscoelastic retraction of single living stress fibers and its impact on cell shape, cytoskeletal organization, and extracellular matrix mechanics," *Biophysical Journal*, vol. 90, no. 10, pp. 3762–3773, 2006.
- [132] K. Katoh, Y. Kano, and Y. Noda, "Rho-associated kinase-dependent contraction of stress fibres and the organization of focal adhesions," *Journal of the Royal Society Interface*, vol. 8, no. 56, pp. 305–311, 2011.
- [133] S. P. Palecek, J. C. Loftus, M. H. Ginsberg, D. A. Lauffenburger, and A. F. Horwitz, "Integrin-ligand binding properties govern cell migration speed through cell-substratum adhesiveness," *Nature*, vol. 385, no. 6616, pp. 537–540, 1997.
- [134] J. R. Dunlevy and J. R. Couchman, "Interleukin-8 induces motile behavior and loss of focal adhesions in primary fibroblasts.," *Journal of Cell Science*, vol. 108, pp. 311–321, 1995.
- [135] P. A. DiMilla, J. A. Stone, J. A. Quinn, S. M. Albelda, and D. A. Lauffenburger, "Maximal migration of human smooth muscle cells on fibronectin and type IV collagen occurs at an intermediate attachment strength," *Journal of Cell Biology*, vol. 122, no. 3, pp. 729–737, 1993.
- [136] J. Halper and M. Kjaer, "Basic components of connective tissues and extracellular matrix: Elastin, fibrillin, fibulins, fibrinogen, fibronectin, laminin, tenascins and thrombospondins," *Advances in Experimental Medicine and Biology*, vol. 802, pp. 31–47, 2014.
- [137] N. Boudreau and M. J. Bissell, "Extracellular matrix signaling: integration of form and function in normal and malignant cells.," *Current Opinion in Cell Biology*, vol. 10, no. 5, pp. 640–646, 1998.

- 
- [138] D. E. Discher, P. Janmey, and Y. L. Wang, "Tissue cells feel and respond to the stiffness of their substrate," *Science*, vol. 310, no. 5751, pp. 1139–1143, 2005.
- [139] C. T. C. Mierke, D. Rösel, B. Fabry, and J. Brábek, "Contractile forces in tumor cell migration," *European Journal of Cell Biology*, vol. 87, no. 8-9, pp. 669–676, 2008.
- [140] P. Friedl and K. Wolf, "Tumour-cell invasion and migration: diversity and escape mechanisms.," *Nature Reviews Cancer*, vol. 3, no. 5, pp. 362–374, 2003.
- [141] S. Guido and R. T. Tranquillo, "A methodology for the systematic and quantitative study of cell contact guidance in oriented collagen gels. Correlation of fibroblast orientation and gel birefringence.," *Journal of Cell Science*, vol. 105, pp. 317–331, 1993.
- [142] H. G. Sundararaghavan, R. L. Saunders, D. A. Hammer, and J. A. Burdick, "Fiber alignment directs cell motility over chemotactic gradients," *Biotechnology and Bioengineering*, vol. 110, no. 4, pp. 1249–1254, 2013.
- [143] G. A. Dunn and A. F. Brown, "Alignment of fibroblasts on grooved surfaces described by a simple geometric transformation.," *Journal of Cell Science*, vol. 83, no. 1, pp. 313–40, 1986.
- [144] J. Renkawitz and M. Sixt, "Mechanisms of force generation and force transmission during interstitial leukocyte migration," *EMBO Reports*, vol. 11, no. 10, pp. 744–750, 2010.
- [145] K. F. Swaney, C.-H. Huang, and P. N. Devreotes, "Eukaryotic chemotaxis: a network of signaling pathways controls motility, directional sensing, and polarity.," *Annual Review of Biophysics*, vol. 39, no. 1, pp. 265–289, 2010.
- [146] C. Janetopoulos and R. A. Firtel, "Directional sensing during chemotaxis," *FEBS Letters*, vol. 582, no. 14, pp. 2075–2085, 2008.
- [147] R. H. Insall, "Understanding eukaryotic chemotaxis: A pseudopod-centred view," *Nature Reviews Molecular Cell Biology*, vol. 11, no. 6, pp. 453–458, 2010.
- [148] M. A. Thomas, A. B. Kleist, and B. F. Volkman, "Decoding the chemotactic signal," *Journal of Leukocyte Biology*, no. February, pp. 1–16, 2018.
- [149] S. Bi and V. Sourjik, "Stimulus sensing and signal processing in bacterial chemotaxis," *Current Opinion in Microbiology*, vol. 45, pp. 22–29, 2018.
- [150] O. D. Weiner, "Regulation of cell polarity during eukaryotic chemotaxis: The chemotactic compass," *Current Opinion in Cell Biology*, vol. 14, no. 2, pp. 196–202, 2002.
- [151] C. A. Parent, B. J. Blacklock, W. M. Froehlich, D. B. Murphy, and P. N. Devreotes, "G protein signaling events are activated at the leading edge of chemotactic cells," *Cell*, vol. 95, no. 1, pp. 81–91, 1998.
- [152] A. Bagorda and C. A. Parent, "Eukaryotic chemotaxis at a glance," *Journal of Cell Science*, vol. 121, no. 16, pp. 2621–2624, 2008.
- [153] P. Rickert, O. D. Weiner, F. Wang, H. R. Bourne, and G. Servant, "Leukocytes navigate by compass: Roles of PI3K $\gamma$  and its lipid products," *Trends in Cell Biology*, vol. 10, no. 11, pp. 466–473, 2000.
- [154] H. R. Bourne and O. Weiner, "A chemical compass," *Nature*, vol. 419, no. 6902, p. 21, 2002.
- [155] I. C. Schneider and J. M. Haugh, "Mechanisms of gradient sensing and chemotaxis: Conserved pathways, diverse regulation," *Cell Cycle*, vol. 5, no. 11, pp. 1130–1134, 2006.
- [156] S. Funamoto, R. Meili, S. Lee, L. Parry, and R. A. Firtel, "Spatial and temporal regulation of 3-phosphoinositides by PI 3-kinase and PTEN mediates chemotaxis," *Cell*, vol. 109, no. 5, pp. 611–623, 2002.

- 
- [157] J. M. Haugh, F. Codazzi, M. Teruel, and T. Meyer, "Spatial sensing in fibroblasts mediated by 3' phosphoinositides," *The Journal of Cell Biology*, vol. 151, no. 6, pp. 1269–1279, 2000.
- [158] I. C. Schneider and J. M. Haugh, "Quantitative elucidation of a distinct spatial gradient-sensing mechanism in fibroblasts," *Journal of Cell Biology*, vol. 171, no. 5, pp. 883–892, 2005.
- [159] R. J. Petrie, A. D. Doyle, and K. M. Yamada, "Random versus directionally persistent cell migration," *Nature Reviews Molecular Cell Biology*, vol. 10, no. 8, pp. 538–549, 2009.
- [160] P. R. Fisher, R. Merkl, and G. Gerisch, "Quantitative analysis of cell motility and chemotaxis in *Dictyostelium discoideum* by using an image processing system and a novel chemotaxis chamber providing stationary chemical gradients," *The Journal of Cell Biology*, vol. 108, no. 3, pp. 973–984, 1989.
- [161] J. Schlessinger, "Cell Signaling by Receptor Tyrosine Kinases," *Cell*, vol. 103, no. 2, pp. 211–225, 2000.
- [162] C. S. Park, I. C. Schneider, and J. M. Haugh, "Kinetic analysis of platelet-derived growth factor receptor/phosphoinositide 3-kinase/Akt signaling in fibroblasts," *Journal of Biological Chemistry*, vol. 278, no. 39, pp. 37064–37072, 2003.
- [163] O. Hoeller and R. R. Kay, "Chemotaxis in the Absence of PIP3 Gradients," *Current Biology*, vol. 17, no. 9, pp. 813–817, 2007.
- [164] A. T. Melvin, E. S. Welf, Y. Wang, D. J. Irvine, and J. M. Haugh, "In chemotaxing fibroblasts, both high-fidelity and weakly biased cell movements track the localization of PI3K signaling," *Biophysical Journal*, vol. 100, no. 8, pp. 1893–1901, 2011.
- [165] C. Wu, S. B. Asokan, M. E. Berginski, E. M. Haynes, N. E. Sharpless, J. D. Griffith, S. M. Gomez, and J. E. Bear, "Arp2/3 is critical for lamellipodia and response to extracellular matrix cues but is dispensable for chemotaxis," *Cell*, vol. 148, no. 5, pp. 973–987, 2012.
- [166] Y. Tsukada, K. Aoki, T. Nakamura, Y. Sakumura, M. Matsuda, and S. Ishii, "Quantification of local morphodynamics and local GTPase activity by edge evolution tracking," *PLoS Computational Biology*, vol. 4, no. 11, p. e1000223, 2008.
- [167] E. S. Welf, S. Ahmed, H. E. Johnson, A. T. Melvin, and J. M. Haugh, "Migrating fibroblasts reorient directionality: By a metastable, PI3K-dependent mechanism," *Journal of Cell Biology*, vol. 197, no. 1, pp. 105–114, 2012.
- [168] P. J. M. Van Haastert, "Chemotaxis: insights from the extending pseudopod," *Journal of Cell Science*, vol. 123, no. 18, pp. 3031–3037, 2010.
- [169] R. Insall, "The interaction between pseudopods and extracellular signalling during chemotaxis and directed migration," *Current Opinion in Cell Biology*, vol. 25, no. 5, pp. 526–531, 2013.
- [170] N. Andrew and R. H. Insall, "Chemotaxis in shallow gradients is mediated independently of PtdIns 3-kinase by biased choices between random protrusions," *Nature Cell Biology*, vol. 9, no. 2, pp. 193–200, 2007.
- [171] G. Gerisch and H. U. Keller, "Chemotactic reorientation of granulocytes stimulated with micropipettes containing fMet-Leu-Phe.," *Journal of Cell Science*, vol. 52, no. 1, pp. 1–10, 1981.
- [172] Z. Pujic, D. Mortimer, J. Feldner, and G. J. Goodhill, "Assays for Eukaryotic Cell Chemotaxis," *Combinatorial Chemistry & High Throughput Screening*, vol. 12, pp. 580–588, 2009.
- [173] S. F. Sun, *Physical Chemistry of Macromolecules : basic principles and issues*. Hoboken, New Jersey: John Wiley, second ed., 2004.

- 
- [174] J. Adler, "Chemotaxis in bacteria.," *Science*, vol. 153, no. 3737, pp. 708–16, 1966.
- [175] S. Boyden, "The chemotactic effect of mixtures of antibody and antigen on polymorphonuclear leucocytes.," *The Journal of Experimental Medicine*, vol. 115, no. 3, pp. 453–466, 1962.
- [176] R. D. Nelson, P. G. Quie, and R. L. Simmons, "Chemotaxis under agarose: a new and simple method for measuring chemotaxis and spontaneous migration of human polymorphonuclear leukocytes and monocytes.," *Journal of Immunology*, vol. 115, no. 6, pp. 1650–1656, 1975.
- [177] Z. Pujic, C. E. Giacomantonio, D. Unni, W. J. Rosoff, and G. J. Goodhill, "Analysis of the growth cone turning assay for studying axon guidance," *Journal of Neuroscience Methods*, vol. 170, no. 2, pp. 220–228, 2008.
- [178] L. Soon, G. Mouneimne, J. Segall, J. Wyckoff, and J. Condeelis, "Description and characterization of a chamber for viewing and quantifying cancer cell chemotaxis," *Cell Motility and the Cytoskeleton*, vol. 62, no. 1, pp. 27–34, 2005.
- [179] S. A. Grando, A. M. Crosby, B. D. Zelickson, and M. V. Dahl, "Agarose Gel Keratinocyte Outgrowth System as a Model of Skin Re-epithelization: Requirement of Endogenous Acetylcholine for Outgrowth Initiation.," *Journal of Investigative Dermatology*, vol. 101, no. 6, pp. 804–810, 1993.
- [180] A. Vasaturo, S. Caserta, I. Russo, V. Preziosi, C. Ciacci, and S. Guido, "A Novel Chemotaxis Assay in 3-D Collagen Gels by Time-Lapse Microscopy," *PloS One*, vol. 7, no. 12, p. e52251, 2012.
- [181] D. M. Knapp, E. F. Helou, and R. T. Tranquillo, "A fibrin or collagen gel assay for tissue cell chemotaxis: Assessment of fibroblast chemotaxis to GRGDSP," *Experimental Cell Research*, vol. 247, no. 2, pp. 543–553, 1999.
- [182] T. M. Keenan and A. Folch, "Biomolecular gradients in cell culture systems," *Lab on a Chip*, vol. 8, no. 1, pp. 34–57, 2007.
- [183] W. J. Rosoff, J. S. Urbach, M. A. Esrick, R. G. McAllister, L. J. Richards, and G. J. Goodhill, "A new chemotaxis assay shows the extreme sensitivity of axons to molecular gradients," *Nature Neuroscience*, vol. 7, no. 6, pp. 678–682, 2004.
- [184] J. M. Rhodes, "Measurement of chemotaxis in Boyden chamber filter assays. Is the checkerboard correction valid?," *Journal of Immunological Methods*, vol. 49, pp. 235–236, 1982.
- [185] D. Zicha, G. A. Dunn, and A. F. Brown, "A new direct-viewing chemotaxis chamber," *Journal of Cell Science*, vol. 99, no. 4, pp. 769–775, 1991.
- [186] A. J. Muinonen-Martin, D. M. Veltman, G. Kalna, and R. H. Insall, "An improved chamber for direct visualisation of chemotaxis," *PloS One*, vol. 5, no. 12, p. e15309, 2010.
- [187] E. K. Sackmann, A. L. Fulton, and D. J. Beebe, "The present and future role of microfluidics in biomedical research.," *Nature*, vol. 507, no. 7491, pp. 181–189, 2014.
- [188] S. Toetsch, P. Olwell, A. Prina-Mello, and Y. Volkov, "The evolution of chemotaxis assays from static models to physiologically relevant platforms.," *Integrative Biology*, vol. 1, no. 2, pp. 170–181, 2009.
- [189] Y. Xia and G. M. Whitesides, "Soft Lithography," *Angewandte Chemie International Edition*, vol. 37, no. 5, pp. 550–575, 1998.
- [190] C. Beta and E. Bodenschatz, "Microfluidic tools for quantitative studies of eukaryotic chemotaxis," *European Journal of Cell Biology*, vol. 90, no. 10, pp. 811–816, 2011.
- [191] S. Kim, H. J. Kim, and N. L. Jeon, "Biological applications of microfluidic gradient devices," *Integrative Biology*, vol. 2, no. 11-12, pp. 584–603, 2010.

- 
- [192] M. Tehrani-Rokh, A. Z. Kouzani, and J. R. Kanwar, "Gradient generating microfluidic devices for cell cultivation," in *Procedia Engineering*, vol. 29, pp. 1740–1744, 2012.
- [193] J. Wu, X. Wu, and F. Lin, "Recent developments in microfluidics-based chemotaxis studies," *Lab on a Chip*, vol. 13, no. 13, pp. 2484–2499, 2013.
- [194] A. G. Toh, Z. P. Wang, C. Yang, and N. T. Nguyen, "Engineering microfluidic concentration gradient generators for biological applications," *Microfluidics and Nanofluidics*, vol. 16, no. 1-2, pp. 1–18, 2014.
- [195] O. C. Amadi, M. L. Steinhauser, Y. Nishi, S. Chung, R. D. Kamm, A. P. McMahon, and R. T. Lee, "A low resistance microfluidic system for the creation of stable concentration gradients in a defined 3D microenvironment," *Biomedical Microdevices*, vol. 12, no. 6, pp. 1027–1041, 2010.
- [196] Y. Shin, S. Han, J. S. Jeon, K. Yamamoto, I. K. Zervantonakis, R. Sudo, R. D. Kamm, and S. Chung, "Microfluidic assay for simultaneous culture of multiple cell types on surfaces or within hydrogels," *Nature Protocols*, vol. 7, no. 7, pp. 1247–1259, 2012.
- [197] W. Saadi, S. W. Rhee, F. Lin, B. Vahidi, B. G. Chung, and N. L. Jeon, "Generation of stable concentration gradients in 2D and 3D environments using a microfluidic ladder chamber," *Biomedical Microdevices*, vol. 9, no. 5, pp. 627–635, 2007.
- [198] Y. Fu, L. K. Chin, T. Bourouina, A. Q. Liu, and A. M. Vandongen, "Nuclear deformation during breast cancer cell transmigration," *Lab on a Chip*, vol. 12, no. 19, pp. 3774–3778, 2012.
- [199] D. Irimia, G. Charras, N. Agrawal, T. Mitchison, and M. Toner, "Polar stimulation and constrained cell migration in microfluidic channels.," *Lab on a Chip*, vol. 7, pp. 1783–1790, dec 2007.
- [200] B. Mosadegh, C. Huang, J. W. Park, H. S. Shin, B. G. Chung, S.-K. Hwang, K.-H. Lee, H. J. Kim, J. Brody, and N. L. Jeon, "Generation of Stable Complex Gradients Across Two-Dimensional Surfaces and Three-Dimensional Gels," *Langmuir*, vol. 23, no. 22, pp. 10910–10912, 2007.
- [201] S. Rao, U. Tata, V. Lin, and J.-C. Chiao, "The Migration of Cancer Cells in Gradually Varying Chemical Gradients and Mechanical Constraints," *Micromachines*, vol. 5, no. 1, pp. 13–26, 2014.
- [202] A. Shamloo, N. Ma, M.-M. Poo, L. L. Sohn, and S. C. Heilshorn, "Endothelial cell polarization and chemotaxis in a microfluidic device.," *Lab on a Chip*, vol. 8, no. 8, pp. 1292–1299, 2008.
- [203] G. M. Walker, J. Sai, A. Richmond, M. Stremler, C. Y. Chun, and J. P. Wikswo, "Effects of flow and diffusion on chemotaxis studies in a microfabricated gradient generator," *Lab on a Chip*, vol. 5, no. 6, pp. 611–618, 2005.
- [204] C. Zhang, M. P. Barrios, R. M. Alani, M. Cabodi, and J. Y. Wong, "A microfluidic Transwell to study chemotaxis," *Experimental Cell Research*, vol. 342, no. 2, pp. 159–165, 2016.
- [205] U. Tata, S. M. Rao, A. Sharma, K. Pabba, K. Pokhrel, B. Adhikari, V. K. Lin, and J. C. Chiao, "Study of lung-metastasized prostate cancer cell line chemotaxis to epidermal growth factor with a BIOMEMS device," *Advances in Natural Sciences: Nanoscience and Nanotechnology*, vol. 3, no. 3, pp. 35007–35012, 2012.
- [206] W. K. Raja, B. Gligorijevic, J. Wyckoff, J. S. Condeelis, and J. Castracane, "A new chemotaxis device for cell migration studies," *Integrative Biology*, vol. 2, no. 11-12, pp. 696–706, 2010.
- [207] E. Berthier, J. Surfus, J. Verbsky, A. Huttenlocher, and D. Beebe, "An arrayed high-content chemotaxis assay for patient diagnosis," *Integrative Biology*, vol. 2, pp. 630–638, 2010.



- 
- [208] E. Ezra Tsur, M. Zimerman, I. Maor, A. Elrich, and Y. Nahmias, “Microfluidic Concentric Gradient Generator Design for High-Throughput Cell-Based Studies,” *Frontiers in Bioengineering and Biotechnology*, vol. 5, p. 21, 2017.
- [209] X. H. Liao, N. P. Meena, N. Southall, L. Liu, M. Swaroop, A. L. Zhang, J. J. Xiang, C. A. Parent, W. Zheng, and A. R. Kimmel, “A High-Throughput, Multi-Cell Phenotype Assay for the Identification of Novel Inhibitors of Chemotaxis/Migration,” *Scientific Reports*, vol. 6, p. 22273, 2016.
- [210] K. L. Butler, V. Ambravaneswaran, N. Agrawal, M. Bilodeau, M. Toner, R. G. Tompkins, S. Fagan, and D. Irimia, “Burn injury reduces neutrophil directional migration speed in microfluidic devices,” *PloS One*, vol. 5, no. 7, p. e11921, 2010.
- [211] V. Biswenger, N. Baumann, J. Jürschick, M. Häckl, C. Battle, J. Schwarz, E. Horn, and R. Zantl, “Characterization of EGF-guided MDA-MB-231 cell chemotaxis in vitro using a physiological and highly sensitive assay system,” *PloS One*, vol. 13, no. 9, p. e0203040, 2018.
- [212] M. Samereier, M. Schleicher, H. Roth, D. Brechtefeld, B. Walzog, and A. Müller-Taubenberger, “EB1 contributes to proper front-to-back polarity in neutrophil-like HL-60 cells,” *European Journal of Cell Biology*, vol. 96, no. 2, pp. 143–153, 2017.
- [213] S. Kamakura, M. Nomura, J. Hayase, Y. Iwakiri, A. Nishikimi, R. Takayanagi, Y. Fukui, and H. Sumimoto, “The cell polarity protein minsc regulates neutrophil chemotaxis via a noncanonical G protein signaling pathway,” *Developmental Cell*, vol. 26, no. 3, pp. 292–302, 2013.
- [214] M. Horsthemke, A. C. Bachg, K. Groll, S. Moyzio, B. Mütter, S. A. Hemkemeyer, R. Wedlich-Söldner, M. Sixt, S. Tacke, M. Bähler, and P. J. Hanley, “Multiple roles of filopodial dynamics in particle capture and phagocytosis and phenotypes of Cdc42 and Myo10 deletion,” *Journal of Biological Chemistry*, vol. 292, no. 17, pp. 7258–7273, 2017.
- [215] P. Suraneni, B. Rubinstein, J. R. Unruh, M. Durnin, D. Hanein, and R. Li, “The Arp2/3 complex is required for lamellipodia extension and directional fibroblast cell migration,” *Journal of Cell Biology*, vol. 197, no. 2, pp. 239–251, 2012.
- [216] S. Corallino, C. Malinverno, B. Neumann, C. Tischer, A. Palamidessi, E. Frittoli, M. Panagiotakopoulou, A. DiSanza, G. Malet-Engra, P. Nastaly, C. Galli, C. Luise, G. Bertalot, S. Pece, P. P. Di Fiore, N. Gauthier, A. Ferrari, P. Maiuri, and G. Scita, “A RAB35-p85/PI3K axis controls oscillatory apical protrusions required for efficient chemotactic migration,” *Nature Communications*, vol. 9, no. 1, p. 1475, 2018.
- [217] D. Terheyden-Keighley, B. Brand-Saber, and C. Theiss, “Real-Time Imaging of Accessible Axon Guidance Assays in Three-Dimensional Culture,” *Journal of Neurology and Experimental Neuroscience*, 2016.
- [218] L. Zhang, V. Luga, S. K. Armitage, M. Musiol, A. Won, C. M. Yip, S. V. Plotnikov, and J. L. Wrana, “A lateral signalling pathway coordinates shape volatility during cell migration,” *Nature Communications*, vol. 7, p. 11714, 2016.
- [219] M. Théry, “Micropatterning as a tool to decipher cell morphogenesis and functions,” *Journal of Cell Science*, vol. 123, no. 24, pp. 4201–13, 2010.
- [220] Y. Ito, “Surface micropatterning to regulate cell functions,” *Biomaterials*, vol. 20, no. 23–24, pp. 2333–2342, 1999.
- [221] M. Thery, V. Racine, M. Piel, A. Pepin, A. Dimitrov, Y. Chen, J.-B. Sibarita, and M. Bornens, “Anisotropy of cell adhesive microenvironment governs cell internal organization and orientation of polarity,” *Proceedings of the National Academy of Sciences*, vol. 103, no. 52, pp. 19771–19776, 2006.
- [222] T. Vignaud, R. Galland, Q. Tseng, L. Blanchoin, J. Colombelli, and M. Thery, “Reprogramming cell shape with laser nano-patterning,” *Journal of Cell Science*, vol. 125, no. 9, pp. 2134–2140, 2012.

- 
- [223] M. Bailly, J. S. Condeelis, and J. E. Segall, "Chemoattractant-induced lamellipod extension," *Microscopy Research and Technique*, vol. 43, no. 5, pp. 433–443, 1998.
- [224] A. D. Doyle, F. W. Wang, K. Matsumoto, and K. M. Yamada, "One-dimensional topography underlies three-dimensional fibrillar cell migration," *Journal of Cell Biology*, vol. 184, no. 4, pp. 481–490, 2009.
- [225] A. D. Doyle, M. L. Kutys, M. A. Conti, K. Matsumoto, R. S. Adelstein, and K. M. Yamada, "Micro-environmental control of cell migration - myosin IIA is required for efficient migration in fibrillar environments through control of cell adhesion dynamics," *Journal of Cell Science*, vol. 125, no. 9, pp. 2244–2256, 2012.
- [226] D. R. Jung, R. Kapur, T. Adams, K. A. Giuliano, M. Mrksich, H. G. Craighead, and D. L. Taylor, "Topographical and physicochemical modification of material surface to enable patterning of living cells," *Critical Reviews in Biotechnology*, vol. 21, no. 2, pp. 111–154, 2001.
- [227] H.-C. Moeller, M. K. Mian, S. Shrivastava, B. G. Chung, and A. Khademhosseini, "A microwell array system for stem cell culture.," *Biomaterials*, vol. 29, no. 6, pp. 752–63, 2008.
- [228] A. K. Marel, S. Rappl, A. Piera Alberola, and J. O. Rädler, "Arraying cell cultures using PEG-DMA micromolding in standard culture dishes," *Macromolecular Bioscience*, vol. 13, no. 5, pp. 595–602, 2013.
- [229] P. J. F. Röttgermann, A. P. Alberola, and J. O. Rädler, "Cellular self-organization on micro-structured surfaces," *Soft Matter*, vol. 10, no. 14, p. 2397, 2014.
- [230] A. S. Piotrowski-Daspit and C. M. Nelson, "Engineering Three-dimensional Epithelial Tissues Embedded within Extracellular Matrix," *Journal of Visualized Experiments*, no. 113, pp. e54283–e54283, 2016.
- [231] E. Ruoslahti, "Fibronectin and its Receptors," *Annual Review of Biochemistry*, vol. 57, no. 1, pp. 375–413, 1988.
- [232] C. D. James, R. C. Davis, L. Kam, H. G. Craighead, M. Isaacson, J. N. Turner, and W. Shain, "Patterned Protein Layers on Solid Substrates by Thin Stamp Microcontact Printing," *Langmuir*, vol. 14, no. 4, pp. 741–744, 1998.
- [233] N. Nath, J. Hyun, H. Ma, and A. Chilkoti, "Surface engineering strategies for control of protein and cell interactions," *Surface Science*, vol. 570, no. 1-2, pp. 98–110, 2004.
- [234] R. Michel, S. Pasche, M. Textor, and D. G. Castner, "Influence of PEG architecture on protein adsorption and conformation," *Langmuir*, vol. 21, no. 26, pp. 12327–12332, 2005.
- [235] P. J. F. Röttgermann, S. Hertrich, I. Berts, M. Albert, F. J. Segerer, J.-F. Moulin, B. Nickel, and J. O. Rädler, "Cell Motility on Polyethylene Glycol Block Copolymers Correlates to Fibronectin Surface Adsorption," *Macromolecular Bioscience*, vol. 14, no. 12, pp. 1755–1763, 2014.
- [236] D. Falconnet, G. Csucs, H. Michelle Grandin, and M. Textor, "Surface engineering approaches to micropattern surfaces for cell-based assays," *Biomaterials*, vol. 27, no. 16, pp. 3044–3063, 2006.
- [237] R. S. Kane, S. Takayama, E. Ostuni, D. E. Ingber, and G. M. Whitesides, "Patterning proteins and cells using soft lithography," *Biomaterials*, vol. 20, no. 23-24, pp. 2363–2376, 1999.
- [238] R. Singhvi, A. Kumar, G. P. Lopez, G. N. Stephanopoulos, D. I. Wang, G. M. Whitesides, and D. E. Ingber, "Engineering cell shape and function," *Science*, vol. 264, no. 5159, pp. 696–698, 1994.
- [239] A. Bernard, J. P. Renault, B. Michel, H. R. Bosshard, and E. Delamarche, "Microcontact Printing of Proteins," *Advanced Materials*, vol. 12, no. 14, pp. 1067–1070, 2000.

- 
- [240] E. Delamarche, A. Bernard, H. Schmid, A. Bietsch, B. Michel, and H. Biebuyck, "Microfluidic Networks for Chemical Patterning of Substrates: Design and Application to Bioassays," *Journal of the American Chemical Society*, vol. 120, no. 3, pp. 500–508, 1998.
- [241] A. Folch, B. H. Jo, O. Hurtado, D. J. Beebe, and M. Toner, "Microfabricated elastomeric stencils for micropatterning cell cultures," *Journal of Biomedical Materials Research*, vol. 52, no. 2, pp. 346–353, 2000.
- [242] A. Tourovskaia, T. Barber, B. T. Wickes, D. Hirdes, B. Grin, D. G. Castner, K. E. Healy, and A. Folch, "Micropatterns of chemisorbed cell adhesion-repellent films using oxygen plasma etching and elastomeric masks," *Langmuir*, vol. 19, no. 11, pp. 4754–4764, 2003.
- [243] N. Hampe, T. Jonas, B. Wolters, N. Hersch, B. Hoffmann, and R. Merkel, "Defined 2-D microtissues on soft elastomeric silicone rubber using lift-off epoxy-membranes for biomechanical analyses," *Soft Matter*, vol. 10, no. 14, p. 2431, 2014.
- [244] D. Wright, B. Rajalingam, J. M. Karp, S. Selvarasah, Y. Ling, J. Yeh, R. Langer, M. R. Dokmeci, and A. Khademhosseini, "Reusable, reversibly sealable parylene membranes for cell and protein patterning," *Journal of Biomedical Materials Research*, vol. 85, no. 2, pp. 530–538, 2008.
- [245] H. Kaji, G. Camci-Unal, R. Langer, and A. Khademhosseini, "Engineering systems for the generation of patterned co-cultures for controlling cell-cell interactions.," *Biochimica et Biophysica Acta*, vol. 1810, no. 3, pp. 239–50, 2011.
- [246] M. J. Hynes and J. A. Maurer, "Lighting the path: Photopatternable substrates for biological applications," *Molecular BioSystems*, vol. 9, no. 4, pp. 559–564, 2013.
- [247] A. Azioune, M. Storch, M. Bornens, M. Thery, and M. Piel, "Simple and rapid process for single cell micro-patterning.," *Lab on a Chip*, vol. 9, no. 11, pp. 1640–1642, 2009.
- [248] J. Nakanishi, Y. Kikuchi, T. Takarada, H. Nakayama, K. Yamaguchi, and M. Maeda, "Spatiotemporal control of cell adhesion on a self-assembled monolayer having a photocleavable protecting group," *Analytica Chimica Acta*, vol. 578, no. 1, pp. 100–104, 2006.
- [249] W. S. Dillmore, M. N. Yousaf, and M. Mrksich, "A photochemical method for patterning the immobilization of ligands and cells to self-assembled monolayers," *Langmuir*, vol. 20, no. 17, pp. 7223–7231, 2004.
- [250] J. M. Bélisle, D. Kunik, and S. Costantino, "Rapid multicomponent optical protein patterning.," *Lab on a Chip*, vol. 9, pp. 3580–3585, 2009.
- [251] E. K. U. Larsen, M. B. L. Mikkelsen, and N. B. Larsen, "Facile photoimmobilization of proteins onto low-binding PEG-coated polymer surfaces," *Biomacromolecules*, vol. 15, no. 3, pp. 894–899, 2014.
- [252] E. K. U. Larsen, M. B. L. Mikkelsen, and N. B. Larsen, "Protein and cell patterning in closed polymer channels by photoimmobilizing proteins on photografted poly(ethylene glycol) diacrylate," *Biomicrofluidics*, vol. 8, no. 6, pp. 064127–1, 2014.
- [253] M. a. Cole, N. H. Voelcker, H. Thissen, and H. J. Griesser, "Stimuli-responsive interfaces and systems for the control of protein-surface and cell-surface interactions," *Biomaterials*, vol. 30, no. 9, pp. 1827–1850, 2009.
- [254] J. Nakanishi, T. Takarada, K. Yamaguchi, and M. Maeda, "Recent Advances in Cell Micropatterning Techniques for Bioanalytical and Biomedical Sciences," *Analytical Sciences*, vol. 24, no. 1, pp. 67–72, 2008.
- [255] A. Higuchi, Q. D. Ling, S. S. Kumar, Y. Chang, T. C. Kao, M. a. Munusamy, A. a. Alarfaj, S. T. Hsu, and A. Umezawa, "External stimulus-responsive biomaterials designed for the culture and differentiation of ES, iPS, and adult stem cells," *Progress in Polymer Science*, vol. 39, no. 9, pp. 1585–1613, 2014.

- 
- [256] C. G. Rolli, H. Nakayama, K. Yamaguchi, J. P. Spatz, R. Kemkemer, and J. Nakanishi, "Switchable adhesive substrates: Revealing geometry dependence in collective cell behavior," *Biomaterials*, vol. 33, no. 8, pp. 2409–2418, 2012.
- [257] K. Uhlig, H. Boerner, E. Wischerhoff, J.-F. Lutz, M. Jaeger, A. Laschewsky, and C. Duschl, "On the Interaction of Adherent Cells with Thermoresponsive Polymer Coatings," *Polymers*, vol. 6, no. 4, pp. 1164–1177, 2014.
- [258] S. F. M. Van Dongen, P. Maiuri, E. Marie, C. Tribet, and M. Piel, "Triggering cell adhesion, migration or shape change with a dynamic surface coating," *Advanced Materials*, vol. 25, no. 12, pp. 1687–1691, 2013.
- [259] A. Khademhosseini, R. Langer, J. Borenstein, and J. P. Vacanti, "Microscale technologies for tissue engineering and biology.," *Proceedings of the National Academy of Sciences of the United States of America*, vol. 103, no. 8, pp. 2480–7, 2006.
- [260] A. Revzin, R. J. Russell, V. K. Yadavalli, W. G. Koh, C. Deister, D. D. Hile, M. B. Mellott, and M. V. Pishko, "Fabrication of poly(ethylene glycol) hydrogel microstructures using photolithography," *Langmuir*, vol. 17, no. 18, pp. 5440–5447, 2001.
- [261] M. S. Hahn, J. S. Miller, and J. L. West, "Three-dimensional biochemical and biomechanical patterning of hydrogels for guiding cell behavior," *Advanced Materials*, vol. 18, no. 20, pp. 2679–2684, 2006.
- [262] E. K. F. Yim, R. M. Reano, S. W. Pang, A. F. Yee, C. S. Chen, and K. W. Leong, "Nanopattern-induced changes in morphology and motility of smooth muscle cells.," *Biomaterials*, vol. 26, no. 26, pp. 5405–13, 2005.
- [263] A.-K. Marel, M. Zorn, C. Klingner, R. Wedlich-Söldner, E. Frey, and J. O. Rädler, "Flow and Diffusion in Channel-Guided Cell Migration," *Biophysical Journal*, vol. 107, no. 5, pp. 1054–1064, 2014.
- [264] A. D. Doyle, N. Carvajal, A. Jin, K. Matsumoto, and K. M. Yamada, "Local 3D matrix microenvironment regulates cell migration through spatiotemporal dynamics of contractility-dependent adhesions," *Nature Communications*, vol. 6, p. 8720, 2015.
- [265] B. D. Fairbanks, M. P. Schwartz, A. E. Halevi, C. R. Nuttelman, C. N. Bowman, and K. S. Anseth, "A Versatile Synthetic Extracellular Matrix Mimic via Thiol-Norbornene Photopolymerization," *Advanced Materials*, vol. 21, no. 48, pp. 5005–5010, 2009.
- [266] M. S. Hahn, "Patterning of PEG-based Hydrogels - Engineering Spatial Complexity," *Material Matters*, no. 5.3, p. 62, 2010.
- [267] C.-C. Lin, C. S. Ki, and H. Shih, "Thiol-norbornene photoclick hydrogels for tissue engineering applications," *Journal of Applied Polymer Science*, vol. 132, no. 8, 2015.
- [268] B. D. Fairbanks, M. P. Schwartz, C. N. Bowman, and K. S. Anseth, "Photoinitiated polymerization of PEG-diacrylate with lithium phenyl-2,4,6-trimethylbenzoylphosphinate: polymerization rate and cytocompatibility," *Biomaterials*, vol. 30, no. 35, pp. 6702–6707, 2009.
- [269] S. Bäckström, J. Benavente, R. W. Berg, K. Stibius, M. S. Larsen, H. Bohr, C. Hélix-Nielsen, R. W. Berg, K. Stibius, M. S. Larsen, H. Bohr, and C. Hélix-Nielsen, "Tailoring Properties of Biocompatible PEG-DMA Hydrogels with UV Light," *Materials Sciences and Applications*, vol. 03, no. 06, pp. 425–431, 2012.
- [270] M. Dietrich, H. Le Roy, D. B. Brückner, H. Engelke, R. Zantl, J. O. Rädler, and C. P. Broedersz, "Guiding 3D cell migration in deformed synthetic hydrogel microstructures," *Soft Matter*, vol. 14, no. 15, pp. 2816–2826, 2018.
- [271] J. Schindelin, I. Arganda-Carreras, E. Frise, V. Kaynig, M. Longair, T. Pietzsch, S. Preibisch, C. Rueden, S. Saalfeld, B. Schmid, J. Y. Tinevez, D. J. White, V. Hartenstein, K. Eliceiri, P. Tomancak, and A. Cardona, "Fiji: An open-source platform for biological-image analysis," *Nature Methods*, vol. 9, no. 7, pp. 676–682, 2012.

- 
- [272] J. Schindelin, C. T. Rueden, M. C. Hiner, and K. W. Eliceiri, "The ImageJ ecosystem: An open platform for biomedical image analysis," *Molecular Reproduction and Development*, vol. 82, no. 7-8, pp. 518–529, 2015.
- [273] Ibidi, "Appl. Note 17: 2D and 3D Chemotaxis Assays Using  $\mu$ -Slide Chemotaxis," tech. rep., 2012.
- [274] S. R. Sternberg, "Biomedical Image Processing," *IEEE Computer*, vol. 16, no. 1, pp. 22–34, 1983.
- [275] J. M. S. Prewitt and M. L. Mendelsohn, "The Analysis Of Cell Images," *Annals of the New York Academy of Sciences*, vol. 128, no. 3, pp. 1035–1053, 1966.
- [276] N. Stuurman, A. Edelstein, N. Amodaj, K. Hoover, and R. Vale, "Computer control of microscopes using manager," oct 2010.
- [277] C. M. Cesa, N. Kirchgeßner, D. Mayer, U. S. Schwarz, B. Hoffmann, and R. Merkel, "Micropatterned silicone elastomer substrates for high resolution analysis of cellular force patterns," *Review of Scientific Instruments*, vol. 78, no. 3, p. 034301, 2007.
- [278] J. R. Soiné, N. Hersch, G. Dreissen, N. Hampe, B. Hoffmann, R. Merkel, and U. S. Schwarz, "Measuring cellular traction forces on non-planar substrates," *Interface Focus*, vol. 6, no. 5, 2016.
- [279] N. Hersch, B. Wolters, G. Dreissen, R. Springer, N. Kirchgeßner, R. Merkel, and B. Hoffmann, "The constant beat: cardiomyocytes adapt their forces by equal contraction upon environmental stiffening," *Biology Open*, vol. 2, no. 3, pp. 351–361, 2013.
- [280] S. Houben, N. Kirchgeßner, and R. Merkel, "Estimating force fields of living cells - Comparison of several regularization schemes combined with automatic parameter choice," in *Proceedings of the DAGM Symposium, Lecture Notes in Computer Sciences*, vol. 6376, pp. 71–80, Springer, Berlin, Heidelberg, 2010.
- [281] L. Tomasova, Z. Guttenberg, B. Hoffmann, and R. Merkel, "Advanced 2D/3D cell migration assay for faster evaluation of chemotaxis of slow-moving cells," *PloS One*, vol. 14, no. 7, p. e0219708, 2019.
- [282] M. Stoker and E. Gherardi, "Regulation of cell movement: the motogenic cytokines," *Biochimica et Biophysica Acta*, vol. 1072, no. 1, pp. 81–102, 1991.
- [283] S. Verrier, S. Pallu, R. Bareille, A. Jonczyk, J. Meyer, M. Dard, and J. Amédée, "Function of linear and cyclic RGD-containing peptides in osteoprogenitor cells adhesion process," *Biomaterials*, vol. 23, no. 2, pp. 585–596, 2002.
- [284] B. D. Fairbanks, S. P. Singh, C. N. Bowman, and K. S. Anseth, "Photodegradable, photoadaptable hydrogels via radical-mediated disulfide fragmentation reaction," *Macromolecules*, vol. 44, no. 8, pp. 2444–2450, 2011.
- [285] M. W. Toepke, N. a. Impellitteri, J. M. Theisen, and W. L. Murphy, "Characterization of thiol-ene crosslinked PEG hydrogels," *Macromolecular Materials and Engineering*, vol. 298, no. 6, pp. 699–703, 2013.
- [286] M. P. Schwartz, R. E. Rogers, S. P. Singh, J. Y. Lee, S. G. Loveland, J. T. Koepsel, E. S. Witze, S. I. Montanez-Sauri, K. E. Sung, E. Y. Tokuda, Y. Sharma, L. M. Everhart, E. H. Nguyen, M. H. Zaman, D. J. Beebe, N. G. Ahn, W. L. Murphy, and K. S. Anseth, "A quantitative comparison of human HT-1080 fibrosarcoma cells and primary human dermal fibroblasts identifies a 3D migration mechanism with properties unique to the transformed phenotype.," *PloS One*, vol. 8, no. 12, p. e81689, 2013.
- [287] W. Li, J. Fan, M. Chen, and D. T. Woodley, "Mechanisms of human skin cell motility," *Histology and Histopathology*, vol. 19, no. 4, pp. 1311–1324, 2004.
- [288] M. Tomasz, "Mitomycin C: small, fast and deadly (but very selective)," *Chemistry and Biology*, vol. 2, no. 9, pp. 575–579, 1995.

- 
- [289] M. S. Pepper, J. D. Vassalli, R. Montesano, and L. Orci, "Urokinase-type plasminogen activator is induced in migrating capillary endothelial cells," *Journal of Cell Biology*, vol. 105, no. 6 Pt 1, pp. 2535–2541, 1987.
- [290] C. Zhang, S. Jang, O. C. Amadi, K. Shimizu, R. T. Lee, and R. N. Mitchell, "A sensitive chemotaxis assay using a novel microfluidic device," *BioMed Research International*, vol. 2013, pp. 1–8, 2013.
- [291] M. Bindschadler and J. L. McGrath, "Sheet migration by wounded monolayers as an emergent property of single-cell dynamics," *Journal of Cell Science*, vol. 120, no. 5, pp. 876–884, 2007.
- [292] L. R. Kark, J. M. Karp, and J. E. Davies, "Platelet releasate increases the proliferation and migration of bone marrow-derived cells cultured under osteogenic conditions," *Clinical Oral Implants Research*, vol. 17, no. 3, pp. 321–327, 2006.
- [293] P. V. Peplow and M. P. Chatterjee, "A review of the influence of growth factors and cytokines in in vitro human keratinocyte migration," *Cytokine*, vol. 62, no. 1, pp. 1–21, 2013.
- [294] S. Pastore, F. Mascia, V. Mariani, and G. Girolomoni, "The epidermal growth factor receptor system in skin repair and inflammation," *Journal of Investigative Dermatology*, vol. 128, no. 6, pp. 1365–1374, 2008.
- [295] S. D. Rodgers, *Characterizing the Motogenic Response of Human Keratinocytes to Epidermal Growth Factor and Transforming Growth Factor-Alpha*. PhD thesis, Massachusetts Institute of Technology, 1996.
- [296] C. S. Kim, I. P. Mitchell, A. W. Desotell, P. K. Kreeger, and K. S. Masters, "Immobilized epidermal growth factor stimulates persistent, directed keratinocyte migration via activation of PLC $\gamma$ 1.," *FASEB Journal*, vol. 30, no. 7, pp. 2580–2590, 2016.
- [297] G. Schultz, D. S. Rotatori, and W. Clark, "EGF and TGF- $\alpha$  in Wound Healing and Repair," *Journal of Cellular Biochemistry*, vol. 45, pp. 346–352, 1991.
- [298] H. Björkelund, L. Gedda, and K. Andersson, "Comparing the epidermal growth factor interaction with four different cell lines: Intriguing effects imply strong dependency of cellular context," *PloS One*, vol. 6, no. 1, p. e16536, 2011.
- [299] M. M. Moasser, A. Basso, S. D. Averbuch, and N. Rosen, "The tyrosine kinase inhibitor ZD1839 ("Iressa") inhibits HER2-driven signaling and suppresses the growth of HER2-overexpressing tumor cells," *Cancer Research*, vol. 61, no. 19, pp. 7184–7188, 2001.
- [300] Y. Nakamura, C. Sotozono, and S. Kinoshita, "The epidermal growth factor receptor (EGFR): Role in corneal wound healing and homeostasis," *Experimental Eye Research*, vol. 72, no. 5, pp. 511–517, 2001.
- [301] S. K. Repertinger, E. Campagnaro, J. Fuhrman, T. El-Abaseri, S. H. Yuspa, and L. A. Hansen, "EGFR enhances early healing after cutaneous incisional wounding," *Journal of Investigative Dermatology*, vol. 123, no. 5, pp. 982–989, 2004.
- [302] R. C. Harris, E. Chung, and R. J. Coffey, "EGF receptor ligands," *Experimental Cell Research*, vol. 284, no. 1, pp. 2–13, 2003.
- [303] M. R. Schneider and E. Wolf, "The epidermal growth factor receptor ligands at a glance," *Journal of Cellular Physiology*, vol. 218, no. 3, pp. 460–466, 2009.
- [304] A. R. French, D. K. Tadaki, S. K. Niyogi, and D. A. Lauffenburger, "Intracellular trafficking of epidermal growth factor family ligands is directly influenced by the pH sensitivity of the receptor/ligand interaction," *Journal of Biological Chemistry*, vol. 270, no. 9, pp. 4334–4340, 1995.

- 
- [305] T. Ronan, J. L. Macdonald-Obermann, L. Huelsmann, N. J. Bessman, K. M. Naegle, and L. J. Pike, "Different Epidermal Growth Factor Receptor (EGFR) agonists produce unique signatures for the recruitment of downstream signaling proteins," *Journal of Biological Chemistry*, vol. 291, no. 11, pp. 5528–5540, 2016.
- [306] Y. Yarden, "The EGFR family and its ligands in human cancer," *European Journal of Cancer*, vol. 37, pp. 3–8, 2001.
- [307] K. J. Wilson, J. L. Gilmore, J. Foley, M. A. Lemmon, and D. J. Riese, "Functional selectivity of EGF family peptide growth factors: Implications for cancer," *Pharmacology and Therapeutics*, vol. 122, no. 1, pp. 1–8, 2009.
- [308] Y. Liu, M. Petreaca, and M. Martins-Green, "Cell and molecular mechanisms of insulin-induced angiogenesis," *Journal of Cellular and Molecular Medicine*, vol. 13, no. 11-12, pp. 4492–4504, 2009.
- [309] M. F. Cordeiro, "Beyond mitomycin: TGF- $\beta$  and wound healing," *Progress in Retinal and Eye Research*, vol. 21, no. 1, pp. 75–89, 2002.
- [310] J. N. Mansbridge and P. C. Hanawalt, "Role of transforming growth factor beta in the maturation of human epidermal keratinocytes," *Journal of Investigative Dermatology*, vol. 90, no. 3, pp. 336–341, 1988.
- [311] Y. Sarret, D. T. Woodley, K. Grigsby, K. Wynn, and E. J. O'Keefe, "Human keratinocyte locomotion: The effect of selected cytokines," *Journal of Investigative Dermatology*, vol. 98, no. 1, pp. 12–16, 1992.
- [312] W. Halfter, J. Candiello, H. Hu, P. Zhang, E. Schreiber, and M. Balasubramani, "Protein composition and biomechanical properties of in vivo-derived basement membranes," *Cell Adhesion and Migration*, vol. 7, no. 1, pp. 64–71, 2013.
- [313] S. Hiroyasu, Z. T. Colburn, and J. C. Jones, "A hemidesmosomal protein regulates actin dynamics and traction forces in motile keratinocytes," *FASEB Journal*, vol. 30, no. 6, pp. 2298–2310, 2016.
- [314] K. Mandal, I. Wang, E. Vitiello, L. A. C. Orellana, and M. Balland, "Cell dipole behaviour revealed by ECM sub-cellular geometry," *Nature Communications*, vol. 5, no. 1, p. 5749, 2014.
- [315] A. Gandalovičová, D. Rosel, M. Fernandes, P. Veselý, P. Heneberg, V. Čermák, L. Petruželka, S. Kumar, V. Sanz-Moreno, and J. Brábek, "Migrastatics—Anti-metastatic and Anti-invasion Drugs: Promises and Challenges," *Trends in Cancer*, vol. 3, no. 6, pp. 391–406, 2017.
- [316] D. Rosel, M. Fernandes, V. Sanz-Moreno, and J. Brábek, "Migrastatics: Redirecting R&D in Solid Cancer Towards Metastasis?," *Trends in Cancer*, vol. 5, no. 12, pp. 755–756, 2019.
- [317] S. A. Eccles, C. Box, and W. Court, "Cell migration/invasion assays and their application in cancer drug discovery," *Biotechnology Annual Review*, vol. 11, pp. 391–421, 2005.
- [318] M. Vinci, C. Box, and S. A. Eccles, "Three-dimensional (3D) tumor spheroid invasion assay," *Journal of Visualized Experiments*, no. 99, p. e52686, 2015.
- [319] N. Kramer, A. Walzl, C. Unger, M. Rosner, G. Krupitza, M. Hengstschläger, and H. Dolznig, "In vitro cell migration and invasion assays," *Reviews in Mutation Research*, vol. 752, no. 1, pp. 10–24, 2013.
- [320] T. Majima, W. Schnabel, and W. Weber, "Phenyl-2,4,6-trimethylbenzoylphosphinates as water-soluble photoinitiators. Generation and reactivity of O=P(C<sub>6</sub>H<sub>5</sub>)(O<sup>-</sup>) radical anions," *Macromolecular Chemistry and Physics*, vol. 192, no. 10, pp. 2307–2315, 1991.





# List of Figures

1.1	Scheme of wound closure . . . . .	4
1.2	End-point chemotaxis assay: the basic idea . . . . .	7
1.3	Traction Force Microscopy . . . . .	10
1.4	Light-sheet Fluorescence Microscopy . . . . .	11
2.1	Actin treadmilling. . . . .	15
2.2	Cell migration along 2D substrate. . . . .	17
2.3	Scheme of a chemotaxing cell . . . . .	23
2.4	Chemotaxis compass and chemotaxis bias models. . . . .	25
2.5	Evolution of a diffusion-based gradient. . . . .	27
2.6	Micropipette chemotaxis assay. . . . .	28
2.7	Under-agarose chemotaxis assay. . . . .	29
2.8	Boyden chamber assay . . . . .	30
2.9	Bridge assays . . . . .	31
2.10	Microfluidic-based chemotaxis assays . . . . .	32
2.11	$\mu$ -Slide Chemotaxis. . . . .	34
2.12	Parameters for analysing chemotaxis in the $\mu$ -Slide Chemotaxis. . . . .	35
2.13	Micro-patterning methods . . . . .	40
2.14	Fabrication of 3D structures from PEG-norb . . . . .	42
3.1	Fabrication of PEG-DMA microwells. . . . .	44
3.2	Fibronectin micro-patterning with silicon stencil . . . . .	45
3.3	Photolithographic in-channel micro-patterning of passivated surfaces . . . . .	46
3.4	8-arm PEG-norbornene . . . . .	48
3.5	Photomask for PEG4norb structures . . . . .	48
3.6	Centre of mass displacement . . . . .	53
4.1	Cell distribution in the $\mu$ -Slide Chemotaxis at the beginning and at the end of an chemotaxis experiment. . . . .	60
4.2	PEG-DMA micro-wells . . . . .	61
4.3	Distribution of HT1080 cells in the PEG-DMA micro-well over time . . . . .	62
4.4	Cell adhesion and chemotaxis on round fibronectin patterns. . . . .	63
4.5	Cell adhesion on an in-channel micro-patterned surface . . . . .	65

4.6	Scheme of the hydrogel-enclosed migration arena in the $\mu$ -Slide Chemotaxis. . .	65
4.7	Function of the migration arena. . . . .	66
4.8	Fabrication of the migration arena by photolithography . . . . .	67
4.9	Visualisation of the gradient in the migration arena assay assay . . . . .	68
4.10	HT1080 model of chemotaxis of slow moving cells. . . . .	69
4.11	Cell viability in the 3D migration arena assay . . . . .	70
4.12	Stabilisation of the 3D collagen matrix in the migration arena . . . . .	71
4.13	Chemotaxis of HT1080 in a 3D migration arena assay . . . . .	72
4.14	Verification of the results of a 3D migration arena assay . . . . .	72
4.15	Chemotaxis of HT1080 in the 2D migration arena assay . . . . .	74
4.16	Analysis of cell migration trajectories in the arena assay . . . . .	76
5.1	GF-induced nHEK chemotaxis: scheme of the experimental set-up. . . . .	83
5.2	Automated and manual analysis of COMD . . . . .	85
5.3	nHEK distribution at the end-point of chemotaxis assay. . . . .	86
5.4	Time-lapse analysis of nHEK chemotaxis: EGF and TGF $\alpha$ . . . . .	87
5.5	Time-lapse analysis of nHEK chemotaxis: TGF $\beta$ , insulin, and BPE. . . . .	88
5.6	GF-induced chemotaxis of nHEK cells . . . . .	89
5.7	Inhibition of cell proliferation—optimisation of MMC treatment. . . . .	91
5.8	Chemotaxis of non-proliferating cells. . . . .	92
5.9	Effect of gradients of combined GFs on nHEK chemotaxis. . . . .	93
5.10	EGF- and TGF $\alpha$ -induced chemotaxis is EGFR dependent. . . . .	94
6.1	Scheme of the chemotaxis slide with a TFM-substrate . . . . .	100
6.2	Distribution of cell forces. . . . .	102
6.3	Contractile forces of nHEKs in chemotaxis and chemokinesis . . . . .	103
6.4	Gradient visualisation in the FEP tube . . . . .	105
6.5	HT1080 cell migrating through a 3D collagen matrix visualised by the light-sheet fluorescence microscopy . . . . .	106
6.6	Stabilisation of the collagen matrix in the FEP container. . . . .	107

# Acknowledgements

Thourough my PhD studies I was fortunate to recieve valuable pieces of advice, support and guidance from many, whom I wish to thank.

Foremost, my sincere thanks belong to my supervisors, Dr. Zeno von Guttenberg and Prof. Dr. Rudolf Merkel. Thank you for entrusting me this fascinating topic. And thank you for your kind guidance and mentoring, and all the invaluable pieces of advice.

I also thank my co-supervisor, Dr. Bernd Hoffmann, and Prof. Dr. Rudolf Leube, Prof. Dr. Reinhard Windoffer, Prof. Dr. Alexander Bershadsky, and all members of the InCeM consortium for fruitful discussions and many helpful pieces of advice, especially — but not only — on the topic of keratinocyte migration.

Dr. Roman Zantl, Dr. Valentin Kahl, Dr. Jan Schwarz, Dr. Miriam Balles, Shokoufeh Teymouri, Elias Horn, Helga Wagner, Verena Biswenger, Nina Bauman, Johannes Jürschick, Trung Pham, and the whole ibidi R&D department, for the helpful scientific discussions and constructive feedback throughout my PhD studies. Thank you, Elias, Verena, and Nina for sharing your experience with the chemotaxis assay.

Dr. Miriam Balles, for introducing me to the world microstructuring and micropatterning methods, and sharing her experience with the 3D hydrogel. Also for synthetising the LAP photoinitiator.

Dr. Jan Schwarz, for his help with micropatterning, as well as for constructive feedback and many thought-provoking discussions.

And thank you, Miriam and Shokoufeh, for all the brainstorming sessions in our office that led to many interesting scientific ideas.

Prof. Dr. Reinhard Windoffer, Dr. Volker Buck, and Dr. Sebastian Kant for introducing me to the light-sheet microscopy, as well as Dr. Nicole Schwarz, Dr. Marcin Moch, Dr. Nadiéh Kuijpers, Dr. Anne Pora, and the whole team of the MOCA Institute for their help and support during my secondment at the RWTH Aachen.

Dr. Bernd Hoffmann, Nico Hampe, Dr. Erik Noetzel, Dr. Ronald Springer, and Georg Dreissen, for their help with the traction force microscopy and soft lithography. Gloria, Galia, Kritika, Niels, and the whole team of ICS-7, Forschungszentrum Jülich, for all the kind help I received during my secondment there.

Many thanks to Zeno, Anna, and Anita, for proofreading the thesis, and helping me to get rid of errors, typos, and overly long sentences. And Johannes, thank you for the most helpful discussion regarding commas.

Thank you, Julia, Zeno, Miriam, Shokoufeh, Jan, Louise, Brigitte, Anita, Moritz, JJ, Trung, Irina, and all ibidis from all departments, for providing support in many forms, for creating the wonderful, inspiring working atmosphere, and for being the most amazing colleagues I could wish for.

I am extremely grateful to my friends and family for their continuous support throughout the time of my studies, and beyond. Special thanks to Anna for all her help, and Anita, Anna, Sonni and Erich, Irina, and Hanne and Rainer, for constant motivation and for giving me the extra push that was needed at times when I got too side-tracked from finishing writing the thesis.

Thanks to my fellow InCeM PhD candidates, Tina, Nadieh, Roman, Anne, Nikos, Kritika, Rutuja, Galyia, Katarina, Dima, Davide, Shore, Victor, Laura, for all the great time we spent together during the project meetings, making science having fun, or just having fun, making (no) science out of it. It was epic indeed.

And last but not least, I want to thank my amazing parents with all my heart, for always being there for me with their unconditional support. Thank you.



# A. List of Abbreviations

$\mu$ CP	micro-contact printing
$\mu$ FLP	microfluidic patterning
2D	two dimensional
3D	three dimensional
ADP	adenosine diphosphate
AF	actin filaments
ATP	adenosine triphosphate
BM	basal medium
BPE	bovine pituitary extract
cAMP	cyclic adenosin monophosphate
CM	complete medium
COM	centre of mass
COMD	centre of mass displacement
DNA	deoxyribonucleic acid
ECM	extracellular matrix
EDC	ethyl-dimethyl-aminopropylcarbodiimide
EGF	epithelial growth factor
FA, FAs	focal adhesion, adhesions
F-actin	filamentous actin polymer
FBS	fetal bovine serum
FDA	fluorescein diacetate
FEP	fluorinated ethylene propylene
FITC	fluorescein isothiocyanate
FMI	forward migration indices
GAPs	GTPase activating proteins
GDI	guanine nucleotide dissociation inhibitors
GDP	guanosine diphosphate
GEFs	guanosine nucleotide exchange factors
GF, GFs	growth factor, factors
GPRC	G-protein coupled receptor
GTP	guanosine triphosphate
h	hours
KC, KCs	keratinocyte, keratinocytes
LAP	lithium phenyl-2,4,6-trimethylbenzoylphosphinate

LSFM	light-sheet fluorescence microscopy
min	minutes
MLC	myosin light-chain
MMC	mitomycin C
MMPs	matrix metalloproteinases
nHEK, nHEKs	normal human epithelial keratinocyte, keratinocytes
NHS	N-hydroxy-succinimide
PDGF	platelet-derived growth factor
PDMS	polydimethylsiloxane
PEG	polyethylene glycol
PEG4norb	4-arm polyethylene glycol norbornene
PEG8norb	8-arm polyethylene glycol norbornene
PEG-DT	polyethylene glycol dithiol
PEG-DMA	polyethylene glycol dimethylacrylate
PI	propidium iodide
PI3K	phosphoinositide 3-kinase
PIP3	phosphatidylinositol-3,4,5-phosphate
PLL	poly-L-lysine
PTEN	PIP3-regulating phosphatase
RGD	arginin-glycin-aspartate peptide
RTK	receptor tyrosine kinase
s	seconds
SD	standard deviation
SEM	standard error of mean
TFM	traction force microscopy
TGF $\alpha$	transforming growth factor alpha
TGF $\beta$	transforming growth factor beta
TKI	tyrosine kinase inhibitor tyrphostin
UV	ultraviolet







## B. List of Materials

Chemicals	Supplier
3-aminopropyl triethoxysilane (APTES)	Sigma-Aldrich, St. Louis, MO, USA
4-arm polyethylene glycol norbornene, 20 kDa (PEG4norb)	JenKem Technology USA, Plano, TX, USA
4-benzoyl benzylamide hydrochloride	Fluorochem, Hadfield, UK
6-fluorescein-alkyne (6-FAM)	Jena Bioscience, Jena, Germany
8-arm polyethylene glycol norbornene, 20 kDa (PEG8norb)	JenKem Technology USA, Plano, TX, USA
acetone, HPLC grade	Carl Roth GmbH, Karlsruhe, Germany
Alexa Fluor488	invitrogen, Waltham, MA, USA
bovine pituitary extract (BPE)	part of DermaLife K Life-Factors kit, Lifeline Cell Technology, Frederick, MD, USA
Click-iT Cell Reaction Buffer Kit	invitrogen, Waltham, MA, USA
collagen type I solution, bovine (PureCol, 3mg/ml)	Advanced BioMatrix, Carlsbad, CA, USA
cyclic RGD-azide (cyclo[RGDFK(azide)])	Peptides International, Gardner, MA, USA
DermaLife K LifeFactors kit	Lifeline Cell Technology, Frederick, MD, USA
DermaLife medium	Lifeline Cell Technology, Frederick, MD, USA
DMEM, low glucose, 10x	Sigma-Aldrich, St. Louis, MO, USA
Dulbecco's Modified Eagle's Medium, high glucose	Sigma-Aldrich, St. Louis, MO, USA
EGFR monoclonal antibody 225, mouse, anti-human	invitrogen, Waltham, MA, USA
epithelial growth factor (EGF)	PromoCell, Heidelberg, Germany
ethanol, 96%	VWR, Radnor, PA, USA
ethyl-dimethyl-aminopropylcarbodiimide (EDC)	Sigma-Aldrich, St. Louis, MO, USA
fetal bovine serum (FBS), qualified, Brazil (Cat.No.:10270106)	Gibco, Carlsbad, CA, USA
fibronectin, human, natural (Cat. No. 354008)	Corning, Corning, NY, USA
FITC-dextran, 40 kDa	Sigma-Aldrich, St. Louis, MO, USA
fluorescein diacetate (FDA)	Sigma-Aldrich, St. Louis, MO, USA
FluoSpheres Carboxylate, 0.2 $\mu$ m, crimson	invitrogen, Waltham, MA, USA
insulin	part of DermaLife K Life-Factors kit, Lifeline Cell Technology, Frederick, MD, USA
linear RGD peptide (CRGDS)	Iris Biotech, Marktredwitz, Germany
lithium phenyl-2,4,6-trimethylbenzoylphosphinate (LAP)	in house synthesis by Dr. M. Balles, as described in [320]
mitomycin C (MMC)	Sigma-Aldrich, St. Louis, MO, USA
N-hydroxy-succinimide (NHS)	Sigma-Aldrich, St. Louis, MO, USA
Penicillin/Streptomycin	Gibco, Carlsbad, CA, USA
phosphate buffered saline, no Ca and Mg (Cat.No.:1419044)	Gibco, Carlsbad, CA, USA
Pluronic F-127	Sigma-Aldrich, St. Louis, MO, USA
polyethylene glycol dimethylacrylate (PEG-DMA, Mn 550)	Sigma-Aldrich, St. Louis, MO, USA
polyethylene glycol dithiol (PEG-DT, Mn 1000)	Sigma-Aldrich, St. Louis, MO, USA
propidium iodide (PI)	Carl Roth GmbH, Karlsruhe, Germany
sodium bicarbonate (NaHCO <sub>3</sub> , 7.5%)	Sigma-Aldrich, St. Louis, MO, USA
sodium dodecyl sulfate (SDS)	Sigma-Aldrich, St. Louis, MO, USA
sodium hydroxide (NaOH)	Carl Roth GmbH, Karlsruhe, Germany
Sulfo-Cyanine-3-azide	Lumiprobe, Hannover, Germany
Sylgard 184 Silicone Elastomere Kit	Dow Corning, Midland, MI, USA
transforming growth factor alpha	part of DermaLife K Life-Factors kit, Lifeline Cell Technology, Frederick, MD, USA
transforming growth factor beta	Peptotech, Cranbury, NJ, USA
Trypsin Neutralizing Solution	Lifeline Cell Technology, Frederick, MD, USA
trypsin-EDTA (0.5%, 10x, no phenol red)	Gibco, Carlsbad, CA, USA
tyrphostin AG-1478	Sigma-Aldrich, St. Louis, MO, USA
ultra-pure water, ROTIPURAN® p.a., ACS grade	Carl Roth GmbH, Karlsruhe, Germany

<b>Cells</b>	<b>Supplier</b>
HT1080 (human, fibrosarcoma)	DSMZ, Braunschweig, Germany
LifeAct-GFP2 HT1080	ibidi, Gräfelfing, Germany
nHEK (normal human epithelial keratinocytes)	CellSystems, Troisdorf, Germany

<b>Consumables</b>	<b>Supplier</b>
Cell+ tissue culture flasks	Sarstedt, Nümbrecht, Germany
Culture Insert FulTrack	ibidi, Gräfelfing, Germany
FEP tubes Bola S1815-04	Bohlender GmbH, Grünsfeld, Germany
glass coverslips 75x25 mm, thickness no. 0 (0.085-0.115 mm)	Paul Marienfeld GmbH, Lauda-Königshofen, Germany
LifterSlips, 22x25 mm, volume 13,02 µl	Science Services, Munich, Germany
PCR-foil	HJ-Bioanalytik GmbH, Erkelenz, Germany
polymer foil, uncoated, ibiTreat or BioInert, Coverslips for sticky-Slides	ibidi, Gräfelfing, Germany
sticky-Slide Chemotaxis	ibidi, Gräfelfing, Germany
µ-Slide Chemotaxis	ibidi, Gräfelfing, Germany

<b>Instruments</b>	<b>Supplier</b>
302 nm UV bench lamp, XX-series, 15 W	VWR, Radnor, PA, USA
365 nm LED lamp KSL70/365	RappOpto Electronic GmbH, Hamburg, Germany
quarz photomasks	Compugraphics Jena, Jena, Germany
projector Panasonic PT-AH1000E	Panasonic, Kadoma, Japan
EVOS fl inverted microscope	AMG, Mill Creek, WA, USA
Nikon Eclipse Ti inverted microscope	Nikon GmbH, Düsseldorf, Germany
Olympus CKX41 inverted microscope	Olympus Scientific Solutions, Waltham, MA, USA
Zeiss Axiovert 100 microscope	ZEISS, Oberkochen, Germany
Zeiss Lightsheet Z.1 microscope	ZEISS, Oberkochen, Germany
Stage Top Incubation System, Universal Fit, for 4 µ-Slides	ibidi, Gräfelfing, Germany
cell culture CO <sub>2</sub> incubator Heracell 150i	ThermoFisher Scientific, Waltham, MA, USA
vacuum pump ME 2 NT, 70 mbar	vacuubrand, Wertheim, Germany
spincoater WS-650mz-23NPP	Laurell, North Wales, PA, USA